ANALYSIS OF HEAT TREATMENT EFFECT
ON SPRINGBACK IN V- BENDING

A THESIS SUBMITTED TO
THE GRADUATE SCHOOL OF NATURAL AND APPLIED SCIENCES
OF
MIDDLE EAST TECHNICAL UNIVERSITY

BY

ONUR TURGAY SARIKAYA

IN PARTIAL FULFILLMENT OF THE REQUIREMENTS
FOR
THE DEGREE OF MASTER OF SCIENCE
IN
MECHANICAL ENGINEERING

NOVEMBER 2008

Approval of the thesis:

ANALYSIS OF HEAT TREATMENT EFFECT ON SPRINGBACK IN V- BENDING

submitted by **Onur Turgay SARIKAYA** in partial fulfillment of the requirements for the degree of **Master of Science in Mechanical Engineering Department, Middle East Technical University by,**

Prof. Dr. Canan Özgen _______________
Dean, Graduate School of **Natural and Applied Sciences**

Prof. Dr. Süha ORAL _______________
Head of Department, **Mechanical Engineering**

Prof. Dr. Haluk DARENDELİLER _______________
Supervisor, **Mechanical Engineering Dept., METU**

Examining Committee Members:

Prof. Dr.Metin AKKÖK _______________
Mechanical Engineering Dept., METU

Prof. Dr. Haluk DARENDELİLER _______________
Mechanical Engineering Dept., METU

Prof. Dr. Kemal İDER _______________
Mechanical Engineering Dept., METU

Assoc. Prof. Dr. Serkan DAĞ _______________
Mechanical Engineering Dept., METU

Prof. Dr. Can ÇOĞUN _______________
Mechanical Engineering Dept., Gazi University

Date: _______________

I hereby declare that all information in this document has been obtained and presented in accordance with academic rules and ethical conduct. I also declare that, as required by these rules and conduct, I have fully cited and referenced all material and results that are not original to this work.

Name, Last name: Onur Turgay, SARIKAYA

Signature :

ABSTRACT

ANALYSIS OF HEAT TREATMENT EFFECT ON SPRINBACK IN V-BENDING

SARIKAYA, ONUR TURGAY

M.S. , Department of Mechanical Engineering

Supervisor : Prof Dr. Haluk DARENDELİLER

November 2008, 184 Pages

Aluminum based alloys have wide area of usage in automotive and defense industry and bending processes are frequently applied during production. One of the most important design criteria of bending processes is springback, which can be basically defined as elastic recovery of the part during unloading. To overcome this problem, heat treatment is generally applied to the workpiece material to refine tensile properties.

In this study, the effect of heat treatment on springback characteristics of aluminum studied both numerically by using finite element analysis and experimentally. For this purpose, two different materials are selected and various heat treatment procedures are considered. The aluminum sheets having thickness of 1.6 mm, 2 mm and 2.5 mm are bent to 60˚, 90˚ and 120˚. The von Mises stress distributions, plastic strain values and punch load values and comparison of the numerical and experimental results are also given.

Key Words : Springback, Metal Forming, Bending, Finite Element Analysis, Finite Element Method.

ÖZ

ISIL İŞLEMİN V-BÜKME İŞLEMİNDE GERİ YAYLANMAYA ETKİSİ

SARIKAYA, ONUR TURGAY

Yüksek Lisans, Makina Mühendisliği Bölümü

Tez Yöneticisi : Prof Dr. Haluk DARENDELİLER

Kasım 2008, 184 sayfa

Otomotiv ve savunma sanayii endüstrisinde geniş bir kullanım alanı bulan aluminyum temelli alaşımlar, bükme işlemlerinde üretim boyunca sık sık kullanılmaktadır. Bükme işleminin en önemli tasarım kriterlerinden biri, yükleme kaldırıldıktan sonra parçanın eski haline dönme eğilimi olan, geriyaylanmadır. Bu sorunun üstesinden gelmek için iş parçasına genellikle çekme özelliklerini iyileştirmek amacıyla ısıl işlem uygulanır.

Bu çalışmada ısıl işlemin aluminyum malzemenin geri yaylanma karakteristiğine olan etkisi sonlu elemanlar analizi yöntemi kullanılarak nümerik, ve deneysel olarak belirlenmiştir. Bu amaçla, iki farklı alüminyum sac malzeme seçildi ve değişik isıl işlemer uygulandı. 1.6 mm, 2 mm ve 2.5 mm kalınlıklarındaki aluminyum sac malzemelere 60˚, 90˚ ve 120˚ bükme işlemi yapıldı. İncelenen durumlar için, von Mises gerilme dağılımları, plastik gerinme değerleri, kalıp kuvvetleri ve nümerik değerlerle deneysel sonuçların karşılaştırılması da bu çalışma kapsamında yapılmıştır.

Anahtar Kelimeler : Geri yaylanma, Metal Şekillendirme, Bükme, Sonlu Elemanlar Analizi, Sonlu Elemanlar Yöntemi.

This thesis is dedicated to my parents Gülsen and Hüseyin SARIKAYA.

ACKNOWLEDGEMENTS

First and foremost, I would like to express a great deal of thanks and gratitude to Prof. Dr. Haluk DARENDELİLER for his encouragement, insight and close guidance. Prof. DARENDELİLER far exceeded my expectations from an advisor and made my entire graduate experience unforgettable.

I also want to thank Prof. Dr. Metin AKKÖK, Prof. Dr. Can Çoğun, Prof. Dr. Kemal İder and Assoc. Prof. Dr. Serkan DAĞ for their comments.

I would also take the opportunity to thank all my colleagues in TÜBİTAKSAGE, Mechanical Production Division, especially to Mahmut BEŞİR and Egemen Varlı, for their help and invaluable discussing during my study.

I would like to express my gratefulness to my colleagues, İlker Atik, Dr.Bülent Özkan, Dr. Kemal Yaman, Ahmet Akbulut, Aydın Tüzün and Burak Durak for their valuable comments and advices during this thesis.

TABLE OF CONTENTS

LIST OF TABLES

TABLES

LIST OF FIGURES

FIGURES

CHAPTER 1

INTRODUCTION

1.1 Bending

1.1.1 Definition and Terminology

Bending is the forming of solid parts, where angled or ring-shaped workpieces are produced from sheet or strip metal. The process consists of uniformly straining flat sheets or strips of metal around a linear axis, but it also may be used to bend tubes, drawn profiles bars, and wire [2]. In bending, the plastic state is brought by a bending load [1]. In fact, one of the most common processes for sheet metal forming is bending, which is used not only to form pieces such as L, U or V-profiles, but also to improve the stiffness of a piece by increasing its moment of inertia.

Bending has the greatest number of applications in the automotive, aircraft and defense industries and for the production of other sheet metal products. Typical examples of sheet-metal bends are illustrated in Figure 1.1.

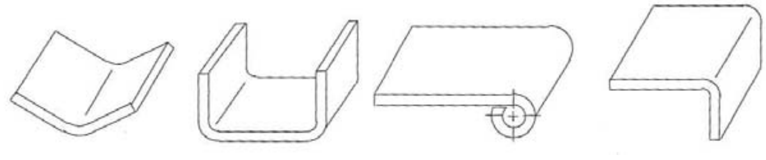

Figure 1.1 Typical examples of sheet metal bend parts. [2]

The basic characteristic of bending is stretching (tensile elongation) imposed on the outer surface and compression on the inner surface as shown Figure 1.2 [3].

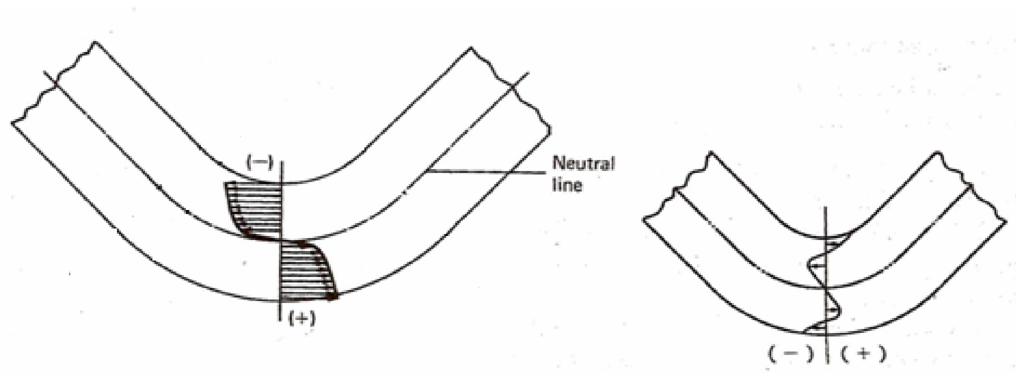

(a) (b)

Figure 1.2 In the course of bending (a) the entire stress-strain curve is transversed ; (b) elastic stresses result in springback and the residual stress pattern [3].

In this sence, the terms used in bending are defined in the drawing in Figure 1.3

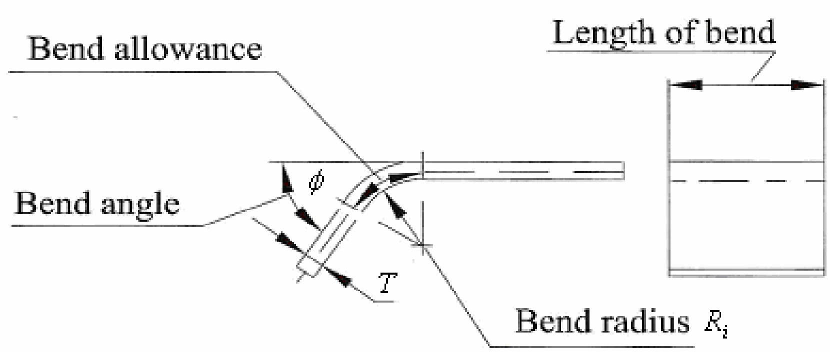

Figure 1.3 Schematic illustration of terminology, used in bending process. [2]

Here, the bend radius R_i is measured on the inner surface of the bend piece. The bend angle ϕ is the angle of the bent piece and T is the material thickness [2].

In bending process, since the outer fibers of the material are placed in tension and the inner fibers are placed in compression, theoretically the strain values on the outer and inner fibers are equal in magnitude and are given by the following equation:

$$e_0 = e_1 = \frac{1}{(2R_i/T)+1} \tag{1.1}$$

Experimental researches indicate that this formula is more precise for the deformation of the inner fibers of the material, e_1, than for the deformation of the outer fibers, e_0 . The deformation in the outer fibers is notably greater, which is why neutral fibers move to the inner side of the bent piece. The width of the piece on the outer side is smaller and on the inner side is larger than the original width. As R_i/T ratio decreases, the bend radius becomes smaller; the tensile strain at the outer fibers increases and the material eventually cracks.

1.1.2 Moment of Bending

Suppose that there is have a long, thin straight beam having cross-section (bxT) and length L, bent into a curve by moments (M). The beam and moments lie in the vertical plane nxz, as shown in Figure 1.4. At a distance x from the left end, the deflection of the beam is given by distance z. Figure 1.4b shows, enlarged, two slices $A-B$ and $A'-B'$ of different angles dx, cut from the beam at location x.The planes cutting $A-B$ and $A'-B'$ are taken perpendicular to the longitudinal axis x of the original straight beam. It is customary to assume that these cross-sections will remain planar and perpendicular to the longitudinal elements of the beam after moments (M) are applied. Laboratory experiments have in general verified this assumption.

After bending, some of the fibers have been extended $(B-B')$, some have been compressed $(A-A')$, and at the location, called the neutral surface, no change in length has taken place $(n-n)$.

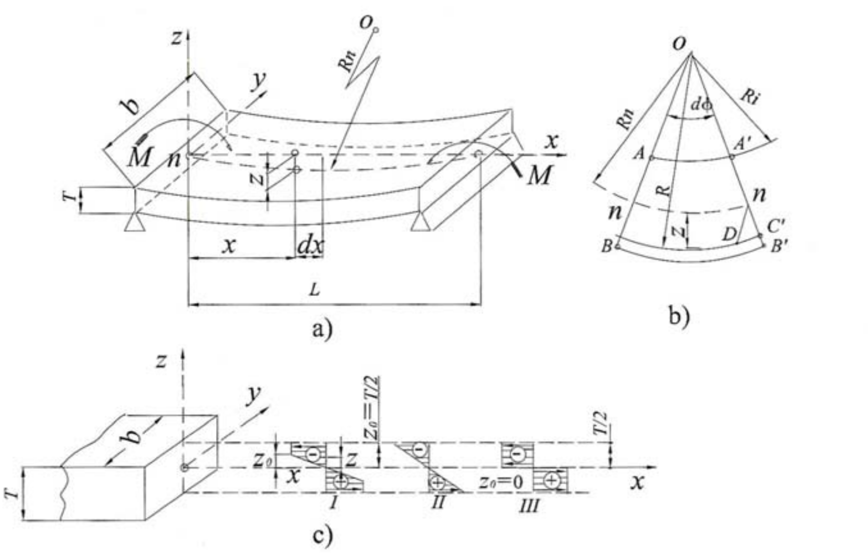

Figure 1.4 Schematic illustration of bending beam: a) bending beam; b) neutral line; c) bending stress in elastic-plastic zone.

The loading of Figure 1.4 is called pure bending. No shear or tangential stress will exist on the end surfaces $A-B$ and $A'-B'$, and the only stress will be σ, the acting normally on the surface. An equation can be derived to give the value of this bending stress at any desired distance z from the neutral surface. Let O be the center of curvature for slice $(n-n)$ of the deformation beam, $d\varphi$ the small angle included between the cutting planes, and R_n the radius of curvature. Consider a horizontal element located a distance z below the neutral surface. Draw a line $n-D$ parallel to $O-B$. The angle $D-n-C'$ and the following proportional relationship results:

$$\frac{z}{R_n} = \frac{d\varphi}{dx} = \varepsilon \tag{1.2}$$

Since the total deformation of the element $2d\varphi$ divided by the original length dx is the unit deformation or strain, Equation (1.2) indicates that the elongation of the element will vary directly with the distance z from a neutral surface.

For a more detailed definition of the stress-strain relationship in bending process, the concept of a reduction in the radius of neutral curvature (R_r) is useful. This value is the ratio to the bend radius of the neutral surface-to-material thickness.

$$R_r = \frac{R_n}{T} \tag{1.3}$$

where;

R_r = reduction radius of the neutral curvature surface. [2]

1.1.2.1 Moment of Bending in Elastic-Plastic Domain

The engineering moment of bending in elastic-plastic domain can be expressed as the sum of the moments of bending in the elastic and plastic zones for the same axis, and is given by general formula,

$$M = YS\left[\frac{2}{z_0}\int_0^{z} z^2 dA + 2\int_{z_0}^{T/2} zdA\right] \tag{1.4}$$

The first segment of this equation is the moment of resistance in the elastic deformation zone with regard to the y - axis:

$$W = \frac{2}{z_0}\int_0^{z_0} z^2 dA \tag{1.5}$$

The second segment of the equation is the moment of static at the plastic deformation zone with regard to the y - axis:

$$S = 2\int_{z_0}^{T/2} zdA \tag{1.6}$$

Therefore, the bending moment in the elastic-plastic domain in the final form is:

$$M = YS(W + S) \tag{1.7}$$

where;

$\beta =$ Hardening Coefficient of Material

$k =$ True Strain of Material

$b =$ Width of Beam (length of bending), and

$T =$ Material Thickness

For a rectangular cross- section of a beam, the bending moment in the elastic-plastic domain is given by the formula:

$$M = \frac{(YS)b}{12}\left(3T^2 - 4z_0^2\right) \tag{1.8}$$

The value of z_0 can be calculated by Hooke's law:

$$YS = E \cdot \varepsilon_0 = E\frac{z_0}{R_n} \tag{1.9}$$

where;

R_n = Radius of Curvature

E = Elastic Modulus

Hence,

$$z_0 = \frac{(YS) \cdot R_n}{E} \tag{1.10}$$

When the above expression is substituted for z_0 in equation (1.8), equation (1.8) is changes to:

$$M = \frac{(YS)b}{12}\left[3T^2 - \left(\frac{2(YS) \cdot R_n}{E}\right)^2\right] \tag{1.11}$$

Respecting equation (1.3) the bending moment may be expressed as the reduction radius of curvature (R_r) :

$$M = (YS)\frac{bT^2}{12}\left[3 - \left(\frac{2(YS)R_n}{E}\right)^2\right] \tag{1.12}$$

However, with bending in the elastic-plastic domain $5 \le R_r \le 200$ the influence of part of the equation $\left(\frac{2YS \cdot R_r}{E}\right)^2$ is very slight, and the engineering calculation can be disregarded. Setting aside this part of the equation, we may assume, as a matter of fact, that the entire cross-section of the beam experiences linear-plastic deformation Figure 1.4c, so that the moment of the bending beam is loaded by stresses in the linear-plastic domain:

$$M = (YS)\frac{bT^2}{4} \tag{1.13}$$

1.1.2.2. Moment of Bending in the Purely Plastic Domain

The moment of bending in purely plastic domain for a rectangular cross-section is given by the formula:

$$M = \beta \cdot k\frac{bT^2}{4} \tag{1.14}$$

$\beta =$ Hardening coefficient of material

$k =$ True strain of material

$b =$ Width of beam (length of bending), and

$T =$ Material thickness

This expression can be simplified to:

$$M = n\left(UTS\,\frac{bT^2}{4}\right) \tag{1.15}$$

Where:

n = Correction coefficient hardening of the material (n=1.6 to 1.8)
UTS = Ultimate tensile strength of the material
b = Width of beam (lentgh of bending), and
T = Material thickness [2]

1.1.3. Types of Bending Operations

Bending of sheet metals can be accomplished through utilization of several manufacturing processes. A distinction can be made as depending on the part's support; supported bending and unsupported bending.

Unsupported bending is similar to the process of stretching, where a flat piece of metal retained in a die, stretches along with the application of tool pressure.

U-die and V-die bending processes are both considered unsupported bending processes at their beginning stages, as shown Figure 1.5. As the bending process continues and the material is pulled down into the recess, all the way down, the bending becomes supported, as shown in Figure 1.6.

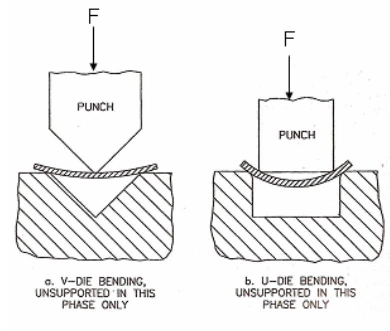

Figure 1.5 Unsupported bending

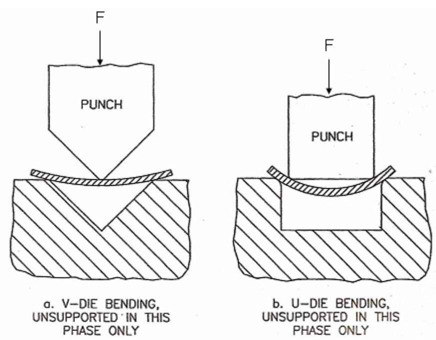

Figure 1.6 Supported and partially supported bending

Supported bending may be considered any bending where a spring-loaded pad, is included for support of the formed part as given in Figure 1.7 [4].

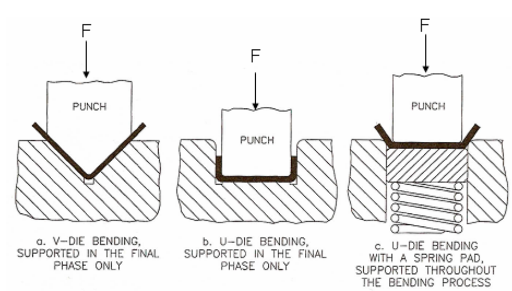

Figure 1.7 Supported bending.

1.1.3.1. V-Die Bending

V-die bending is widely used thought industry because of its simple tooling. During V-die bending, the punch moves down, coming first to a contact with the unsupported sheet metal. By progressing farther down, it forces the material to follow along, until bottoming on V shape of the die at final stage [4].

In the case of V-die bending, because of the mechanics of the process, the two end regions of the bent-up sheet leave the die and lean on the punch just before the fully loaded stage [4]. As the punch proceeds further to move downwards, the ends of the sheet are bent towards the die again and secondary bent-up regions are formed on both sides just above the main bent-up region. At the fully loaded state, the sheet is fully supported by the die and the punch. After the removal of the sheet from the punch and die, the secondary bent-up regions, which are formed during bending, also cause springback in the opposite direction to the one resulted by the main bent-up region [61].

V-die bending and is illustrated in Figure 1.8 and some examples are shown in Figure 1.9 [4].

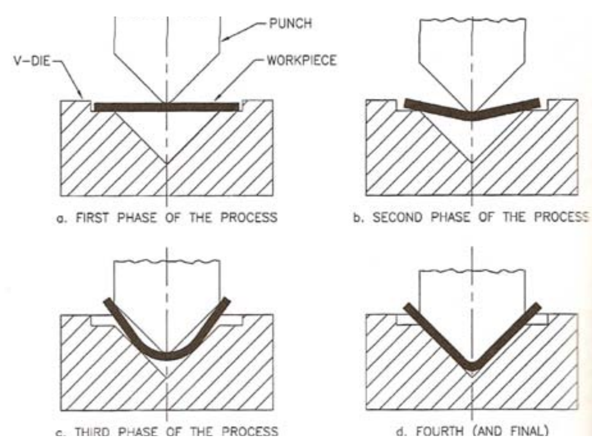

Figure 1.8 V-die Bending

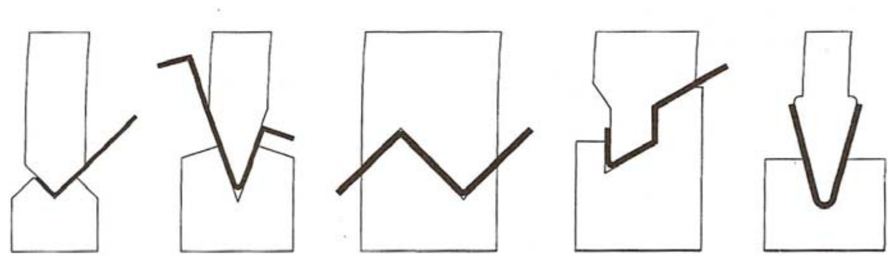

Figure 1.9 V-die bending samples.

If the angle of the die face is γ in Figure 1.10a and there is some friction between the sheet and die, the force on the sheet will be at an angle ψ to the normal, where the coefficient of friction is $\mu = \tan\psi$. The force on the punch, *P,* is

$$P = 2\cos(\alpha - \psi) \tag{1.16}$$

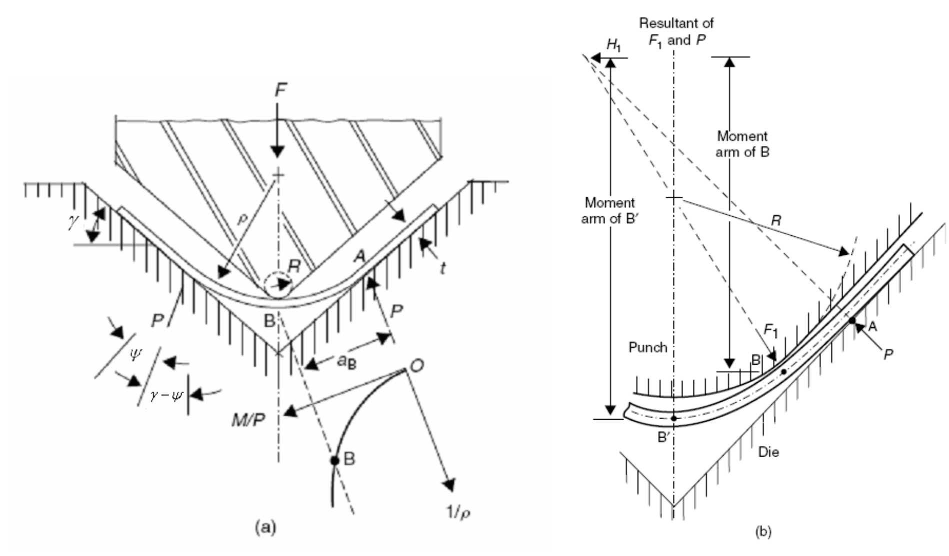

Figure 1.10 Bending a strip in a V-die with a punch of nose radius *R* (a) At the start of the process. (b) When the punch has nearly reached the bottom of its stroke.

In the initial stages, the curvature of the sheet at the nose of the punch will be less than the nose radius, as shown in Figure 1.10 (a). The curvature is given by the point B in the bending line construction shown. As the bending progresses, the punch force will increase and the curvature at the point of contact increase until it just matches the punch curvature. On further bending, the point of contact with the punch will move away from the nose to some point B as shown in Figure 1.10 (b). Since only a frictionless condition has been considered, the force is normal to the tool at the point of contact. It is seen that there is a difference between the line of action of the force exerted by the die at point A and that through the point of contact B with the punch. These forces converge as shown, and by symmetry, their resultant must be horizontal, i.e. the force *H*. As the moment arm of the force bending the sheet at the centre-line B' is greater than that at the punch contact B, the curvature at B' must be greater than at B, and there will be a gap between the sheet and the punch at B'. If close conformity between the punch and the sheet is required, the V-die is made with a radius at the bottom to match the punch and a large force is applied at the end of the process. A problem with such an arrangement is that small variations in thickness or strength in the sheet or in friction may cause appreciable changes in springback [5].

1.1.3.2. Air Bending

In air bending, the tooling, punch and die are used only to convey energy. The workpieces rests on two points. The punch carries out the bending movement. A curvature sets in, growing the centre. Air bending is used mainly to straighten workpieces [1].

Principle of the process is illustrated in Figure 1.11

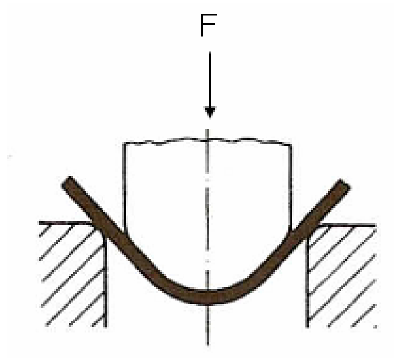

Figure 1.11 Principle of air bending.

1.1.3.3. U-Bending

In this type of bending, the process begins with a strip or sheet of metal positioned over a U-shaped opening or an insert of such a shape. As the punch comes down, it contacts the sheet metal material first and pulls it along on a further descent, forcing in into the U-shaped opening as shown in Figure 1.12 [4].

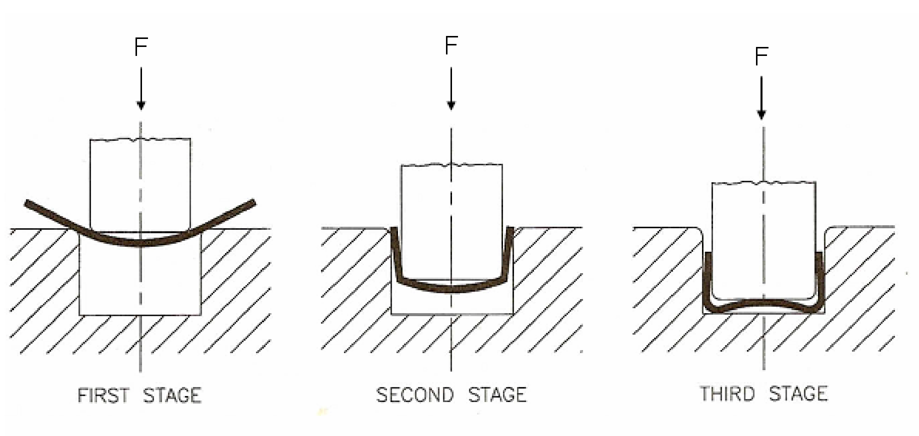

Figure 1.12 U-die bending process.

In this case, to prevent the bottom form bulging out during bending, a backing pad is often used. During the bending process, it already starts pressing against the bottom of the workpiece [1].

1.1.3.4. Wipe Bending

In wipe bending methods of producing bends, the blank is retained in a fixed position by spring-loaded pressure pad (Figure 1.13). The forming punch comes down toward the spring-loaded pressure pad. This type of bending may be preferred when the bent flange is relatively shorter than the remaining part of the sheet [4].

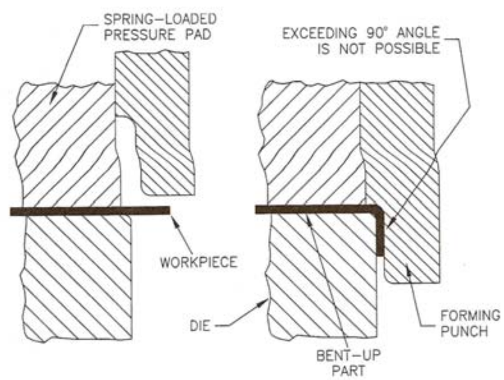

Figure 1.13 Wipe bending process

1.1.3.5. Rotary Bending

Rotary bending has several advantages over traditional types of bending. It does not only utilize 50 to 80 percent less bending force than wipe bending process, but also it generally does not need a pressure pad for retention of material, as the rocker provides for it automatically as seen Figure 1.14 [4].

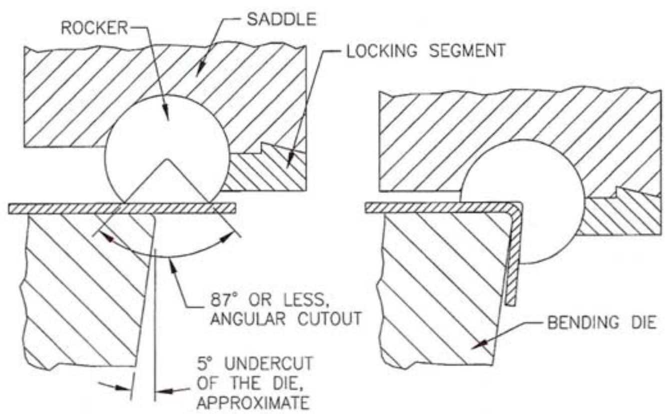

Figure 1.14 Rotary bending process using ready bender

As the tool comes down, the rocker lands on the material, positioning itself with one edge over the die and with the other over the gap. Coming farther down, its pressure bends down the flange, but it does not stop at 90°; it continues farther to attain 3° overbend as a protection against springback [4].

1.1.4. Factors Effecting Bending

Bend radius or die radius R_i, is one of the most important parameter, which considerably affects all bending operations of sheet metals. The bend radius in bending operations always pertains to the inside radius of the bend. Minimum bend radius is dependent on the material thickness and the mechanical properties of the material. Minimum bend radii vary for various metals; generally, most annealed metals can be bent to a radius equal to the thickness, T and sometimes to $T/2$, for a given bend angle and bend length.

Bend angle is another crucial factor in bending operations. As the bend angle becomes larger, especially with bend angles over 90°, many difficulties arise. In this case, the amount of bend radius become more critical and the material hardness becomes more detrimental to the success of the bending process.

In bending process, some deformations occur in the bent-up region of the workpiece depending on the dimensions of the workpiece, bend angle, and bend radius. As the strength of the workpiece is limited, the deformations should be restrained in some limits [61].

1.2. Springback Phenomenon

Springback is generally referred as to undesirable change of part shape that occurs upon removal of constraints after forming. It can be considered a dimensional change which happens during unloading, due to the occurrence of primarily elastic recovery of the part. [21]. In the other words, springback describes the change in shape of formed sheet upon removal from tooling [30].

Springback is one of the key factors to influence quality of stamped sheet metal parts in sheet metal manufacturing areas [17].

Springback is influenced by several factors, such as; [53]

- Sheet thickness
- Elastic modulus
- Yield stress
- Work hardening exponent
- Die and punch radii
- Punch stroke etc.

1.2.1. Mechanics and Terminology of Springback

Every plastic deformation is followed by elastic recovery. As a consequence of this phenomenon, changes occur in the dimensions of the plastic-deformed workpiece upon removing the load.

While a workpiece is loaded, it will have the following characteristic dimensions as a consequence of plastic deformation. (Figure 1.15)

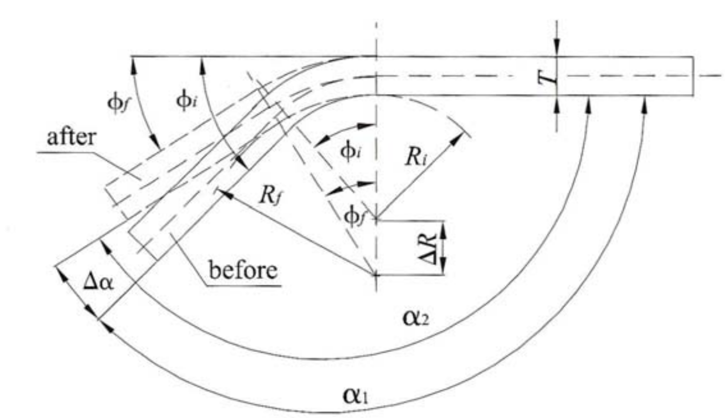

Figure 1.15 Schematic illustration of springback.

- Bend radius (R_i),
- Bend angle $(\phi_i = 180^\circ - \alpha_1)$, and
- Profile angle (α_1)

All workpiece materials have a finite modulus of elasticity, so each will undergo a certain elastic recovery upon loading. In bending, this recovery is known as a springback. The final dimensions of the workpiece after bending unloaded are:

- Bend Radius (R_f),
- Bend Angle (α_2), and
- Profile Angle $(\phi_f = 180^\circ - \alpha_2)$.

The final angle after springback is smaller $(\phi_f < \phi_i)$ and the final bend radius is larger $(R_f > R_i)$ than before.

There are two ways to understand and compensate for springback. One is to obtain or develop a predictive model of the amount of springback. The other way is to define a quantity to describe the amount of springback. A quantity characterizing springback is the springback factor (K), which is determined as follows:

The bend allowance of the neutral line (L_n) is the same before and after bending, so the following relationship is obtained by the formula:

$$L_n = \left(R_i + \frac{T}{2}\right)\phi_i = \left(R_f + \frac{T}{2}\right)\phi_f \qquad (1.17)$$

From this relationship, the springback factor is [4, 7]:

$$K = \frac{R_i + \frac{T}{2}}{R_f + \frac{T}{2}} = \frac{\frac{2R_i}{T} + 1}{\frac{2R_f}{T} + 1} = \frac{\phi_f}{\phi_i} = \frac{180^\circ - \alpha_2}{180^\circ - \alpha_1} \qquad (1.18)$$

The springback factor (K) depends on R/T. A springback factor of $K=1$ indicates no springback and $K=0$ indicates the complete elastic recovery. To estimate springback, an approximate formula has been developed in terms of the radii R_i and R_f as follows [2] ;

$$\frac{R_i}{R_f}=4\left(\frac{R_i(YS)}{ET}\right)^3-3\left(\frac{R_i(YS)}{ET}\right)+1 \qquad (1.19)$$

In case of plane strain bending, the following formula can be used [6]

$$\frac{R_i}{R_f}=4\left(\frac{R_i}{T}\frac{YS}{E}\left(1-\upsilon^2\right)\right)^3-3\left(\frac{R_i}{T}\frac{YS}{E}\right)\left(1-\upsilon^2\right)+1 \qquad (1.20)$$

In V-die bending, the part radius at the unloaded state, *R*, may be estimated by:

$$R_p=\frac{1}{\frac{1}{R}+3\frac{YS}{TE}} \qquad (1.21)$$

where, R_p is punch radius [61].

1.3. Heat Treatment

In this thesis, AA 2014 and AA 6061 are preferred as workpiece material. Different heat treatments are applied these alloys in order to observe springback amounts under different temper types and bend angles.

1.3.1. Heat Treatment of Aluminum Alloys

Heat treating is the broadest sense, refers to any of the heating and cooling operations that are performed for changing the mechanical properties, the metallurgical structure, or the residual stress state of the metal product. When the term is applied to aluminum alloys, however, its use frequently is restricted to the specific operations employed to increase strength and hardness of the precipitation-hardenable wrought and cast alloys. These usually are referred to as the "*heat-treatable*" alloys to distinguish them from those alloys in which no significant strengthening can be achieved by heating and cooling. The latter, generally referred to as "*not heat-treatable*" alloys depend primarily and cold work to increase strength. Heating to decrease strength and increase ductility (annealing) is used with alloys of both types; metallurgical reactions may vary with type alloy and with degree of softening desired [11].

Heat treatment to increase strength of aluminum alloys is a three-step process:

- Solution heat treatment: dissolution of soluble phases
- Quenching: development of supersaturation
- Age hardening: precipitation of solute atoms either at room temperature (natural aging) or at elevated temperature (artificial aging or precipitation heat treatment).

1.3.2. Temper Designations

Designations for the heat-treated tempers utilized in this study, and descriptions of the sequences of operations used to produce those tempers, are as bellows.

1.3.2.1. O, annealed

Applies to wrought products that are annealed to obtain lowest strength temper and to cast products that are annealed to improve ductility and dimensional stability. The O may be followed by a digit other than zero.

1.3.2.2. T4, Solution Heat Treated and Naturally Aged to a Substantially Stable Condition

This signifies products that are not cold worked after solution heat treatment and for which mechanical properties have been stabilized by room-temperature aging. If the products are flattened or straightened, the effects of the cold work imparted by flattening or straightening are not accounted for in specified property limits.

1.3.2.3. T6, Solution Heat Treated and Artificially Aged

This group encompasses products that are not cold worked after solution heat treatment and for which mechanical properties or dimensional stability, or both, have been substantially improved by precipitation heat treatment. If the products are flattened or straightened, the effects of the cold work imparted by flattening or straightening are not accounted for in specified property limits [9].

CHAPTER 2

LITERATURE SURVEY ON BENDING AND SPRINGBACK

2.1 Previous Studies

Since sheet metal forming industry has become one of the major manufacturing centers for automobile and aerospace and defense industries, the popularity of sheet metal products is attributable to their light weight, great interchangeability, good surface finish, and low cost [12].

There has been a growing interest during the past decade in using finite element method for springback prediction following forming of arbitrary shapes. While it is apparently simple in concept, the prediction of springback has proven challenging for a variety of reasons, including numerical sensitivity, physical sensitivity, and poorly characterized material behavior under reverse loading and unloading conditions [20]. Springback of sheet metal parts after forming causes deviation from the designed target shape and produces downstream quality problems as well as assembly difficulties. Its economic impact in terms of delayed production, tooling revision costs, and rejection of unqualified parts is estimated to exceed $50 million per year in the U.S. automotive industry alone [20]. It is obvious that controlling sprinback is a vital concern in manufacturing.

Several studies have been done for past decades in order to develop springback reduction and compensation methods. S. Nishino et al. examined a new method of predicting a shape fixation property by combining free bending test data with the results of the computer simulations conducted using the finite element method (FEM) [13]. In that study, they proposed a highly accurate evaluation technique of experimental data in free and bottoming bending tests with the FEM simulation data that are the elastic strain values in the bent sheet. In the study of Chou and Hung, [14] several springback reduction techniques used in the U-channel bending processes have been analyzed with finite element method, which include arc bottoming, pinching die, spanking, and movement techniques. Here, a commercial finite element program and optimization program for implicit problems were utilized. Results of the authors's research for optimization provide acceptable sets of design variables, which show that the use of coupled finite element optimization analysis is both practical and efficient in solving the problem of springback control. Karafillis and Boyce [15] developed a "Deformation Transfer Function (DTF)" for changing the shape of the tool to compensate for springback in sheet metal forming using FEM. Also, H. Palanisway et al. [16] studied to formulate an optimization problem to find the optimum blank dimensions that minimize the springback in the manufacturing of a cone shaped part while Sang-Wook Lee [17] worked on the bi-directional springback of a drawn sheet metal using modified U-draw bending process. In the latter study, they used a strip with the fixed width which is drawn by the elliptical tool and laid freely. Li-ping Lei et al. [12] developed an elasto-plastic finite element solution based on solid element and finite-strain plasticity for free bending and square cup drawing process of stainless steel. They used a solid element to consider bending stiffness and two-face contact instead of membrane elements in which is impossible with the use of membrane elements. They also investigated that springback rapidly decreased with a decrease in clearance.

Beyond these attempts, K.M. Zhao et al. [18] showed that bending process tends to a steady cycle upon applying repeated cycles of displacements. In this study, they applied different hardening laws with simplified non-contact finite element model and attained following results.

- The isotropic hardening law over-estimates the hardening component by missing the Bauschinger Effect and the plastic shakedown.

- The kinematic hardening rule under-estimates the hardening component and exaggerates the Bauschinger Effect and the plastic shakedown.

- The hardening parameters in the combined model are indentified inversely by using a micro-genetic algorithm.

Moreover, many studies were carried out for controlling and compensating springback. W.Gan et al. [19] claimed that reducing springback lies in designing tooling in such a way that to compensate for springback. They employed "displacement adjustment (DA) method" which is briefly referred as to move surface nodes defining the die surface in the direction opposite to the springback error.

Similarly, L. Wu [20] proposed tooling mesh generation technique for iterative FEM die surface design algorithm to compensate for springback in sheet metal stamping. Sheet metal parts, when removed from dies after forming, are subject to springback due to the resultant in-plane forces and moments throughout the sheet at the end of the forming processes. Negative of those forces and moments can be applied to the formed parts with FEM simulation such the part deform in a manner opposite to springback. The process is referred as spring-forward. Technique is simply as follows:

- Generating tool mesh based on computer aided drawing (CAD) file
- Running FEM simulation to form the part and evaluating forces and moments (f)

- Multiplying forces and moments with a scalar quantity such as -1 (α)

- Running FEM simulation with α relevant application to the formed part in step 2

- Generating tool mesh based on the deformed part shape
- Running simulation of forming followed by springback simulation.

Another springback compensation method is proposed by H.S. Cheng. et al. [21] The past studies related to this issue require few iteration steps before converting to the desired tooling shape. In this study, they additionally built upon existing methods, a new methodology is proposed by incorporating pure geometry correction with fundamental mechanic analysis. Consequently, the convergence becomes much faster and certain. Their innovation called "accelerated springback compensation method" is compared with other methods, namely "Deformation Transfer Function (DTF) method, "Force Descriptor Method (FDM) and DA method.

Numerical models are also employed when predicting springback in sheet metal forming processes. In this sense, R.H Wagoner et al. [22] proposed a numerical approach. They have evaluated numerical integration error and have investigated roles of tension force, number of iteration points, radius to thickness ratio, and material properties etc. to this variation. To obtain accurate numerical solutions, mechanical models implemented in simulation algorithms should use reliable descriptions of the materials' elastoplastic behavior, namely a description of the anisotropy and work-hardening behaviors. M.C. Oliveira et al. [23] have studied on the influence of work hardening modeling in springback prediction employing Numisheet'05 "Benchmark 3": the U-shape "Channel Draw". Another important numerically springback prediction study has been done by B.L. Fu et al. [24] They have first introduced the conceptions of forming springback anti-coupled systems and equations of bending beam with large deflection. T.B. Hilditch et al. [25] studied the influence of low-strain deformation behavior on curl and springback in High Speed Steels using under-tension test.

Today apart from CAD/CAM activities, engineering simulation tools based on the finite element method are employed regularly in the design of stamping dies for sheet metal parts in industry. With the increased use Finite Element Simulation in tooling departments, the forming analyses of sheet metal components are used more frequently in the design feasibility studies of production tooling. These computer based tools allow the design engineer to investigate the process and material parameters controlling the material floe over the die surfaces [26]. Several studies were done in past decade. M. Firat [26] studied U-Channel forming analysis to predict springback. He established a kinematic hardening model based on additive backstress form in order to improve the predicted sheet metal deformation response. [26] S.K. Panthi et al. [27] were also studied on a large deformation algorithm based on Total-Elastic-Incremental-Plastic Strain (TEIP) which was used for modeling a typical sheet metal bending process. The process involves large strain, rotation as well as springback. N.Narasimham et al. [28] aimed to introduce a coupled explicit-to-implicit finite element approach for predicting springback deformations in sheet metal stamping that can be utilized for minimizing die prototype design time. In this study, they have utilized the explicit method initially to analyze the contact based forming operation of stamping process. Then an implicit solution has been performed to simulate the springback developing in a blank after the forming pressure removed. They have coupled ANSYS/LS-DYNA explicit and ANSYS implicit codes to solve sheet metal forming processes that involves a high degree of springback.

One of the important studies of finite element analysis of springback in bending was done by V. Esat [29]. In the mentioned work, V. Esat et al. developed a finite element simulation in order to simulate springback by means of a springback factor using commercially available finite element program. They reached a good agreement between the finite element simulation and empirical data. A similar study was done by L. Papeleux et al. [30] They employed the U-draw bending presented in NUMISHEET'93 Conference. Their finite element model is based on 2-D shell elements and Chung-Hulbert dynamic implicit as time integration scheme. They used penalty method on analytically defined rigid bodies to handle contact algorithm. D.W.Park et al. [31] proposed a new shell element to improve accuracy and efficiency of springback simulation by describing complicated bending deformation accurately. They applied the new element both implicit Finite Element Method and explicit Finite Element Method to conduct springback simulation. They implied that the shell element described in this study has twice faster convergence rate than previous shell element in springback simulation. Kawka et al. [60] employed a static emplicit FEM code for the simulation of multi-step sheet metal forming process. S. Sriram et al. [32] developed a method for adding approximate bending stiffness to three-dimensional membrane and tested and applied to several forming operations. H. Livatyali et al. [33-34] presented a computer aided design method for springback in straight flanging process using finite element method and validated the predictions with some laboratory experiments. L.M. Kutt [35] et al. employed a non-linear finite element method to investigate the complicated, springback behavior of double curved, titanium, sheet metal parts that are formed with reconfigurable tooling [35].

Some of experimental and numerical studies were also done in order to analysis bending operation and springback phenomenon. Dongye Fei et al. [36] focused attention on springback behavior of cold rolled transformation induced plasticity steels in air v-bending process experimentally. They also simulated the process by implicit finite element method Abaqus/Standard using subroutine USDFLD. They attested that, for better accuracy in v- bending, the change in Young's modulus due to the plastic deformation should be taken into consideration. M.L. Garcia-Romeu et al. [37] et al. studied sprigback determination of sheet metals in an air bending process based on an experimental work. M. Zhan et al. [38] analyzed the springback mechanism and laws of tube bending by employing a numerical-analytic method proposed by authors. Another experimental study was done by O. Tekaslan [39]. They determined springback amount of steel sheet metal has 0.5 mm. thickness in V bending dies. Similarly, Z. Tekiner [40] studied springback behavior of steel in different bend angles by employing V bend die. Hsu and Shien [41] presented a computational method based on the bending theory for the analysis of axisymmetric sheet metal forming process. Authors investigated the effects of including bending in the modeling of sheet metal forming operations by using finite element method based on a shell theory incorporating finite membrane and bending strains. Their claim was the effect of bending depends on the ratio of the punch (or die) radius to the sheet thickness and it is more apparent in the plane strain condition than those in the axisymmetric condition. Also the experimental results which are in good agreement with the calculated results show FEM to be effective design of tooling in sheet metal forming operations. Similarly Müderrisoğlu et al. [42] proposed am improved design methodology for pre-hemming and hemming of auto body panels, which focuses on the effect of input parameters on final hem quality.

Many studies had been carried out on different perspectives of springback. Micari et al. [43] presented a springback prediction technique in three dimensional stamping processes which is based on a combined approach in which an explicit finite element code has been employed to simulate the forming phase while a traditional implicit procedure has been used to analyze the springback phase. Gau and Kinzel [44] performed an experimental study for determining the Bauschinger Effect on springback predictions which seems very significant in wipe bending operations.

Since springback is a vital concern in manufacturing industry, beyond evaluating and simulating attempts of springback, some researchers studied the parameters that effect springback in sheet metal forming operations in order to control these disturbing parameters. X. Li et al. [45] conducted an experiment and analytical calculation for determining effect of material hardening mode on the springback simulation accuracy of V-free bending. Authors considered the change in material's Young's Modulus with plastic deformation and successfully investigated that material-hardening mode directly affects the springback simulation accuracy. L. Antonelli et al. [46] deduced a new identification method of elasto-plastic characteristics by means of simple testing. The outcome of their procedure is the true stress versus true strain curve. C. Bruni et al. [47] studied on the effects of process parameters on springback of AZ31 magnesium alloy by performing air bending test under warm and hot forming conditions. To this purpose, they carried out air bending experiments in the temperature range varying 100 to 400$^\circ C$ with different values of punch speed. The results showed that the springback ratio is influenced by punch radius and temperature. K.C Chan et al. [48] focused grain shape dependence of springback of integrated circuit (IC) leadframes. In this study the authors mentioned that grain shape, which is the source of plastic anisotropy, has significant effects on springback of a cold rolled copper alloy as integrated circuit leadframe.

W. C. Carden et al. [49] studied for measuring springback by generating constituve equations emphasizing low-strain behavior for automobile body alloys. In the study of C. Jiang et al. [50] an uncertain optimization method is suggested to obtain the optimal variable binder force in U-shaped forming. The friction coefficient is regarded as the uncertain coefficient, and stepped variable binder force model is used. The finite element method is employed to simulate the forming process, and an uncertain objective function which represents the springback magnitude is created. Zhong Hu [51] studied to establish an elasto-plastic model for the calculation of springback angle. In another study of S.W. Lee et al. [52], authors presented an assessment of numerical parameters influencing springback in explicit finite element analysis of sheet metal forming process. The numerical parameters were, contact damping parameter (CDP), penalty parameter (PP), blank element size (BES) and Number of corner elements (NCE). To clarify effect of each factor, the U-draw bending process is chosen as an evaluation problem because of its large springback. Y.H. Moon et al. [53] successfully analyzed the effect of tool temperature on the reduction of the springback of aluminum sheets. Author's research showed that, the combination of hot die and cold punch can reduce the amount of springback up to %20 when compared to conventional room temperature bending test. Similarly H.S. Kim et al. [54] investigated the effect of temperature gradient on the final part quality (i.e, springback) in warm forming of lightweight materials. Thermo-mechanically coupled finite element analysis (FEA) models encompassing the heating of the sheet blanks and tooling, forming, part ejection, and cooling were developed for simple channel drawing process. M.V. Inamdar et al. [55] studied on effects of geometric parameters on springback by dealing with yield strength, Young's modulus, and strain hardening exponent as material properties, punch nose radius, die radius and the sheet thickness as geometric properties. Significance of these factors and their interactions is thus established and the physical interpretation of the results has been given. Lumin Geng et al. [56] discussed the role of plastic anisotropy and its evolution on sprinback by employing a new anisotropic hardening model. The new anisotropic hardening model extends existing kinematic/isotropic and nonlinear kinematic formulations. This hardening model was implemented in ABAQUS in conjunction with four yield functions: Von Misses, Hill Quadratic, Barlat three-parameter and Barlat 1996. In the work of S.A. Asgari et al. [57], the authors focused on development of a method to statistically study forming and springback problems of Transformation Induced Plasticity (TRIP) through an industrial case study. A Design of Experiments (DOE) approach was used to study the sensitivity of predictions to four user input parameters in implicit and explicit sheet metal forming codes. Numerical results were compared to experimental measurements of parts stamped in an industrial production line. J.A. Canteli, et al. [58] presented a theoretical study of air bending at high temperature. Authors developed a thermo-mechanical model able to predict temperature distribution and main bending parameters. Temperature distribution is calculated taking into account heating parameters of the designed heating device for experimental validation. T. Meinders et al. [59] conducted developments in different stages of product design namely, springback prediction, springback compensation and optimization by Finite Element (FE) analysis. Finally the authors present an optimization scheme which is capable of designing optimal and robust metal forming process efficiently.

2.2 Scope of the Thesis

Terminology in bending and springback, theoretical background of bending operation, types of bending, necessary formulations to evaluate bending parameters and springback, heat treatment concept and temper designations and other related information are discussed in Chapter 1. Finite element modeling of the processes discussed in this thesis will be covered in Chapter 3.

In this thesis it is aimed to simulate and analyze V-bending operation in order to observe effect of heat treatment on elastic recovery and springback. Different materials as at different thicknesses are analyzed under 60°, 90°, and 120° bend angles. The effort to try to cover bending operations and springback and heat treatment in a single study is one of the goals of this thesis, which distinguishes the work from previous ones. The results will investigate the compansation of springback in bending dies using appropriate type of heat treatment.

Chapter 4 and chapter 5 will include the case studies, which will contain the analyses of the mentioned bending operations and heat treatment. Results such as springback amounts and stress distrubitions of each material at each temper type will be submitted and the agreement of the calculated results with th emprical data will be investigated.

CHAPTER 3

FINITE ELEMENT MODELING OF V-BENDING

3.1. Introduction

In this thesis, finite element analyses of the bending operations are carried out by using commercially available software, MSC.MARC/MENTAT. The software has also used for pre-processing of the input data and post-processing of the results.

3.2. Kinematics of Deformation

In modeling the forming problems, the kinematics of deformation can be described by following approaches:

- Lagrangian Formulation
- Eularian Formulation
- Arbitrary Eularian-Lagrangian (AEL) Formulation

In this study, Lagrangian Formulation has been employed where the finite element mesh is attached to the material and moves through space along with material and in this case, there is no difficulty in establishing stress or strain histories at a particular material point and the treatment of free surfaces is natural and straightforward.

The Lagrangian approach can be classified into two categories: *the Total Lagrangian Method* and *the Updated Lagrangian Method*. In the total Lagrangian approach, the equilibrium is expressed with the original undeformed state as the reference; in the updated Lagrangian approach, the current configuration acts as the reference state. In this study, the updated Lagrangian procedure has been used, which is employed in large strain and large displacement analyses. Generally, Updated Lagrangian Approach is useful in;

- Analysis of shell and beam structures in which rotations are large so that the nonlinear terms in the curvature expressions may no longer be neglected, and
- Large strain plasticity analysis, for calculations which the plastic deformations cannot be assumed to be infinitesimal.

The equilibrium can be expressed by the principle of virtual work as :

$$\int_{V_0} S_{ij} \delta E_{ij} dV = \int_{V_0} b_i^0 \delta \eta_i dV + \int_{A_0} t_i^0 \delta \eta_i dA \qquad (3.1)$$

where;

S_{ij} : second Piola-Kirchoff stress tensor

E_{ij} : Green-Lagrange strain tensor

b_i^0 : body force in the reference configuration

t_i^0 : traction vector in the reference configuration

η_i : virtual displacements

Direct linearization of the left-hand side Equation 3.1 yields:

$$\int S_{ij}\left(d\left(\delta E_{ij}\right)\right)dV = \int_{V_{n+1}} \nabla\eta_{ik}\sigma_{kj}\nabla\Delta u_{ij}dv \tag{3.2}$$

where Δu and η are actual incremental and virtual displacements respectively, and σ_{kj} Cauchy stress tensor. It can be shown that:

$$\sigma_{ij} = \frac{1}{J}F_{im}S_{mn}F_{jn}$$

$$\delta E_{ij} = F_{mi}\nabla^{S}\eta_{mn}F_{nj} \tag{3.3}$$

$$L_{ijkl} = \frac{1}{J}F_{im}F_{jn}F_{kp}F_{lq}D_{mnpq}$$

where D_{mnpq} represents the material moduli tensor in the reference configuration which is convected to the current configuration, L_{ijkl}. Then:

$$\int_{V_0} dS_{ij}\left(\delta E_{ij}\right)dV = \int_{V_{n+1}} \nabla^{S}\eta_{ij}L_{ijkl}\nabla^{S}\left(\Delta u_{kl}\right)dv \tag{3.4}$$

In the expression above, ∇^{S} denotes the symmetric part of ∇, which represents the gradient operator in the current configuration.

Keeping in view that the reference state is the current state; a rate formulation can be obtained as:

$$\int_{V_{n+1}} \left[\sigma_{ij}{}^{\nabla} \delta d_{ij} + \sigma_{ij} \frac{\partial v_k}{\partial x_i} \frac{\partial \delta \eta_k}{\partial x_j} \right] dv = \int_{V_{n+1}} b_i \delta \eta_i dv + \int_{A_{n+1}} t_i \delta \eta_i da \tag{3.5}$$

Finally,

$$\{K_1 + K_2\} \delta u = F - R \tag{3.6}$$

where K_1 is the material stiffness matrix and K_2 is the geometric stiffness matrix [62].

3.3. Linearity and Non-Linearity Concepts

3.3.1. Linear Analysis

Linear analysis is performed on elastic structures with linear stress-strain relation. The principle of superposition holds under conditions of linearity. Therefore, several individual solutions can be superimposed (summed) to obtain a total solution to a problem.

Linear analysis does not require storing as many quantities as does nonlinear analysis; therefore, it uses the core memory more sparingly [62].

3.3.2. Non-Linear Analysis

There are three main sources of nonlinearity:

- Material non-linearity
- Geometric linearity
- Non-linear boundary conditions.

Material non-linearity results from the non-linear relationship between stresses and strains. There exist various models, which define non-linear material behavior. Elasto-plastic, elasto-viscoplastic, and creep nonlinear behaviors are some examples for material non-linearity.

Geometric nonlinearity results from the nonlinear relationship between strains and displacements as well as the nonlinear relation between stresses and forces. Two main types of geometric nonlinearity problems are buckling problems and large displacement problems.

Boundary conditions and/or loads may also cause nonlinearity. Contact and friction problems lead to nonlinear boundary conditions. This type of nonlinearity manifests itself in several real life situations; for example, metal forming, gears, interference of mechanical components, pneumatic tire contact, and crash [62].

In this work, the three types of non-linearity are taken into consideration in all of case studies.

3.4. Pre- Processing

3.4.1. Mesh Generation

Since plate bending can be considered as plane stain situation, all case studies are modeled as planar to simplify the finite element analysis. At the end of the analyses, the results are expanded through the width direction to obtain whole geometry.

Four node quadrilateral elements are preferred since this element is written by the software for plane strain applications. As this element uses bilinear interpolation functions, the strains tend to be constant throughout the element. The stiffness of this element is formed using four-point Gaussian integration [61]. The Gaussian integration points in the element are illustrated in Figure 3.1.

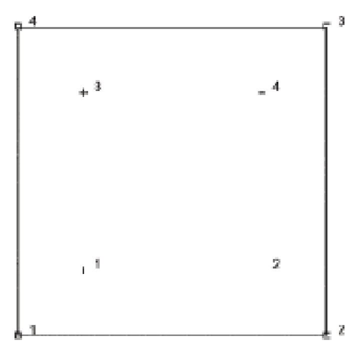

Figure 3.1 Gaussian integration points in the element type 11

Complete geometry and meshed model of V-bending are illustrated in Figure 3.2 and Figure 3.3.

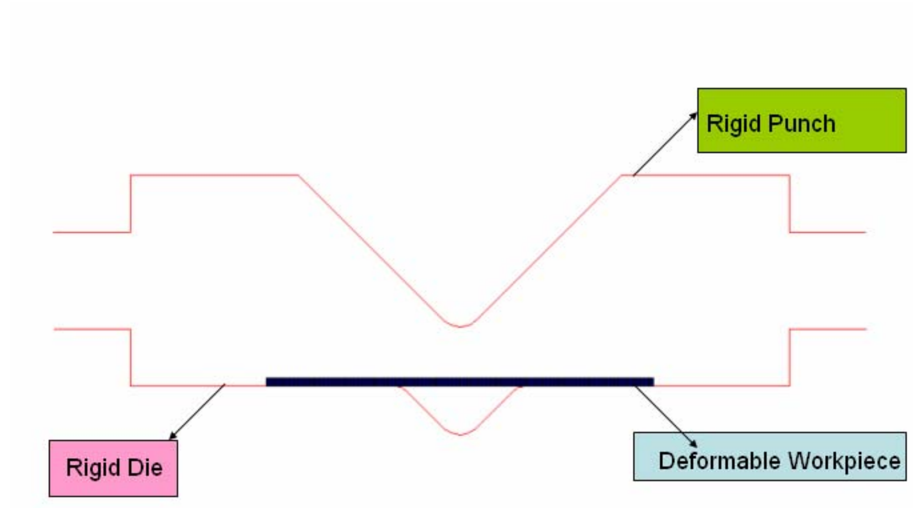

Figure 3.2 Complete geometry of V-bending

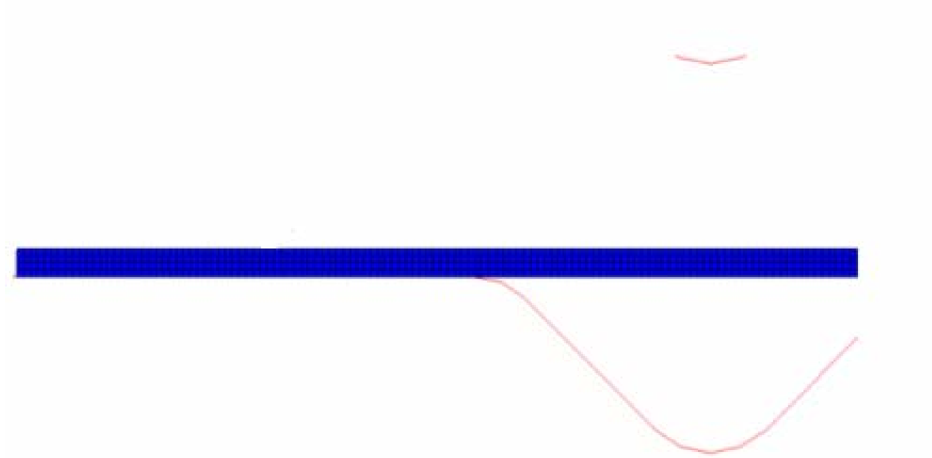

Figure 3.3 Meshed model of sheet metal

3.4.2. Boundary Conditions

As the boundary conditions displacement of the mid-nodes in the x direction is restricted in order to satisfy symmetry (Figure 3.4).

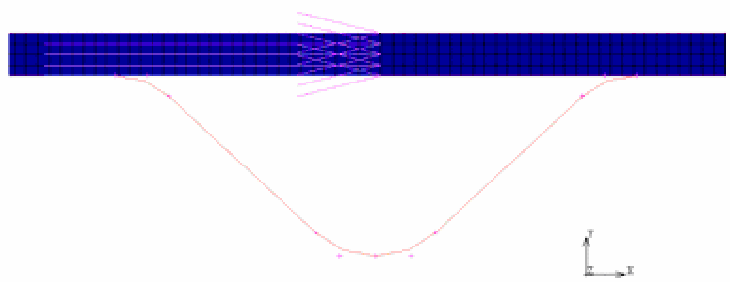

Figure 3.4 Symmetrical boundary condition for sheet metal.

3.4.3. Material Properties

In the software used, the stress-strain curve can be represented by;

- Bilinear representation – constant workhardening slope
- Elastic perfectly-plastic material – no workhardening
- Perfectly-plastic material – no workhardening and no elastic response
- Piecewise linear representation – multiple constant workhardening slopes
- Strain-softening material – negative workhardening slope

Young’s modulus, E, Poisson’s ratio, v, and mass density, ρ, are supplied to the software in order to define material. Piecewise linear representation of the work hardening curve is also employed to define stress-strain relation for plastic deformation. The required data are obtained by tension tests.

In this study, two types of material and three types of temper from each material are considered and modeled as isotropic elastic-plastic materials. The *von Mises* yield criterion is preferred for the isotropic materials used.

The *von Mises* criterion is the most widely used one because of its success due to the continuous nature of the function that defines this criterion and its agreement with the observed behavior for the commonly confronted ductile materials. [61]. The *von Mises* criterion states yielding occurs when the effective (or equivalent) stress ($\overline{\sigma}$) equals the yield stress (σ_y) as measured in a uniaxial test. The von Mises yield criterion for any stress condition is [3]:

$$(\sigma_{xx} - \sigma_{yy})^2 + (\sigma_{yy} - \sigma_{zz})^2 + (\sigma_{zz} - \sigma_{xx})^2 + 6(\tau_{xy}^2 + \tau_{yz}{}^2 + \tau_{zx}{}^2) = 2\sigma^2 \qquad (3.7)$$

where σ ’s and τ ’s are normal and shear stresses, respectively, or

$$(\sigma_1 - \sigma_2)^2 + (\sigma_2 - \sigma_3)^2 + (\sigma_3 - \sigma_1)^2 = 2\sigma^2 \qquad (3.8)$$

in terms of principal stresses σ_1, σ_2, and σ_3.

3.4.4. Contact Analysis

In this study, punch and bottom die are modeled as rigid bodies. *The Penalty Function Method* is the procedure to numerically implement the contact constraints.

Motion of the punch is introduced as prescribed velocities with respect to time, which is entered into definition of FEA problem by employing relevant tables.

3.4.4.1. Friction

Friction is a complex physical phenomenon that involves the characteristics of the surface such as surface roughness, temperature, normal stress, and relative velocity. Friction between a workpiece and tools or dies dominates the strain patterns and performance of many forming operations, and yet is often the least quantified of all phenomena involved in forming [62].

Coulomb Friction Model is the most widely used friction model. Because of this usefulness, *Coulomb Friction Model* is employed upon this study. The Coulomb model can be characterized by:

$$\|\sigma_t\| < \mu\sigma_n \quad (stick) \quad \text{and } \sigma_t = -\mu\sigma_n \cdot t \quad (slip) \tag{3.9}$$

where:

σ_t : Tangential (friction) stress

σ_n : Normal stress

μ **:** Friction coefficient

t **:** Tangential unit vector in the direction of the relative velocity

The Coulomb model can also be written in terms of nodal forces instead of stresses:

$$\|f_t\| < \mu \cdot f_n \quad (stick) \quad \text{and} \quad f_t = -\mu \cdot f_n \cdot t \quad (slip) \tag{3.10}$$

where

f_t : Tangential force

f_n : Normal reaction force [64].

3.5. Analysis

3.5.1. Loadcase

Two types of analyses are carried out in this study. First, by the movement of punch, deformation of the sheet material is analyzed and then releasing the load residual stresses are determined.

3.5.2. Solution Procedure

Nonlinear analysis requires incremental solution schemes and iterations within each load/time increment to ensure that equilibrium is satisfied at the end of each step.

A nonlinear problem does not always have a unique solution. Sometimes a nonlinear problem does not have any solution, although the problem can seem to be defined correctly [62].

In this thesis; *Full Newton-Raphson Algorithm* is preferred. The full Newton-Raphson method provides good results for most nonlinear problems which is also suggested by software in large displacement problems such as bending [62].

3.5.3. Convergence Testing

The convergence criterion, used in this thesis is based on the magnitude of the maximum residual load compared to the maximum reaction force. This method is appropriate since the residuals measure the out-of-equilibrium force, which should be minimized. This technique is also appropriate for Newton methods, where zero-load iterations reduce the residual load. The method has the additional benefit that convergence can be satisfied without iteration.

Finally, total loadcase time and the number of time increments, during which the analysis is carried out, are determined.

CHAPTER 4

FINITE ELEMENT ANALYSIS OF V-DIE BENDING OPERATIONS

4.1 Introduction

In this chapter, V-bending operation of AA 2014 and AA 6061 material at O, T4 and T6 heat treatment conditions have been analyzed by FEM. For this purpose, 1.0 mm, 1.6 mm, 2 mm, 2.5 mm and 3 mm thickness sheets have been bent to 60°, 90° and 120°. Several results such as springback amounts, maximum von Mises streses, stress distributions, plastic strains and punch loads are presented.

The sheet to be bent-up is analyzed by using four node quadratic plane strain elements. Friction between sheet, punch and die has been utilized by Coulomb's law, where the friction coefficient is taken as 0.1 [62]. The input data are the material properties, boundary conditions, time vs. velocity tables to define motion of the punch, stress vs. plastic strain tables to define the strain hardening characteristics of the materials, and definition of the contact model and the loadcases. The aluminum sheets used in this work are assumed to be free of residual stresses before the loading action.

Finite element model used in springback simulations is composed of a rigid punch and die and a deformable sheet metal. For all cases, rigid punch moves down 25 mm to bend the workpiece. The gap between die and punch, at the end of fully bending step, remains as the original thickness of the material and punch does not squeeze to the sheet further (Figure 4.1).

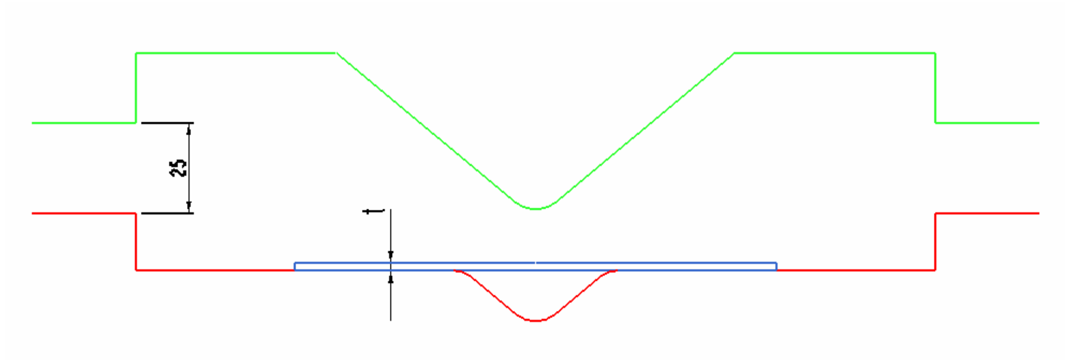

(a)

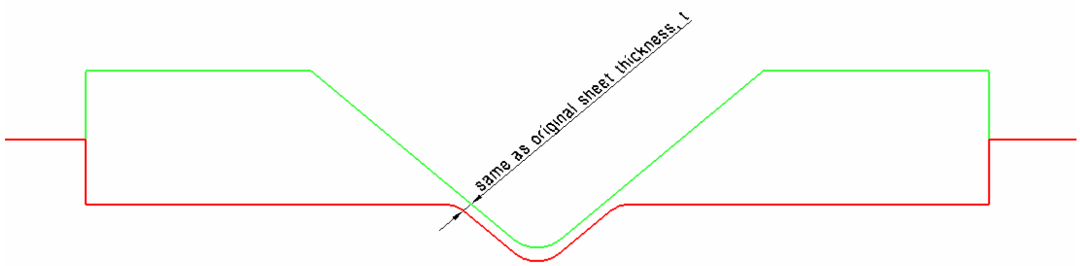

(b)

Figure 4.1 Schematic view of the V-bending process; (a) at beginning of the process, (b) at 25 mm indentation f the punch tip

Necessary dimensions needed to model the processes are illustrated in Figure 4.2, Figure 4.3 and Figure 4.4

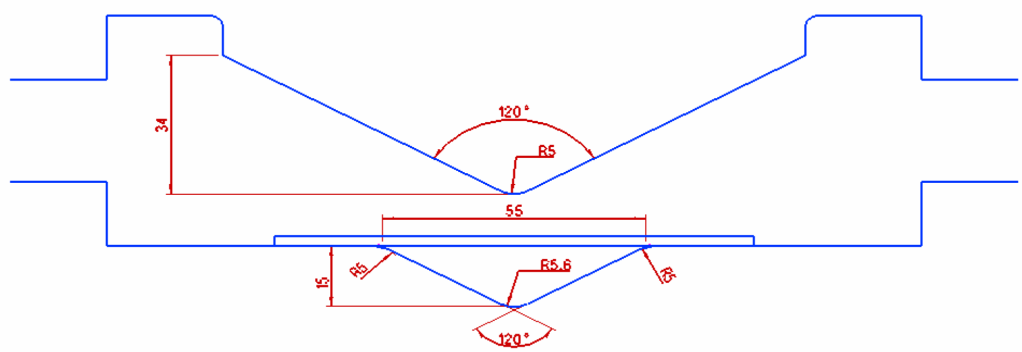

Figure 4.2 Schematic view of 60° V-bending with necessary dimensions

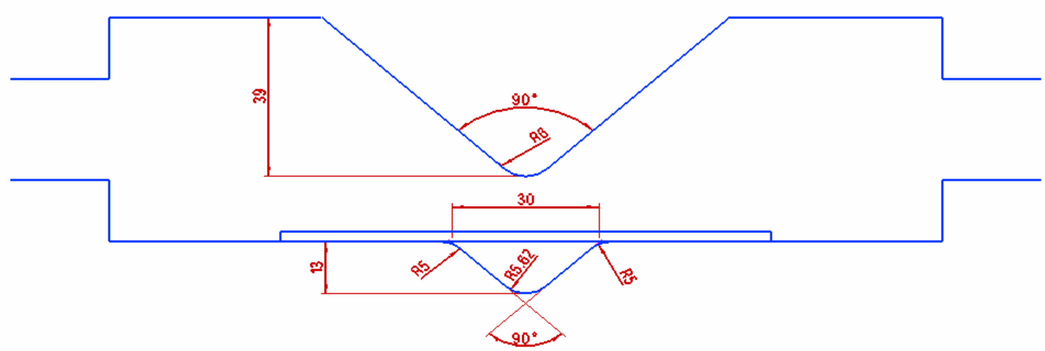

Figure 4.3 Schematic view of 90° V-bending with necessary dimensions

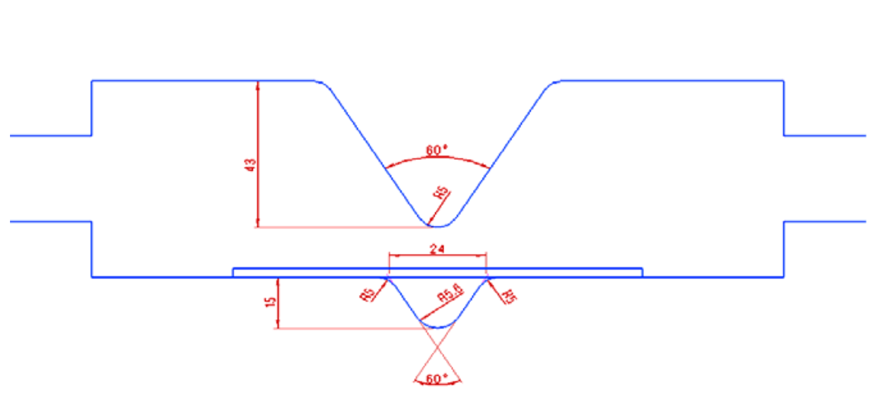

Figure 4.4 Schematic view of 120° V-bending with necessary dimensions

4.1.1 Mesh Size Effect

In all case studies, number of elements along the thickness of the sheet metal is selected as 4. In Figure 4.5 the number of element along the thickness is 4 and total number of elements is 800.

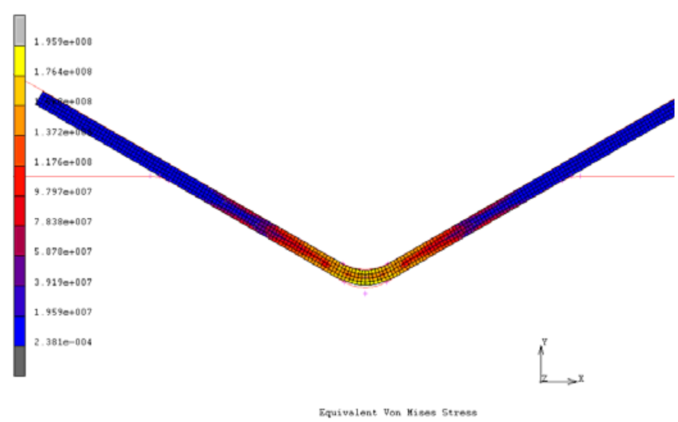

Figure 4.5 Equivalent von Mises stress distribution of AA 2014 O for 60° V bending using 4 elements along the thickness of the sheet metal

On the other hand, to analyze the effect of mesh size for 60° V-bending of AA 2014 O case, the number of the elements along the thickness of the element is taken as 8 and total number of elements becomes 3200 (Figure 4.6).

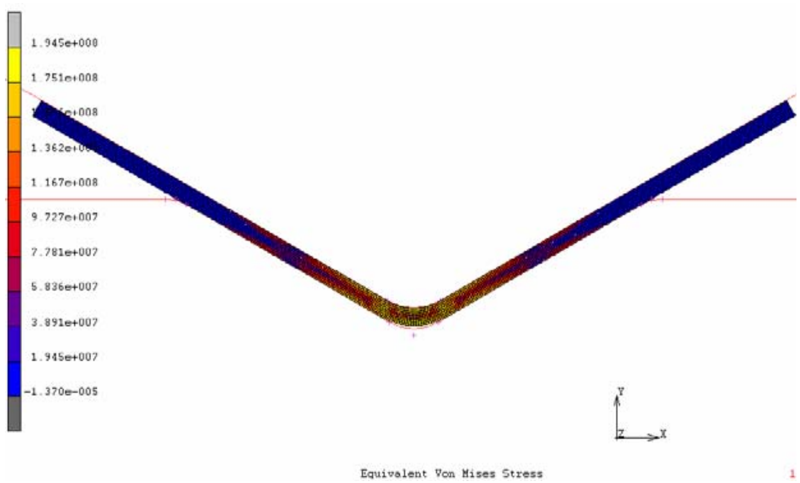

Figure 4.6 Equivalent von Mises stress distribution of AA 2014 O for 60˚ V bending using 8 elements along the thickness of the sheet metal

As seen from the Figure 4.5 and Figure 4.6 and when 8 elements are used along the thickness of the sheet metal, maximum equivalent von Mises stress is evaluated as 194.5 MPa where it is 195.9 MPa when 4 elements used along the thickness. It has been observed that the changes in the maximum von Mises stresses and stress distribution are negligible and number of elements along the thickness is preferred as 4 in order to reduce solution time.

4.1.2 Contact Regions

Stress distributions at the contact regions between sheet and die and punch have also been analyzed to compare the maximum stress values. Contact regions are illustrated in Figure 4.7.

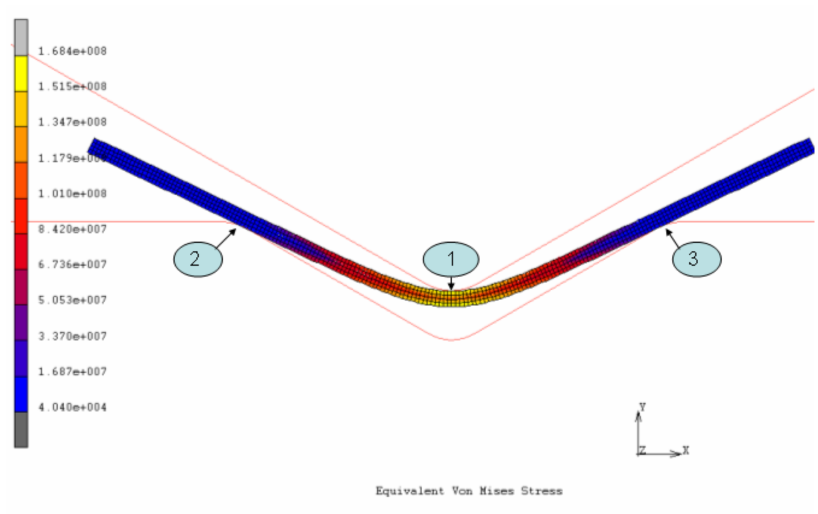

Figure 4.7 Contact Regions of the sheet metal at the 10 mm indentation of the punch tip.

The stress distributions along the thickness direction at region 1 is given in Figure 4.8, and stress distributions along the thickness direction at region 2 and 3 is given in Figure 4.9.

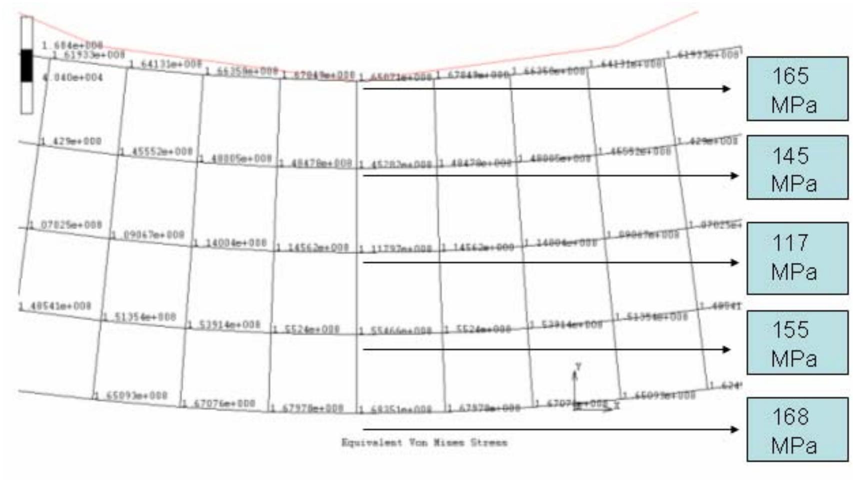

Figure 4.8 Stress distributions at the nodes which are in contact with the rigid punch at 10 mm indentation of the punch tip. (at point 1)

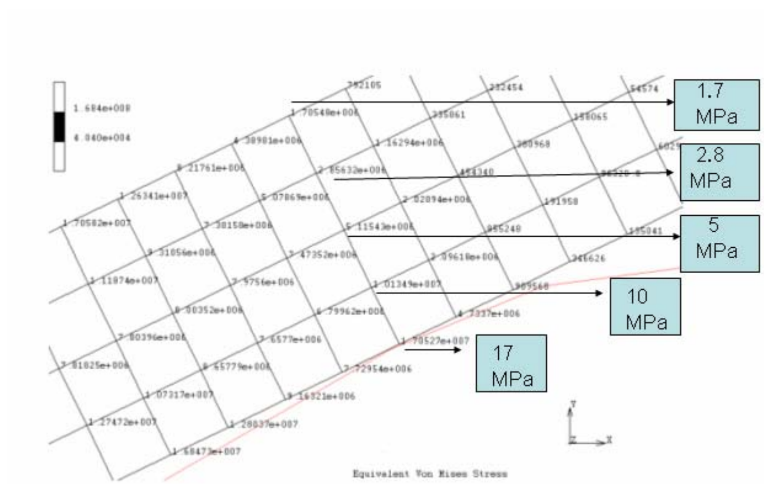

Figure 4.9 Stress distributions at the nodes which are in contact with the rigid die. (at point 3 and 2)

It is observed that stress is maximum at the contact surface whereas decreases towards the free region. However the stresses at region 1 are much higher than region 2 and 3 since the bending is localized in this region.

4.2. Finite Element Analyses

4.2.1. V-bending of AA 2014 at O condition.

In this study, five different thicknesses of AA 2014-O are bent to 60°, 90° and 120° with a punch moving vertically downwards. The alloy AA 2014-O is mainly composed of Al and Cu. Mechanical properties of the alloy are given in Table 4.1

Table 4.1 Mechanical properties of AA 2104-O

Material	Temper	Elasticity Modulus (GPa)	Yield Strength (MPa)	Poisson's Ratio
AA 2014	O	72.4	68.9	0.33

Aluminum sheets with a length of 100 mm, a width of 50 mm and thicknesses of 1.0, 1.6, 2.0, 2.5 and 3.0 mm were analyzed.

In this case study, angles after springback are determined and tabulated and graphically illustrated in Table 4.2, Table 4.3, Table 4.4, and Figure 4.16 respectively. Total equivalent plastic strains and equivalent Von Misses stresses, at different bend angles, occurring in the sheets are gathered from the finite elements analyses are illustrated graphically in Figure 4.17, Figure 4.18, Figure 4.19, Figure 4.20, Figure 4.21 and Figure 4.22. Also, punch loads for each case are also represented in Figure 4.23, Figure 4.24 and Figure 4.25.

Table 4.2 Springback results in terms of part angle for V-Bending to 60°

AA 2014 O at 60° V - Bending			
Thickness (mm)	bend angles (°)	part angle (°)	Springback (°)
1.0	60	58.89	1.13
1.6	60	59.17	0.83
2.0	60	59.44	0.56
2.5	60	59.69	0.31
3.0	60	59.90	0.19

Table 4.3 Springback results in terms of part angle for V-Bending to 90°

AA 2014 O at 90° V - Bending			
Thickness (mm)	bend angles (°)	part angle (°)	Springback (°)
1.0	90	87.85	2.15
1.6	90	88.20	1.80
2.0	90	88.65	1.35
2.5	90	88.97	1.03
3.0	90	89.48	0.78

Table 4.4 Springback results in terms of part angle for V-Bending to 120°

AA 2014 O at 120° V - Bending			
Thickness (mm)	bend angles (°)	part angle (°)	Springback (°)
1.0	120	115.78	4.22
1.6	120	116.24	3.76
2.0	120	116.59	3.41
2.5	120	116.86	3.14
3.0	120	117.25	2.75

In Figure 4.10 and Figure 4.11**,** von misses stresses and total plastic strains in AA 2014-O 2 mm thick sheet in 60˚ V- bending are illustrated respectively.

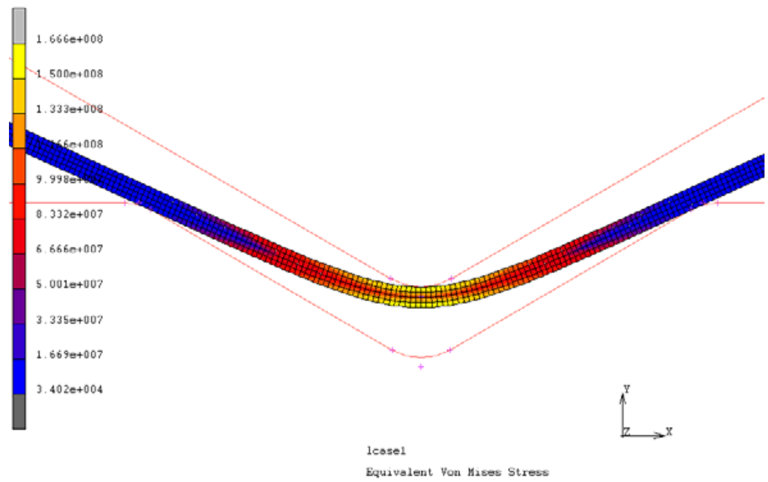

(a)

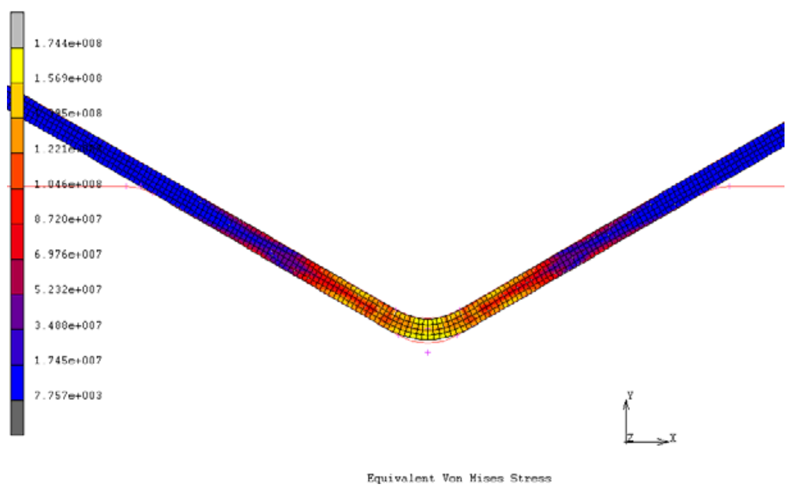

(b)

Figure 4.10 Von Misses stress distribution for AA 2014-O 2 mm-thick sheet , 60˚ V-bending at ; (a) the intermediate stage (b) the fully loaded stage

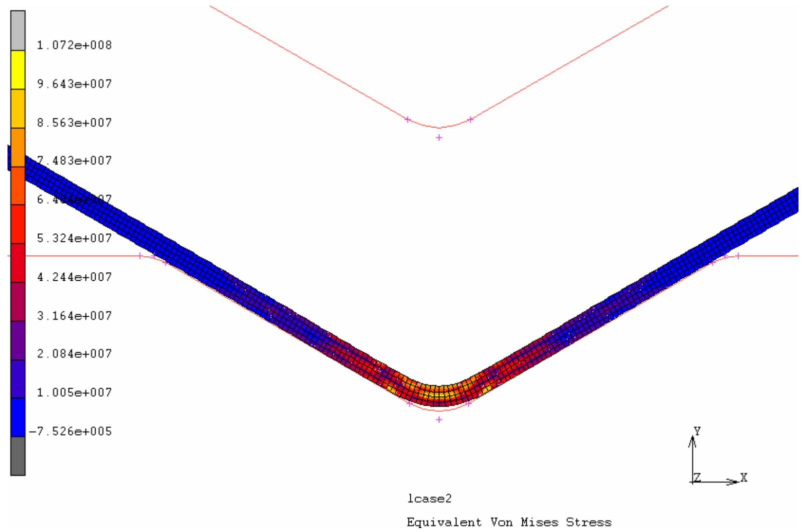

(c)

Figure 4. 10 (cont'd) Von Misses stress distribution for AA 2014-O 2 mm-thick sheet 60˚ V- bending at ; (c) the unloaded stage

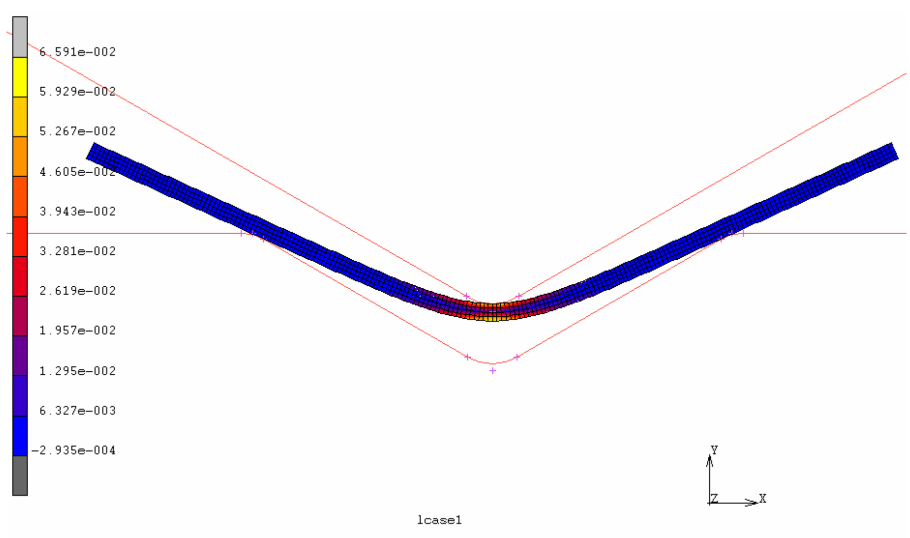

(a)

Figure 4.11 Total-equivalent plastic strain distribution for AA 2014-O 2 mm-thick sheet in 60˚ V- bending at ; (a) the intermediate stage

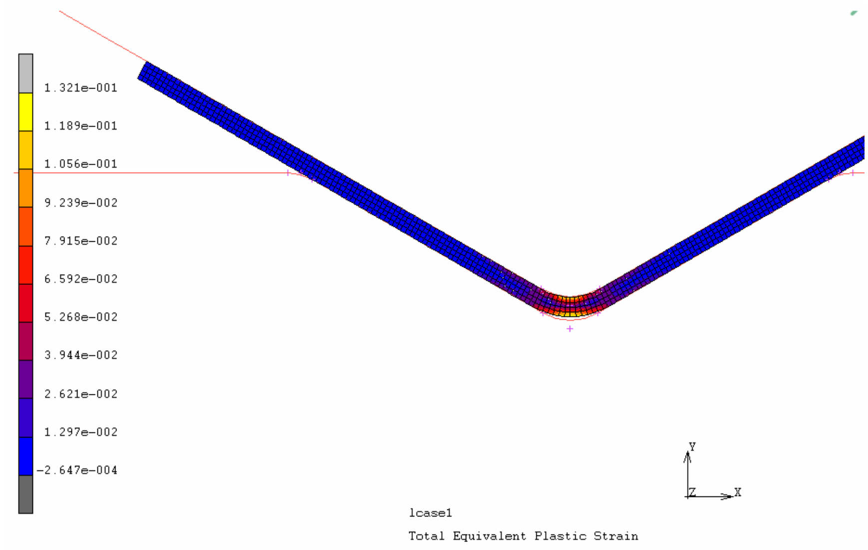

(b)

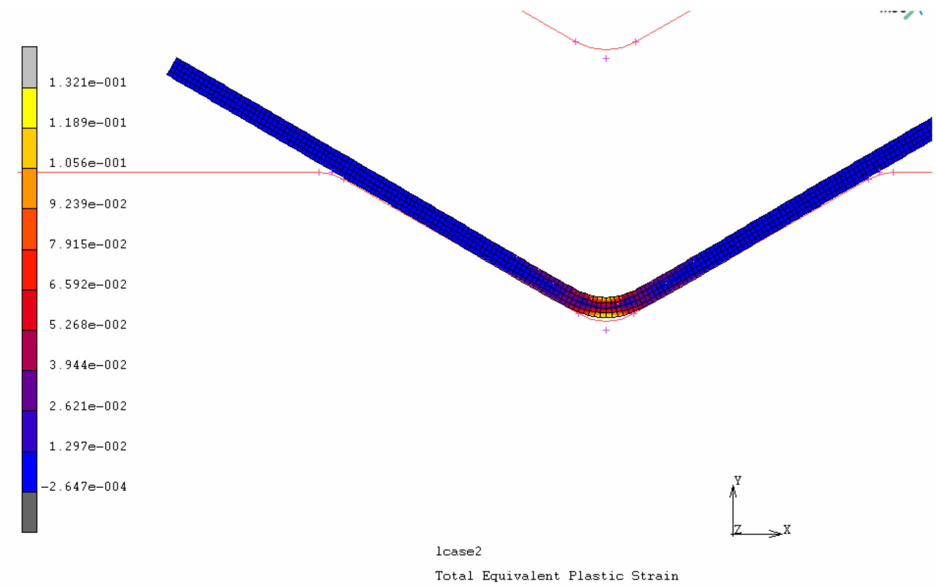

(c)

Figure 4.11 (cont'd) Total-equivalent plastic strain distribution for AA 2014-O 2 mm-thick sheet in 60˚ V- bending at ; (b) the fully loaded stage, (c) the unloaded stage

In Figure 4.12 and Figure 4.13, Von Misses Stresses and Total Plastic Strains in AA 2014-O 2 mm thick sheet in 90˚ V- bending are illustrated respectively.

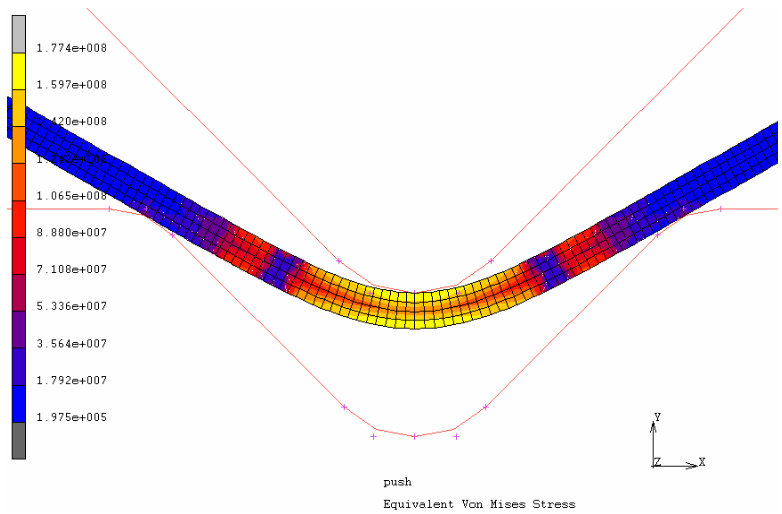

(a)

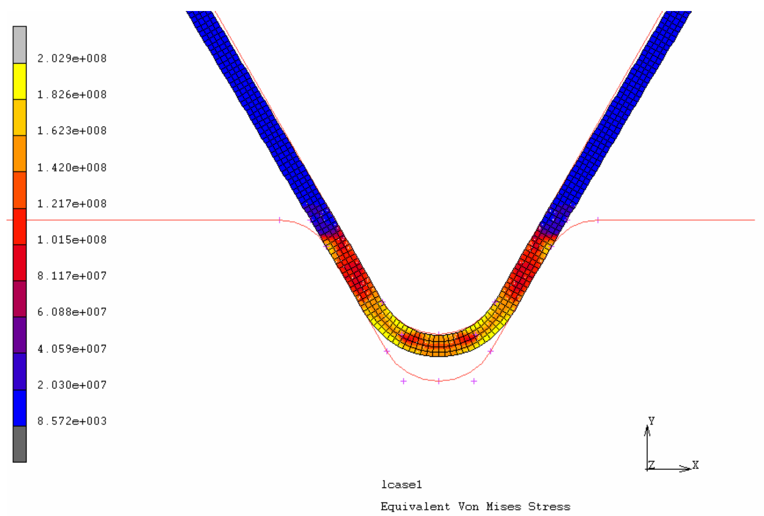

(b)

Figure 4.12 Von Misses stress distribution for AA 2014-O 2 mm-thick sheet in 90˚ V- bending at; (a) the intermediate stage (b) the fully loaded stage

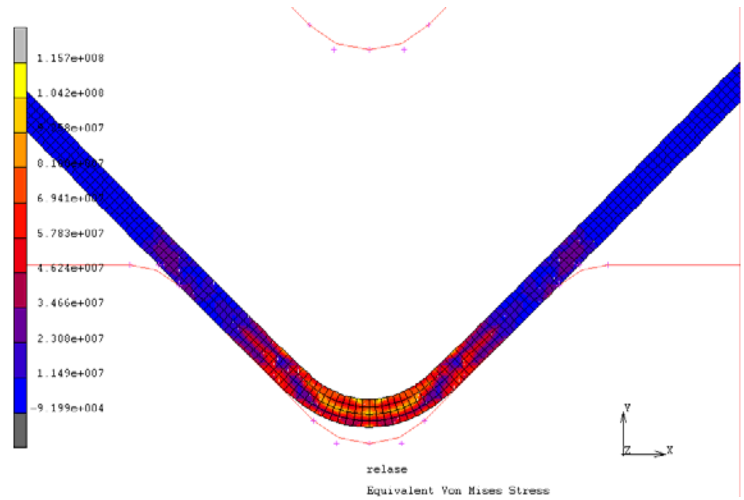

(c)

Figure 4.12 (cont'd)Von Misses stress distribution for AA 2014-O 2 mm-thick sheet in 90˚ V- bending at; (c) the unloaded stage

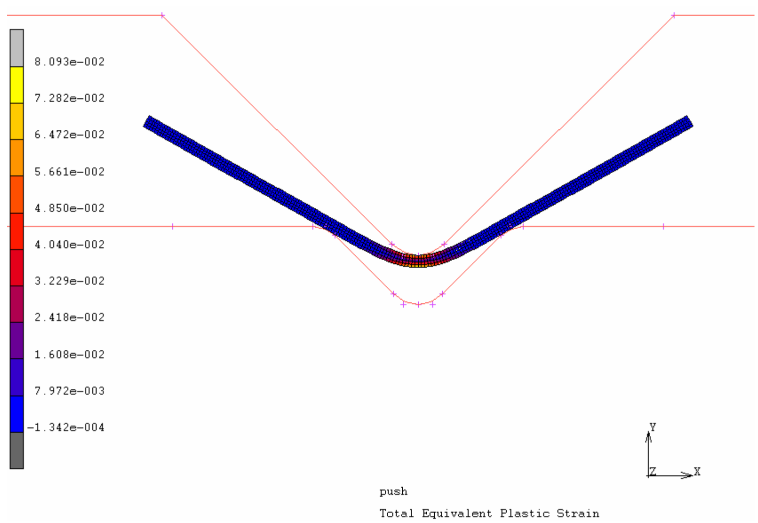

(a)

Figure 4.13 Total-equivalent plastic strain distribution for AA 2014-O 2 mm-thick sheet in 90˚ V- bending at; (a) the intermediate stage

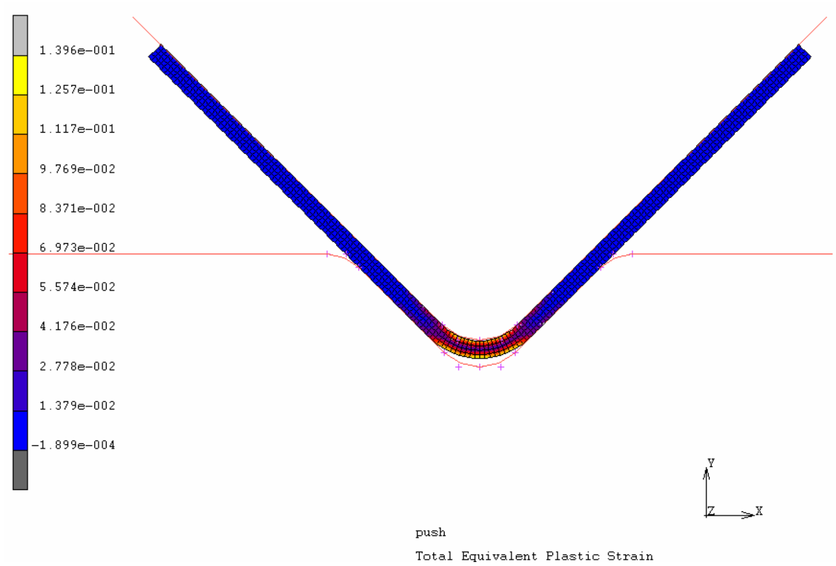

(b)

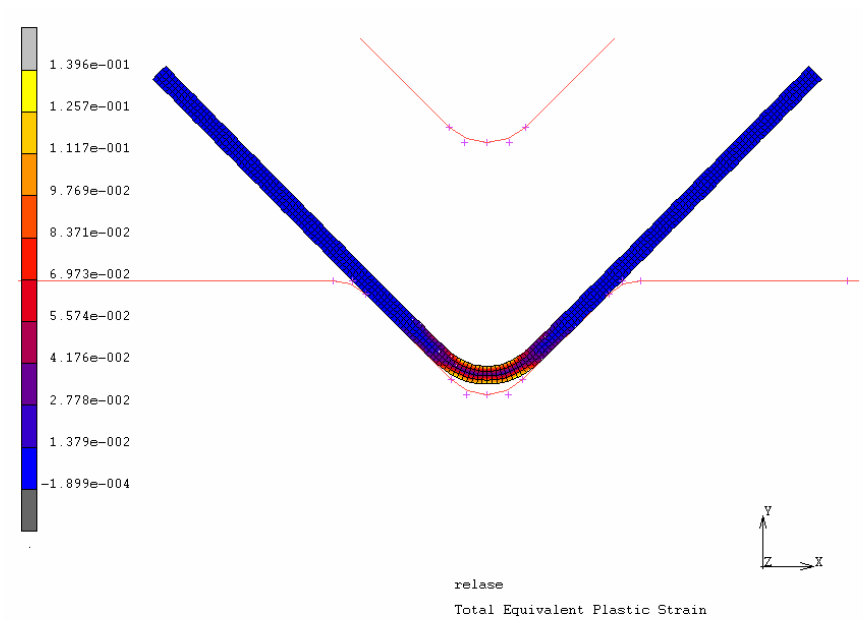

(c)

Figure 4.13 (cont'd) Total-equivalent plastic strain distribution for AA 2014-O 2 mm-thick sheet in 90˚ V- bending at; (b) the fully loaded stage, (c) the unloaded stage

In Figure 4.14 and Figure 4.15, Von Misses Stresses and Total Plastic Strains in AA 2014-O 2 mm thick sheet in 120˚ V- bending are illustrated respectively.

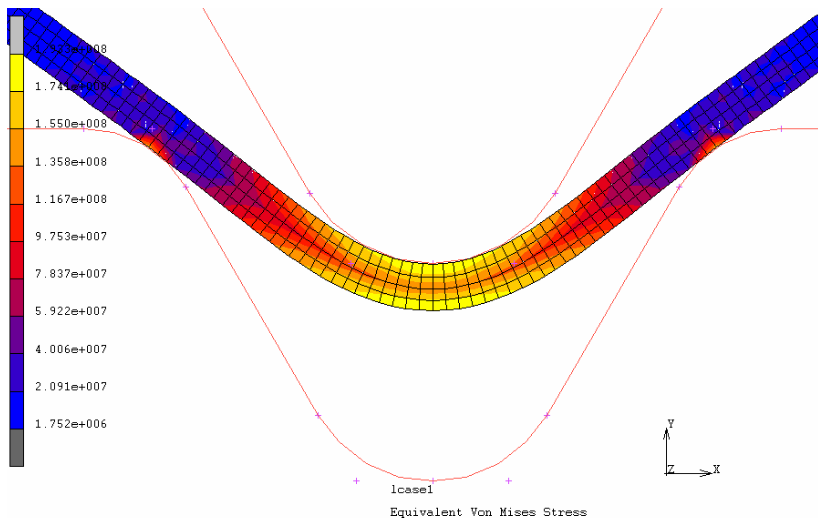

(a)

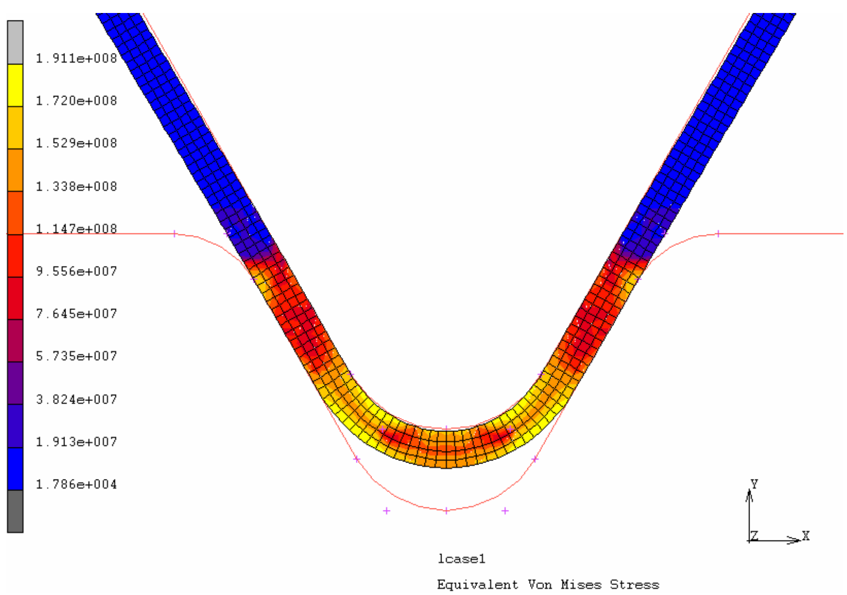

(b)

Figure 4.14 Von Misses stress distribution for AA 2014-O 2 mm-thick sheet in 120˚ V- bending at; (a) the intermediate stage, (b) the fully loaded stage

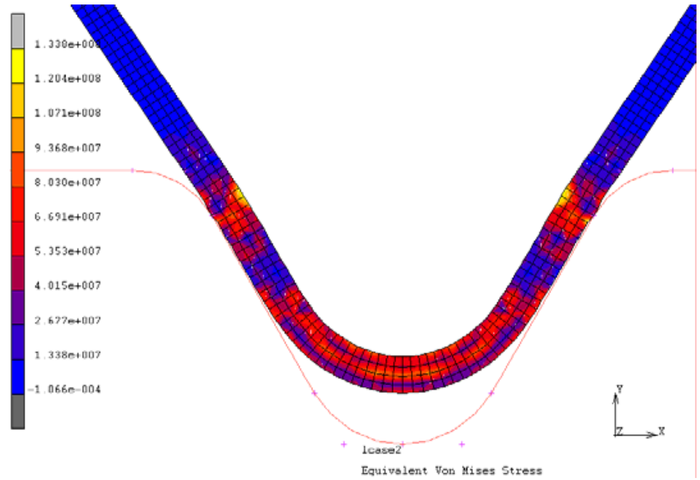

(c)

Figure 4.14 (cont'd) Von Misses stress distribution for AA 2014-O 2 mm-thick sheet in 120˚ V- bending at; (c) the unloaded stage

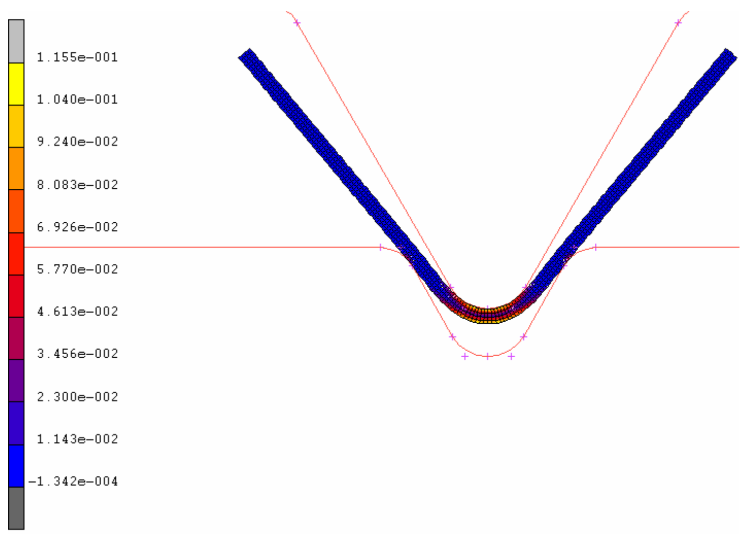

(a)

Figure 4.15 Total-equivalent plastic strain distribution for AA 2014-O 2 mm-thick sheet in 120˚ V- bending at; (a) the intermediate stage.

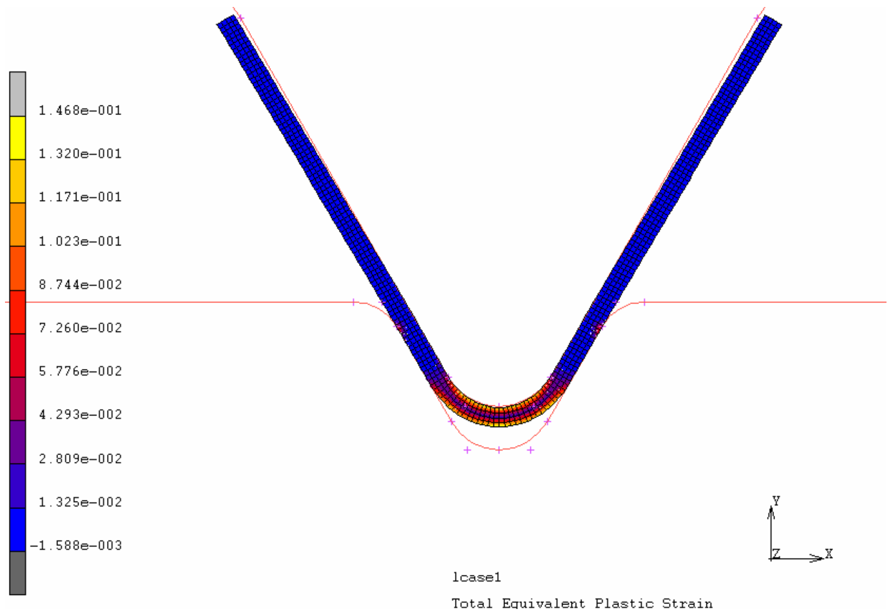

(b)

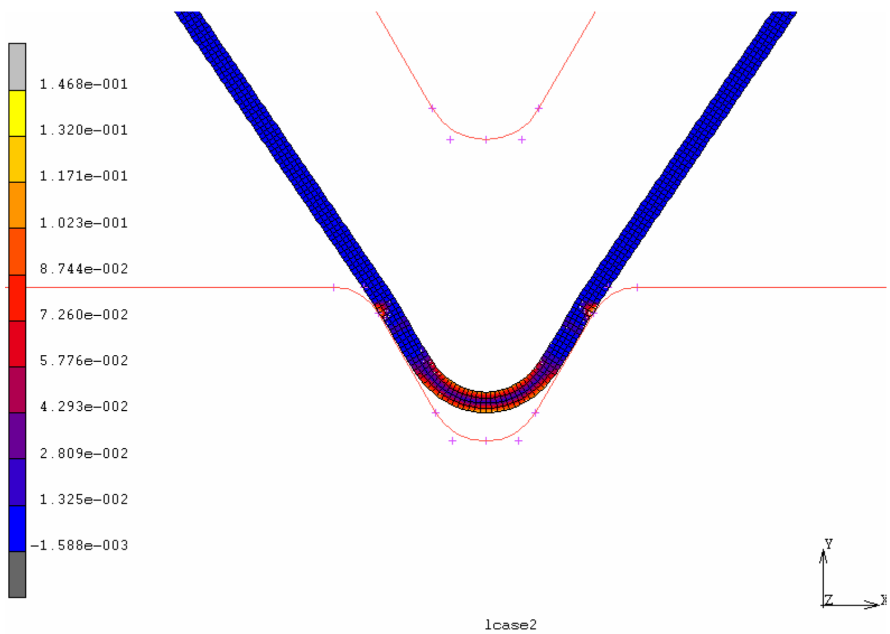

(c)

Figure 4.15 (cont'd) Total-equivalent plastic strain distribution for AA 2014-O 2 mm-thick sheet in 120˚ V- bending at; (b) the fully loaded stage, (c) the unloaded stage

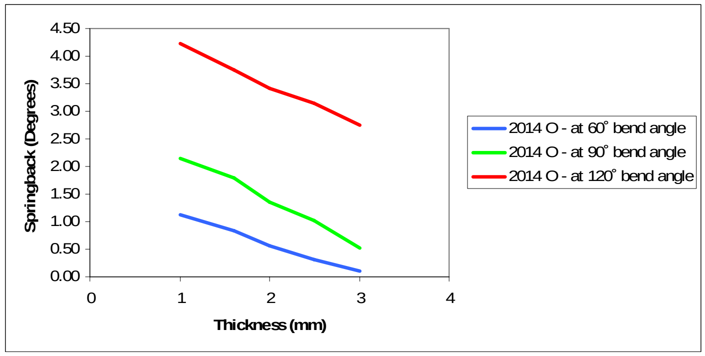

Figure 4.16 Springback data for V-bend of AA 2014 at O condition

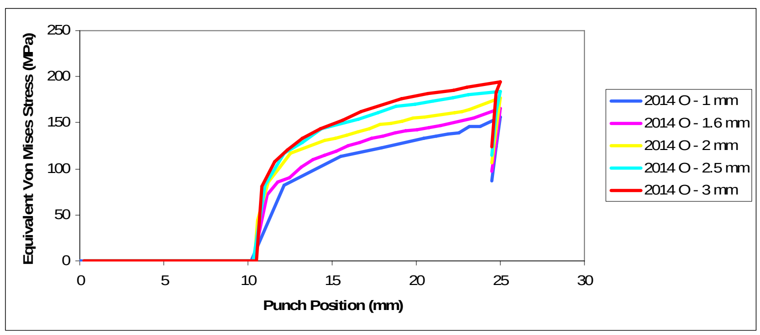

Figure 4.17 Maximum von Mises Stresses vs. position of AA 2014 O for V bending to 60˚

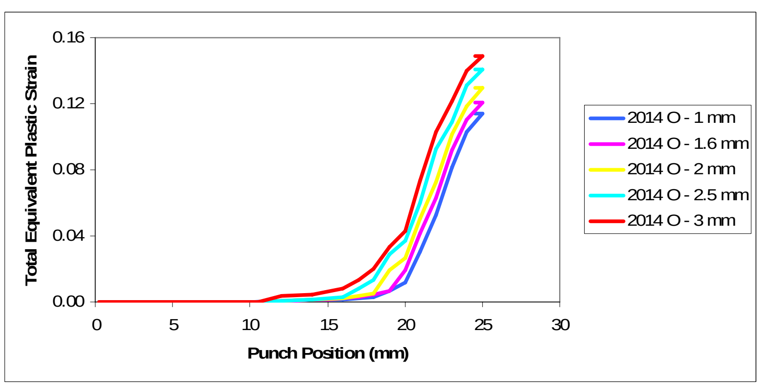

Figure 4.18 Maximum total-equivalent plastic strain vs. position of AA 2014 O for V- bending to 60˚

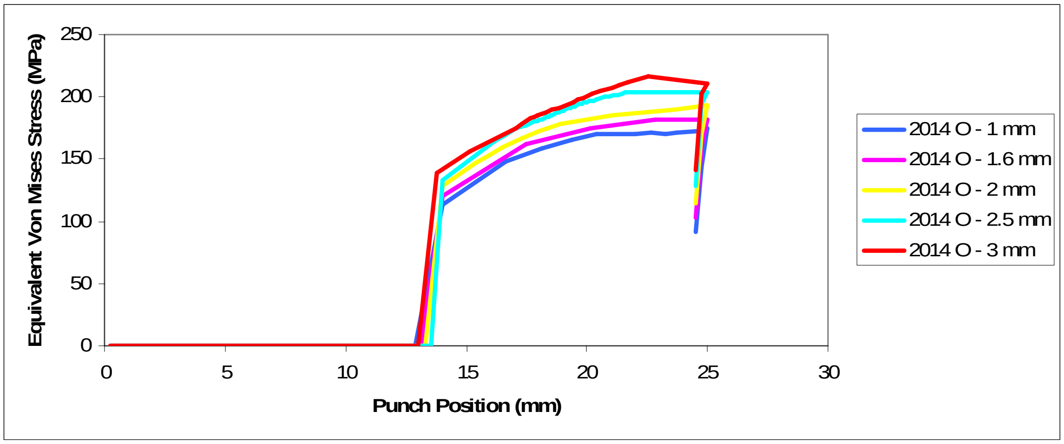

Figure 4.19 Maximum von Mises Stresses vs. punch position of AA 2014 O for V bending to 90˚

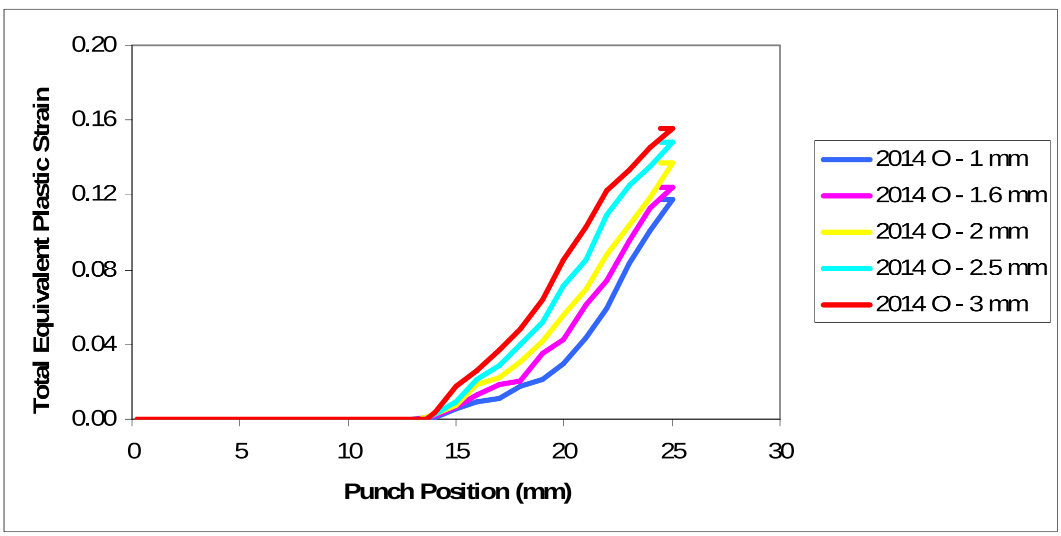

Figure 4.20 Maximum total-equivalent plastic strain vs. punch position of AA 2014 O for V bending to 90˚

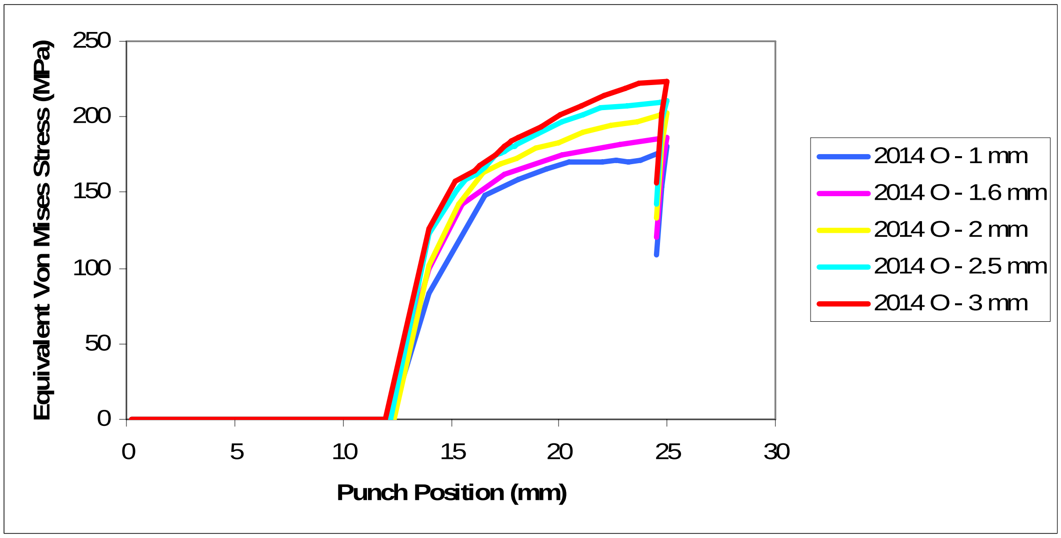

Figure 4.211 Maximum von Mises Stresses vs. punch position of AA 2014 O for V bending to 120˚

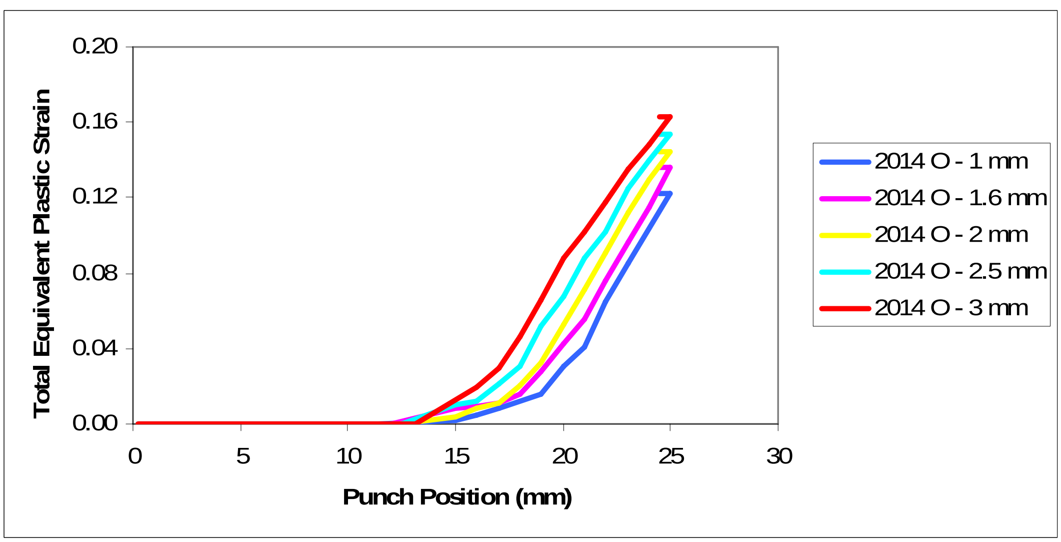

Figure 4.22 Maximum total-equivalent plastic strain vs. punch position of AA 2014 O for V bending to 120˚

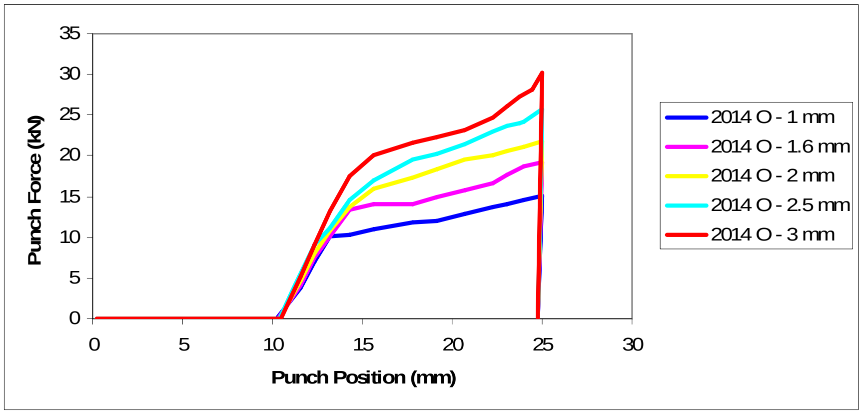

Figure 4.23 Punch load vs. punch position of AA 2014 O for V bending to 60˚

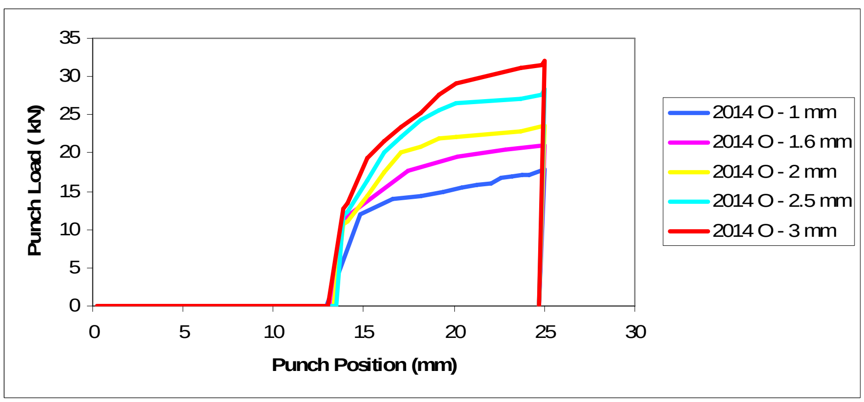

Figure 4.24 Punch load vs. punch position of AA 2014 O for V bending to 90˚

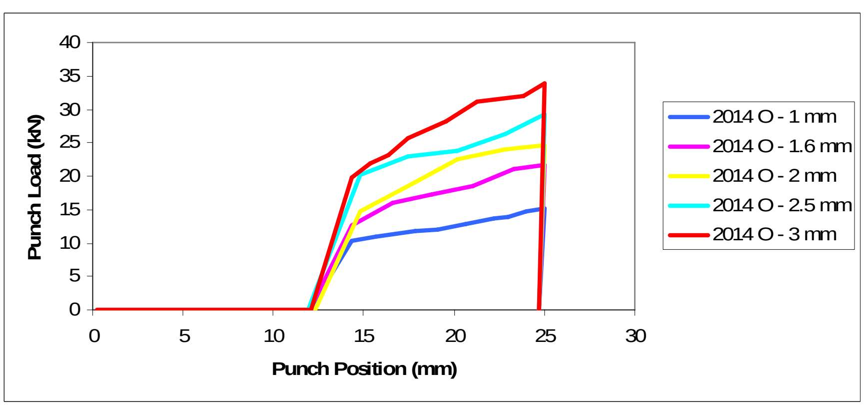

Figure 4. 25 Punch load vs. punch position of AA 2014 O for V bending to 120˚

4.2.2. V-bending of AA 2014 at T4 condition.

In this study, five different thicknesses of AA 2014-T4 are bent to 60°, 90° and 120° with a punch moving vertically downwards. Mechanical properties of the alloy are given in Table 4.5

Table 4.5 Mechanical properties of AA 2104-T4

Material	**Temper**	**Elasticity Modulus (GPa)**	**Yield Strength (MPa)**	**Poisson's Ratio**
AA 2014	T4	72.4	255	0.33

In this case study , aluminum sheets at T4 condition with a length of 100 mm, a width of 50 mm and thicknesses of 1.0, 1.6, 2.0, 2.5 and 3.0 mm. are analyzed. Amount springback is determined and tabulated and graphically illustrated in Table 4.6, Table 4.7, Table 4.8 and Figure 4.26. Total equivalent plastic strains and equivalent von Misses stresses occurring in the sheets are gathered from the finite elements analyses are illustrated graphically in Figure 4.33, Figure 4.34, Figure 4.35, Figure 4.36, Figure 4.37 and Figure 4.38. Also, punch loads for each case are also represented in Figure 4.39, Figure 4.40 and Figure 4.41.

Table 4.6 Springback results in terms of part angle for V-Bending to 60°

AA 2014 T4 at 60° V - Bending			
thickness (mm)	bend angles (°)	part angle (°)	springback (°)
1.0	60	56.30	3.70
1.6	60	56.93	3.07
2.0	60	57.93	2.07
2.5	60	58.85	1.15
3.0	60	59.20	0.80

Table 4.7 Springback results in terms of part angle for V-Bending to 90˚

AA 2014 T4 at 90˚ V - Bending			
thickness (mm)	bend angles (˚)	part angle (˚)	springback (˚)
1.0	90	82.30	7.70
1.6	90	83.93	6.07
2.0	90	84.99	5.01
2.5	90	86.18	3.82
3.0	90	87.75	2.25

Table 4.8 Springback results in terms of part angle for V-Bending to 120˚

AA 2014 T4 at 120˚ V - Bending			
thickness (mm)	bend angles (˚)	part angle (˚)	springback (˚)
1.0	120	109.18	10.82
1.6	120	110.86	9.14
2.0	120	111.71	8.29
2.5	120	112.13	7.87
3.0	120	113.23	6.77

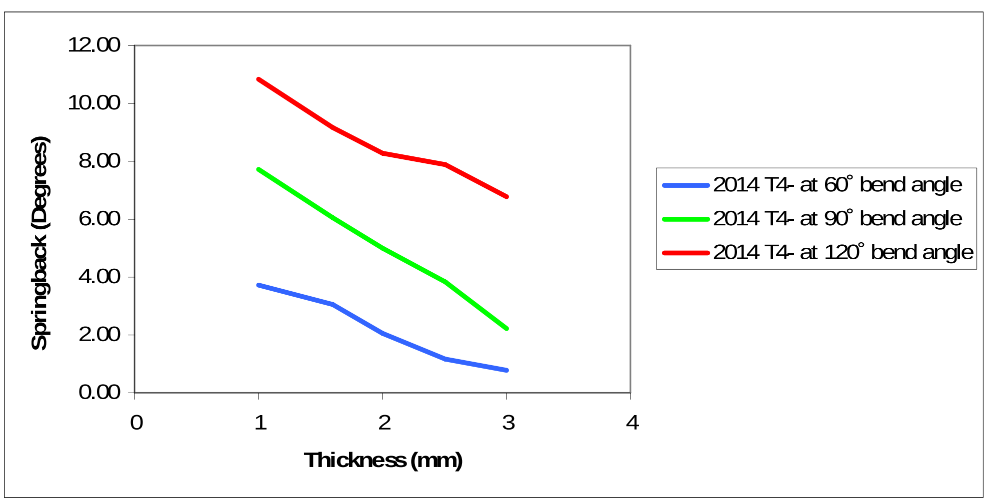

Figure 4.26 Springback data for V-bend of AA 2014 at T4 condition.

In Figure 4.27 and Figure 4.28, Von Misses Stresses and Total Plastic Strains of 2014-T4 2 mm thick sheet in 60˚ V- bending are illustrated respectively.

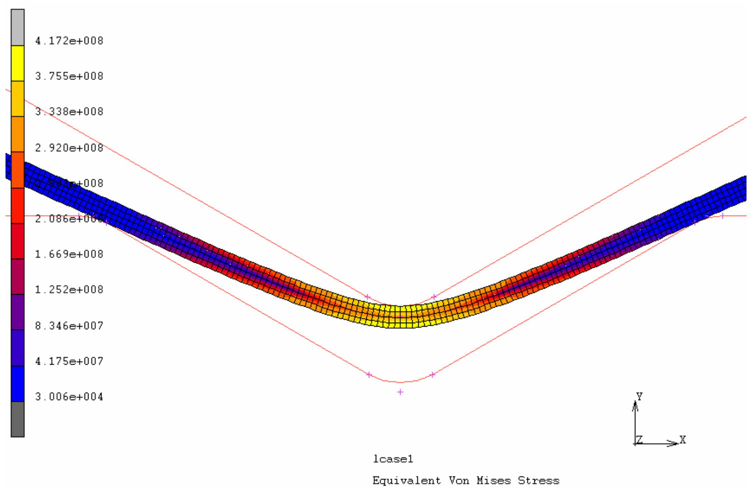

(a)

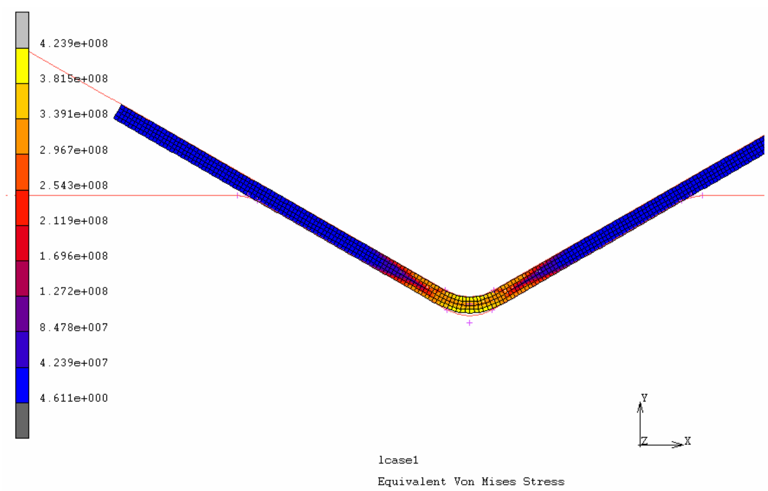

(b)

Figure 4.27 Von Misses stress distribution for AA 2014-T4 2 mm-thick sheet in 60˚ V- bending at ;(a) the intermediate stage , (b) the fully loaded stage

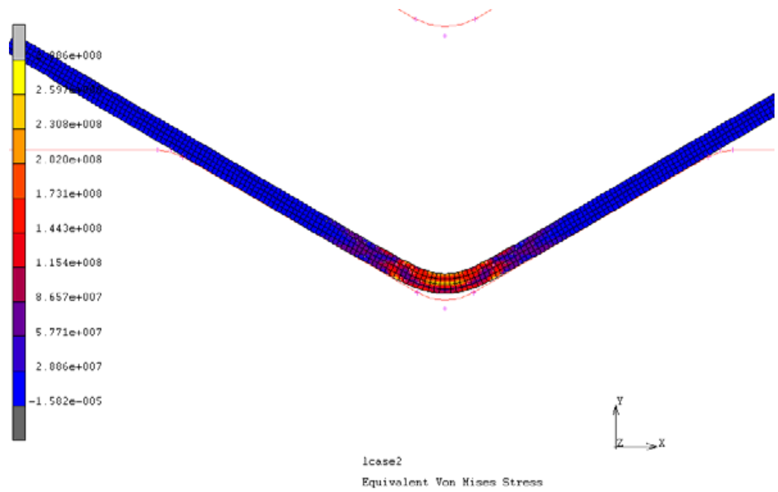

(c)

Figure 4.27 (cont'd) Von Misses stress distribution for AA 2014-T4 2 mm-thick sheet in 60˚ V- bending at ; (c) the unloaded stage.

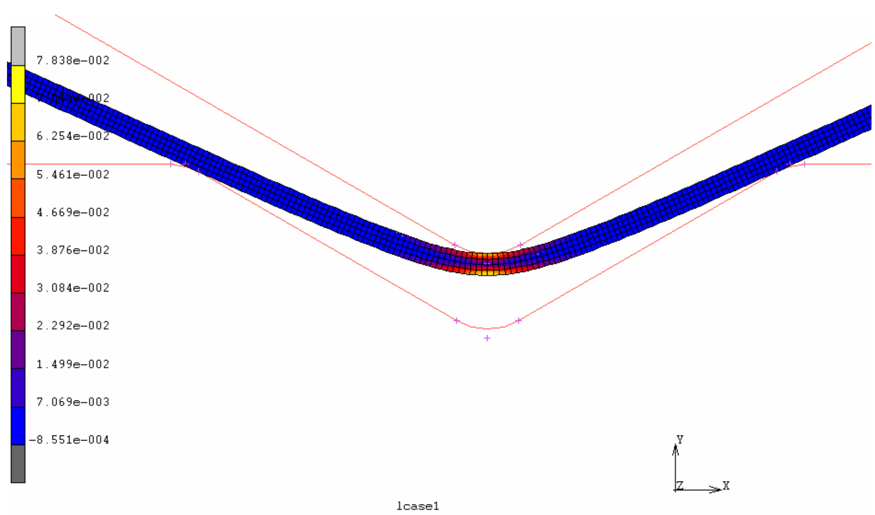

(a)

Figure 4.28 Total-equivalent plastic strain distribution for AA 2014-T4 2 mm-thick sheet in 60˚ V- bending at; (a) the intermediate stage

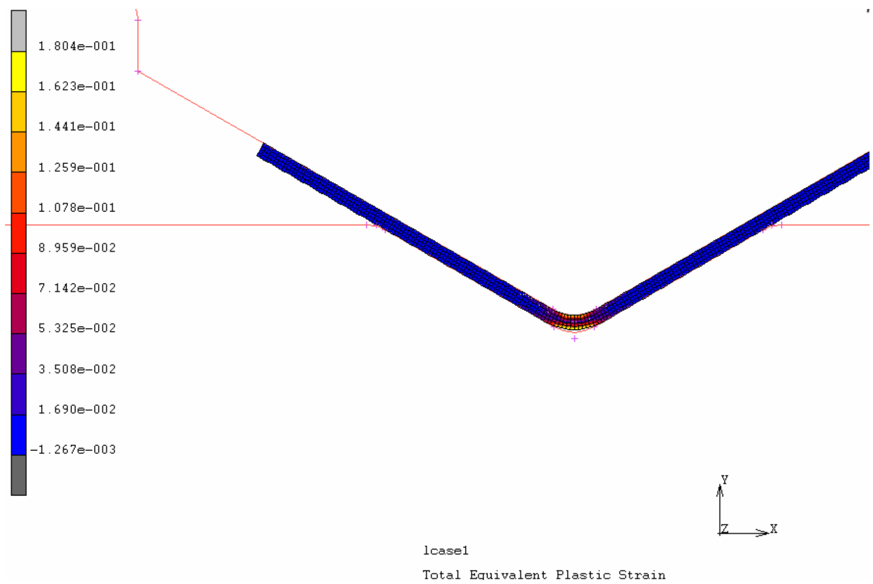

(b)

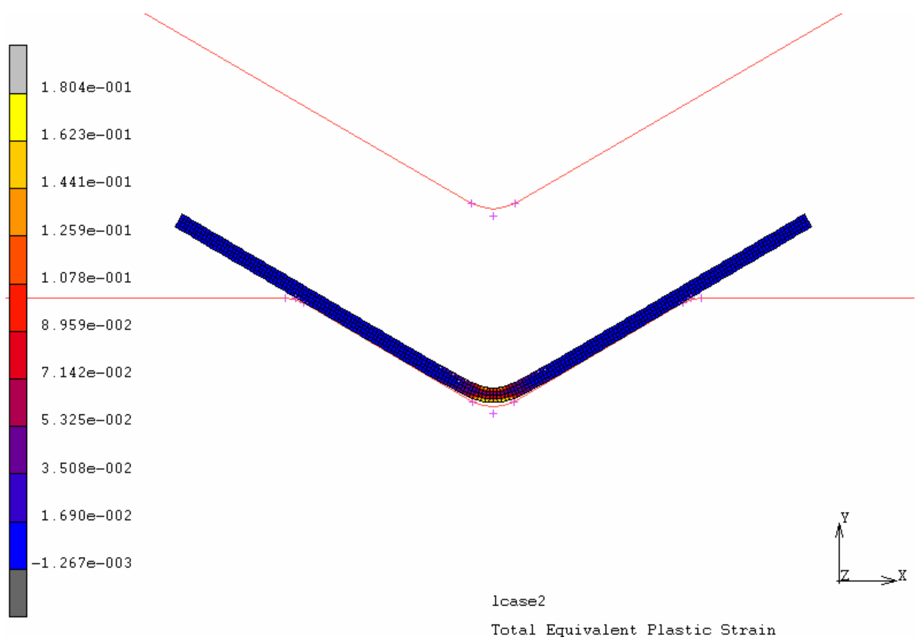

(c)

Figure 4.28 (cont'd) Total-equivalent plastic strain distribution for AA 2014-T4 2 mm-thick sheet in 60˚ V- bending at; b) the fully loaded stage, (c) the unloaded stage

In Figure 4.29 and Figure 4.30, Von Misses Stresses and Total Plastic Strains of AA 2014-T4 2 mm thick sheet in 90˚ V- bending are illustrated respectively.

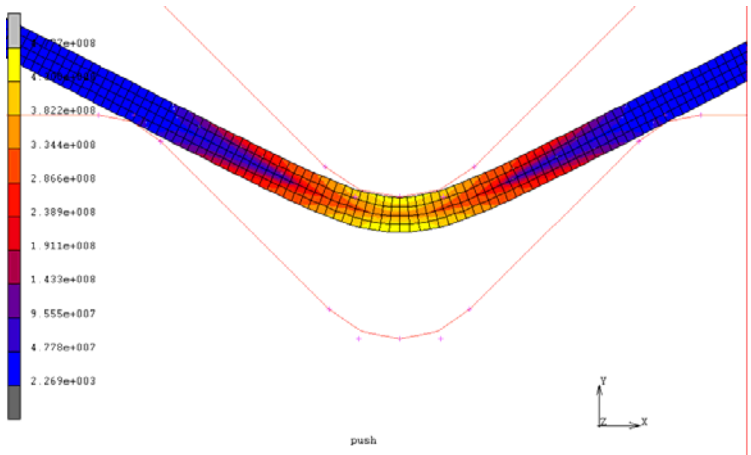

(a)

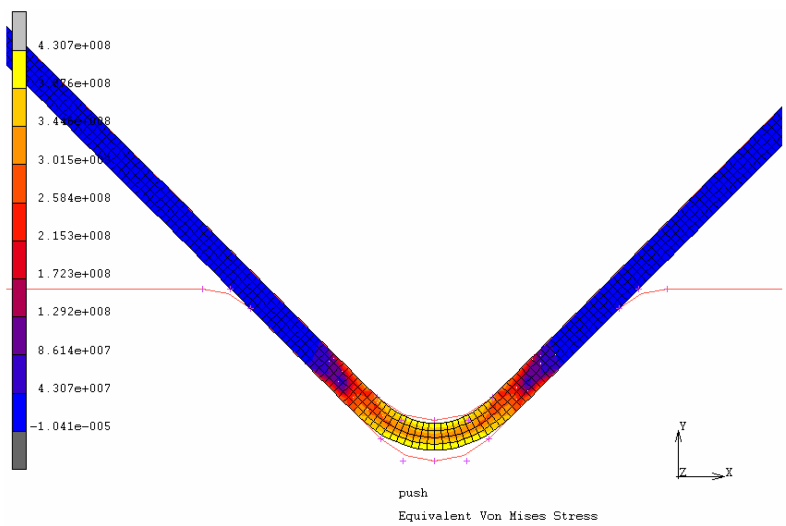

(b)

Figure 4.29 Von Misses stress distribution for AA 2014-T4 2 mm-thick sheet in 90˚ V- bending at; (a) the intermediate stage, (b) the fully loaded stage

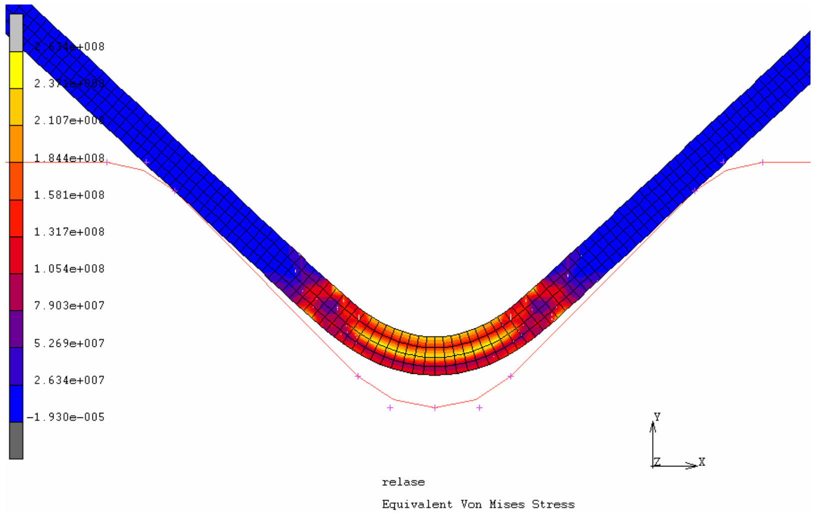

(c)

Figure 4.29 (cont'd) Von Misses stress distribution for AA 2014-T4 2 mm-thick sheet in 90˚ V- bending at; (c) the unloaded stage.

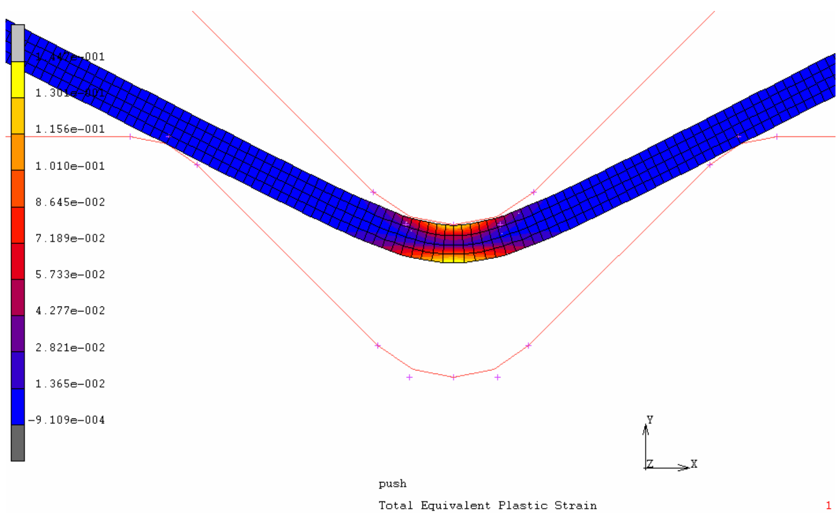

(a)

Figure 4.30 Total-equivalent plastic strain distribution for AA 2014 T4 2 mm-thick sheet in 90˚ V- bending at; (a) the intermediate stage

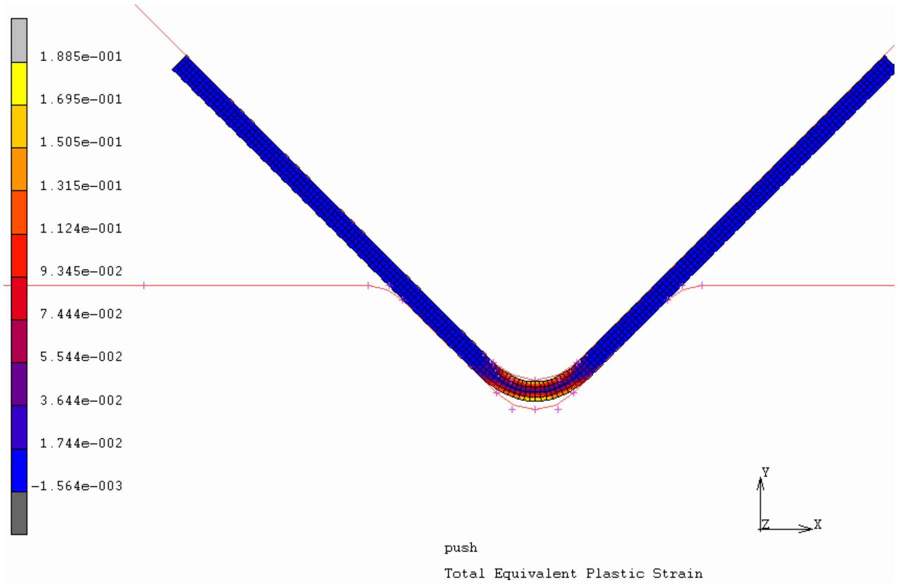

(b)

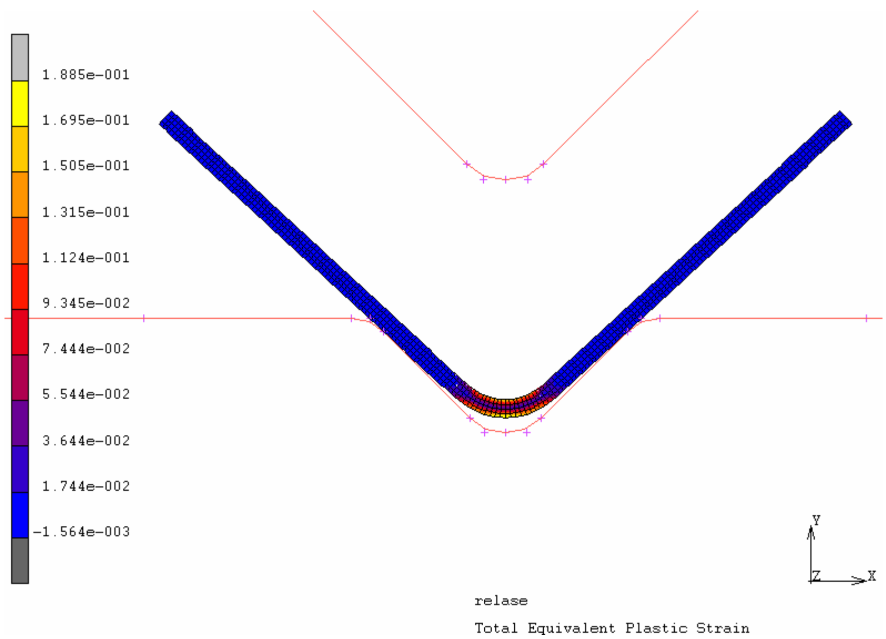

(c)

Figure 4. 30 (cont'd) Total-equivalent plastic strain distribution for AA 2014 T4 2 mm-thick sheet in 90˚ V- bending at; (b) the fully loaded stage, (c) the unloaded stage.

In Figure 4.31 and Figure 4.32, von Misses stresses and total plastic strains of AA 2014-T4 2 mm thick sheet in 120˚ V- bending are illustrated respectively.

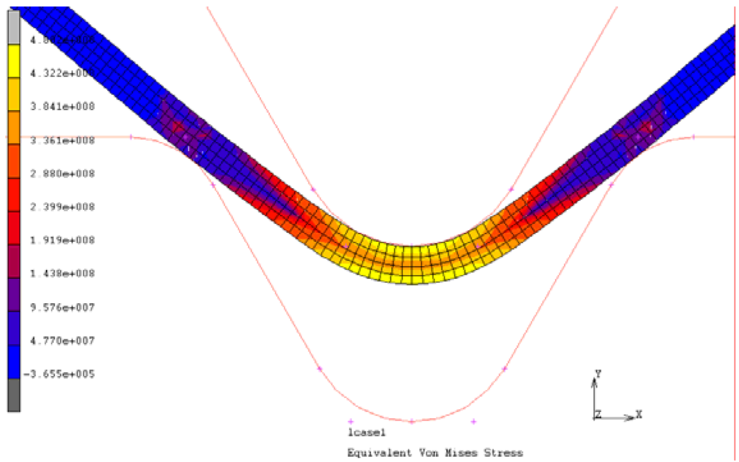

(a)

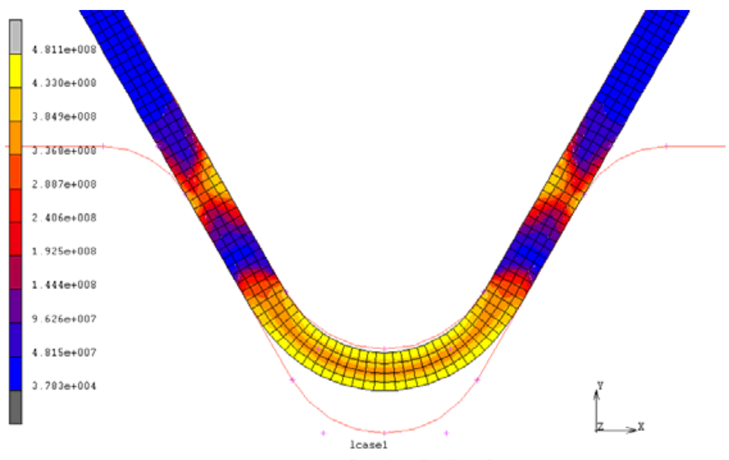

(b)

Figure 4.31 Von Misses stress distribution for AA 2014-T4 2 mm-thick sheet in 120˚ V- bending at ; (a) the intermediate stage, (b) the fully loaded stage

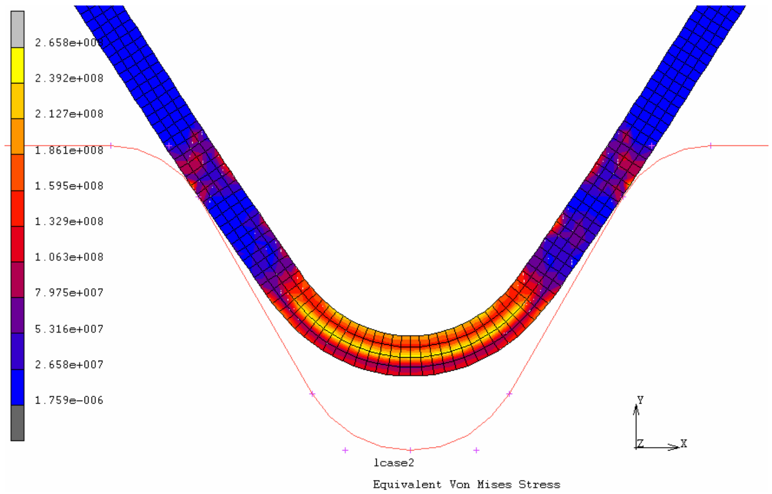

(c)

Figure 4.31 (cont'd) Von Misses stress distribution for AA 2014-T4 2 mm-thick sheet in 120˚ V- bending at ; (c) the unloaded stage

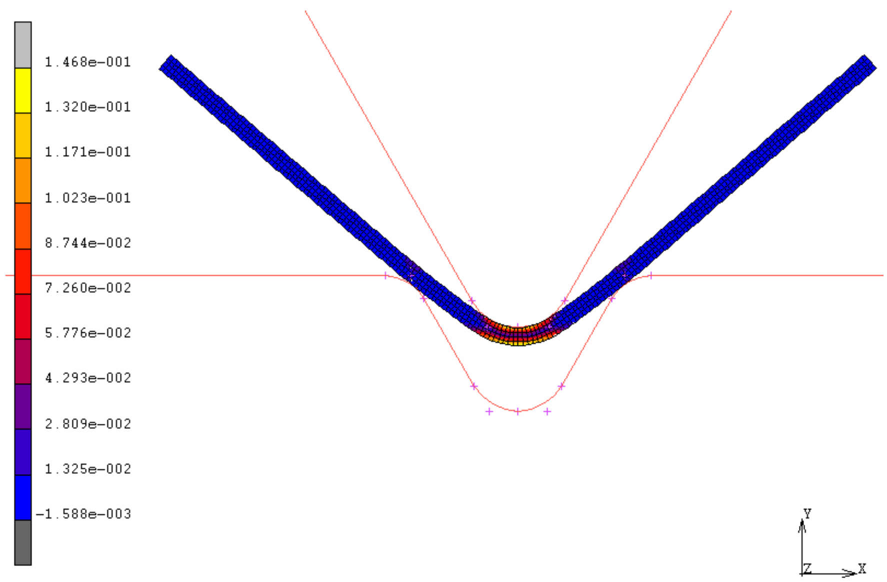

(a)

Figure 4.32 Total-equivalent plastic strain distribution for AA 2014-T4 2 mm-thick sheet in 120˚ V- bending at; (a) the intermediate stage

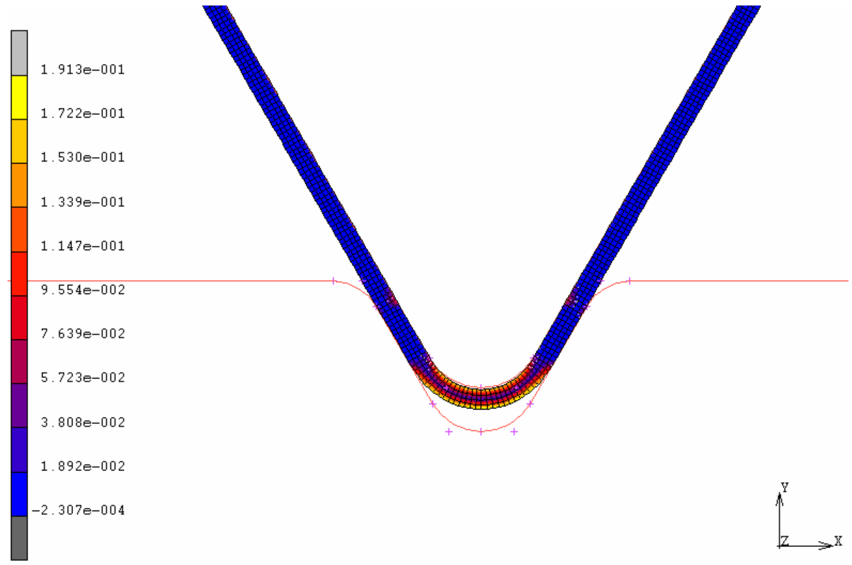

(b)

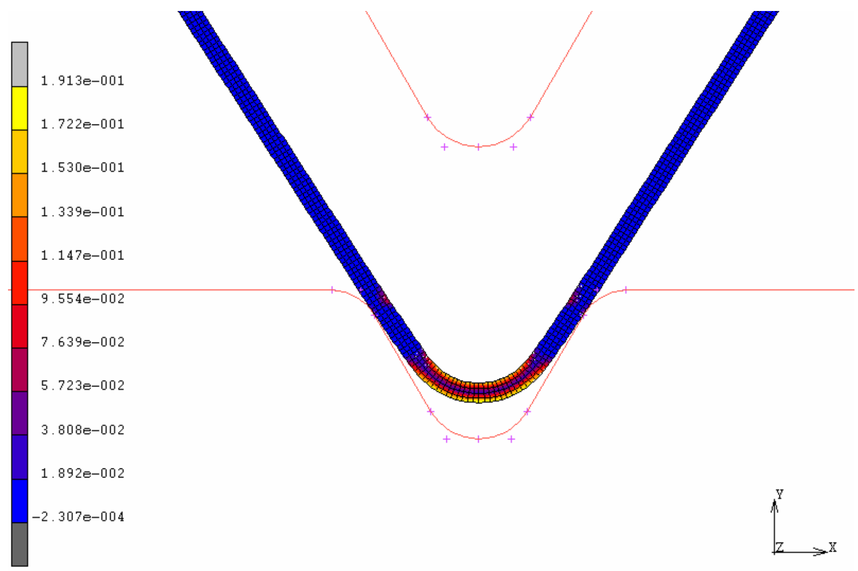

(c)

Figure 4.32 (cont'd) Total-equivalent plastic strain distribution for AA 2014-T4 2 mm-thick sheet in 120˚ V- bending at; (b) the fully loaded stage, (c) the unloaded stage.

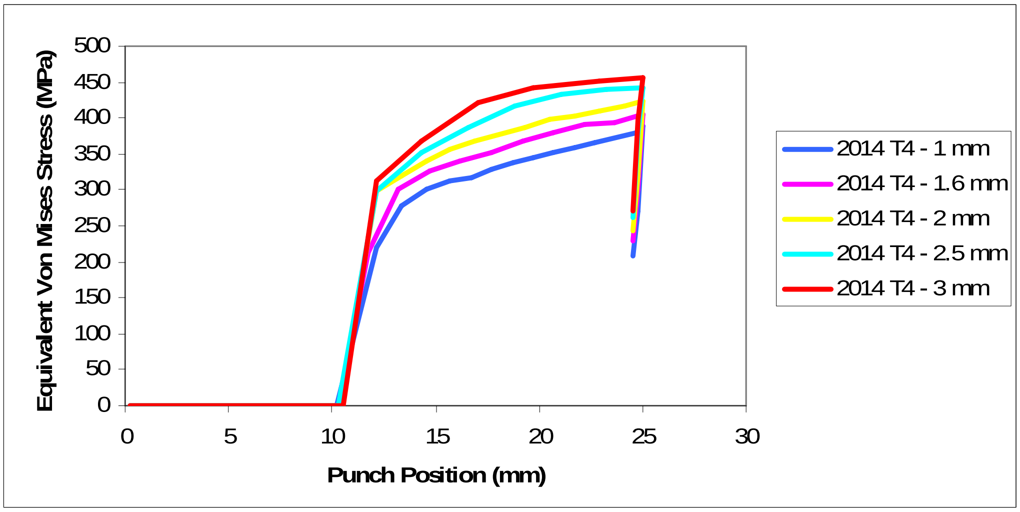

Figure 4.33 Maximum von Mises Stresses vs. punch position of AA 2014 T4 for V-bending to 60˚

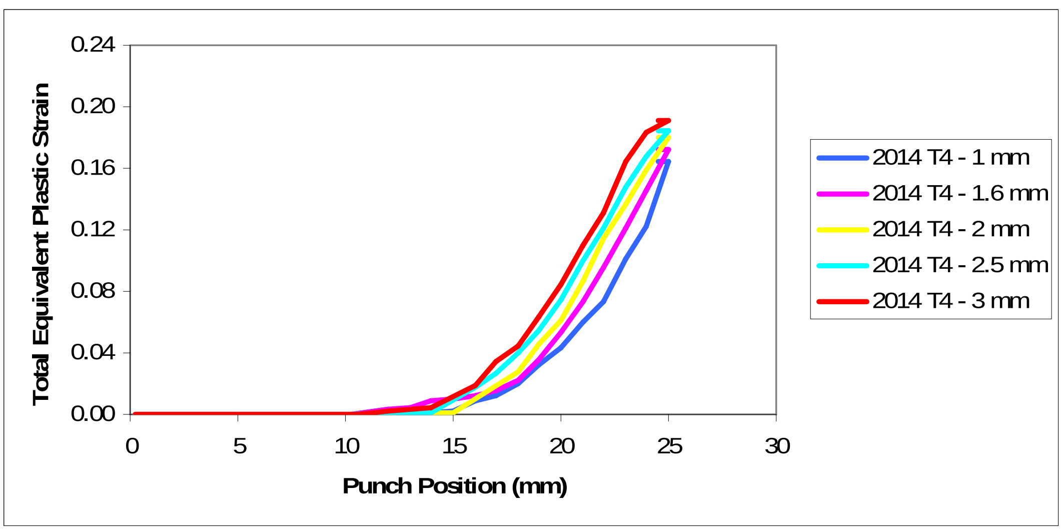

Figure 4.34 Maximum total-equivalent plastic strain vs. punch position of AA 2014 T4 for V-bending to 60˚

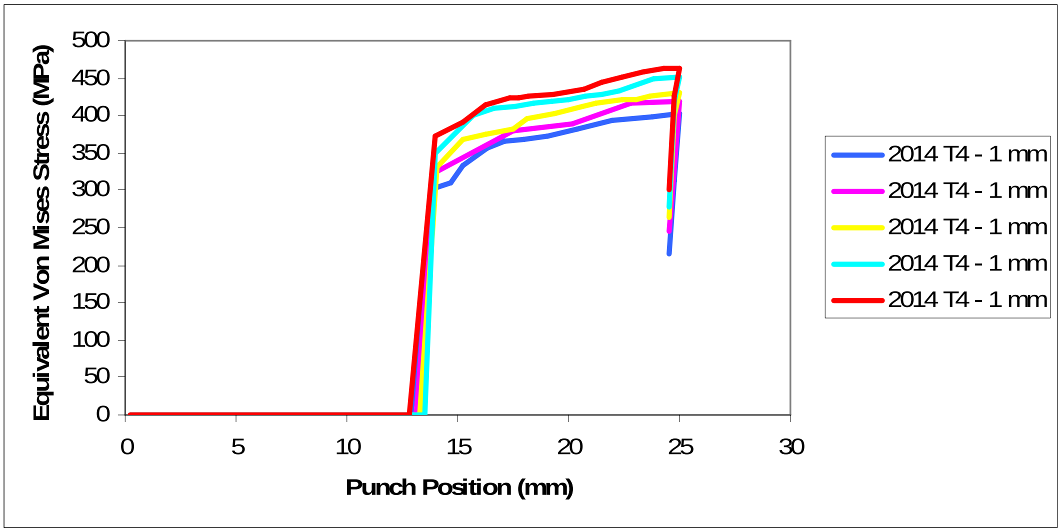

Figure 4.35 Maximum von Mises stresses vs. punch position of AA 2014 T4 for V bending to 90˚

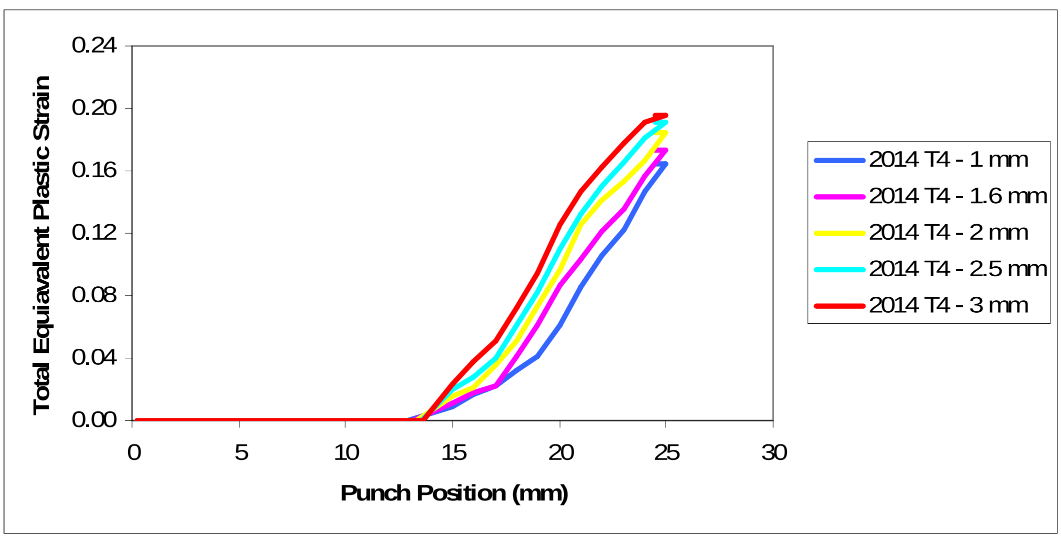

Figure 4.36 Maximum total-equivalent plastic strain vs. punch position of AA 2014 T4 for V bending to 90˚

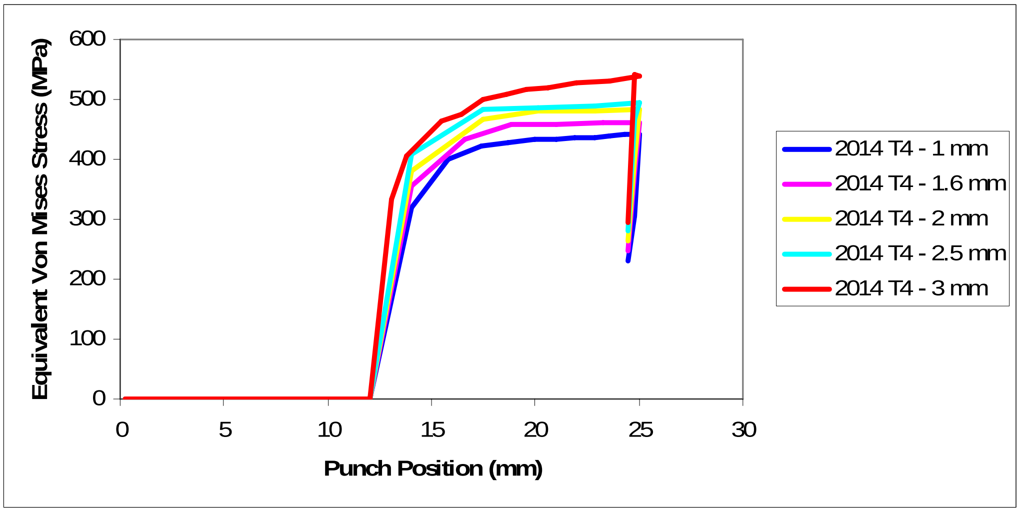

Figure 4.37 Maximum von Mises stresses vs. punch position of AA 2014 T4 for V bending to 120˚

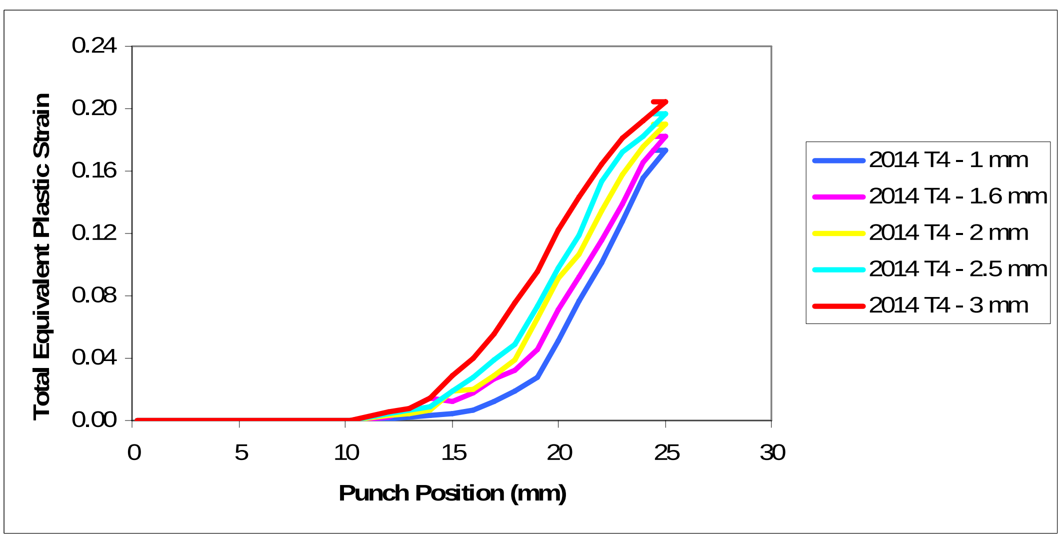

Figure 4. 38 Maximum total-equivalent plastic strain vs. punch position of AA 2014 T4 for V bending to 120˚

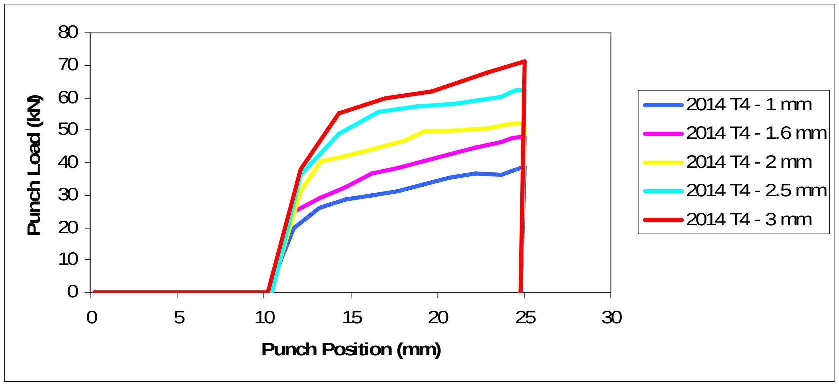

Figure 4.39 Punch load vs. punch position of AA 2014 T4 for V bending to 60˚

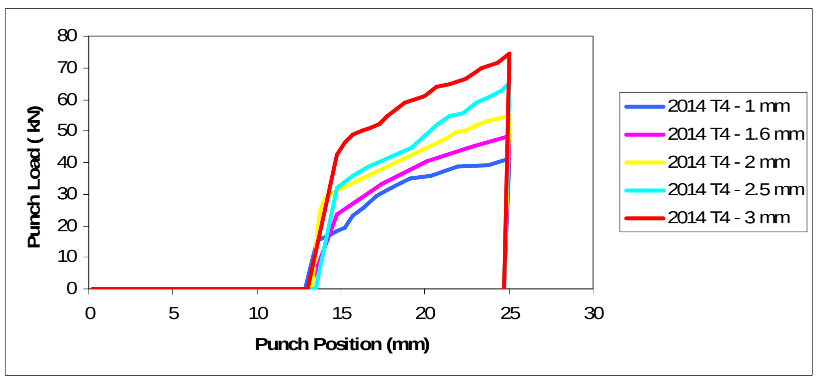

Figure 4.40 Punch load vs. punch position of AA 2014 T4 for V bending to 90˚

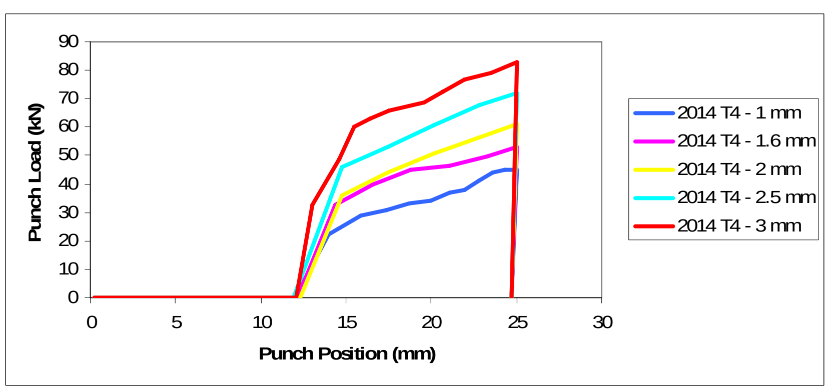

Figure 4.41 Punch load vs. punch position of AA 2014 T4 for V bending to 120˚

4.2.3. V-bending of AA 2014 at T6 condition.

In this part of the study, five different thicknesses of AA 2014-T6 are bent to 60°, 90° and 120° with a punch moving vertically downwards. Mechanical properties of the alloy are given in Table 4.9

Table 4.9 Mechanical properties of AA 2014-T6

Material	Temper	Elasticity Modulus (GPa)	Yield Strength (MPa)	Poisson's Ratio
AA 2014	T6	72.4	414	0.33

In this case study ,aluminum sheets at T6 condition with a length of 100 mm, a width of 50 mm and thicknesses of 1, 1.6, 2, 2.5 and 3 mm. were analyzed. Amount springback is determined and tabulated and graphically illustrated in Table 4.10, Table 4.11, Table 4.12 and Figure 4.42. Total equivalent plastic strains and equivalent Von Misses stresses, at different bend angles, occurring in the sheets are gathered from the finite elements analyses are illustrated graphically in Figure 4.49, Figure 4.50, Figure 4.51, Figure 4.52, Figure 4.53 and Figure 4.54. Also, punch loads for each case are also represented in Figure 4.55, Figure 4.56 and Figure 4.57.

Table 4.10 Springback results in terms of part angle for V-Bending to 60°

AA 2014 T6 at 60° V - Bending			
Thickness (mm)	bend angles (°)	part angle (°)	Springback (°)
1.0	60	53.90	6.10
1.6	60	55.02	4.98
2.0	60	56.64	3.36
2.5	60	57.14	2.86
3.0	60	58.15	1.85

Table 4.11 Springback results in terms of part angle for V-Bending to 90°

AA 2014 T6 at 90° V - Bending			
Thickness (mm)	bend angles (°)	part angle (°)	Springback (°)
1	90	77.53	12.47
1.6	90	79.92	10.08
2	90	81.99	8.01
2.5	90	83.82	6.18
3	90	84.74	5.26

Table 4.12 Springback results in terms of part angle for V-Bending to 120°

AA 2014 T6 at 120° V - Bending			
Thickness (mm)	bend angles (°)	part angle (°)	Springback (°)
1.0	120	104.83	15.17
1.6	120	105.44	14.56
2.0	120	107.49	12.51
2.5	120	108.74	11.26
3.0	120	109.35	10.65

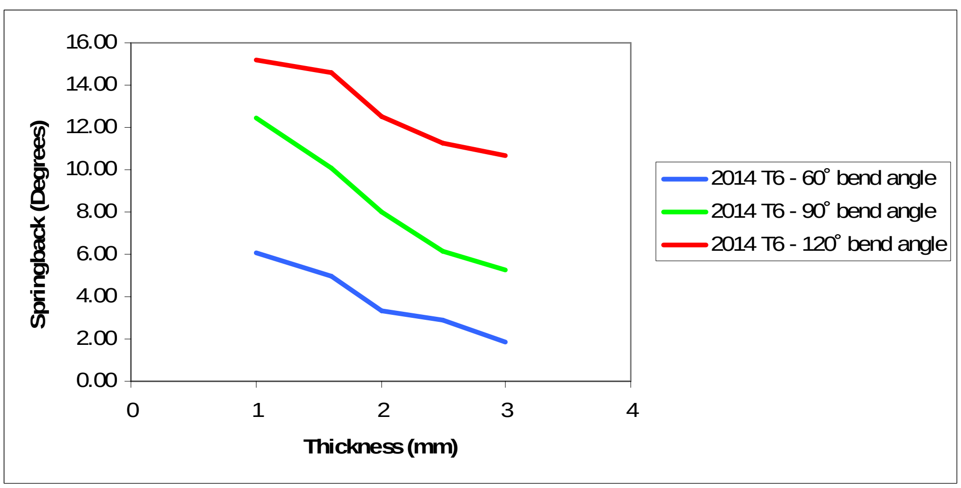

Figure 4.42 Springback data of AA2014 T6 for V-bending.

In Figure 4.43 and Figure 4.44, Von Misses Stresses and total plastic Strains in AA 2014-T6 2 mm thick sheet in 60˚ V- bending are illustrated respectively.

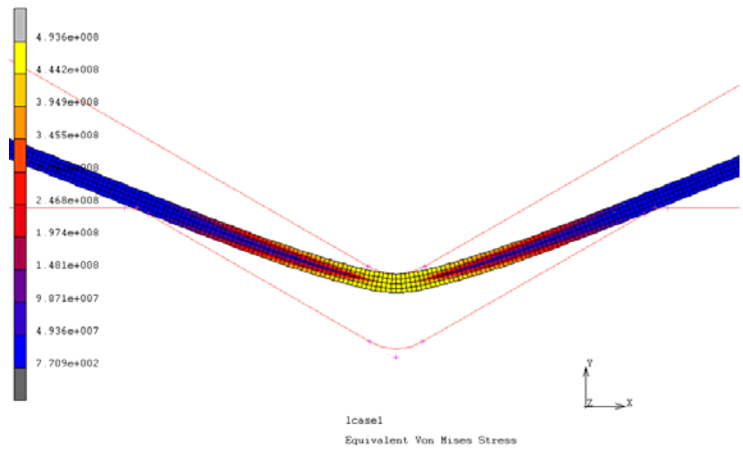

(a)

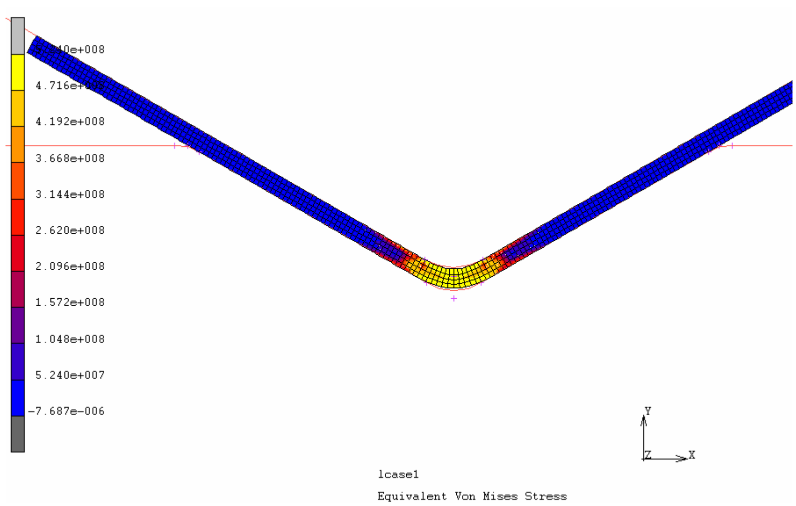

(b)

Figure 4.43 Von Misses stress distribution for AA 2014-T6 2 mm-thick sheet in 60˚ V- bending at; (a) the intermediate stage, (b) the fully loaded stage

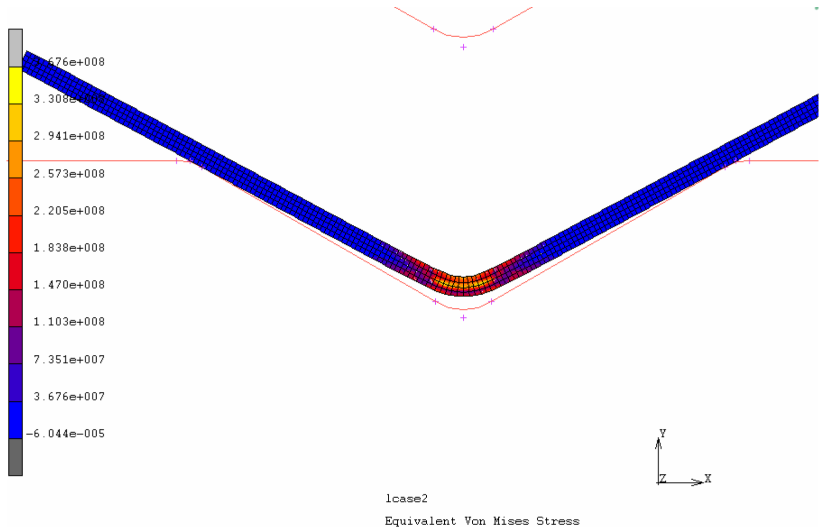

(c)

Figure 4.43 (cont'd) Von Misses stress distribution for AA 2014-T6 2 mm-thick sheet in 60˚ V- bending at; (c) the unloaded stage

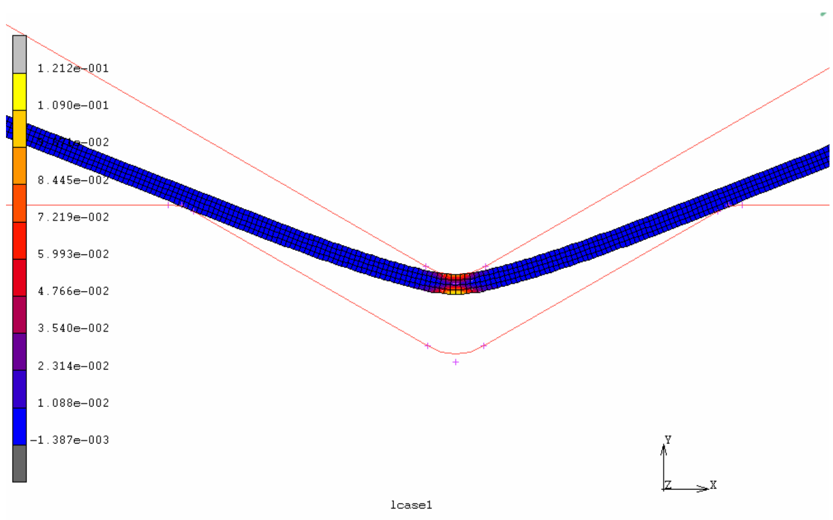

(a)

Figure 4.44 Total-equivalent plastic strain distribution for AA 2014-T6 2 mm-thick sheet in 60˚ V- bending at; (a) the intermediate stage

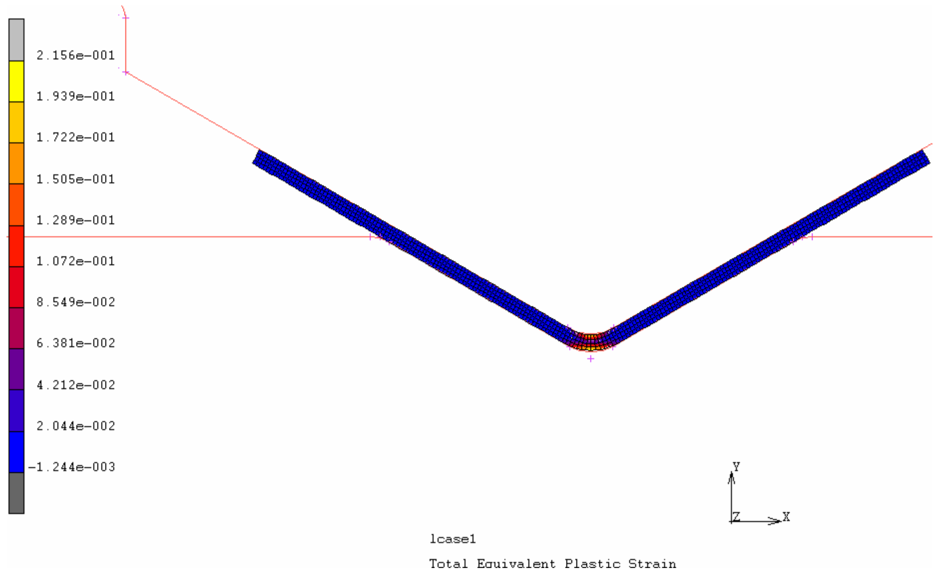

(b)

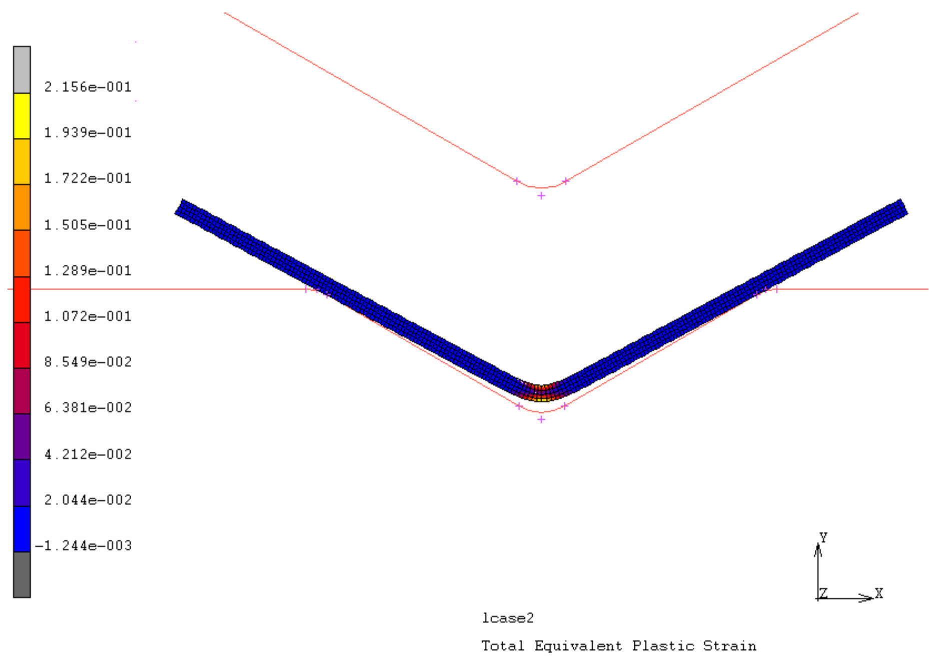

(c)

Figure 4.44 (cont'd) Total-equivalent plastic strain distribution for AA 2014-T6 2 mm-thick sheet in 60˚ V- bending at; (c) the unloaded stage

In Figure 4.45 and Figure 4.46, Von Misses Stresses and total plastic strains in AA 2014-T6 2 mm thick sheet in 90˚ V- bending are illustrated respectively.

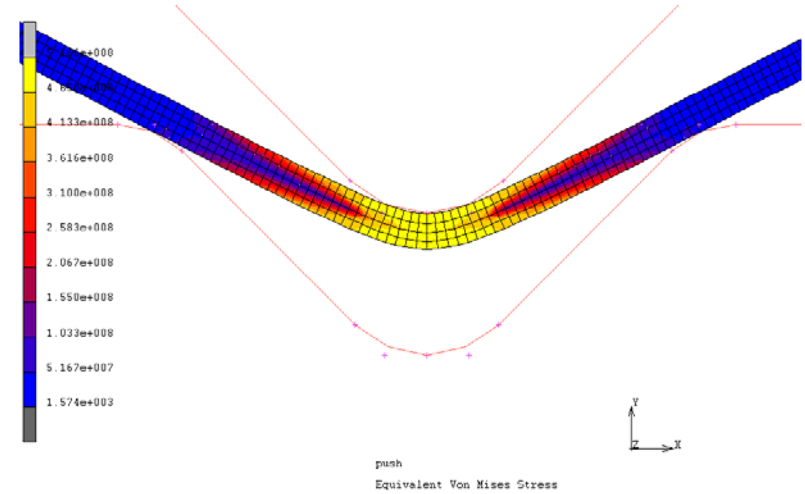

(a)

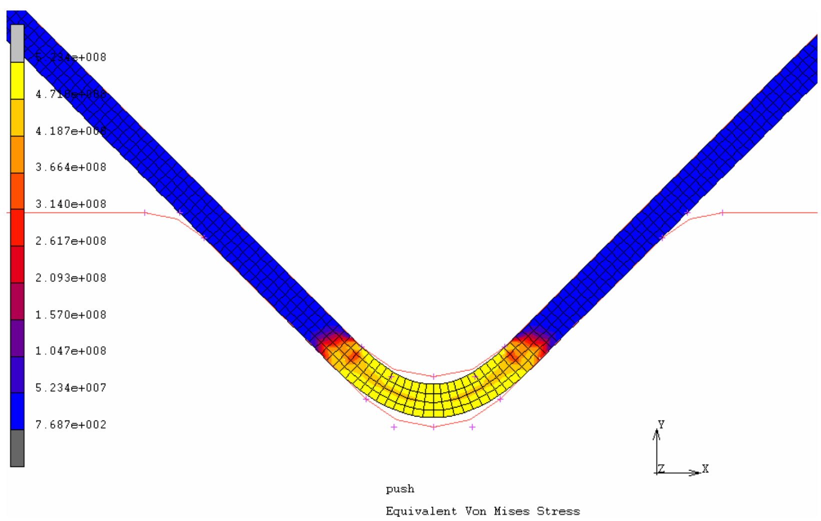

(b)

Figure 4.45 Von Misses stress distribution for 2014-T6 2 mm-thick sheet in 90˚ V-bending at; (a) the intermediate stage, (b) the fully loaded stage

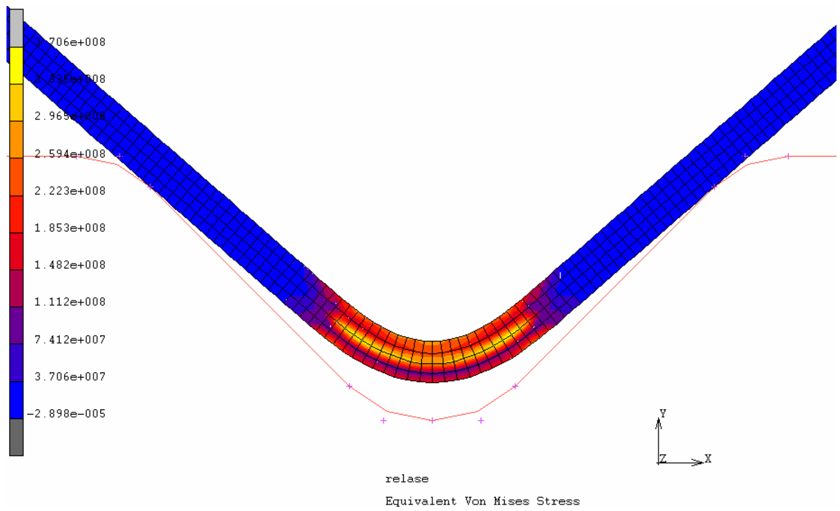

(c)

Figure 4. 45 (cont'd) Von Misses stress distribution for 2014-T6 2 mm-thick sheet in 90˚ V- bending at; (c) the unloaded stage.

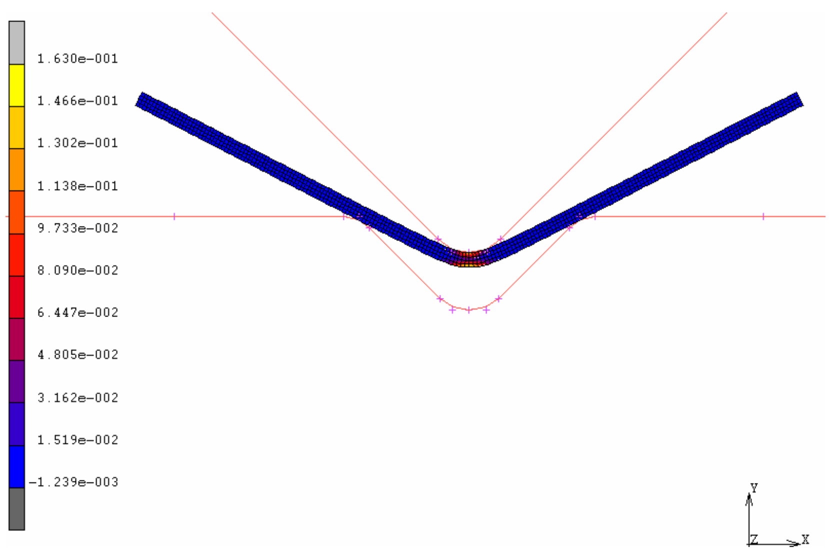

(a)

Figure 4.46 Total-equivalent plastic strain distribution for AA 2014-T6 2 mm-thick sheet in 90˚ V- bending at; (a) the intermediate stage

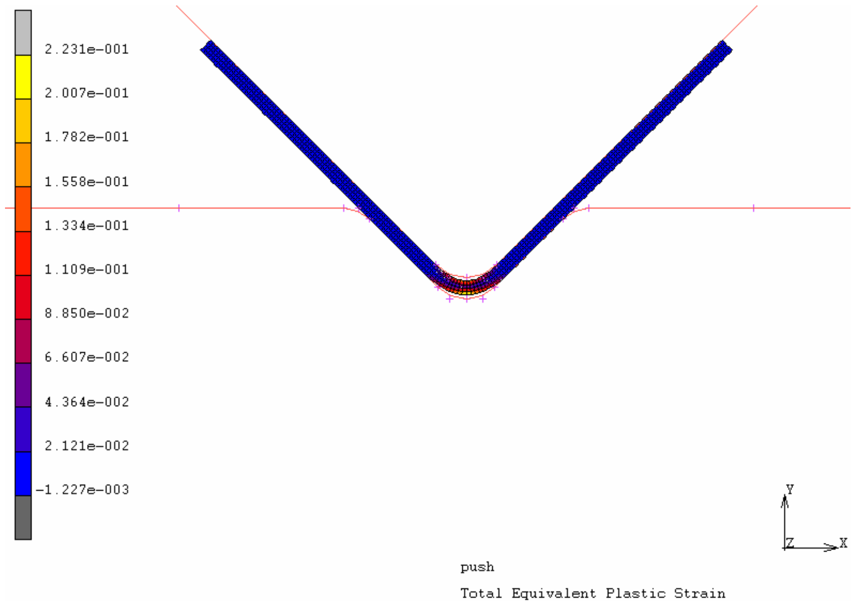

(b)

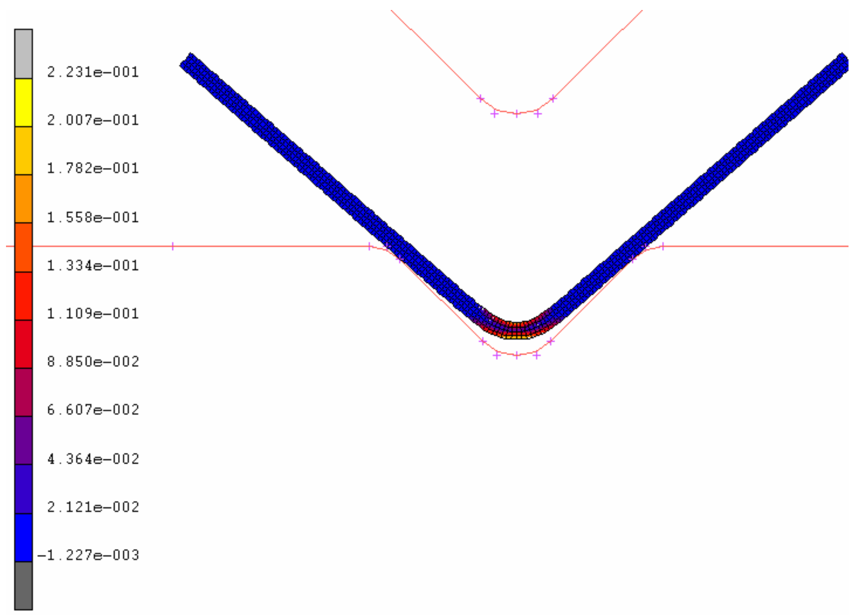

(c)

Figure 4.46 (cont'd) Total-equivalent plastic strain distribution for AA 2014-T6 2 mm-thick sheet in 90˚ V- bending at; (b) the fully loaded stage, (c) the unloaded stage.

In Figure 4.47 and Figure 4.48, Von Misses Stresses and Total Plastic Strains of AA 2014-T6 2 mm thick sheet in 120˚ V- bending are illustrated respectively.

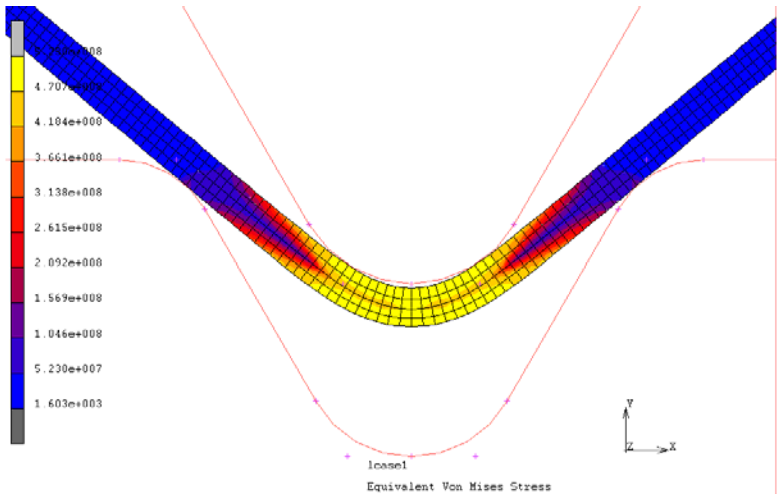

(a)

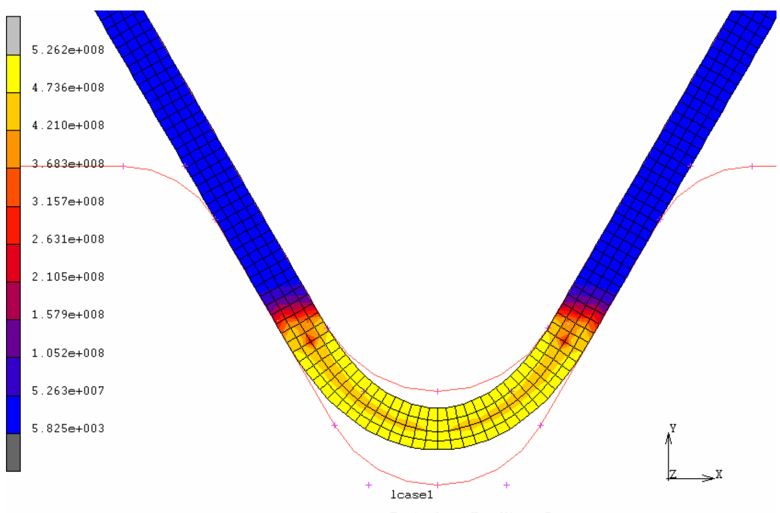

(b)

Figure 4.47 Von Misses stress distribution for AA 2014-T6 2 mm-thick sheet in 120˚ V- bending at; (a) the intermediate stage, (b) the fully loaded stage

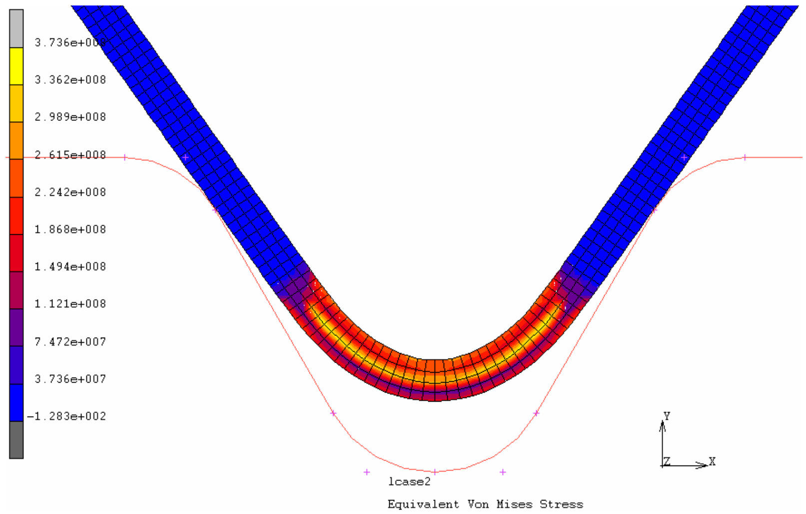

(c)

Figure 4.47 (cont'd) Von Misses stress distribution for AA 2014-T6 2 mm-thick sheet in 120˚ V- bending at; (c) the unloaded stage

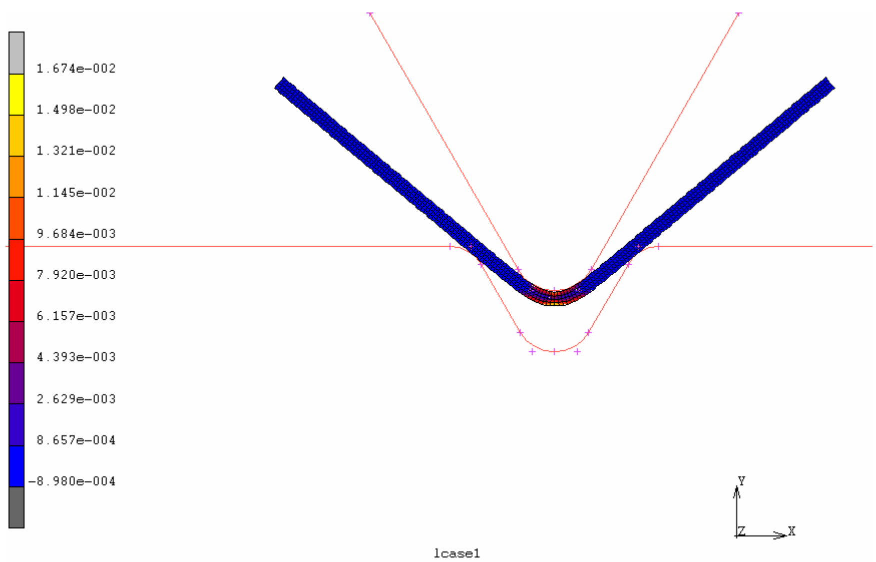

(a)

Figure 4.48 Total-equivalent plastic strain distribution for AA 2014-T6 2 mm-thick sheet in 120˚ V- bending at; (a) the intermediate stage

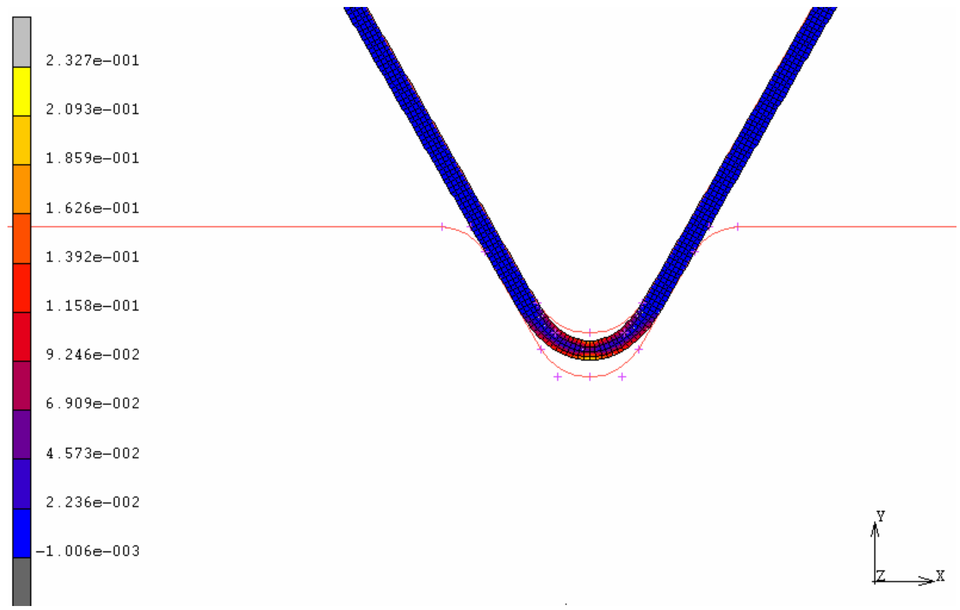

(b)

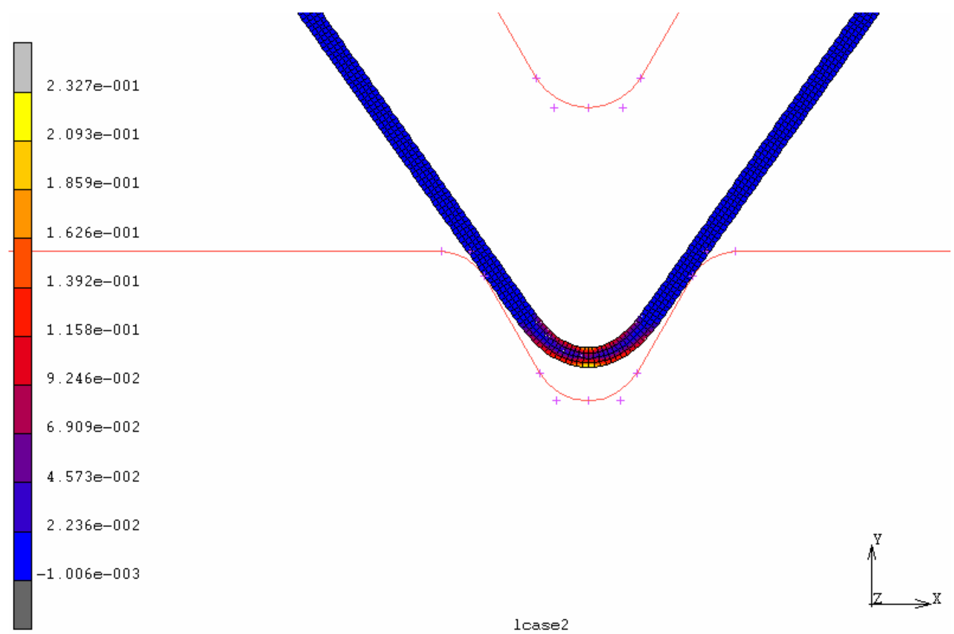

(c)

Figure 4.48 (cont'd) Total-equivalent plastic strain distribution for AA 2014-T6 2 mm-thick sheet in 120˚ V- bending at; (b) the fully loaded stage, (c) the unloaded stage.

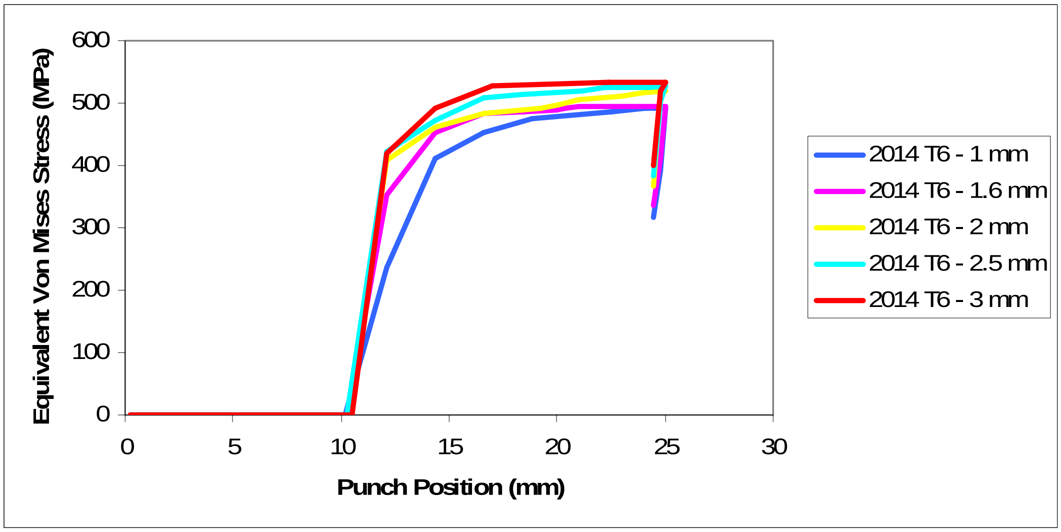

Figure 4.49 Maximum von Mises stresses vs. punch position of AA 2014 T6 for V-bending to 60˚

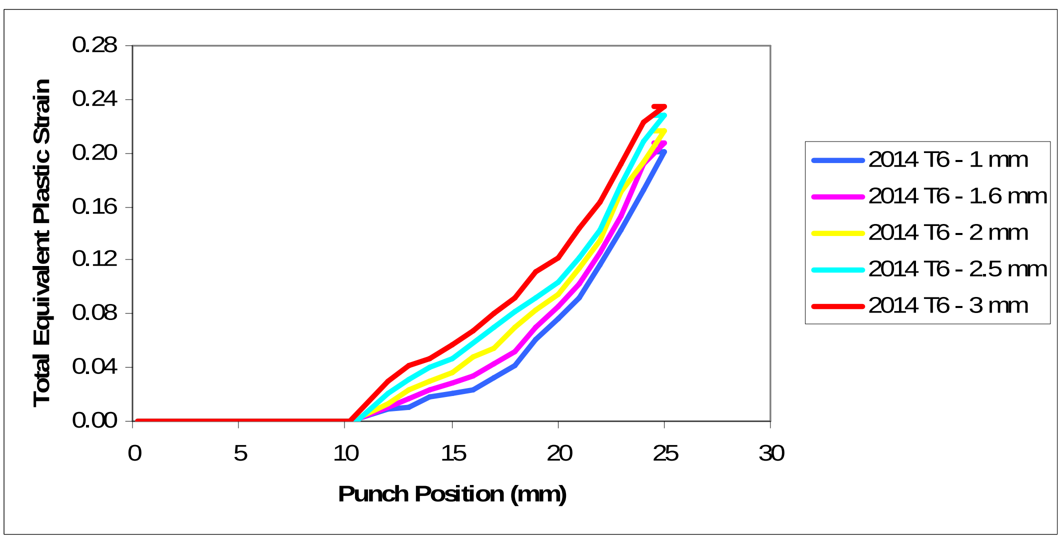

Figure 4.50 Maximum total-equivalent plastic strain vs. punch position of AA 2014 T6 for V-bending to 60˚

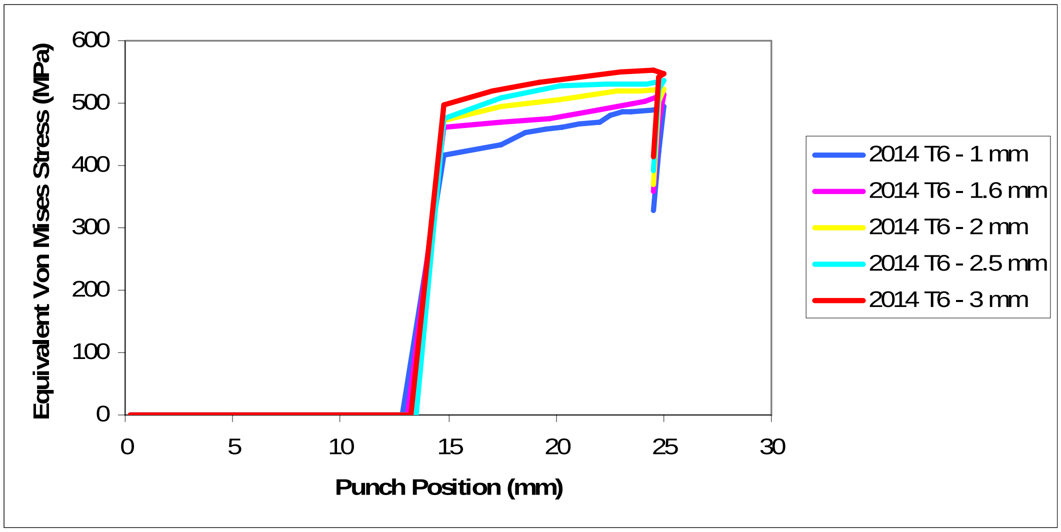

Figure 4.51 Maximum von Mises stresses vs. punch position of AA 2014 T6 for V-bending to 90˚

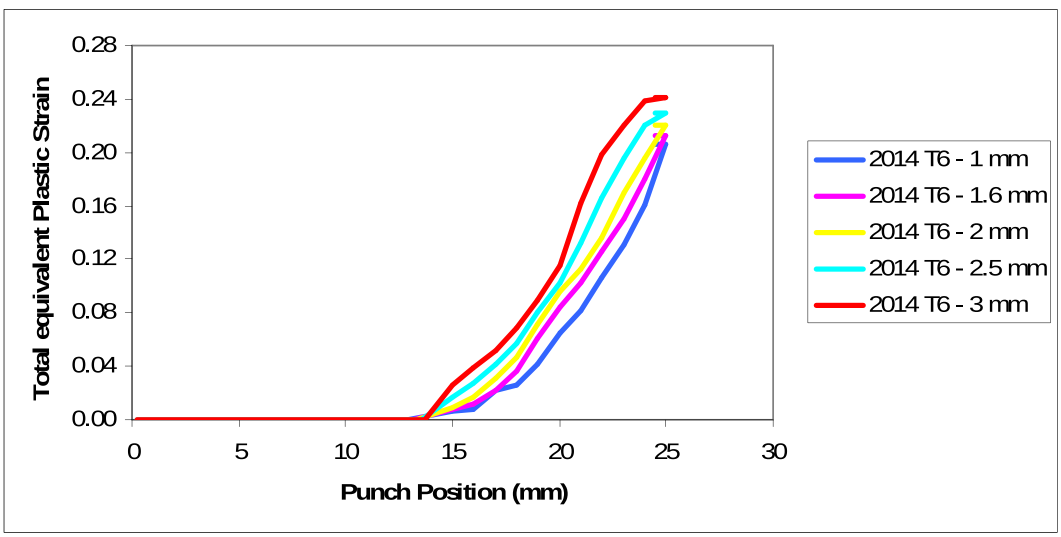

Figure 4.52 Maximum total-equivalent plastic strain vs. punch position of AA 2014 T6 for V-bending to 90˚

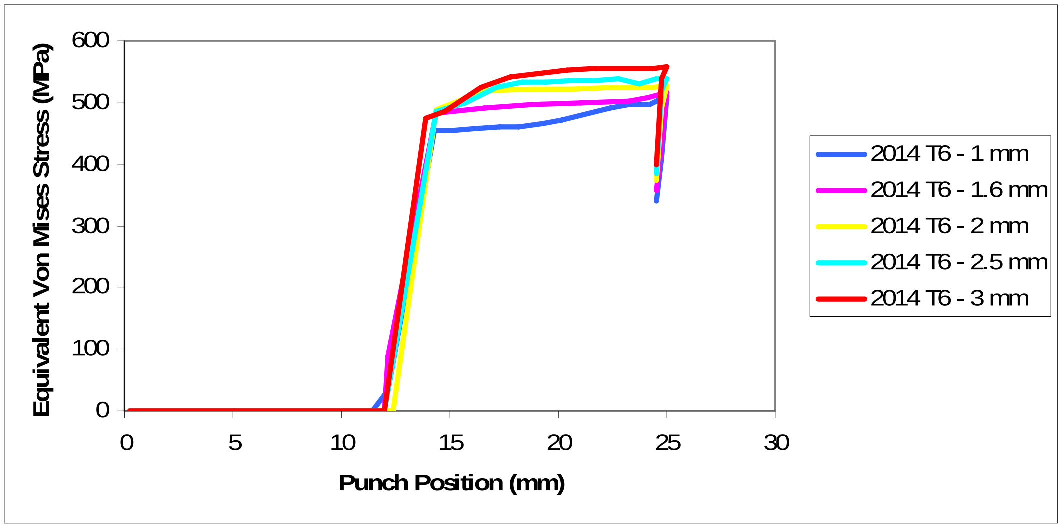

Figure 4.53 Maximum von Mises stresses vs. punch position of AA 2014 T6for V-bending to 120˚

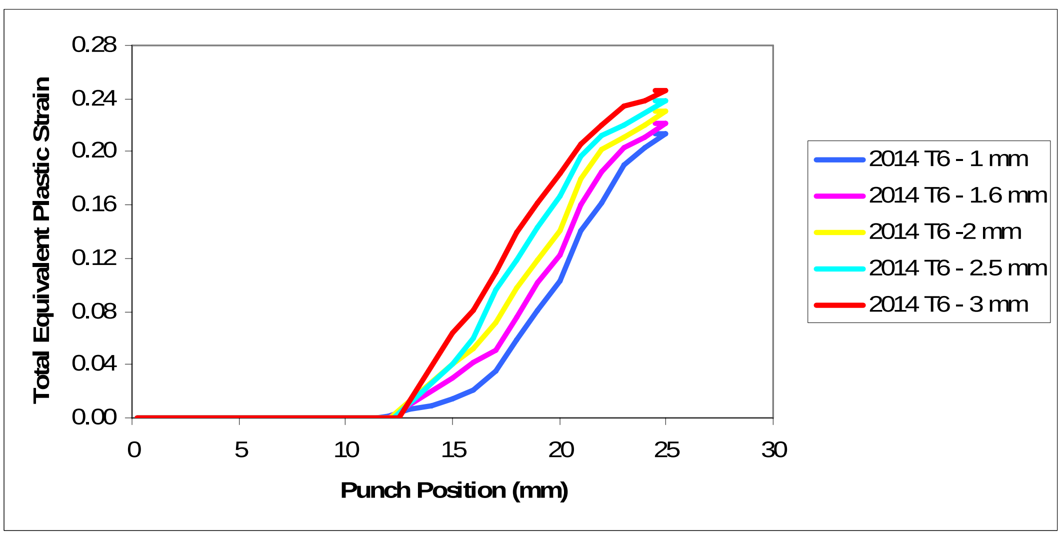

Figure 4.54 Maximum total-equivalent plastic strain vs. punch position of AA 2014 T6 for V-bending to 120˚

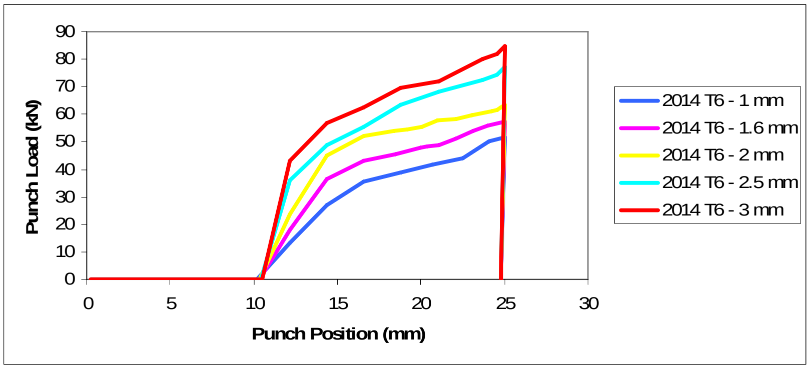

Figure 4.55 Punch load vs. punch position of AA 2014 T6 for V-bending to 60˚

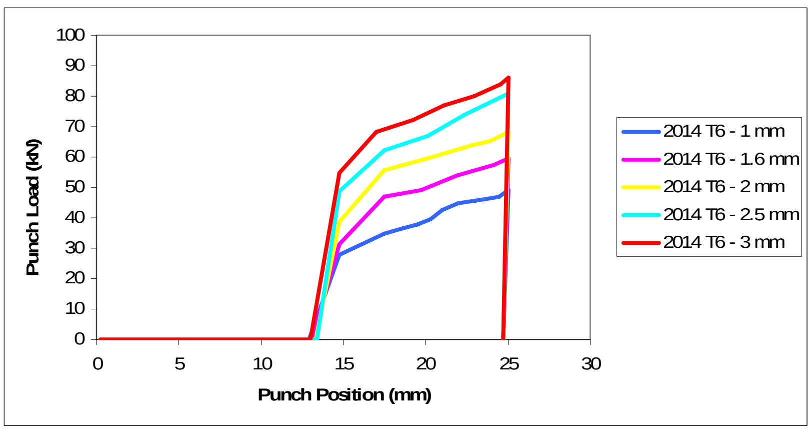

Figure 4.56 Punch load vs. punch position of AA 2014 T6 for V-bending to 90˚

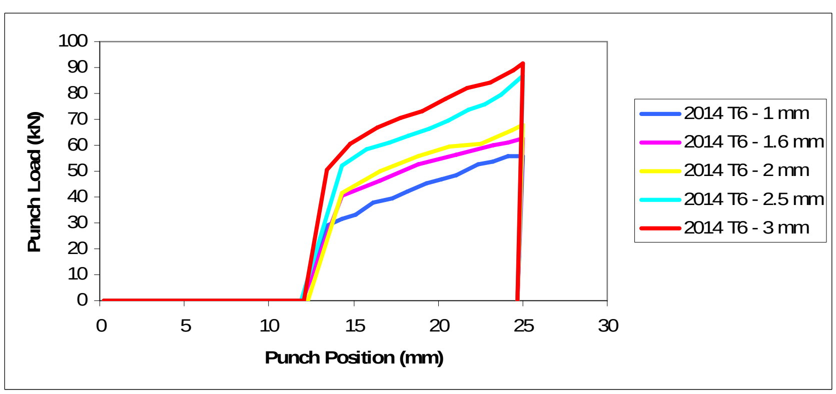

Figure 4.57 Punch load vs. punch position of AA 2014 T6 for V-bending to 120˚

4.2.4. V-bending of AA 6061 at O condition.

In this study, five different thicknesses of AA 6061-O are bent to 60°, 90° and 120° with a punch moving vertically downwards. Mechanical properties of the alloy are given Table 4.13

Table 4.13 Mechanical properties of AA 6061-O

Material	Temper	Elasticity Modulus (GPa)	Yield Strength (MPa)	Poisson's Ratio
AA 6061	O	68.9	55.2	0.33

In this case study ,aluminum sheets at O condition with a length of 100 mm, a width of 50 mm and thicknesses of 1.0 mm, 1.6 mm , 2.0 mm, 2.5 mm and 3 mm. are analyzed. Amount of the springback is determined and tabulated and graphically illustrated in Table 4.14, Table 4.15, Table 4.16 and Figure 4.58. Total equivalent plastic strains and equivalent Von Misses stresses, at different bend angles, occurring in the sheets are gathered from the finite elements analyses are illustrated graphically in Figure 4.65, Figure 4.66, Figure 4.67, Figure 4.68, Figure 4.69 and Figure 4.70. Also, punch loads for each case are also represented in Figure 4.71, Figure 4.72 and Figure 4.73.

Table 4.14 Springback results in terms of part angle for V-Bending to 60°

AA 6061 O at 60° V - Bending			
Thickness (mm)	Bend angle (°)	Part angle (°)	Springback (°)
1.0	60	58.85	0.92
1.6	60	59.35	0.65
2.0	60	59.58	0.42
2.5	60	59.80	0.20
3.0	60	59.90	0.10

Table 4.15 Springback results in terms of part angle for V-Bending to 90˚

AA 6061 O at 90˚ V - Bending			
Thickness (mm)	Bend angle (˚)	Part angle (˚)	Springback (˚)
1.0	90	88.33	1.67
1.6	90	88.59	1.41
2.0	90	88.95	1.05
2.5	90	89.20	0.80
3.0	90	89.43	0.57

Table 4.16 Springback results in terms of part angle for V-Bending to 120˚

AA 6061 O at 120˚ V - Bending			
Thickness (mm)	Bend angle (˚)	Part angle (˚)	Springback (˚)
1.0	120	116.04	3.96
1.6	120	116.83	3.17
2.0	120	117.39	2.61
2.5	120	117.86	2.14
3.0	120	118.54	1.46

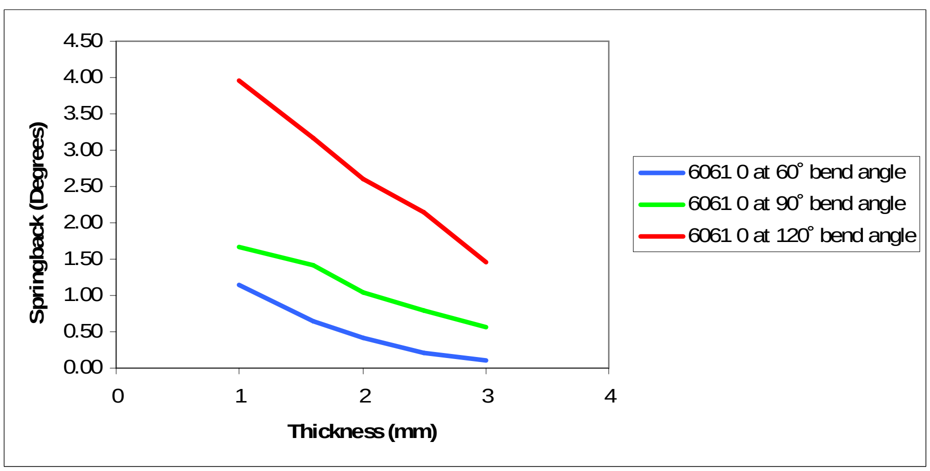

Figure 4.58 Springback data of AA6061 O for V-bending.

In Figure 5.59 and Figure 5.60, Von Misses Stresses and Total Plastic Strains of AA 6061-O 1.6 mm thick sheet in 60˚ V- bending are illustrated respectively.

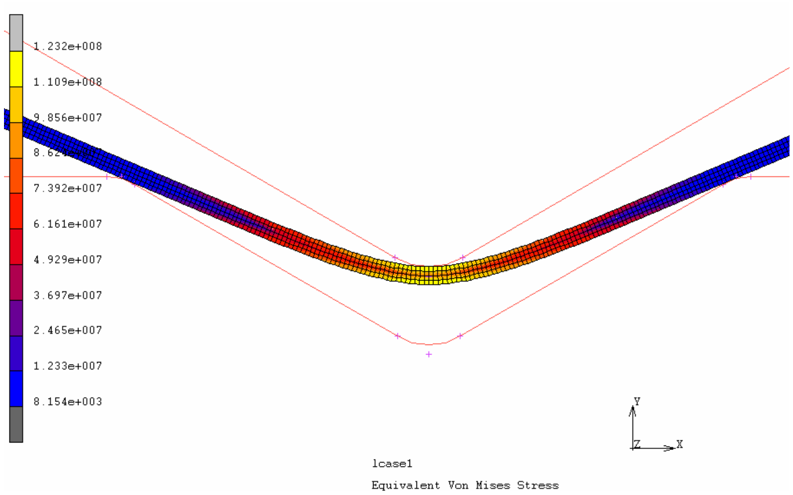

(a)

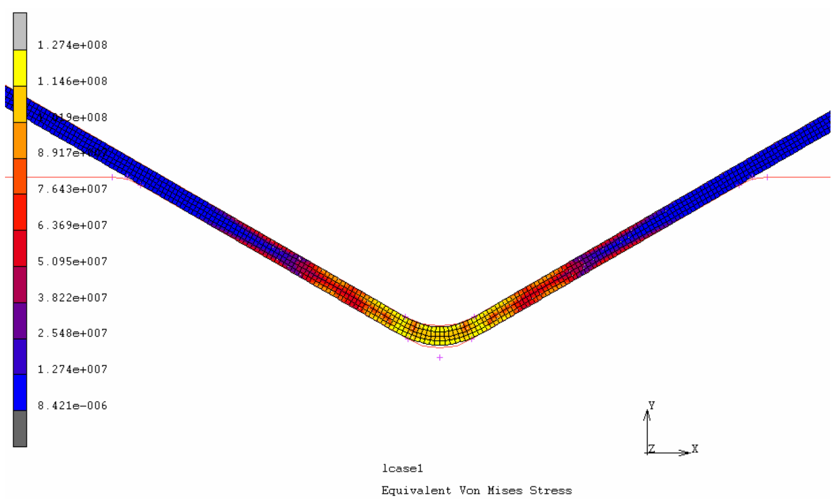

(b)

Figure 4.59 Von Misses stress distribution for AA 6061-O 1.6 mm-thick sheet in 60˚ V- bending at; (a) the intermediate stage, (b) the fully loaded stage

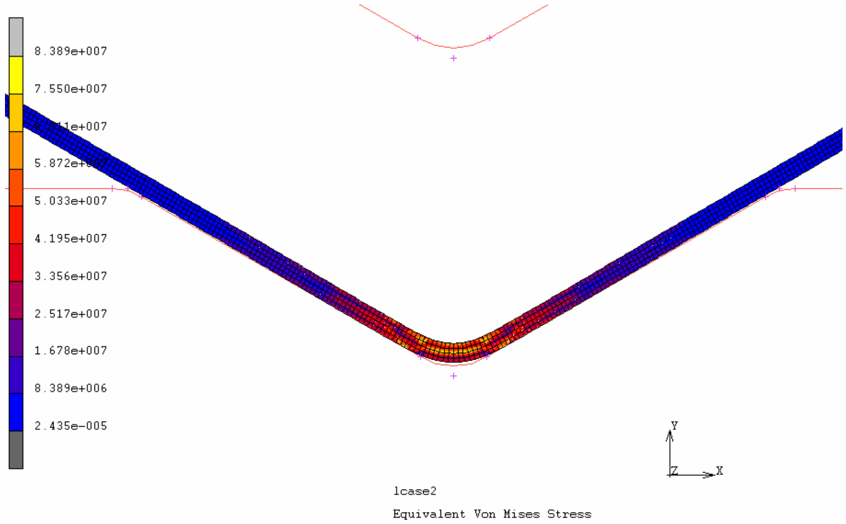

(c)

Figure 4.59 (cont'd) Von Misses stress distribution for AA 6061-O 1.6 mm-thick sheet in 60˚ V- bending at; (c) the unloaded stage.

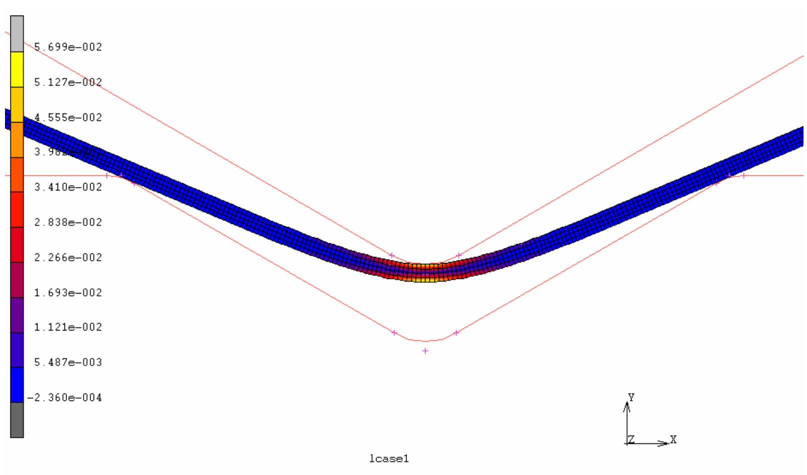

(a)

Figure 4.60 Total-equivalent plastic strain distribution for AA 6061-O 1.6 mm-thick sheet in 60˚ V- bending at; (a) intermediate stage

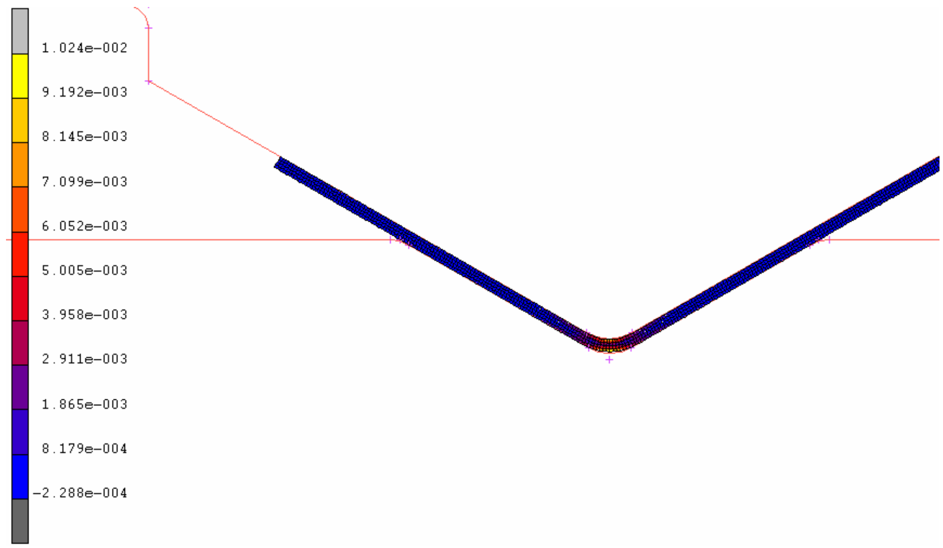

(b)

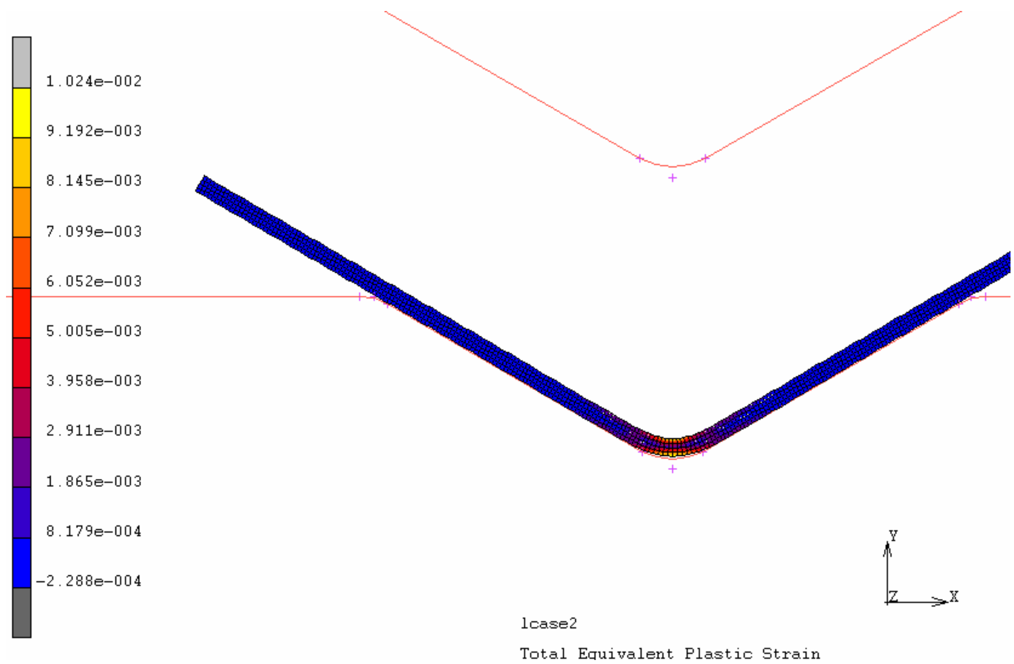

(c)

Figure 4.60 (cont'd) Total-equivalent plastic strain distribution for AA 6061-O 1.6 mm-thick sheet in 60˚ V- bending at; (b) the fully loaded stage, (c) the unloaded stage

In Figure 4.61 and Figure 4.62, Von Misses Stresses and Total Plastic Strains in 6061 O 1.6 mm thick sheet in 90˚ V- bending are illustrated respectively.

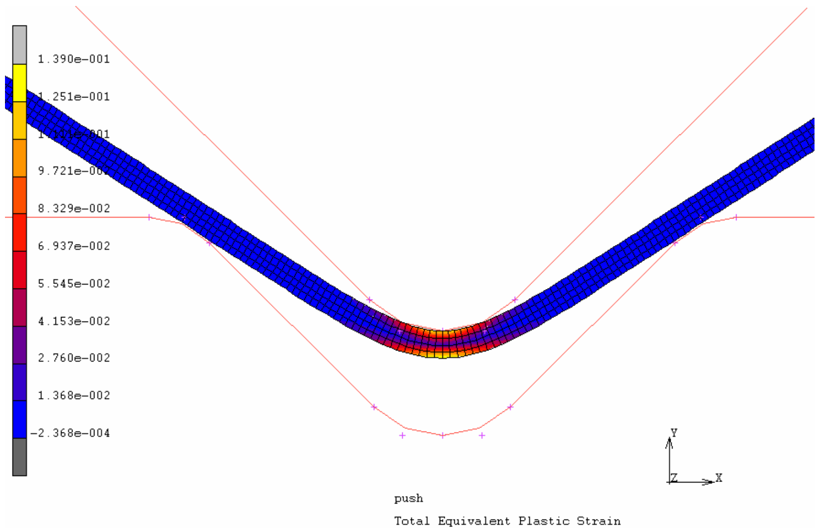

(a)

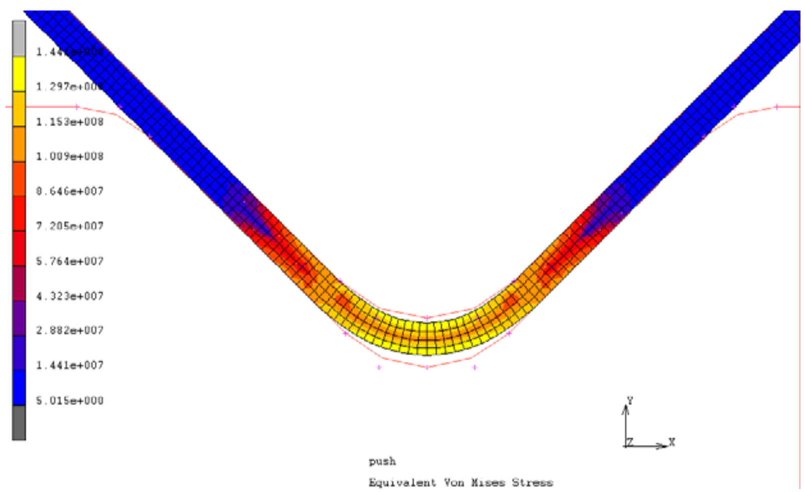

(b)

Figure 4.61 Von Misses stress distribution for AA 6061 O 1.6 mm-thick sheet in 90˚ V- bending at; (a) the intermediate stage, (b) the fully loaded stage

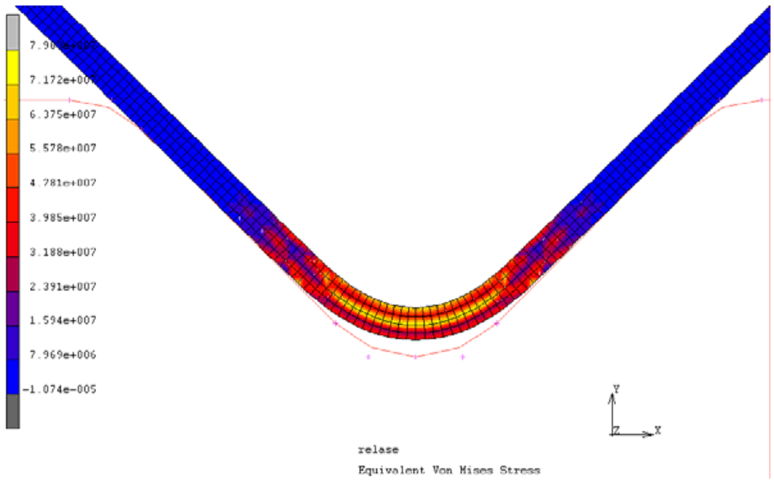

(c)

Figure 4.61 (cont'd) Von Misses stress distribution for AA 6061 O 1.6 mm-thick sheet in 90˚ V- bending at; (c) the unloaded stage

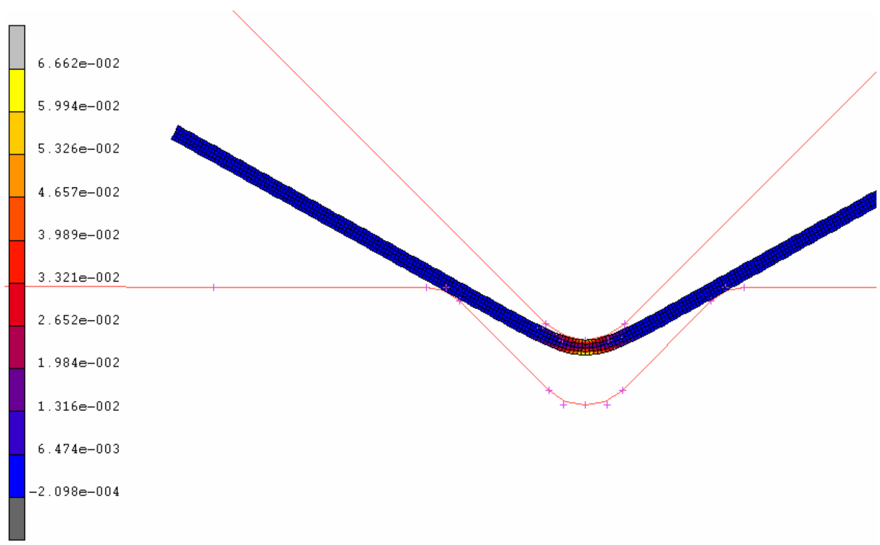

(a)

Figure 4.62 Total-equivalent plastic strain distribution for AA 6061-O 1.6 mm-thick sheet in 90˚ V- bending at; (a) the intermediate stage

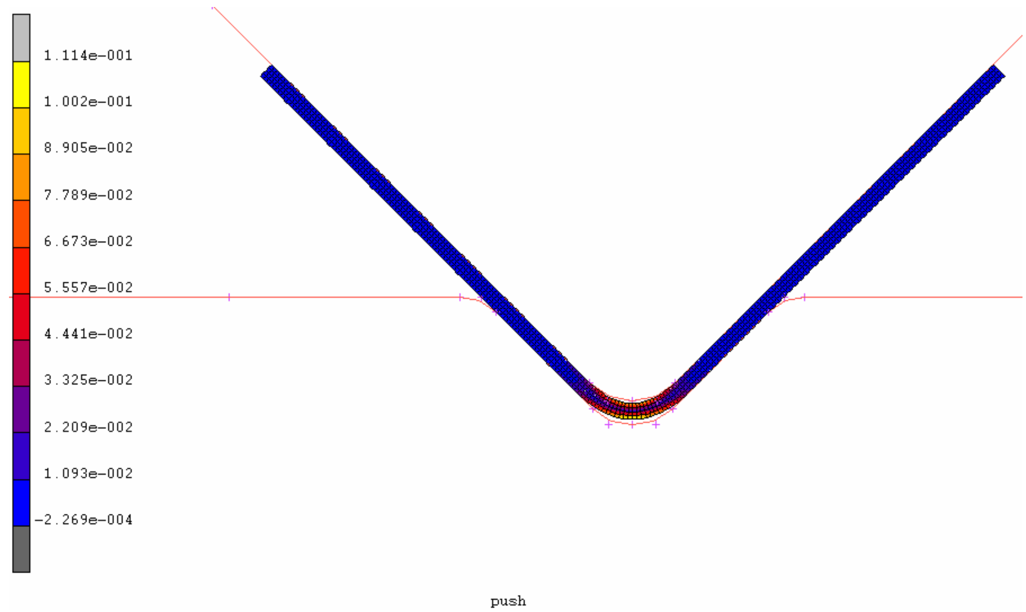

(b)

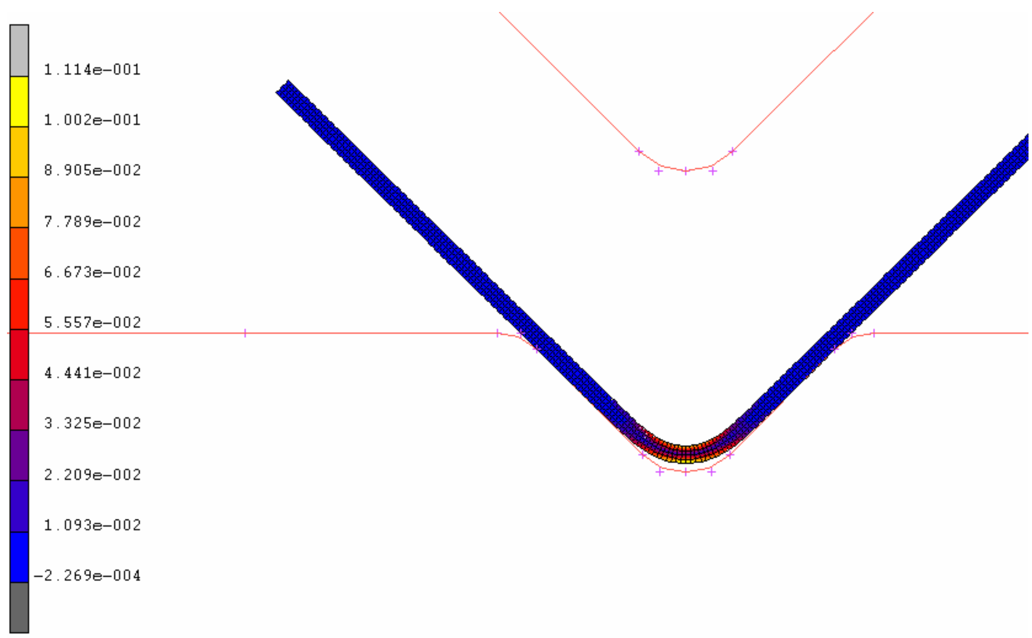

(c)

Figure 4.62 (cont'd) Total-equivalent plastic strain distribution for AA 6061-O 1.6 mm-thick sheet in 90˚ V- bending at;, (b) the fully loaded stage, (c) the unloaded stage

In Figure 4.63 and Figure 4.64, Von Misses Stresses and Total Plastic Strains in 6061 O 1.6 mm thick sheet in 120˚ V- bending are illustrated respectively.

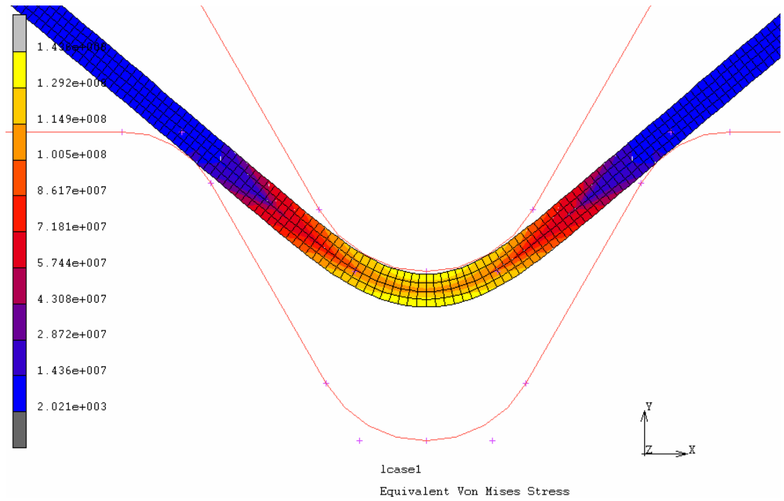

(a)

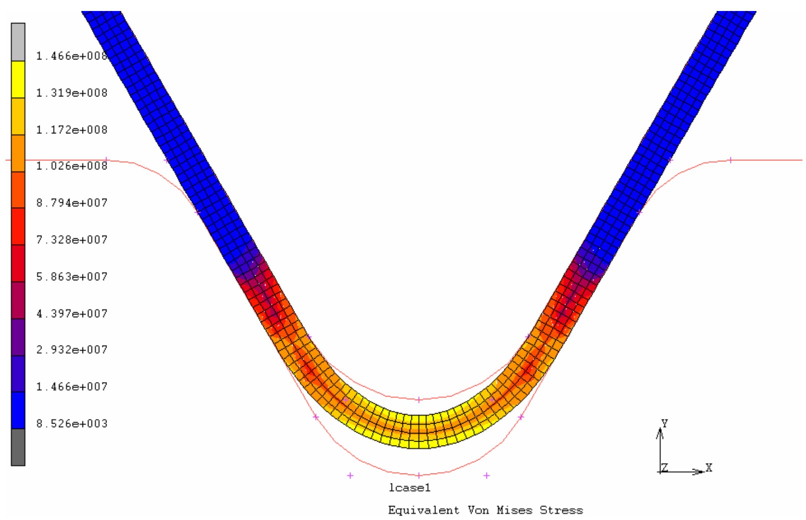

(b)

Figure 4.63 Von Misses stress distribution for AA 6061-O 1.6 mm-thick sheet in 120˚ V- bending at; (a) the intermediate stage, (b) the fully loaded stage

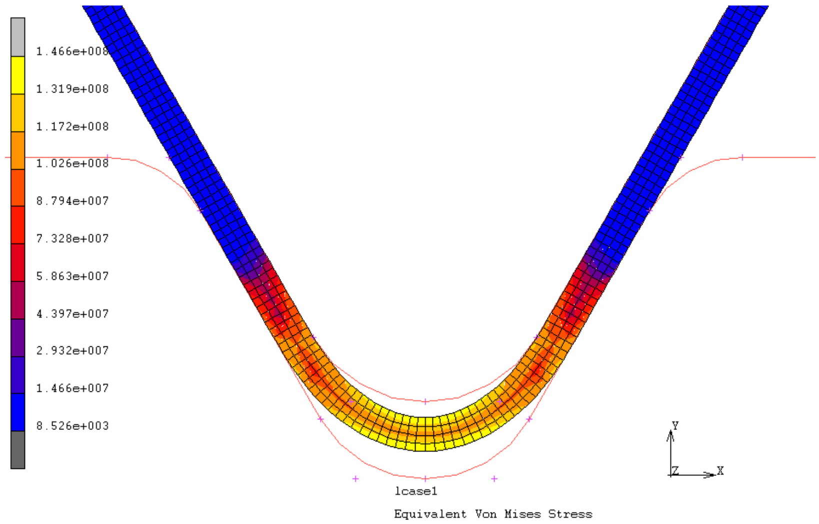

(c)

Figure 4.63 (cont'd) Von Misses stress distribution for AA 6061-O 1.6 mm-thick sheet in 120˚ V- bending at; (c) the unloaded stage

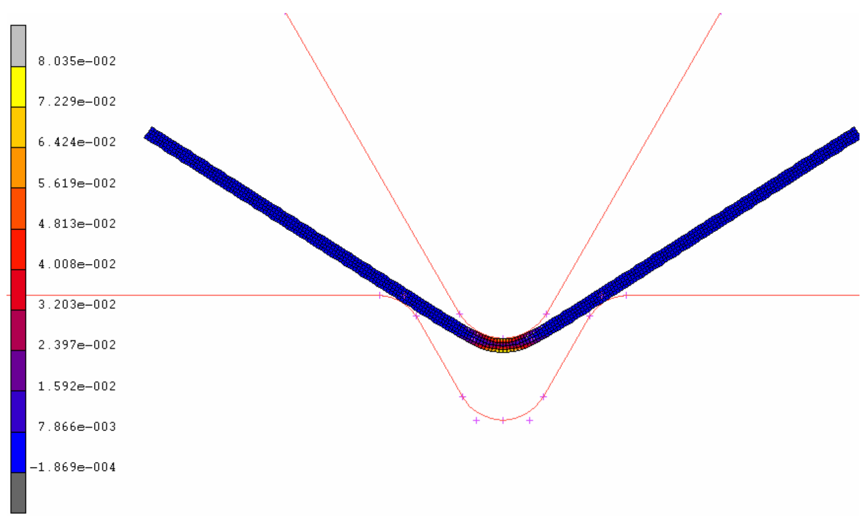

(a)

Figure 4.64 Total-equivalent plastic strain distribution for AA 6061-O 1.6 mm-thick sheet in 120˚ V- bending at; (a) the intermediate stage

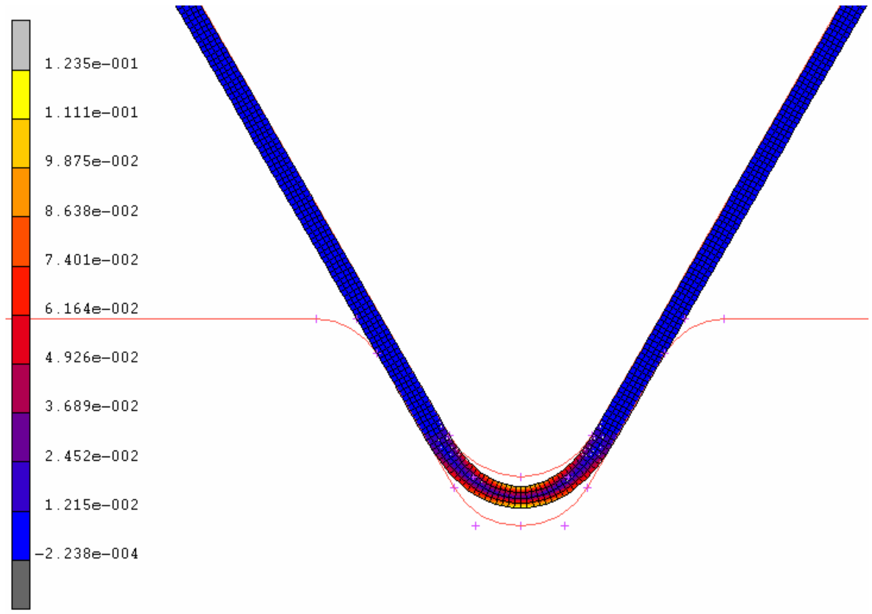

(b)

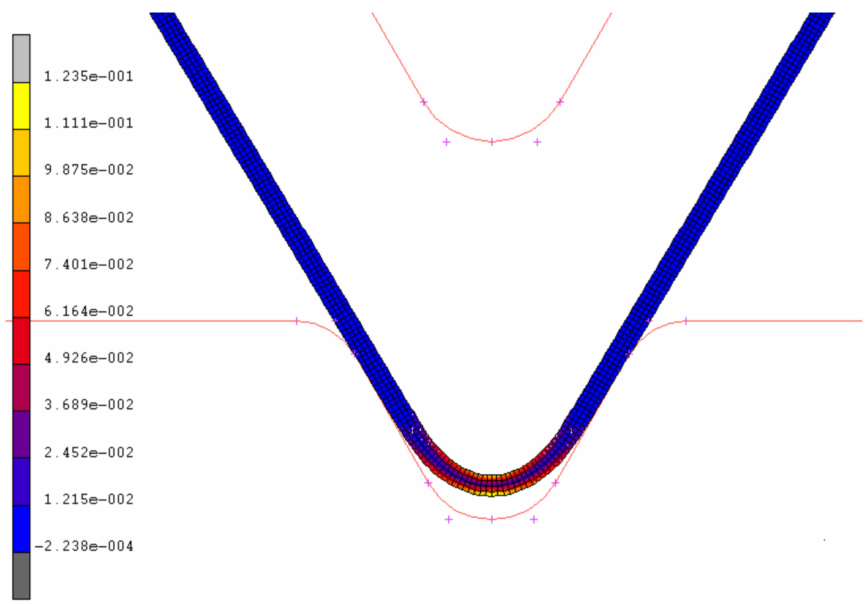

(c)

Figure 4.64 (cont'd) Total-equivalent plastic strain distribution for AA 6061-O 1.6 mm-thick sheet in 120˚ V- bending at; (b) the fully loaded stage, (c) the unloaded stage

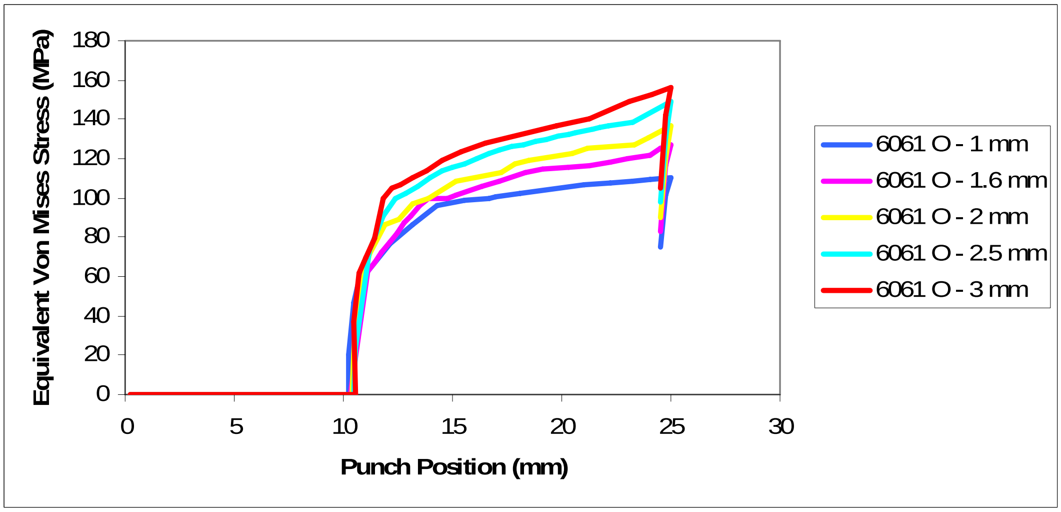

Figure 4.65 Maximum von Mises stresses vs. punch position of AA 6061 O for V-bending to 60˚

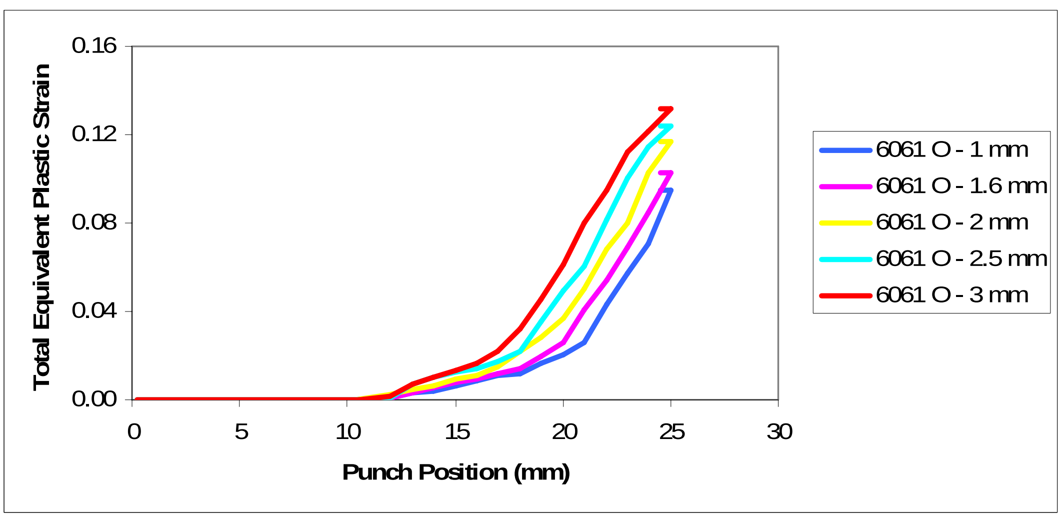

Figure 4.66 Maximum total-equivalent plastic strain vs. punch position of AA 6061 O for V-bending to 60˚

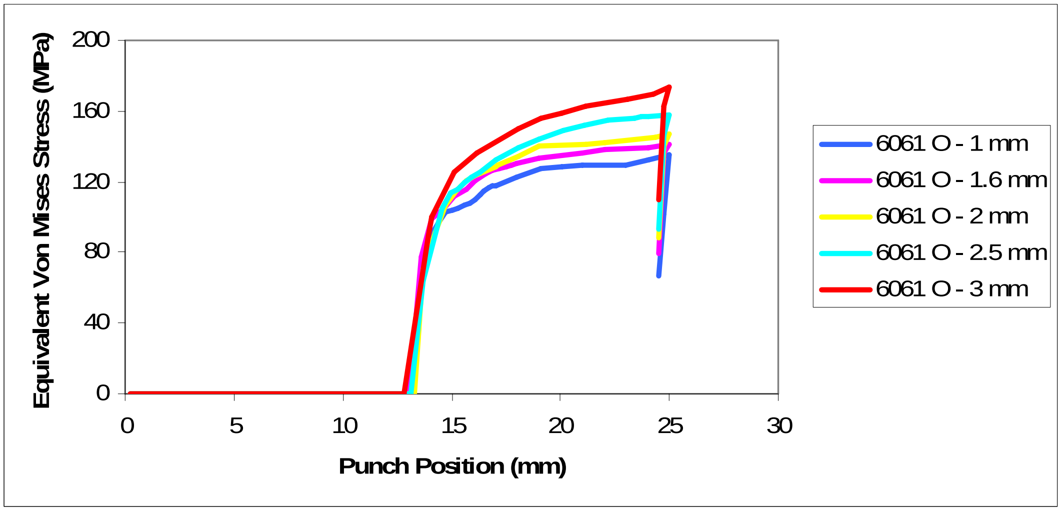

Figure 4.67 Maximum von Mises stresses vs. punch position of AA 6061 O for V-bending to 90˚

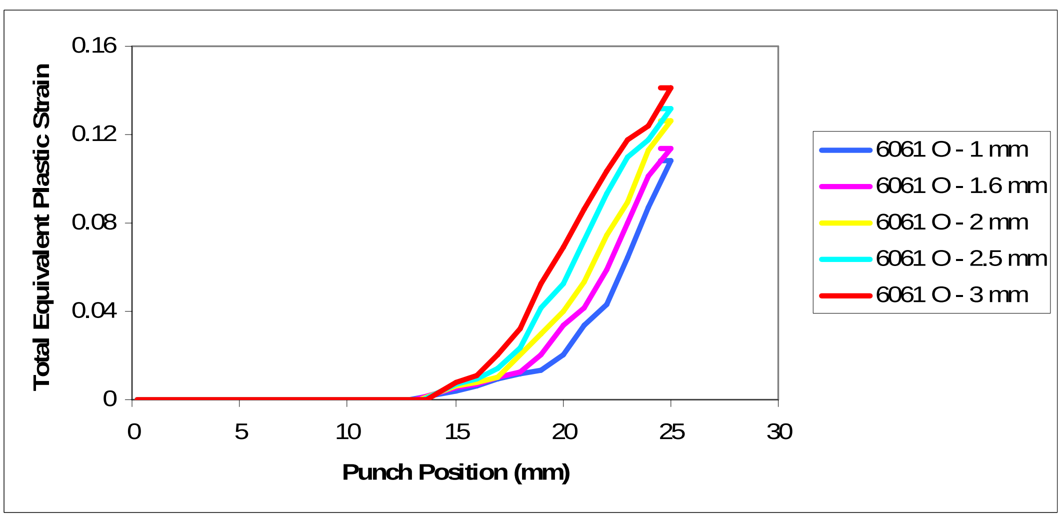

Figure 4.68 Maximum total-equivalent plastic strain vs. punch position of AA 6061 O for V-bending to 90˚

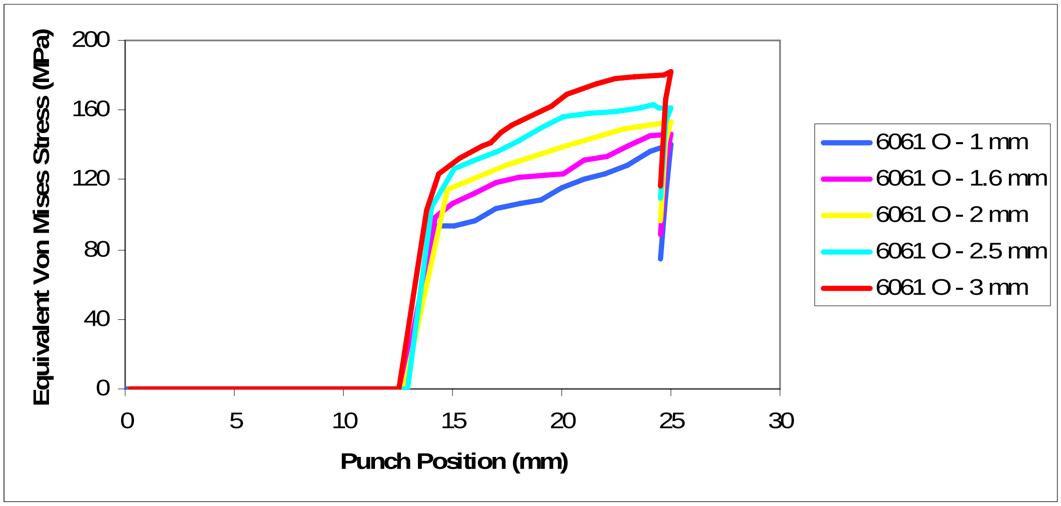

Figure 4.69 Maximum von Mises stresses vs. punch position of AA 6061 O for V-bending to 120˚

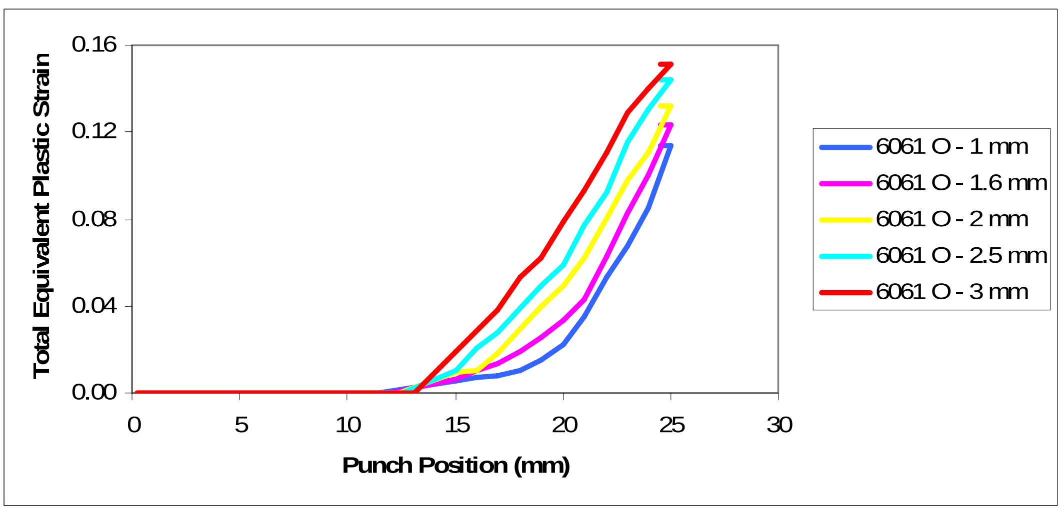

Figure 4.70 Maximum total-equivalent plastic strain vs. punch position of AA 6061 O for V-bending to 120˚

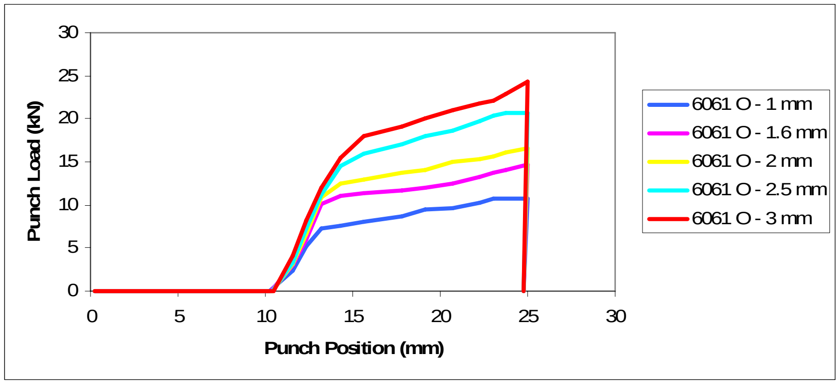

Figure 4.71 Punch load vs. punch position of AA 6061 O for V-bending to 60˚

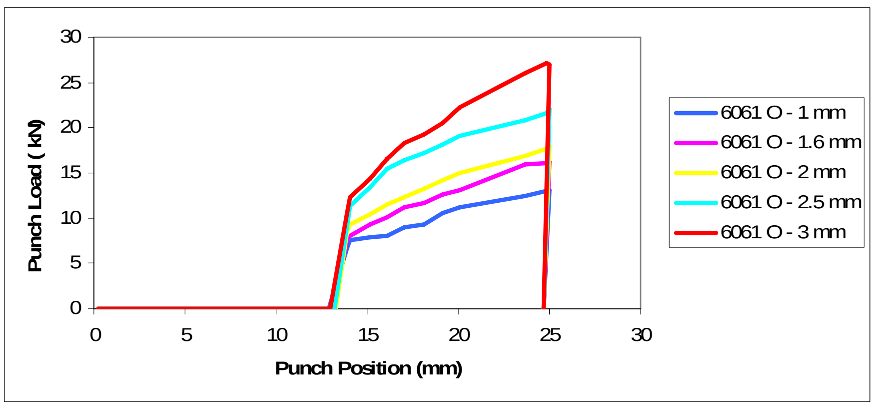

Figure 4.72 Punch load vs. punch position of AA 6061 O for V-bending to 90˚

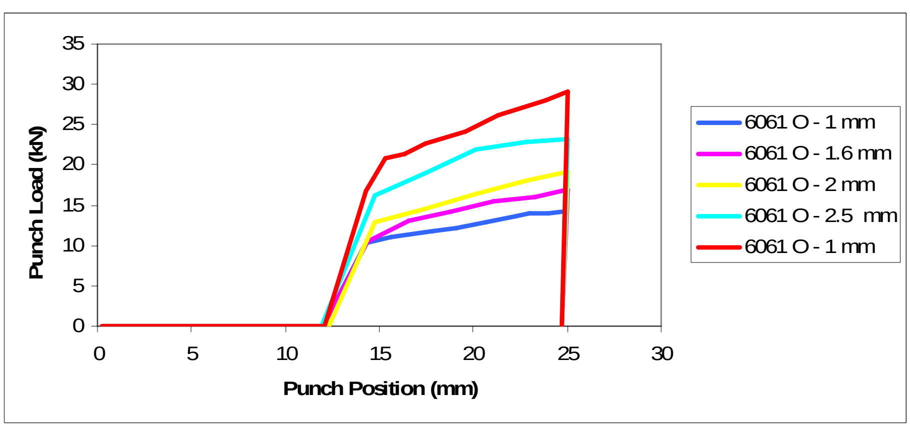

Figure 4.73 Punch load vs. punch position of AA 6061 O for V-bending to 120˚

4.2.5. V-bending of AA 6061 at T4 condition.

In this study, five different thicknesses of AA 6061-T4 are bent to 60°, 90° and 120° with a punch moving vertically downwards. Mechanical properties of the alloy are given in Table 4.17.

Table 4.17 Mechanical properties of AA 6061-T4

Material	Temper	Elasticity Modulus (GPa)	Yield Strength (MPa)	Poisson's Ratio
AA 6061	T4	68.9	145	0.33

In this part of the study, aluminum sheets at T4 condition with a length of 100 mm, a width of 50 mm and thicknesses of 1, 1.6, 2, 2.5 and 3 mm. were analyzed. Amount of springback is determined and tabulated and graphically illustrated in, Table 4.18, Table 4.19, Table 4.20 and Figure 4.74. Total equivalent plastic strains and equivalent Von Misses stresses occurring, at different angles, in the sheets are gathered from the finite elements analyses are illustrated graphically in Figure 4.81, Figure 4.82, Figure 4.83, Figure 4.84, Figure 4.85 and Figure 4.86. Also, punch loads for each case are also represented in Figure 4.87, Figure 4.88 and Figure 4.89

.

Table 4.18 Springback results in terms of part angle for V-Bending to 60°

AA 6061T4 at 60° V - Bending			
Thickness (mm)	Bend angle (°)	Part angle (°)	Springback (°)
1.0	60	57.36	2.64
1.6	60	58.29	1.71
2.0	60	58.90	1.10
2.5	60	59.48	0.52
3.0	60	59.68	0.32

Table 4.19 Springback results in terms of part angle for V-Bending to 90˚

AA 6061T4 at 90˚ V - Bending			
Thickness (mm)	Bend angle (˚)	Part angle (˚)	Springback (˚)
1.0	90	85.63	4.37
1.6	90	86.30	3.70
2.0	90	87.25	2.75
2.5	90	87.92	2.08
3.0	90	88.51	1.49

Table 4.20 Springback results in terms of part angle for V-Bending to 120˚

AA 6061T4 at 120˚ V - Bending			
Thickness (mm)	Bend angle (˚)	Part angle (˚)	Springback (˚)
1.0	120	111.46	8.54
1.6	120	112.25	7.75
2.0	120	113.22	6.78
2.5	120	113.87	6.13
3.0	120	114.56	5.44

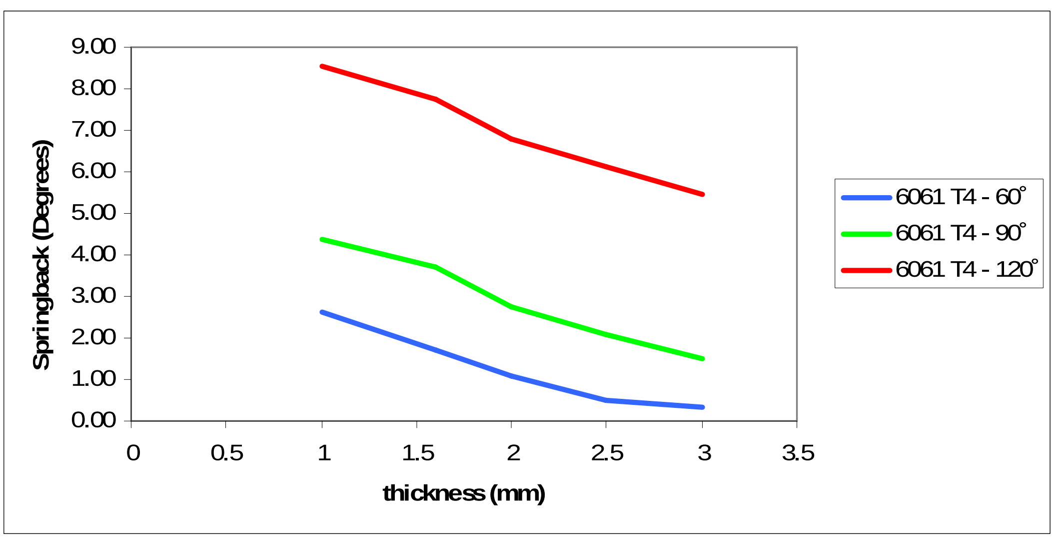

Figure 4.74 Springback data of AA6061 T4 for V-bending.

In Figure 4.75 and Figure 4.76, Von Misses Stresses and Total Plastic Strains of AA 6061-T4 1.6 mm thick sheet in 60˚ V- bending are illustrated respectively.

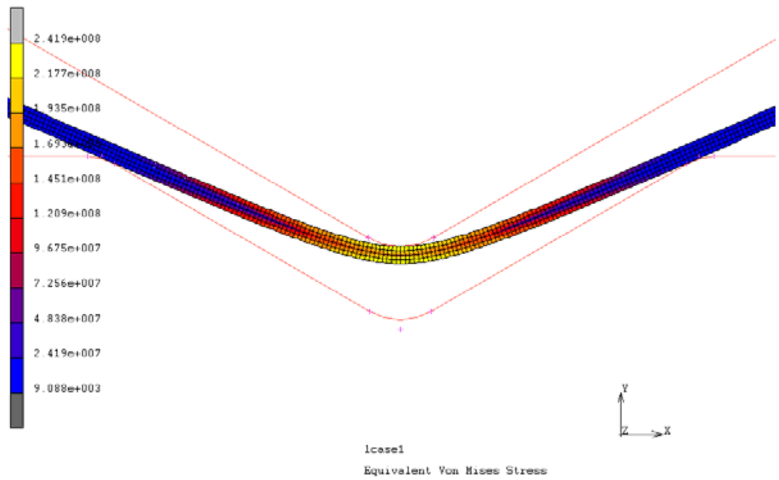

(a)

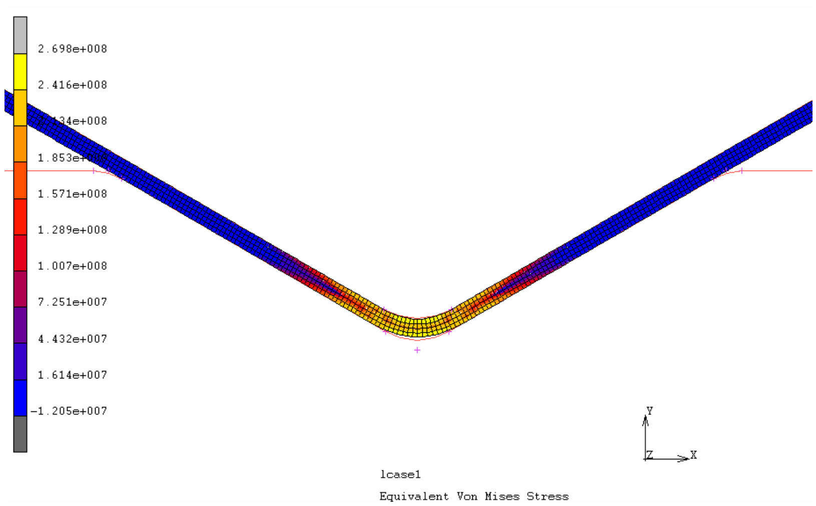

(b)

Figure 4.75 Von Misses stress distribution for AA 6061-T4 1.6 mm-thick sheet, 60˚ V- bending at; (a) the intermediate stage, (b) the fully loaded stage

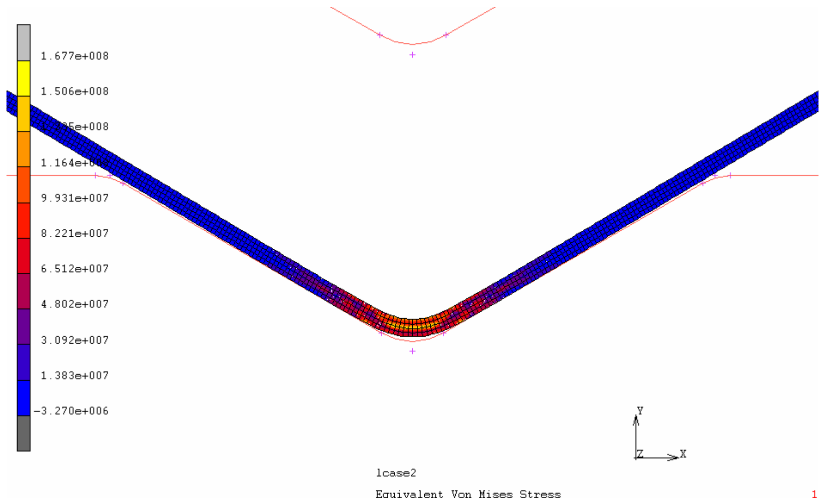

(c)

Figure 4.75 (cont'd) Von Misses stress distribution for AA 6061-T4 1.6 mm-thick sheet, 60˚ V- bending at; (c) the unloaded stage

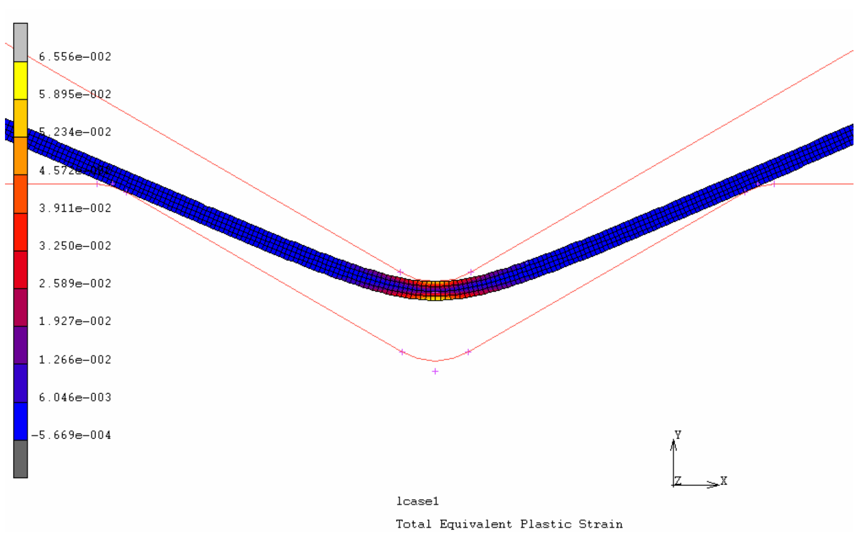

(a)

Figure 4.76 Total-equivalent plastic strain distribution for AA 6061-T4 1.6 mm-thick sheet, 60˚ V- bending at; (a) the intermediate stage

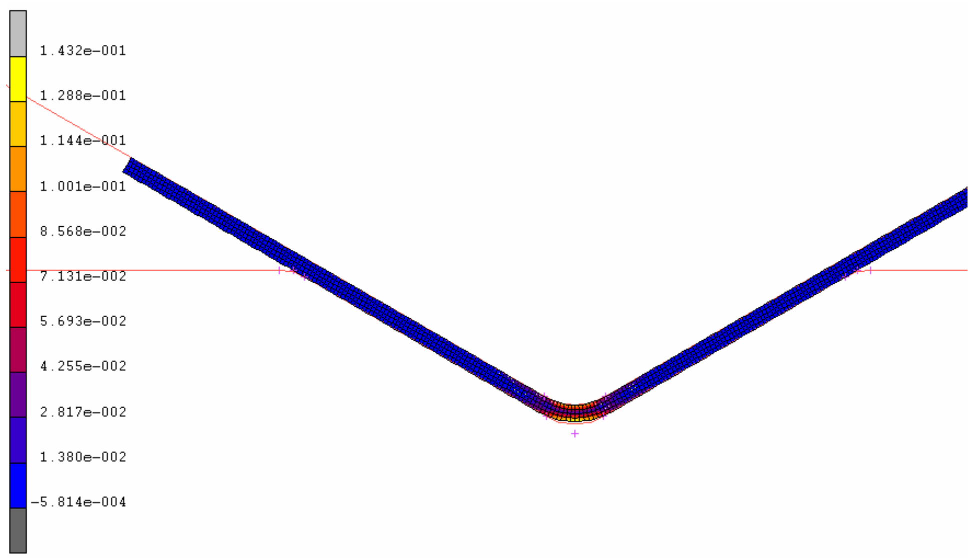

(b)

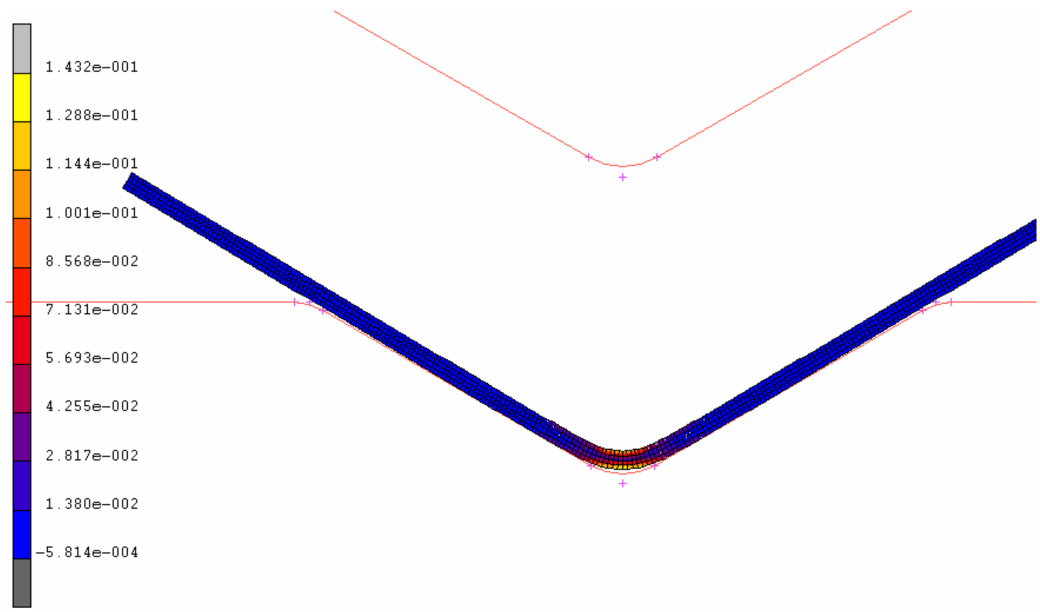

(c)

Figure 4.76 (cont'd) Total-equivalent plastic strain distribution for AA 6061-T4 1.6 mm-thick sheet, 60˚ V- bending at; (b) the fully loaded stage, (c) the unloaded stage

In Figure 4.77 and Figure 4.78, Von Misses Stresses and Total Plastic Strains in AA 6061 T4 1.6 mm thick sheet in 90˚ V- bending are illustrated respectively.

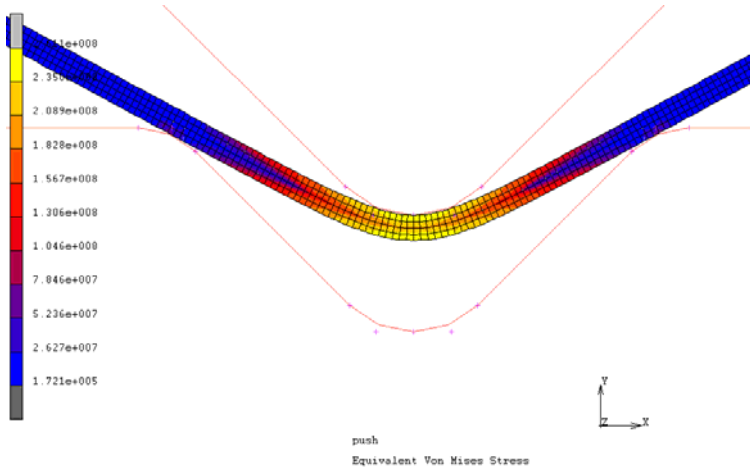

(a)

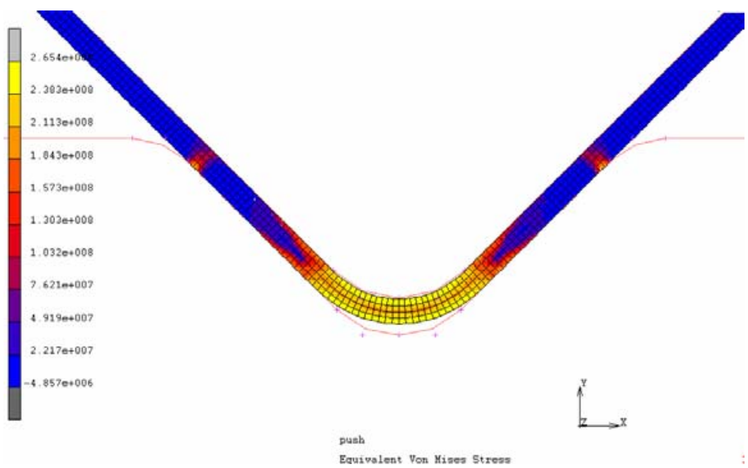

(b)

Figure 4.77 Von Misses stress distribution for in AA 6061 T4 1.6 mm-thick sheet in 90˚ V- bending at; (a) the intermediate stage, (b) the fully loaded stage

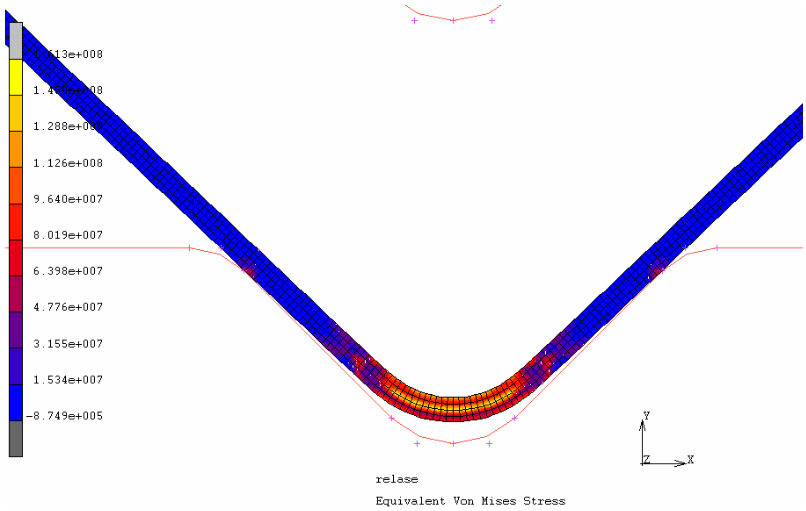

(c)

Figure 4.77 (cont'd) Von Misses stress distribution for in AA 6061 T4 1.6 mm-thick sheet in 90˚ V- bending at; (c) the unloaded stage

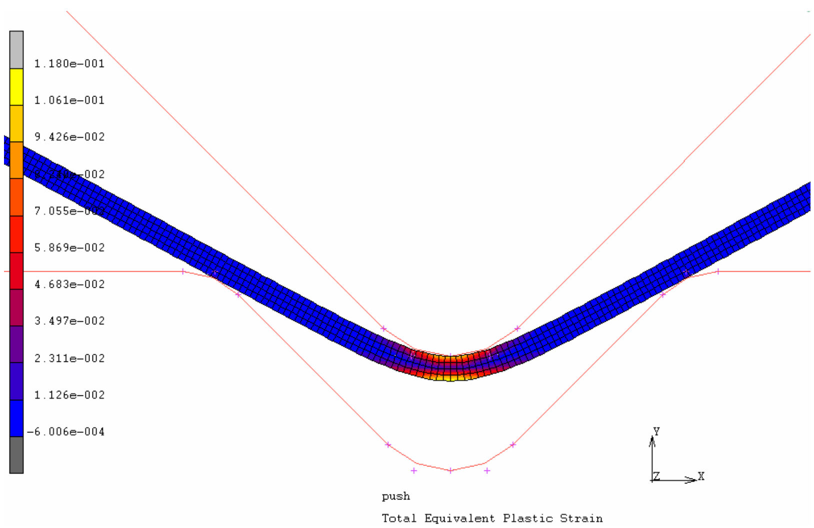

(a)

Figure 4.78 Total-equivalent plastic strain distribution for in AA 6061-T4 1.6 mm-thick sheet in 90˚ V- bending at; (a) the intermediate stage

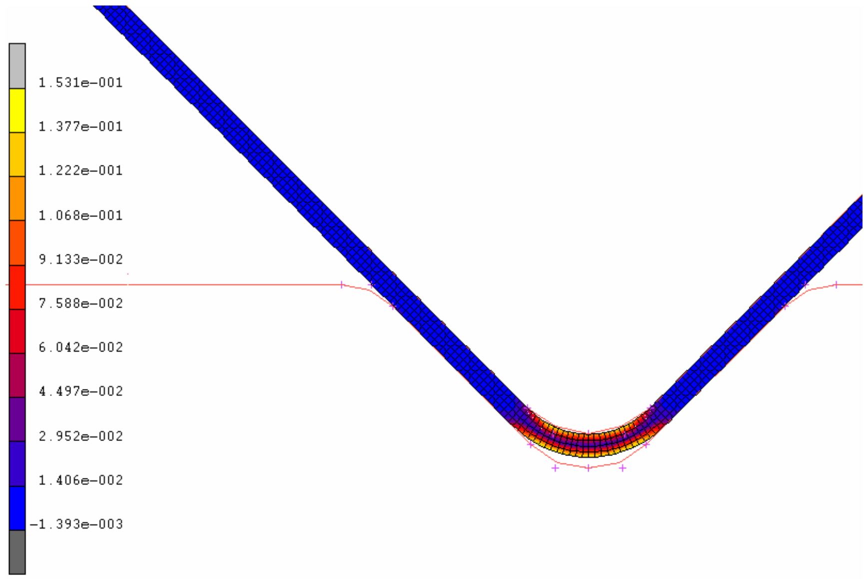

(b)

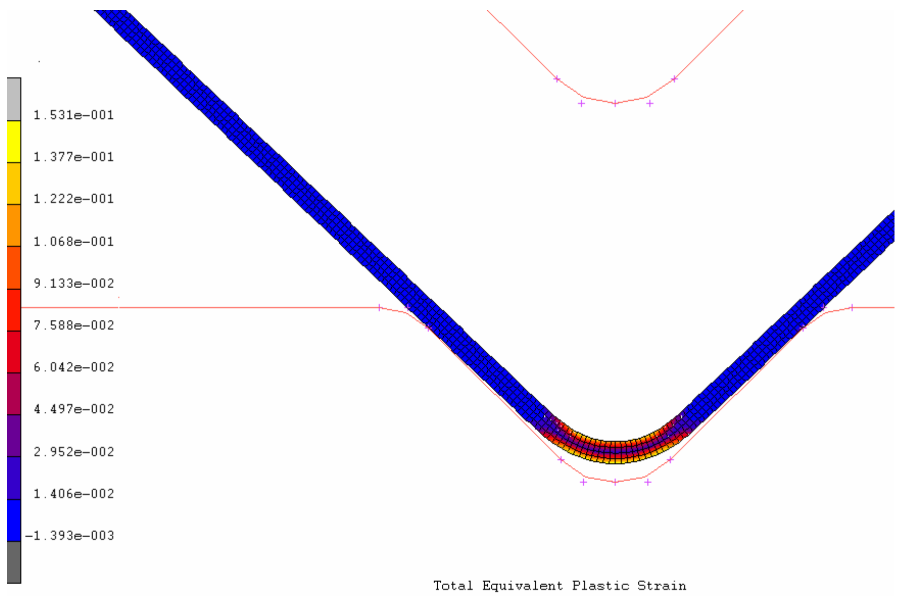

(c)

Figure 4.78 (cont'd) Total-equivalent plastic strain distribution for in AA 6061-T4 1.6 mm-thick sheet in 90˚ V- bending at; (b) the fully loaded stage, (c) the unloaded stage.

In Figure 4.79 and Figure 4.80, Von Misses Stresses and Total Plastic Strains in 6061 T4 1.6 mm thick sheet in 120˚ V- bending are illustrated respectively.

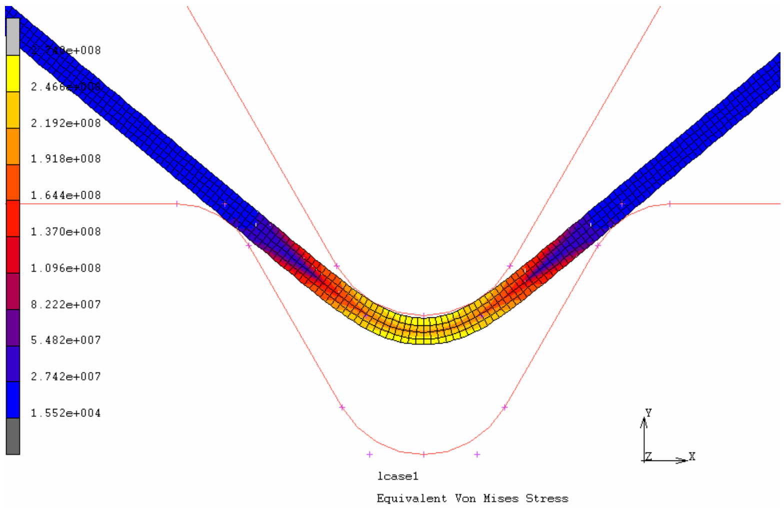

(a)

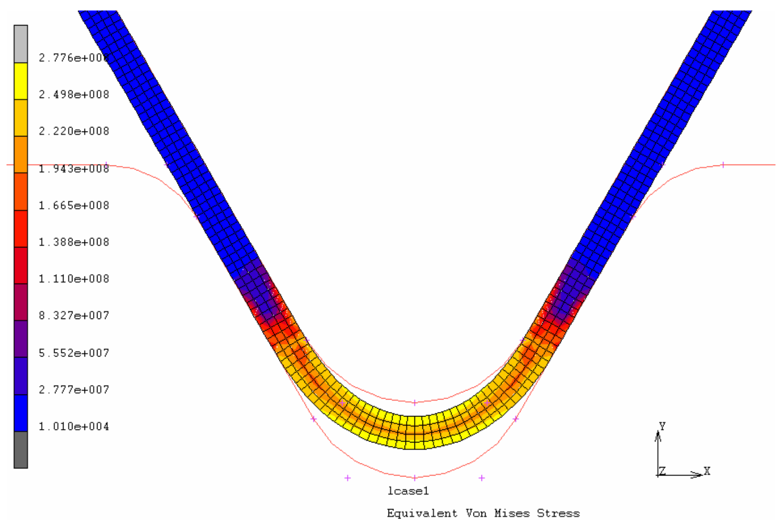

(b)

Figure 4.79 Von Misses stress distribution for in AA 6061-T4 1.6 mm-thick sheet in 120˚ V- bending at; (a) the intermediate stage, (b) the fully loaded stage

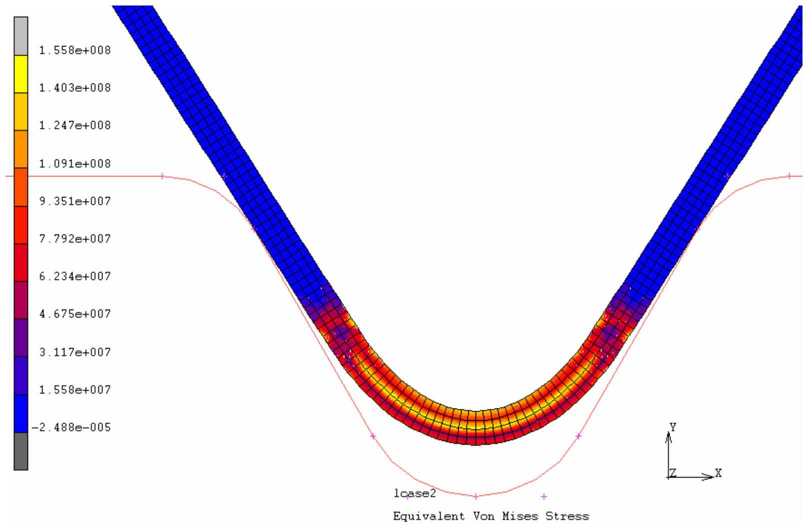

(c)

Figure 4.79 (cont'd) Von Misses stress distribution for in AA 6061-T4 1.6 mm-thick sheet in 120˚ V- bending at; (c) the unloaded stage

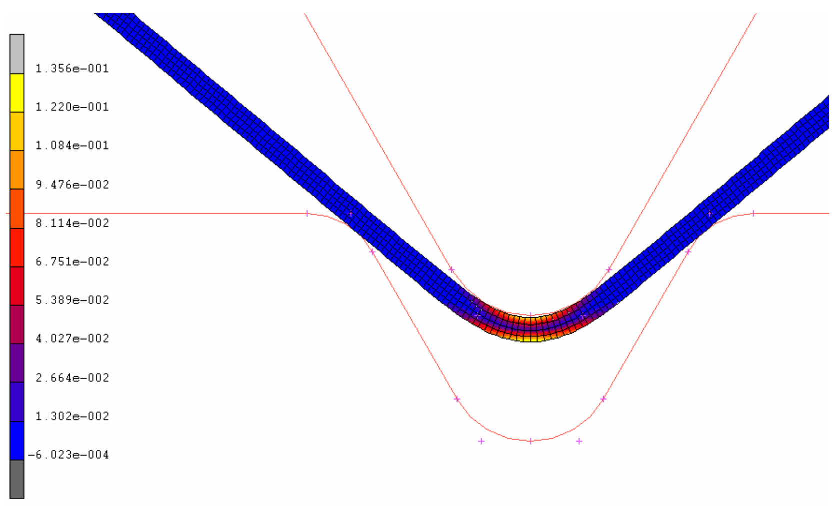

(a)

Figure 4.80 Total-equivalent plastic strain distribution for in AA 6061-T4 1.6 mm-thick sheet in 120˚ V- bending at; (a) the intermediate stage

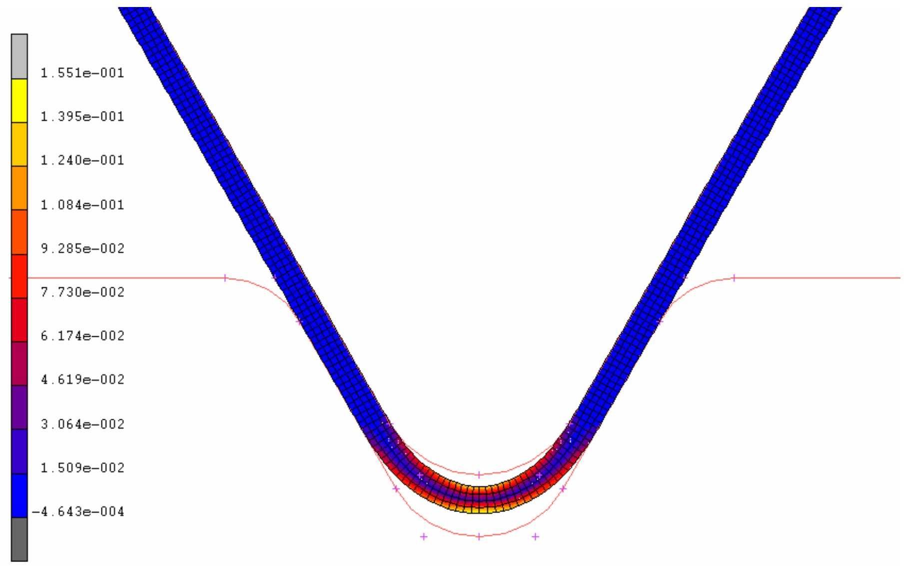

(b)

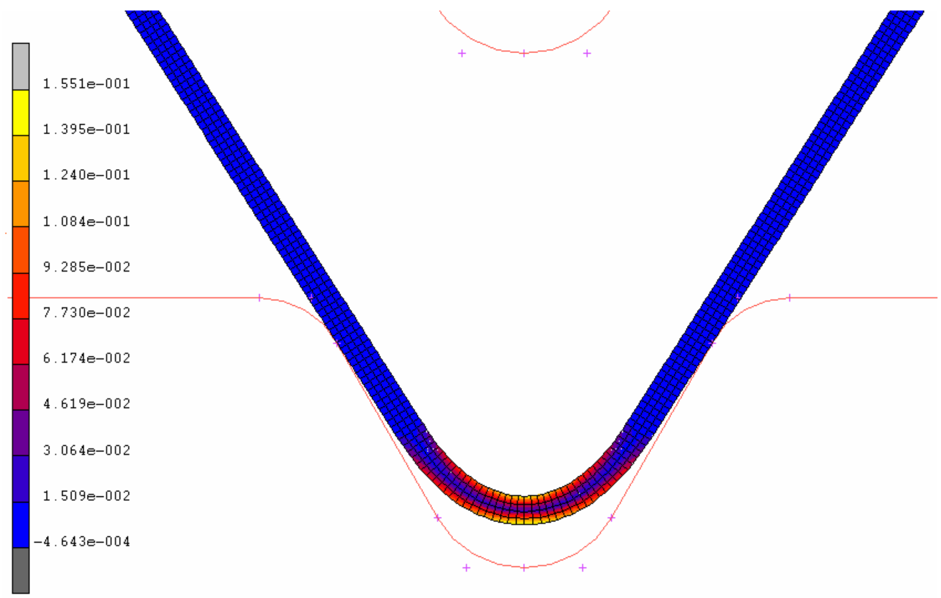

(c)

Figure 4.80 (cont'd) Total-equivalent plastic strain distribution for in AA 6061-T4 1.6 mm-thick sheet in 120˚ V- bending at; (b) the fully loaded stage, (c) the unloaded stage.

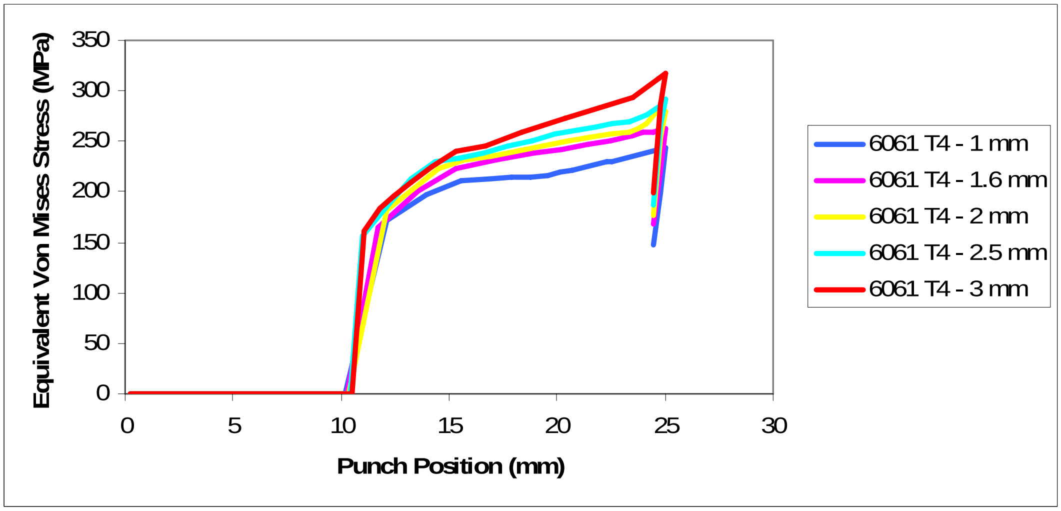

Figure 4.81 Maximum von Mises stresses vs. punch position of AA 6061 T4 for V-bending to 60˚

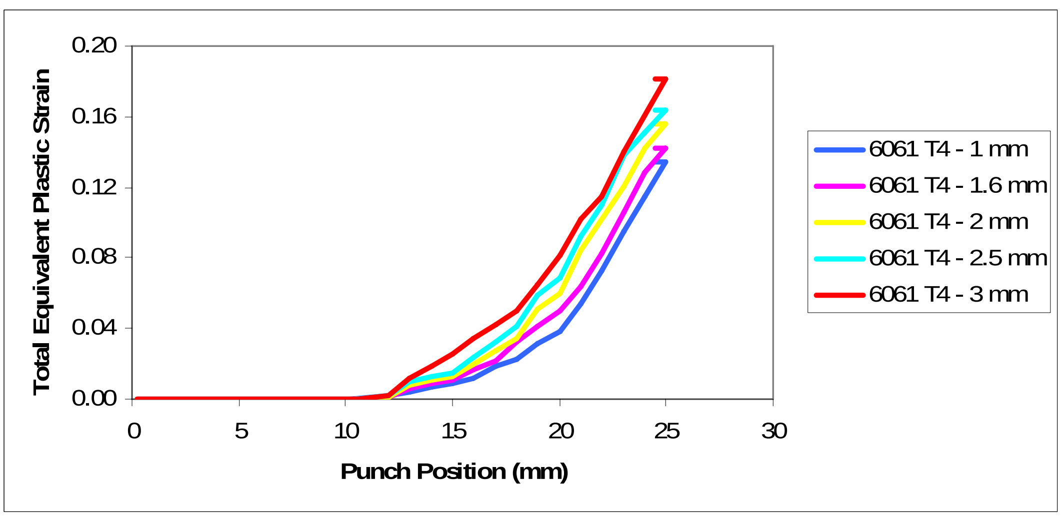

Figure 4.82 Maximum total-equivalent plastic strain vs. punch position of AA 6061 T4 for V-bending to 60˚

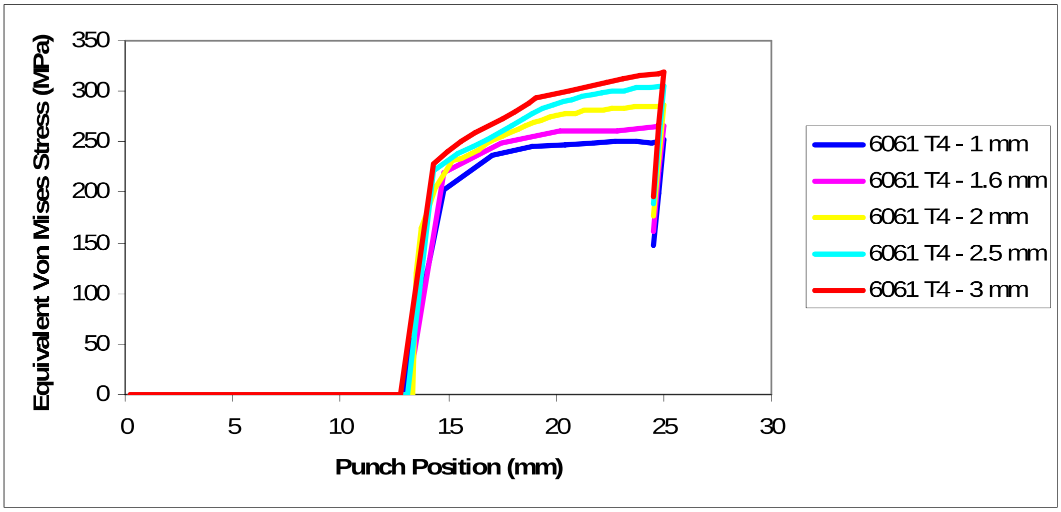

Figure 4.83 Maximum von Mises stresses vs. punch position of AA 6061 T4 for V-bending to 90˚

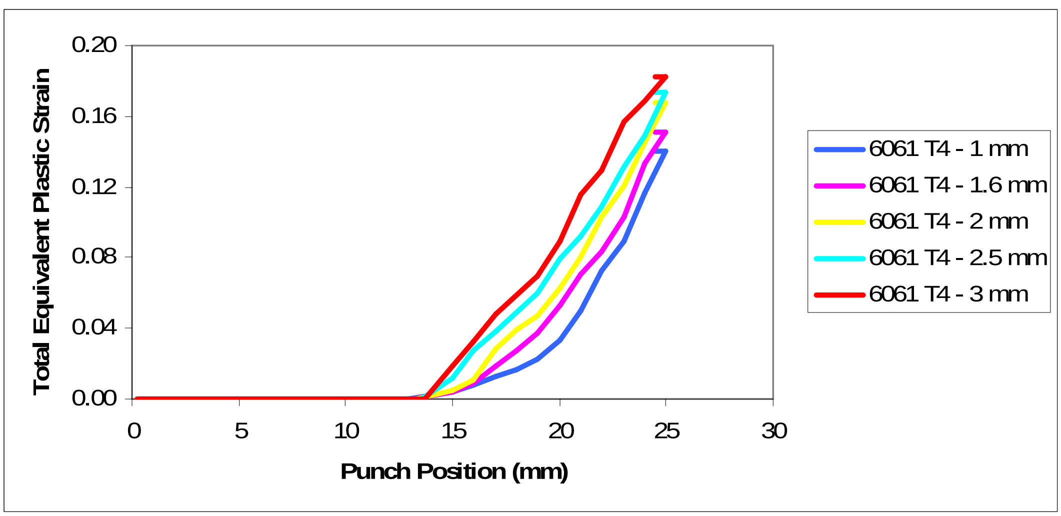

Figure 4.84 Maximum total-equivalent plastic strain vs. punch position of AA 6061 T4 for V-bending to 90˚

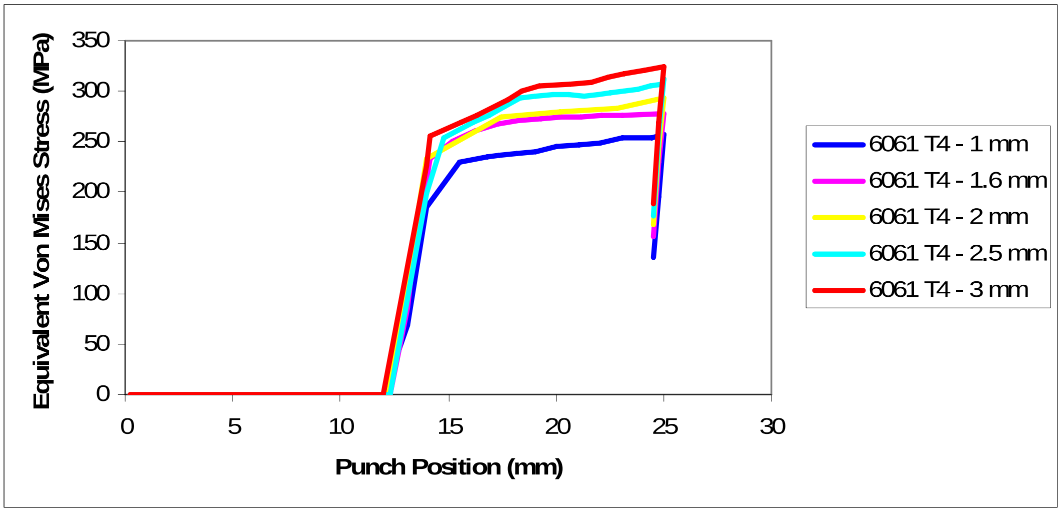

Figure 4.85 Maximum von Mises stresses vs. punch position of 6061 T4 for V-bending to 120˚

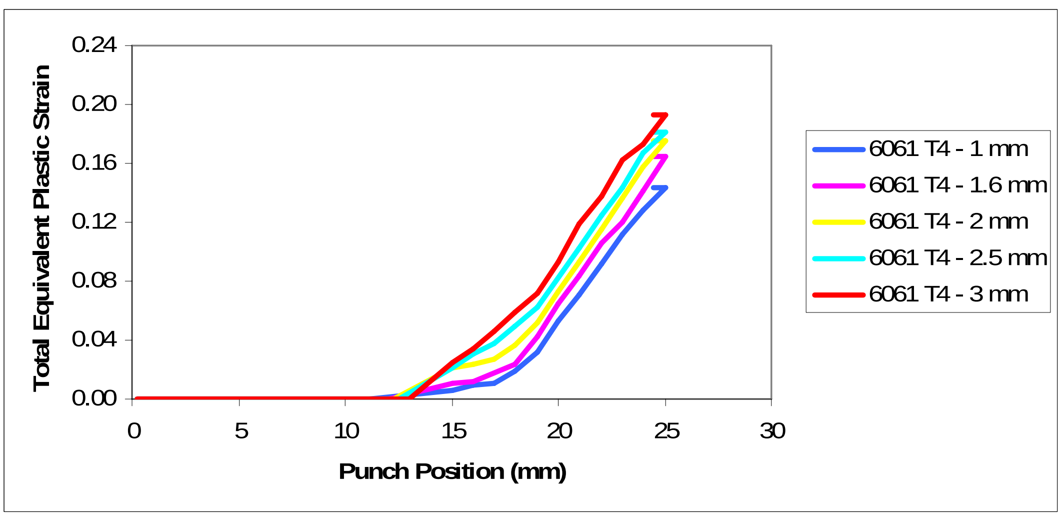

Figure 4.86 Maximum total-equivalent plastic strain vs. punch position of 6061 T4 for V bending to 120˚

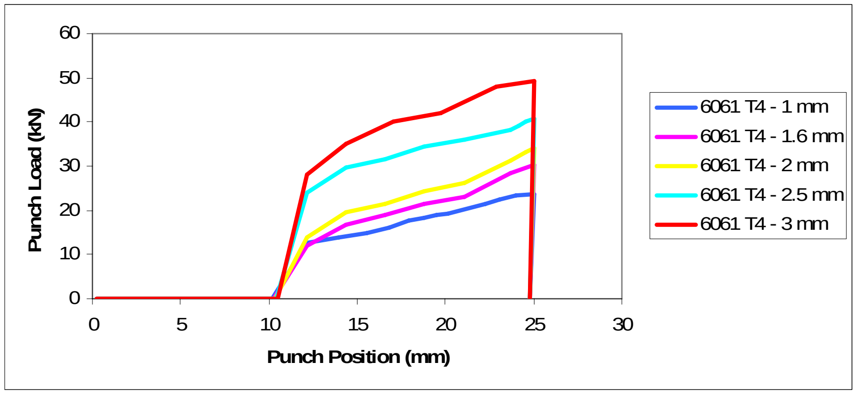

Figure 4.87 Punch load vs. punch position of AA 6061 T4 for V bending to 60˚

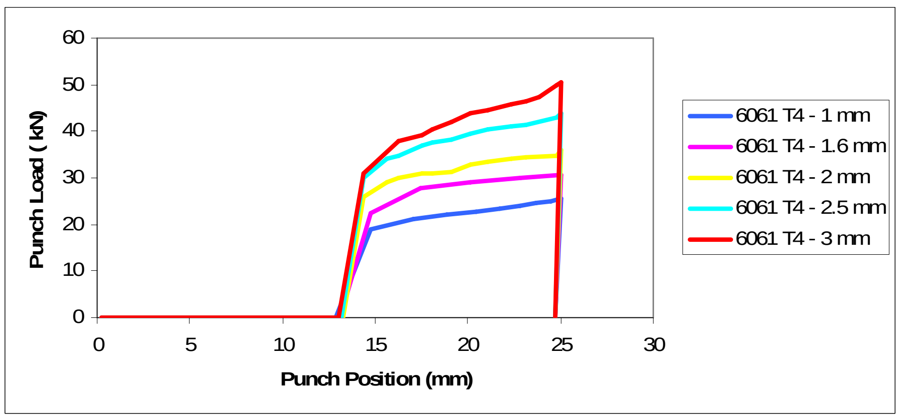

Figure 4.88 Punch load vs. punch position of AA 6061 T4 for V bending to 90˚

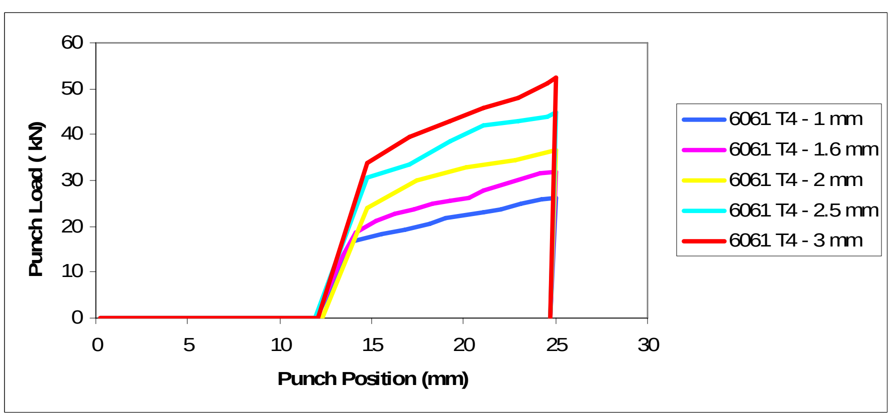

Figure 4.89 Punch load vs. punch position of AA 6061 T4 for V bending to 120˚

4.2.6. V-bending of AA 6061 at T6 condition.

In this study, five different thicknesses of AA 6061-T6 are bent to 60°, 90° and 120° with a punch moving vertically downwards. Mechanical properties of the alloy are given in Table 4.21

Table 4.21 Mechanical properties of AA 6061-T6

Material	Temper	Elasticity Modulus (GPa)	Yield Strength (MPa)	Poisson's Ratio
AA 6061	T6	68.9	276	0.33

In this case study, aluminum sheets at T6 condition with a length of 100 mm, a width of 50 mm and thicknesses of 1.0 mm, 1.6 mm, 2 mm, 2.5 mm and 3 mm are analyzed. Amount of springback is determined and tabulated and graphically illustrated in Table 4.22, Table 4.23, Table 4.24 and Figure 4.90. Total equivalent plastic strains and equivalent von misses stresses occurring, at different angles, in the sheets are gathered from the finite elements analyses are illustrated graphically in Figure 4.97, Figure 4.98, Figure 4.99, Figure 4.100, Figure 4.101 and Figure 4.102. Also, punch loads for each case are also represented in Figure 4.103, Figure 4.104 and Figure 4.105.

Table 4.22 Springback results in terms of part angle for V-Bending to 60°

AA 6061T6 at 60° V - Bending			
Thickness (mm)	Bend angle ($^\circ$)	Part angle ($^\circ$)	Springback ($^\circ$)
1.0	60	55.58	4.42
1.6	60	56.75	3.25
2.0	60	57.79	2.21
2.5	60	58.66	1.34
3.0	60	59.15	1.02

Table 4.23 Springback results in terms of part angle for V-Bending to 90˚

AA 6061T6 at 90˚ V - Bending			
thickness (mm)	bend angles (degrees)	part angle (degrees)	springback (degrees)
1.0	90	81.70	8.30
1.6	90	82.88	7.12
2.0	90	84.75	5.25
2.5	90	85.82	4.18
3.0	90	87.08	2.92

Table 4.24 Springback results in terms of part angle for V-Bending to 120˚

AA 6061T6 at 120˚ V - Bending			
thickness (mm)	bend angles (degrees)	part angle (degrees)	springback (degrees)
1.0	120	108.84	11.16
1.6	120	109.64	10.36
2.0	120	110.88	9.12
2.5	120	111.71	8.29
3.0	120	112.85	7.15

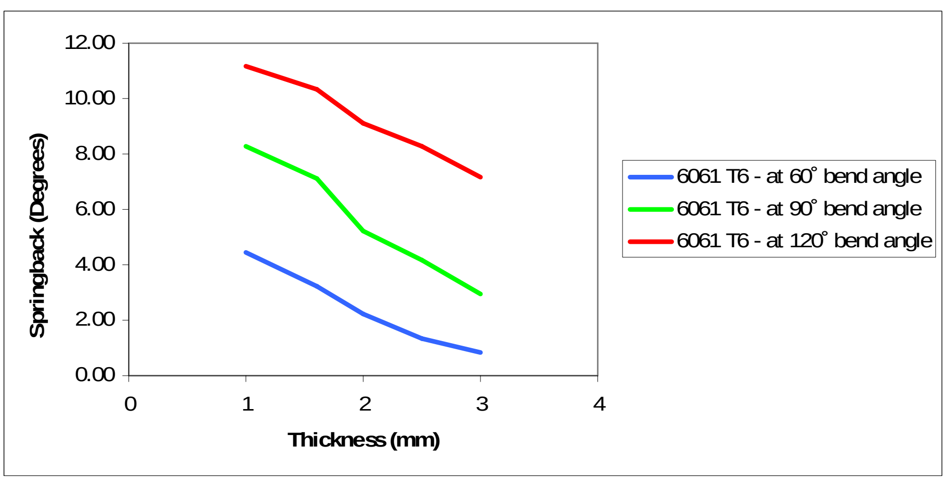

Figure 4.90 Springback data of AA6061 T6 for V-bending.

In Figure 4.91 and Figure 4.92, Von Misses Stresses and total plastic strains in AA 6061-T6 1.6 mm thick sheet in 60˚ V- bending are illustrated respectively.

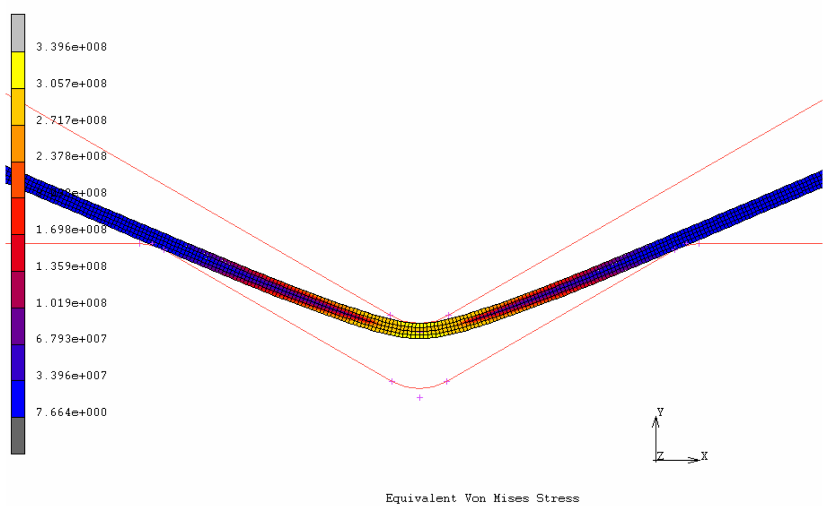

(a)

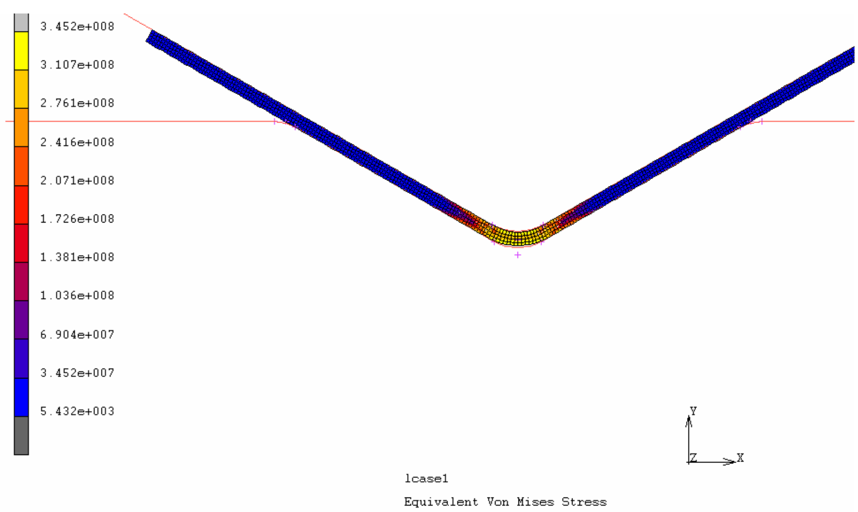

(b)

Figure 4.91 Von Misses stress distribution for AA 6061-T6 1.6 mm-thick sheet in 60˚ V- bending at; (a) the intermediate stage, (b) the fully loaded stage

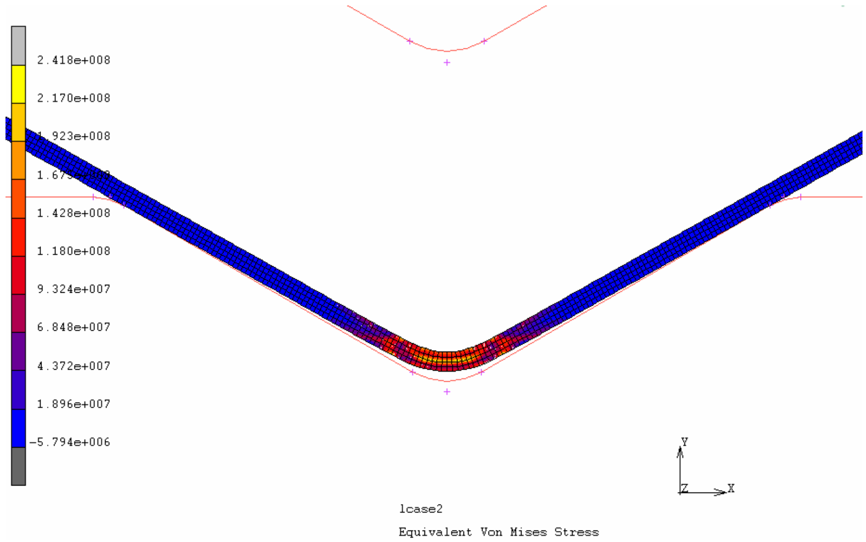

(c)

Figure 4.91 (cont'd) Von Misses stress distribution for AA 6061-T6 1.6 mm-thick sheet in 60˚ V- bending at; (c) the unloaded stage

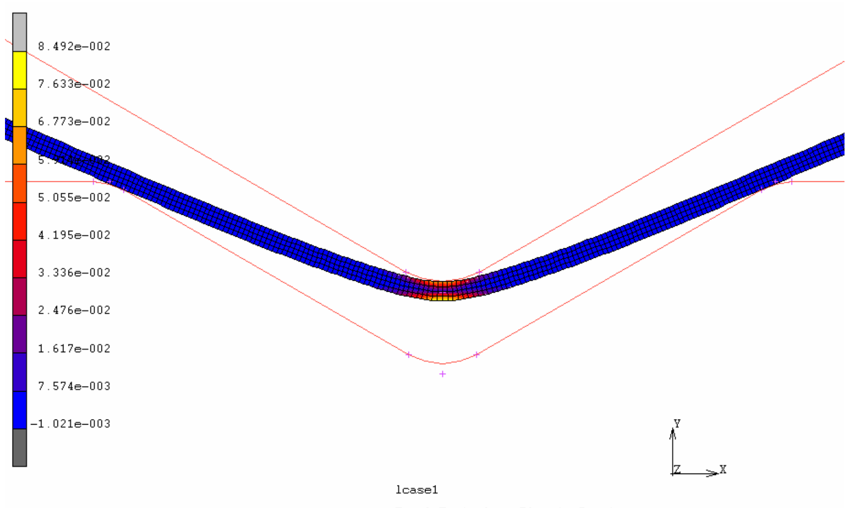

(a)

Figure 4.92 Total-equivalent plastic strain distribution for AA 6061-T6 1.6 mm-thick sheet in 60˚ V- bending at; (a) the intermediate stage

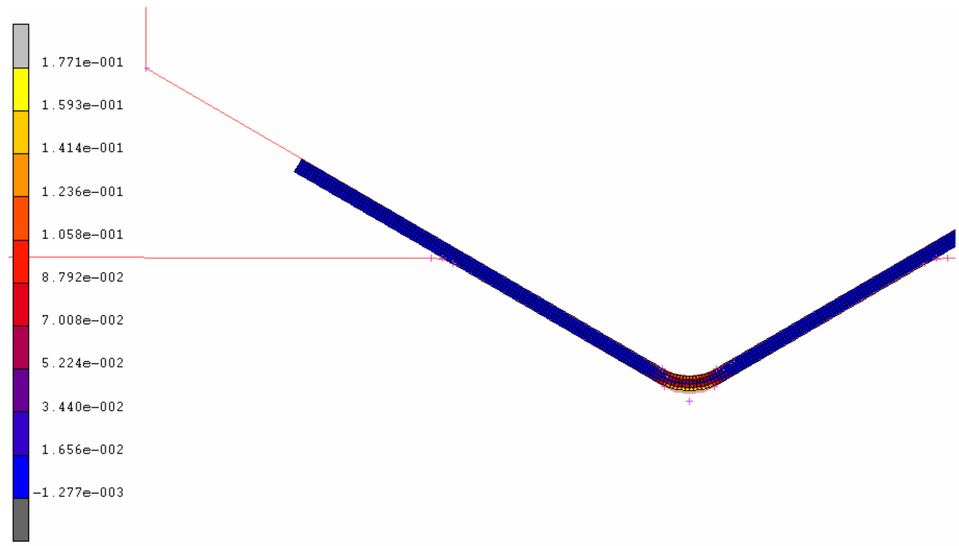

(b)

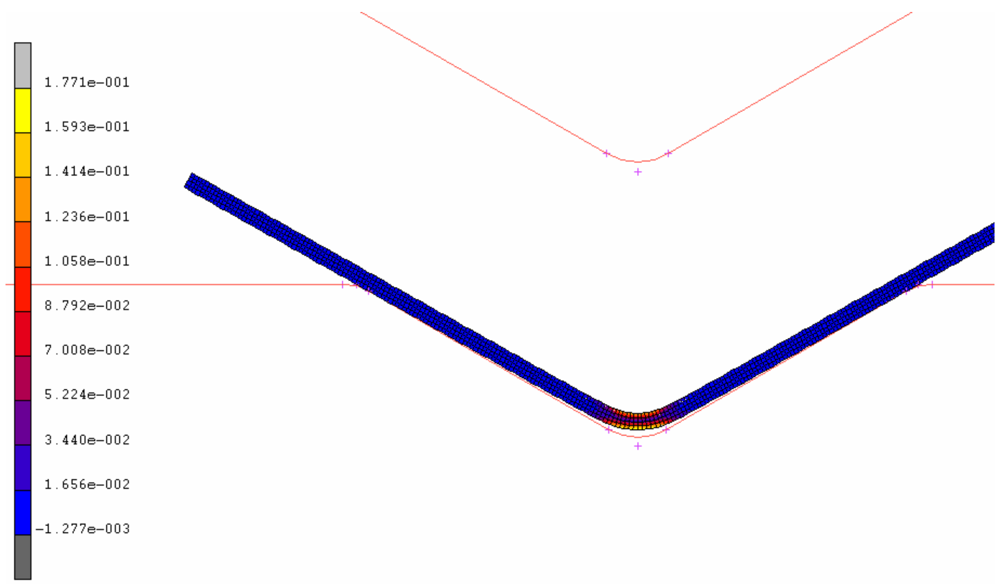

(c)

Figure 4.92 (cont'd) Total-equivalent plastic strain distribution for AA 6061-T6 1.6 mm-thick sheet in 60˚ V- bending at; (b) the fully loaded stage, (c) the unloaded stage.

In Figure 4.93 and Figure 4.94, von Misses stresses and total plastic strains in AA 6061 T6 1.6 mm thick sheet in 90˚ V- bending are illustrated respectively.

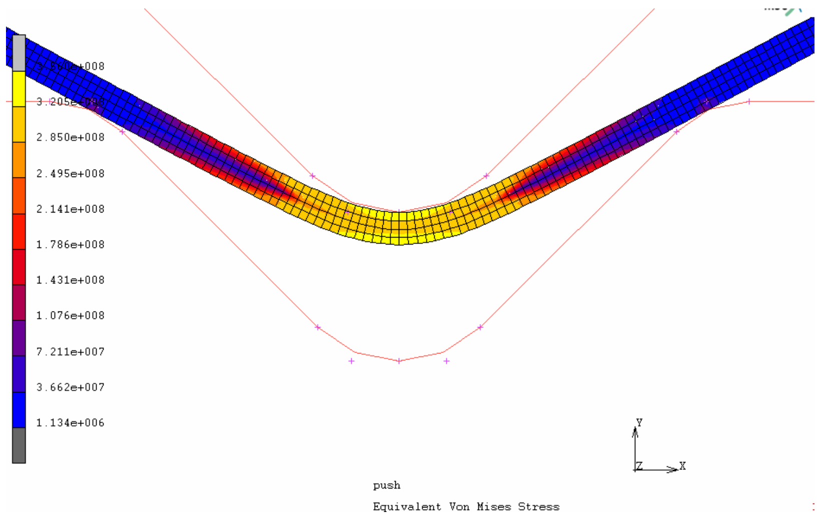

(a)

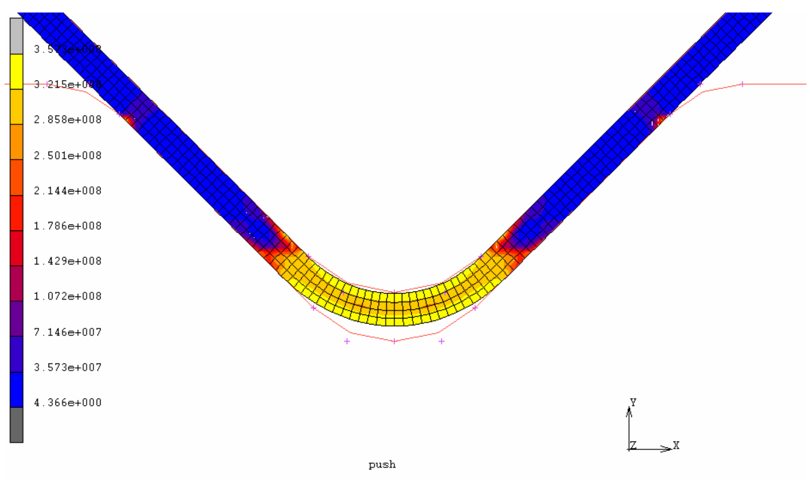

(b)

Figure 4.93 Von Misses stress distribution for AA 6061 T6 1.6 mm-thick sheet in 90˚ V- bending at; (a) the intermediate stage, (b) the fully loaded stage

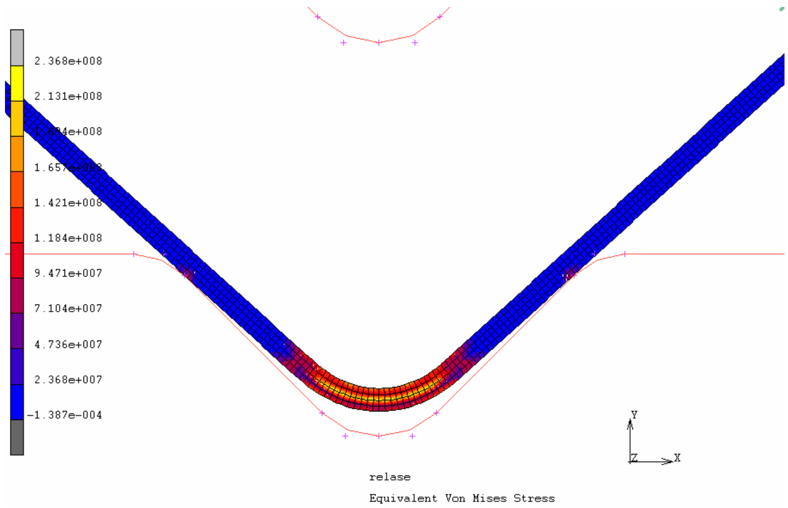

(c)

Figure 4.93 (cont'd) Von Misses stress distribution for AA 6061 T6 1.6 mm-thick sheet in 90˚ V- bending at; (b) the fully loaded stage, (c) the unloaded stage

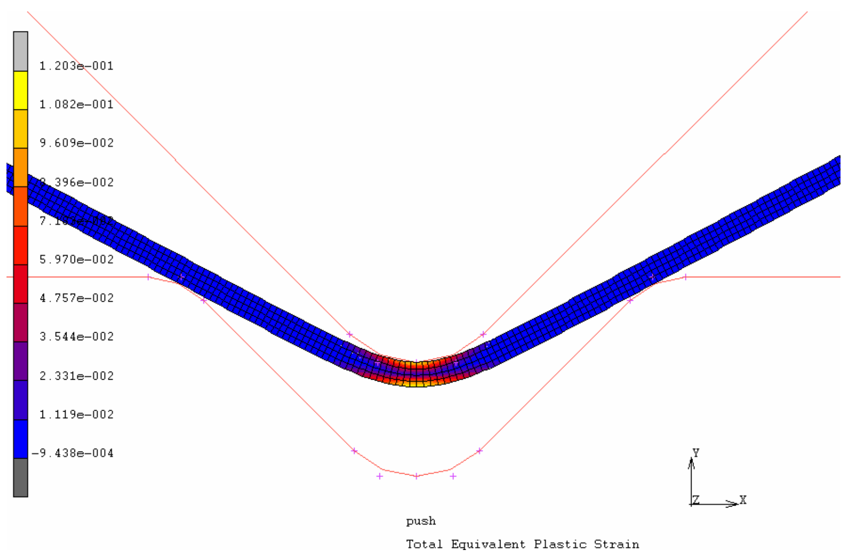

(a)

Figure 4.94 Total-equivalent plastic strain distribution for AA 6061-T6 1.6 mm-thick sheet in 90˚ V- bending at; (a) the intermediate stage

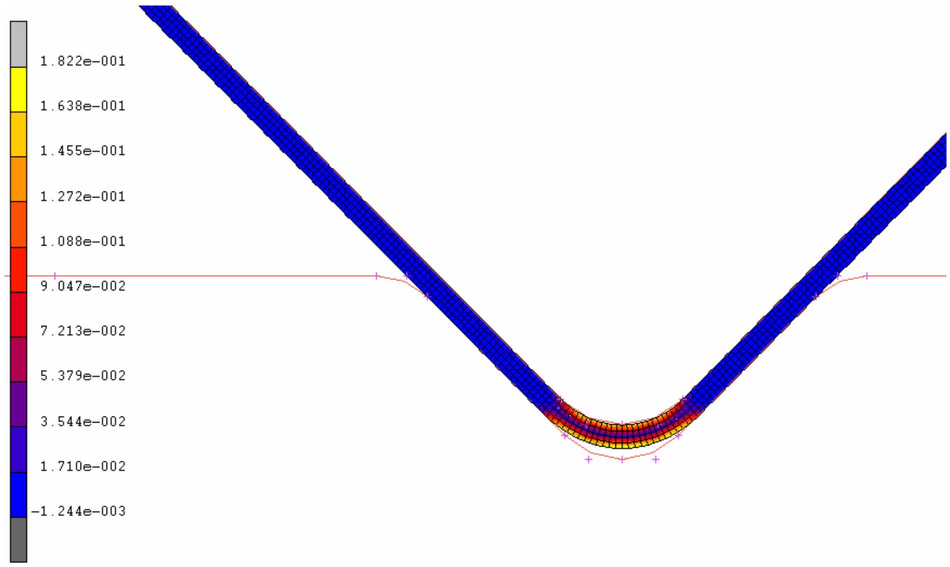

(b)

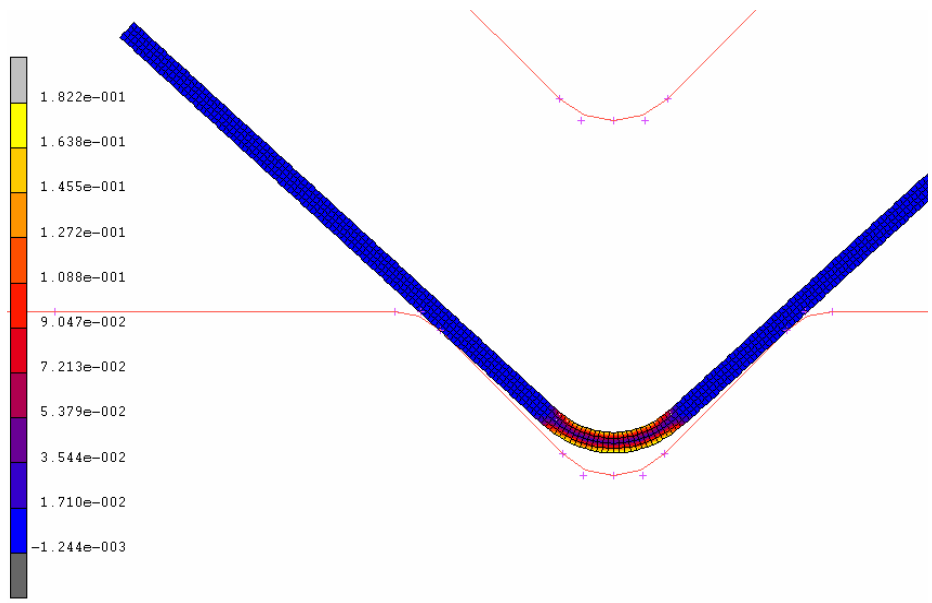

(c)

Figure 4.94 (cont'd) Total-equivalent plastic strain distribution for AA 6061-T6 1.6 mm-thick sheet in 90˚ V- bending at; (b) the fully loaded stage, (c) the unloaded stage

In Figure 4.95 and Figure 4.96, von misses stresses and total plastic strains in AA 6061 T6 1.6 mm thick sheet in 120˚ V- bending are illustrated respectively.

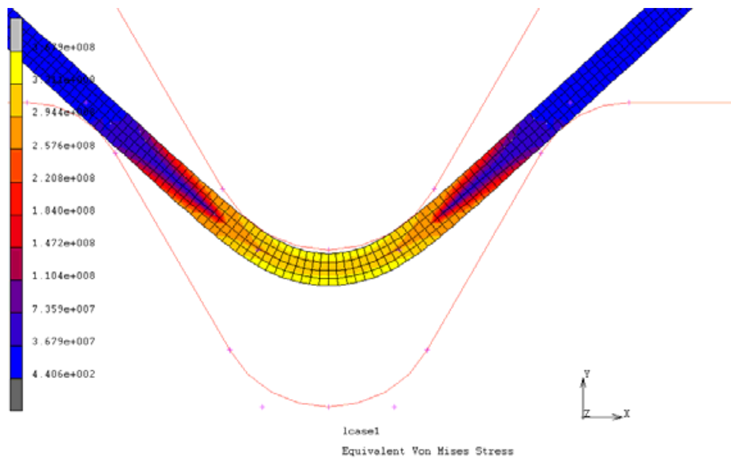

(a)

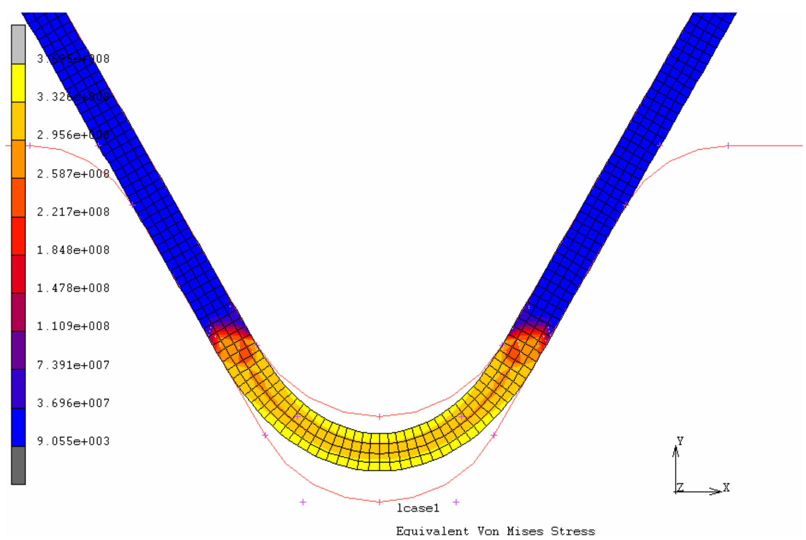

(b)

Figure 4.95 Von Misses stress distribution for AA 6061-T6 1.6 mm-thick sheet in 120˚ V- bending at; (a) the intermediate stage, (b) the fully loaded stage

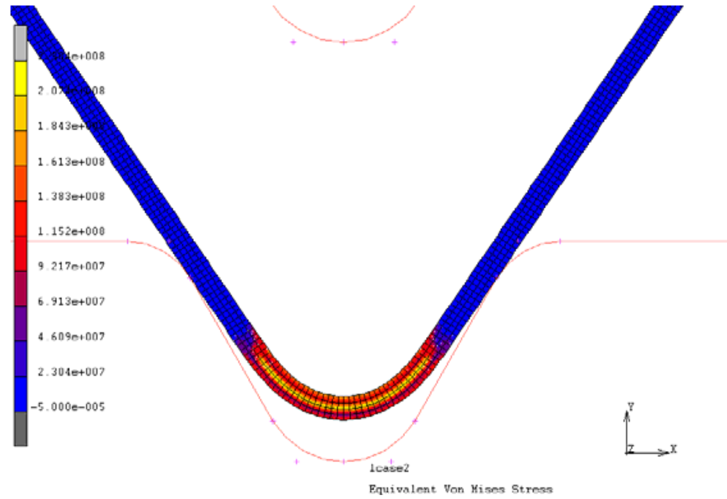

(c)

Figure 4.95 (cont'd) Von Misses stress distribution for AA 6061-T6 1.6 mm-thick sheet in 120˚ V- bending at; (c) the unloaded stage.

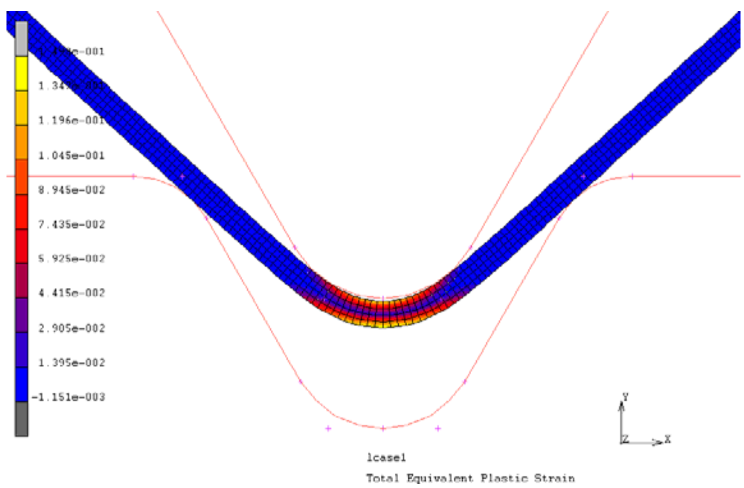

(a)

Figure 4.96 Total-equivalent plastic strain distribution for AA 6061-T6 1.6 mm-thick sheet in 120˚ V- bending at; (a) the intermediate stage

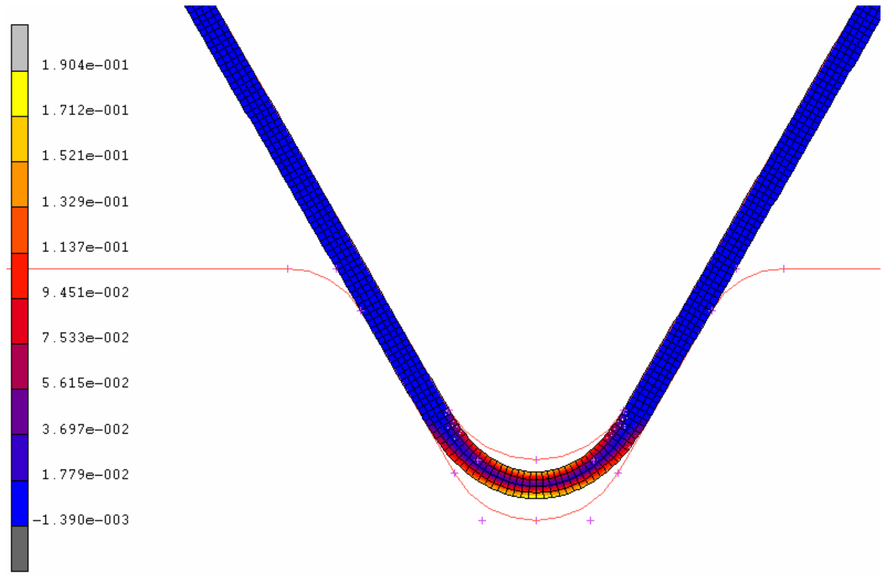

(b)

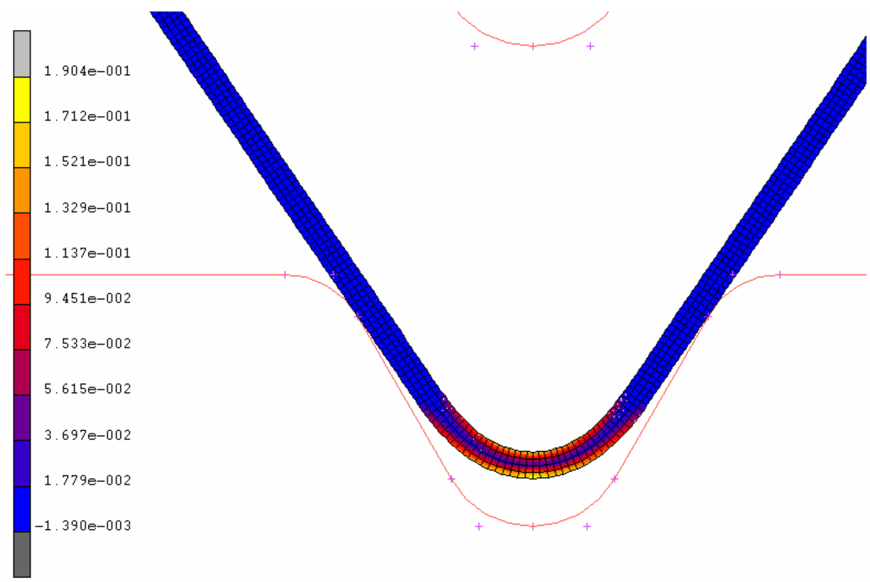

(c)

Figure 4.96 (cont'd) Total-equivalent plastic strain distribution for AA 6061-T6 1.6 mm-thick sheet in 120˚ V- bending at; (b) the fully loaded stage, (c) the unloaded stage.

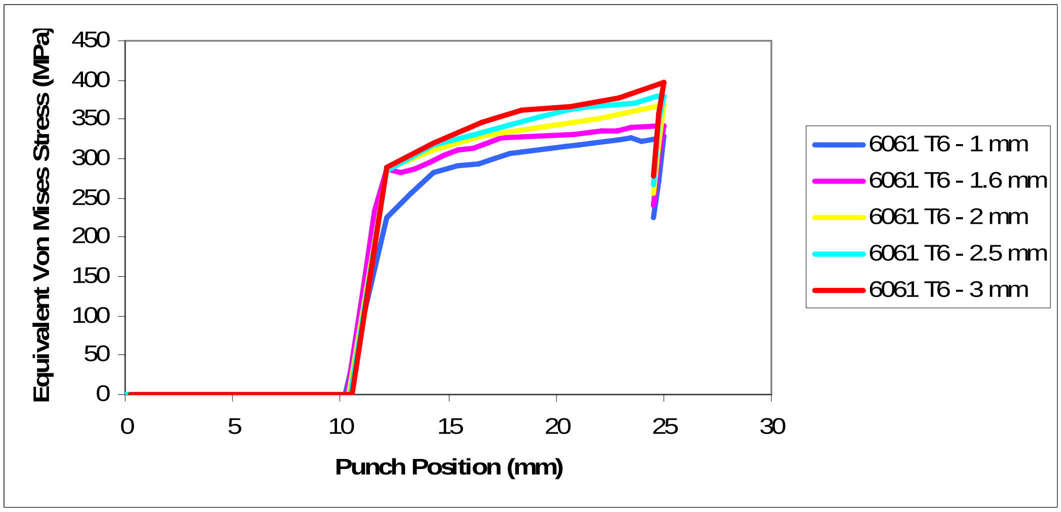

Figure 4.97 Maximum von Mises stresses vs. punch position of 6061 T6 for V bending to 60˚

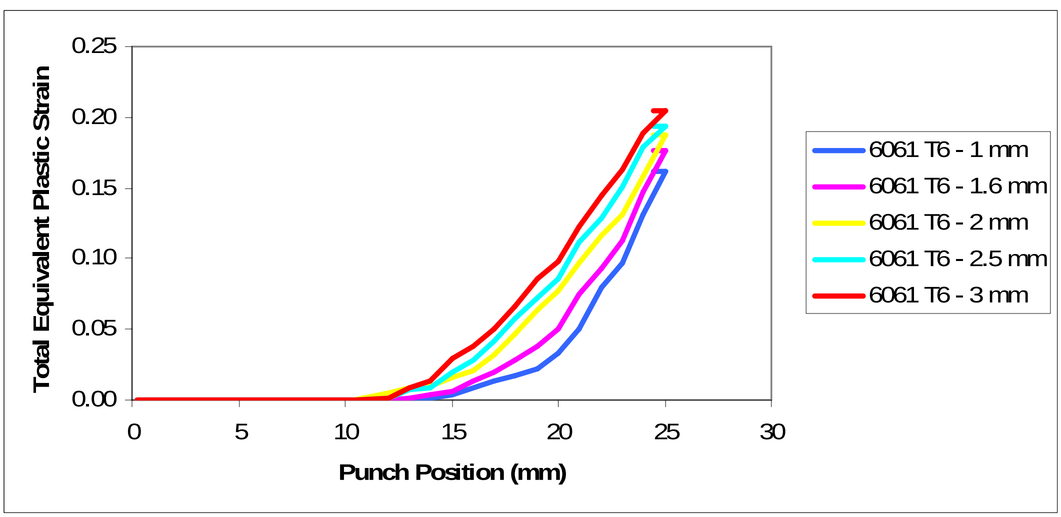

Figure 4.98 Maximum total-equivalent plastic strain vs. punch position of 6061 T6 for V bending to 60˚

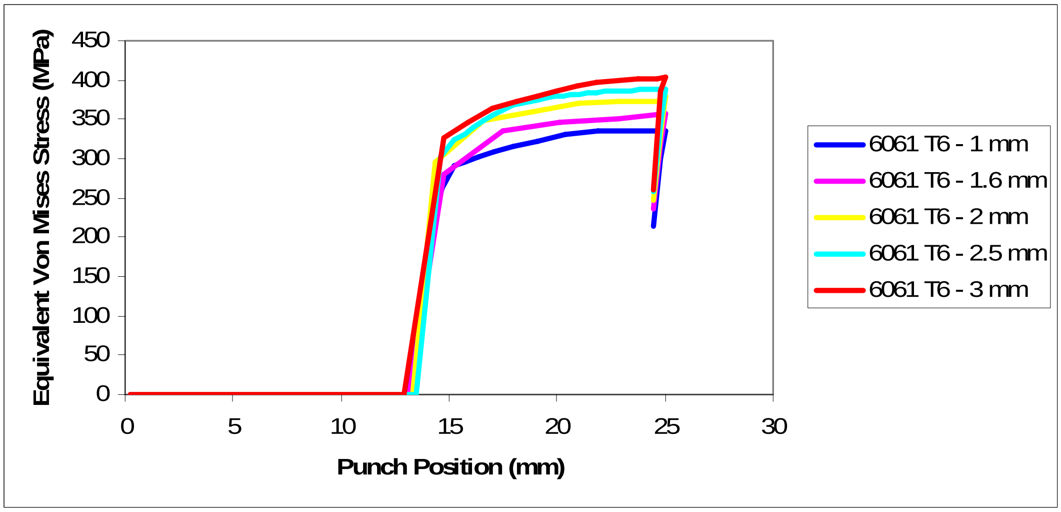

Figure 4.99 Maximum von Mises stresses vs. punch position of 6061 T6 for V bending to 90˚

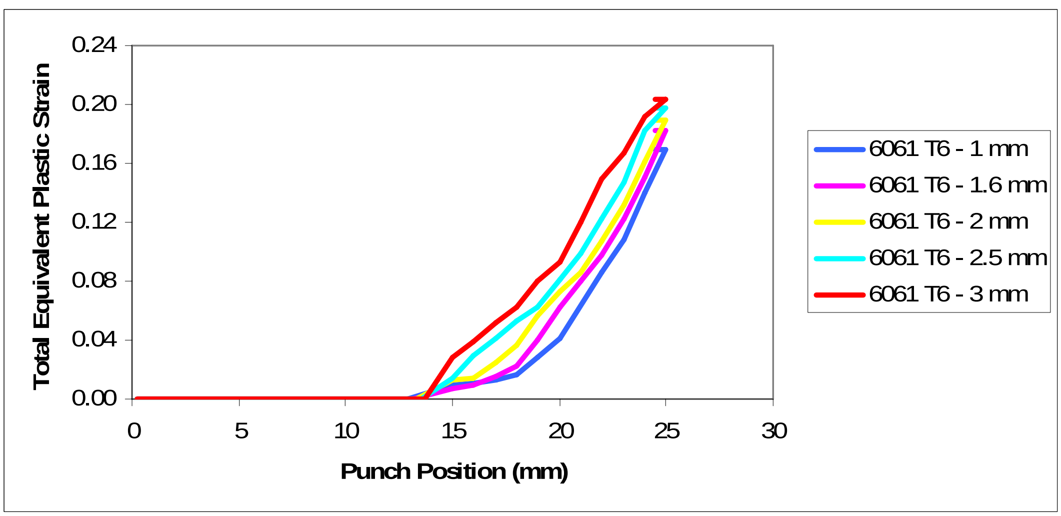

Figure 4.100 Maximum total-equivalent plastic strain vs. punch position of 6061 T6 for V bending to 90˚

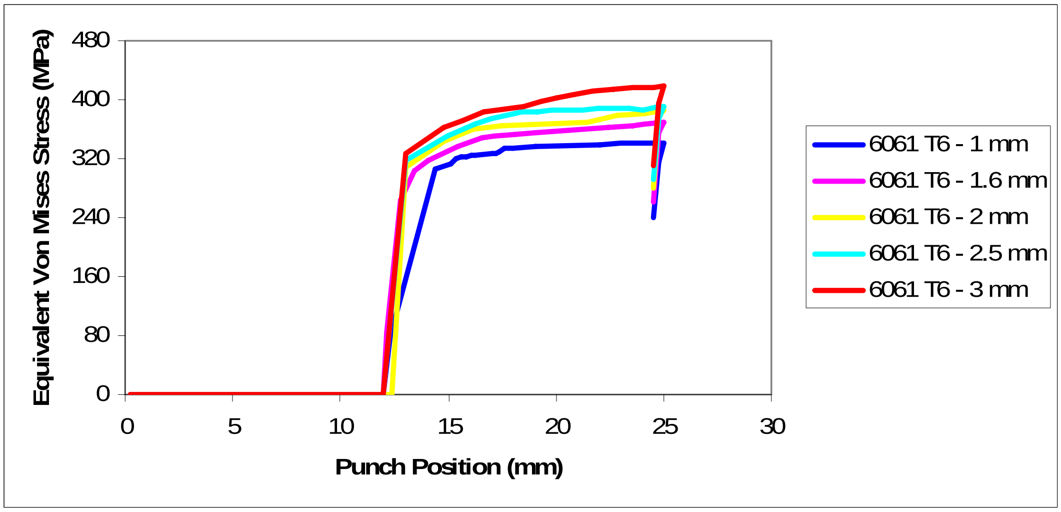

Figure 4.101 Maximum von Mises stresses vs. punch position of 6061 T6 for V bending to 120˚

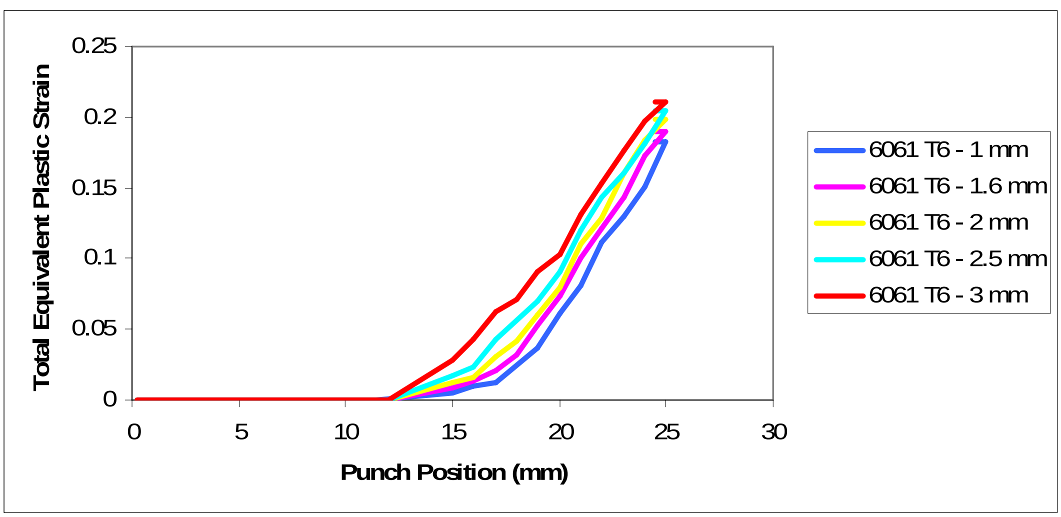

Figure 4.102 Maximum total-equivalent plastic strain vs. punch position of 6061 T6 for V bending to 120˚

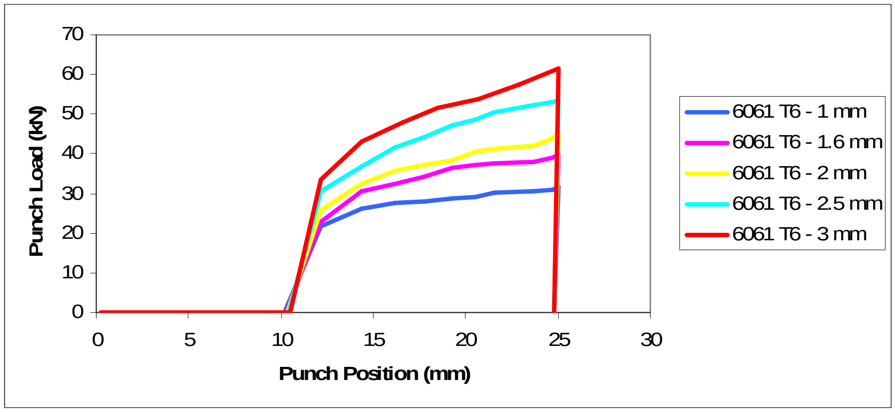

Figure 4.103 Punch load vs. punch position of AA 6061 T6 for V-bending to 60˚

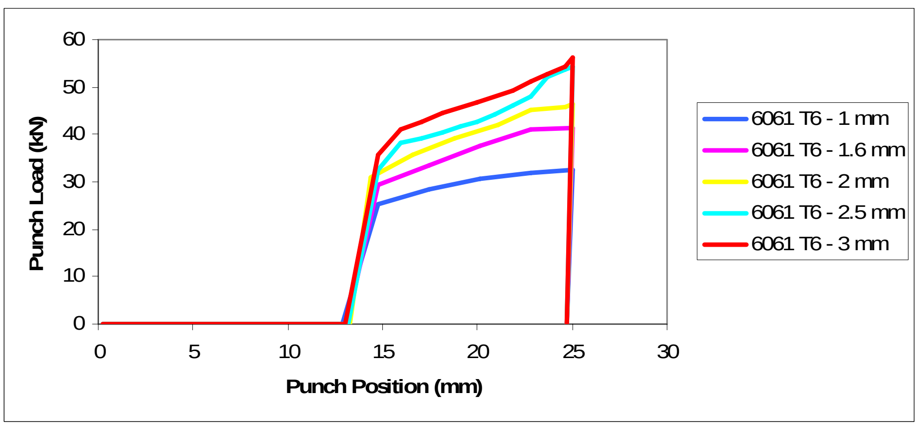

Figure 4.104 Punch load vs. punch position of AA 6061 T6 for V-bending to 90˚

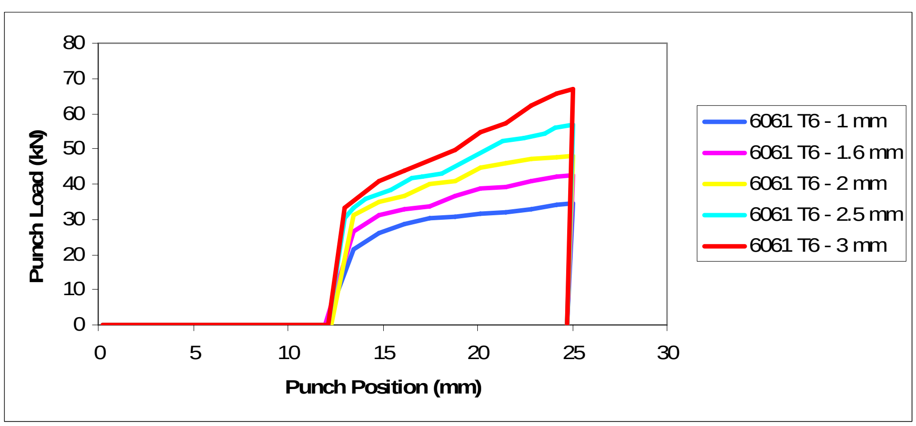

Figure 4. 105 Punch load vs. punch position of AA 6061 T6 for V-bending to 120˚

CHAPTER 5

HEAT TREATMENTS AND EXPERIMENTATION OF V-BENDING OPERATIONS

In this chapter, heat treatment processes and the experiments of the numerically analyzed cases are presented. Heat treatments are carried out in accordance with SAE AMS 2770G standard and the tests of the designed dies are performed in TUBITAK-SAGE.

The experiments have been carried out to measure springback angle of the workpiece after V-bending operation; 3 different tempers of AA 2014 and AA 6061 material under 3 different bend angles, and 3 different thicknesses were analyzed in order to verify FEA results. Number of test sample in each case is 5.

5.1 Material

The materials used in this thesis study are rolled aluminum alloy AA 2014 and AA 6061 Power Plate (registered trademark of Alcoa) with a thickness of 1.6, 2 and 2.5 mm. The plates were produced at the Alcoa Davenport Works, Pittsburgh, with a production lot number of 451661 and a package ticket number of 755624 according to the ASTM B 209-04 standard, which covers the properties of aluminum and aluminum alloy flat sheet, coiled sheet, and plate products.

5.1.1. Specification of Workpiece Materials

5.1.1.1. AA 2014 Alloy Properties

Alloy AA 2014 is a general purpose alloy commonly used in truck hubs, tank wheels and aircraft wheel forgings. It has good machinability and weldability for solution heat treated and artificially aged tempers T4 and T6. Chemical composition of AA 2014 is given in Table 5.1

Table 5.1 Chemical composition of AA 2014

Material Components	Composition Percentage (%)
Aluminum, Al	90.4 - 95.0
Chromium, Cr	<= 0.100
Copper, Cu	3.90 - 5.00
Iron, Fe	<= 0.700
Magnesium, Mg	0.200 - 0.800
Manganese, Mn	0.400 - 1.20
Other, each	<= 0.0500
Other, total	<= 0.150
Silicon, Si	0.500 - 1.20
Titanium, Ti	<= 0.150
Zinc, Zn	<= 0.250

5.1.1.2. AA 6061 Alloy Properties

Alloy AA 6061, a cold finished aluminum wrought product, is suggested for applications requiring high corrosion resistance. This general purpose alloy has excellent corrosion resistance to atmospheric conditions and good corrosion resistance to sea water. Susceptibility to stress corrosion cracking and exfoliation is practically nonexistent. Cold finished alloy 6061 offers relatively high strength and excellent joining characteristics. Typical applications include electrical fittings and connectors, decorative and miscellaneous hardware, hydraulic couplings, brake parts and valve bodies and components for commercial, industrial, automotive and aerospace use. The -T4 temper offers good formability for cold upset and bending applications. [12] Chemical composition of the alloy is submitted in Table 5.2

Table 5.2 Chemical composition of AA 6061

Material Components	Composition Percentage (%)
Aluminum, Al	95.8 - 98.6
Chromium, Cr	.0400 - 0.350
Copper, Cu	0.150 - 0.400
Iron, Fe	<= 0.700
Magnesium, Mg	0.800 - 1.20
Manganese, Mn	<= 0.150
Other, each	<= 0.0500
Other, total	<= 0.150
Silicon, Si	0.400 - 0.800
Titanium, Ti	<= 0.150
Zinc, Zn	<= 0.250

5.1.2. Heat Treatment of AA 2014 and AA 6061 Alloys

In this part of the work; O, T4, and T6 type heat treatments are applied to the AA 2014 and AA6061 sheet metals. For the alloy 2014, 1.6 mm and 2 mm thicknesses of the material were in O condition when it was delivered where 2.5 mm was in T6 condition. First, for the alloy AA 2014, for 2.5 mm thick sheet metal, O condition was achieved by full annealing and later, for all thicknesses, T4 condition is achieved. Finally, T6 condition is achieved for the thicknesses 1.6 mm and 2 mm by solution heat treatment, artificially aging. For the alloy AA 6061, only the 1.6mm thick sheet metal was in T6 condition when it is delivered. By applying full annealing process to 1.6 mm thick sheet metal, O condition is achieved for this material. Later T4 condition and T6 condition is obtained for the thickness of 2 mm and 2.5 mm. Aluminum materials are purchased from Scope Metal Inc. Heat treatment plans of each material is given in Table 5.3 and Table 5.4 respectively.

Table 5.3 Heat treatment scenario of AA 2014 (alclad)

AA 2014		
thickness (mm)	purchased	generated
1.6	O	T4, T6
2.0	O	T4, T6
2.5	T6	O, T6

Table 5.4 Heat treatment scenario of AA 6061

AA 6061		
thickness (mm)	purchased	generated
1.6	T6	O, T6
2.0	O	T4, T6
2.5	O	O, T6

5.1.2.1. Temper Generation for AA 2014 and AA 6061

5.1.2.1.1. Obtaining T4 and T6 Conditions (Solution Heat Treatment)

For the alloy AA 2014, T4 condition is obtained by solutionizing the material at 502 °C with soaking 50 minutes in a air convection aluminum heat treatment furnace and then water quenching. Afterwards material was naturally aged at room temperature for 96 hours, when its hardness and conductivity values according to SAE AMS 2658 standard. After T4 treatment, artificial aging was employed to obtain T6 condition by aging the material at 177 °C for 8 to 9 hours again in air convection furnace.

For the alloy AA 6061, a similar T4 and T6 heat treatment processes were also achieved according to SAE AMS 2770G. T4 condition was obtained by first solution heat treating at 529 °C for 40 minutes and water quenching. After water quenching, material was naturally aged at room temperature, till when its hardness and conductivity values according to SAE AMS 2658 were met, which is typically 96 hours. Once T4 condition reached then artificial aging has taken place for the T6 condition, which was achieved by aging the material at 177 °C for 8 to10 hours.

5.1.2.1.2. Obtaining O Condition (Full Annealing)

For the materials which are originally delivered at T6 condition for both 2014 and 6061 it was necessary to achieve O condition. For both 2014 and 6061 alloys, SAE AMS 2770G directs the same processes for full annealing which was achieved soaking the materials at 427 °C for minimum one hour and then furnace cooled at 28°C /hour maximum to 260 °C and then air cooled to room temperature.

All the heat treatment processes were done according to SAE AMS 2770G standard with using a convection air furnace, which has a temperature uniformity tolerance of ± 6 º C and equipped with a water quenching tank shown in Figure 5.1

(a)

(b)

Figure 5.1 a) Air Furnace, b) Water quenching tank.

After the heat treatments, materials were controlled in terms of their hardness and conductivity values, as well as yield strength and ultimate tensile stress values by employing tension test according to the SAE AMS 2658B standard.

Hardness tests were conducted by using Mettest hardness measurement equipment, and conductivity measurements were performed with Hocking™ Autosigma 3000 (GE Inspection) conductivity measurement device, see Figure 5.2.

(a) (b)

Figure 5.2 a) Hardness tester, b) Hocking™ Autosigma 3000 conductivity measurement device.

The tension tests were utilized in order to obtain true stress – plastic strain values which are needed to define strain hardening behavior of the material in FEM solutions. The tension tests were carried out in the Quality Control Laboratory of TUBITAK-SAGE .

For this purpose, three different specimens are cut from the sheets for each material. The true stress – true strain results of the three specimens from one sheet are plotted, and a mean stress - strain curve is taken to form the strain hardening curve of each material. Tension tests are performed according to ASTM E 8M-04. Test device and necessary dimensions of test specimens are given in Figure 5.3 and Figure 5.4 respectively.

Figure 5.3 Instron Tension test device

E 8M – 04

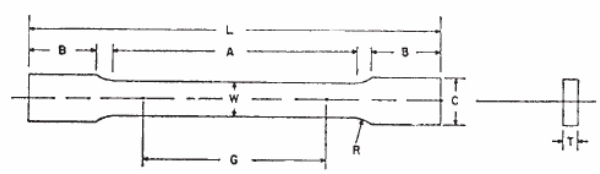

Dimensions, mm			
	Standard Specimens		Subsize Specimen
Nominal Width	Plate-Type 40 mm	Sheet-Type 12.5 mm	6 mm
G— Gage length (Note 1 and Note 2)	200.0 ± 0.2	50.0 ± 0.1	25.0 ± 0.1
W— Width (Note 3 and Note 4)	40.0 ± 2.0	12.5 ± 0.2	6.0 ± 0.1
T— Thickness (Note 5)		thickness of material	
R— Radius of fillet, min (Note 6)	25	12.5	6
L— Overall length, (Note 2, Note 7 and Note 8)	450	200	100
A— Length of reduced section, min	225	57	32
B— Length of grip section, (Note 8)	75	50	30
C— Width of grip section, approximate (Note 4 and Note 9)	50	20	10

Figure 5.4 Dimensions of the tensile test specimen.

True stress – true strain values of the sheet metal after heat treatments are illustrated in Figure 5.5 and Figure 5.6.

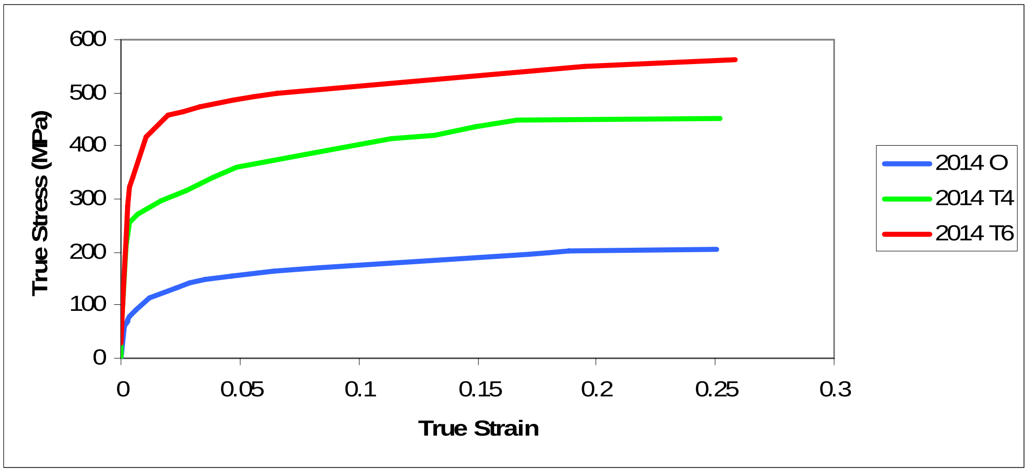

Figure 5.5 True stress – true strain values of AA 2014 at different temper types.

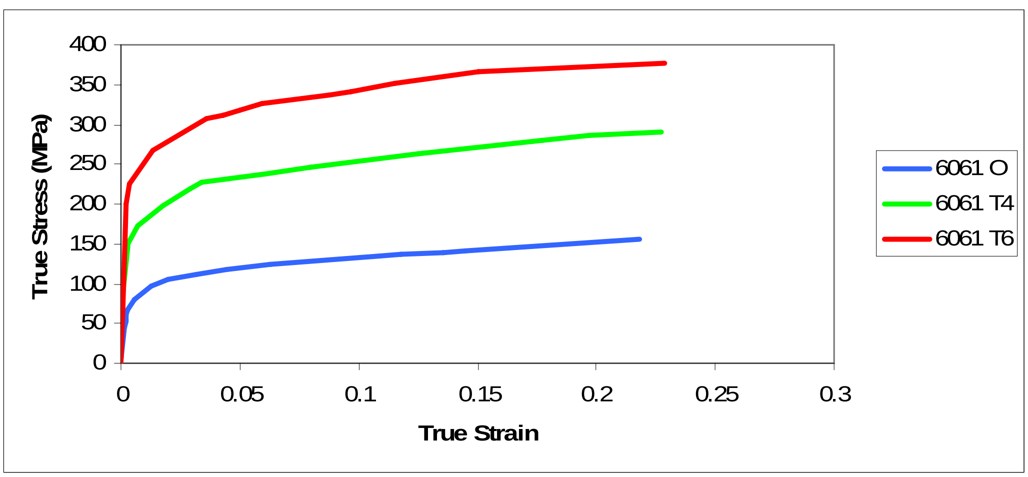

Figure 5.6 True stress – true strain values of AA 6061 at different temper types.

5.2. Experiments

In this study, two different aluminum wrought alloys, 2014 O, 2014 T4, 2014 T6 and 6061 O, 6061 T4 and 6061 T6 are bent.

Dimensions of the sheet metals are investigated in Figure 5.7

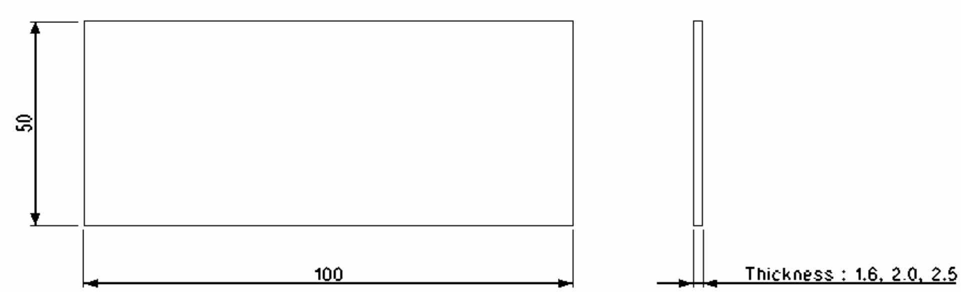

Figure 5.7 Dimensions of the test specimens.

The experiment set-up is composed of a punch, a die and guide pins which are given in Figure 5.8, Figure 5.9 and Figure 5.10. Dimensions of the bending dies are same as the ones used in Finite Element Analysis.

Figure 5.8 60˚ V-Bending die

Figure 5.9 90˚ V-Bending die

Figure 5.10 120˚ V-Bending die

.

A hydraulic press with a capacity of 100 tons is employed during experiments (Figure 5.11)

Figure 5.11 Hydraulic pres machine

Springback angle of the experiment specimen is measured using angle measuring device. (Figure 5.12)

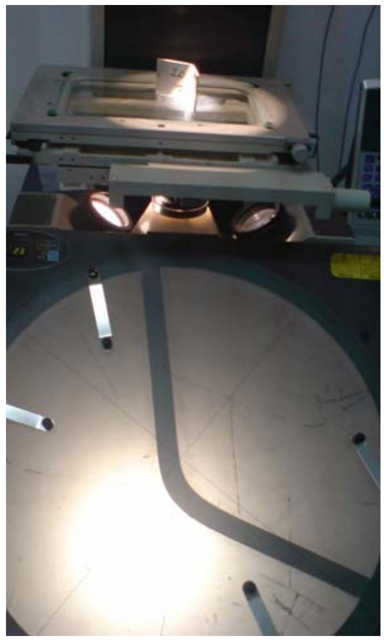

Figure 5.12 Optical angle measuring device

After all experiments, springback angles is measured and mean value of the springback angle is compared with FEA results for each case and tabulated in Table 5.5, Table 5.6, Table 5.7, Table 5.8, Table 5.9 and Table 5.10 respectively.

Table 5.5 Experimental results of AA 2014 O for V-bending

			Experiment Results	
	thickness (mm)	bend angle (deg.)	part angle (deg.)	springback (deg.)
2014 O	1.6	60	59.23	0.77
	2.0		59.56	0.44
	2.5		59.70	0.30
	1.6	90	88.35	1.65
	2.0		88.80	1.20
	2.5		88.98	1.02
	1.6	120	116.44	3.56
	2.0		116.81	3.19
	2.5		117.04	2.96

Table 5.6 Experimental results of AA 2014 T4 for V-bending

			Experiment Results	
	thickness (mm)	bend angle (deg.)	part angle (deg.)	springback (deg.)
2014 T4	1.6	60	57.09	2.91
	2.0		58.02	1.98
	2.5		59.19	0.81
	1.6	90	84.00	6.00
	2.0		85.09	4.91
	2.5		86.41	3.59
	1.6	120	110.98	9.02
	2.0		111.87	8.13
	2.5		112.33	7.67

Table 5.7 Experimental results of AA 2014 T6 for V-bending

			Experiment Results	
	thickness (mm)	bend angle (deg.)	part angle (deg.)	springback (deg.)
2014 T6	1.6	60	55.22	4.78
	2.0		56.97	3.03
	2.5		57.28	2.72
	1.6	90	79.98	10.02
	2.0.0		82.09	7.91
	2.5		83.94	6.06
	1.6	120	105.77	14.23
	2.0		107.75	12.25
	2.5		108.93	11.07

Table 5.8 Experimental results of AA 6061 O for V-bending

			Experiment Results	
	thickness (mm)	bend angle (deg.)	part angle (deg.)	springback (deg.)
6061 O	1.6	60	59.45	0.55
	2.0		59.65	0.35
	2.5		59.81	0.19
	1.6	90	88.70	1.30
	2.0		89.00	1.00
	2.5		89.25	0.75
	1.6	120	116.94	3.06
	2.0		117.79	2.21
	2.5		117.96	2.04

Table 5.9 Experimental results of AA 6061 T4 for V-bending

			Experiment Results	
	thickness (mm)	bend angle (deg.)	part angle (deg.)	springback (deg.)
6061 T4	1.6	60	58.48	1.52
	2.0		59.08	0.92
	2.5		59.50	0.50
	1.6	90	86.50	3.50
	2.0		87.63	2.37
	2.5		87.93	2.07
	1.6	120	112.41	7.59
	2.0		113.32	6.68
	2.5		113.96	6.04

Table 5.10 Experimental results of AA 6061 T6 for V-bending

			Experiment Results	
	thickness (mm)	bend angle (deg.)	part angle (deg.)	springback (deg.)
6061 T6	1.6	60	56.85	3.15
	2.0		57.85	2.15
	2.5		58.76	1.24
	1.6	90	82.94	7.06
	2.0		84.88	5.12
	2.5		85.91	4.09
	1.6	120	109.79	10.21
	2.0		111.06	8.94
	2.5		111.85	8.15

Some of the examples after bending experiments are shown in Figure 5.13

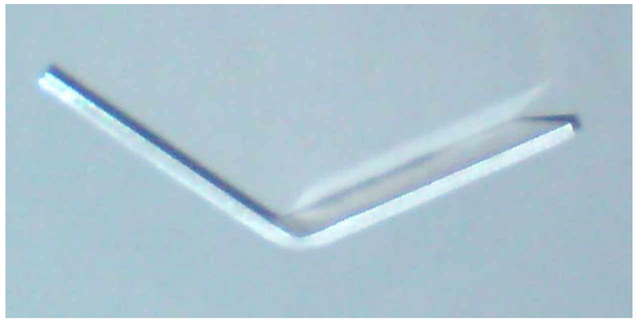

(a)

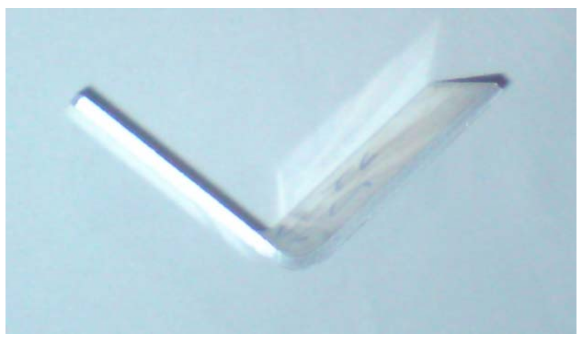

(b)

(c)

Figure 5.13 Bent pieces after a) 60˚ V bending, b) 90˚ V bending, c) 120˚ V bending experiment

CHAPTER 6

DISCUSSIONS OF THE RESULTS

In this chapter, FEM results and experimental results of analyzed cases are compared. Springback amounts, maximum equivalent von Mises stresses, total equivalent plastic strain and punch loads of simulated cases under different heat treatment conditions are given.

6.1. Springback Results

Springback results of simulated cases and experiments for each test material are given in Table 6.1, Table 6.2, Table 6.3, Table 6.4, Table 6.5 and Table 6.6 respectively.

Table 6.1 FEA and experimental results of AA 2014 O for V-bending

			FEA		Experiment	
	thickness (mm)	bend angle (deg.)	part angle (deg)	springback (deg.)	part angle (deg.)	springback (deg.)
2014 O	1.6	60	59.17	0.83	59.23	0.77
	2.0		59.44	0.56	59.56	0.44
	2.5		59.69	0.31	59.70	0.30
	1.6	90	88.20	1.80	88.35	1.65
	2.0		88.65	1.35	88.80	1.20
	2.5		88.97	1.03	88.98	1.02
	1.6	120	116.24	3.76	116.44	3.56
	2.0		116.59	3.41	116.81	3.19
	2.5		116.86	3.14	117.04	2.96

Table 6.2 FEA and experimental results of V-bending of AA 2014 T4

			FEA		Experiment	
	thickness (mm)	bend angle (deg.)	part angle (deg)	springback (deg.)	part angle (deg.)	springback (deg.)
2014 T4	1.6	60	56.93	3.07	57.09	2.91
	2.0		57.93	2.07	58.02	1.98
	2.5		58.85	1.15	59.19	0.81
	1.6	90	83.93	6.07	84.00	6.00
	2.0		84.99	5.01	85.09	4.91
	2.5		86.18	3.82	86.41	3.59
	1.6	120	110.86	9.14	110.98	9.02
	2.0		111.71	8.29	111.87	8.13
	2.5		112.13	7.87	112.33	7.67

Table 6.3 FEA and experimental results of V-bending of AA 2014 T6

			FEA		Experiment	
	thickness (mm)	bend angle (deg.)	part angle (deg)	springback (deg.)	part angle (deg.)	springback (deg.)
2014 T6	1.6	60	55.02	4.98	55.22	4.78
	2.0		56.64	3.36	56.97	3.03
	2.5		57.14	2.86	57.28	2.72
	1.6	90	79.92	10.08	79.98	10.02
	2.0		81.99	8.01	82.09	7.91
	2.5		83.82	6.18	83.94	6.06
	1.6	120	105.44	14.56	105.77	14.23
	2.0		107.49	12.51	107.75	12.25
	2.5		108.74	11.26	108.93	11.07

Table 6. 1 FEA and experimental results of V-bending of AA 6061 O

			FEA		Experiment	
	thickness (mm)	bend angle (deg.)	part angle (deg)	springback (deg.)	part angle (deg.)	springback (deg.)
6061 O	1.6	60	59.35	0.65	59.45	0.55
	2.0		59.58	0.42	59.65	0.35
	2.5		59.80	0.20	59.81	0.19
	1.6	90	88.59	1.41	88.70	1.30
	2.0		88.95	1.05	89.00	1.00
	2.5		89.20	0.80	89.25	0.75
	1.6	120	116.83	3.17	116.94	3.06
	2.0		117.39	2.61	117.79	2.21
	2.5		117.86	2.14	117.96	2.04

Table 6. 2 FEA and experimental results of V-bending of AA 6061 T4

			FEA		Experiment	
	thickness (mm)	bend angle (deg.)	part angle (deg)	springback (deg.)	part angle (deg.)	springback (deg.)
6061 T4	1.6	60	58.29	1.71	58.48	1.52
	2.0		58.90	1.10	59.08	0.92
	2.5		59.48	0.52	59.50	0.50
	1.6	90	86.30	3.70	86.50	3.50
	2.0		87.25	2.75	87.63	2.37
	2.5		87.92	2.08	87.93	2.07
	1.6	120	112.25	7.75	112.41	7.59
	2.0		113.22	6.78	113.32	6.68
	2.5		113.87	6.13	113.96	6.04

Table 6. 3 FEA and experimental results of V-bending of AA 6061 T6

			FEA		Experiment	
	thickness (mm)	bend angle (deg.)	part angle (deg)	springback (deg.)	part angle (deg.)	springback (deg.)
6061 T6	1.6	60	56.75	3.25	56.85	3.15
	2.0		57.79	2.21	57.85	2.15
	2.5		58.66	1.34	58.76	1.24
	1.6	90	82.88	7.12	82.94	7.06
	2.0		84.75	5.25	84.88	5.12
	2.5		85.82	4.18	85.91	4.09
	1.6	120	109.64	10.36	109.79	10.21
	2.0		110.88	9.12	111.06	8.94
	2.5		111.71	8.29	111.85	8.15

Springback amounts of different heat treated materials under different bend angle are graphically illustrated for thickness of 2 mm in Figure 6.1.

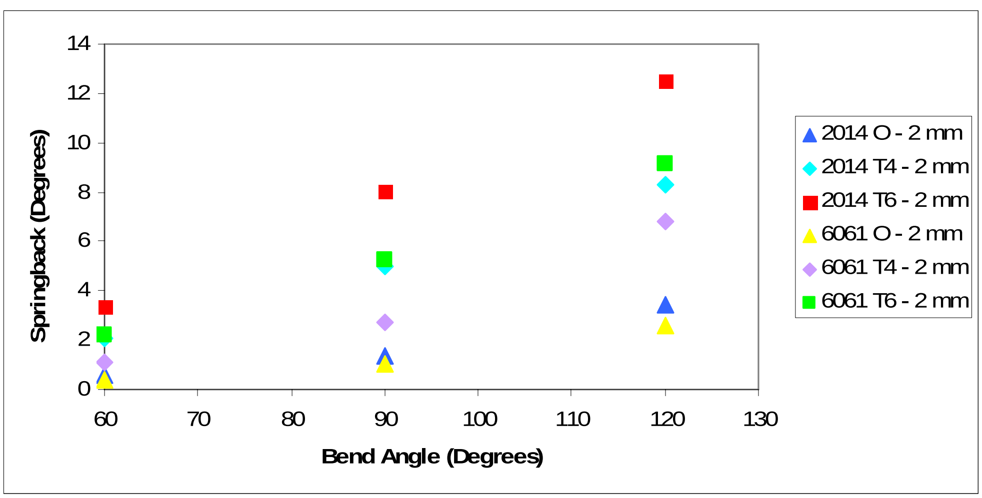

Figure 6.1 FEM results of AA 2014 and AA 6061 under different heat treatments and different bend angles

Due to the changes is mechanical properties after heat treatment, there have been variations in springback angle after the bending operations. For the same material, because of the increase in yield strength from O condition to T6 condition, it has been observed that higher springback is obtained in T6 condition. T6 type heat treatment applied material has higher yield strength than T4 type heat treated material whereas the yield strength of material in O condition is the lowest

6.2. Equivalent Von Mises Stress Values

Maximum von Mises stress values of each heat treated material for 60˚, 90˚, 120˚ V-bending are graphically demonstrated in Figure 6.2, Figure 6.3, Figure 6.4, Figure 6.5 and Figure 6.7.

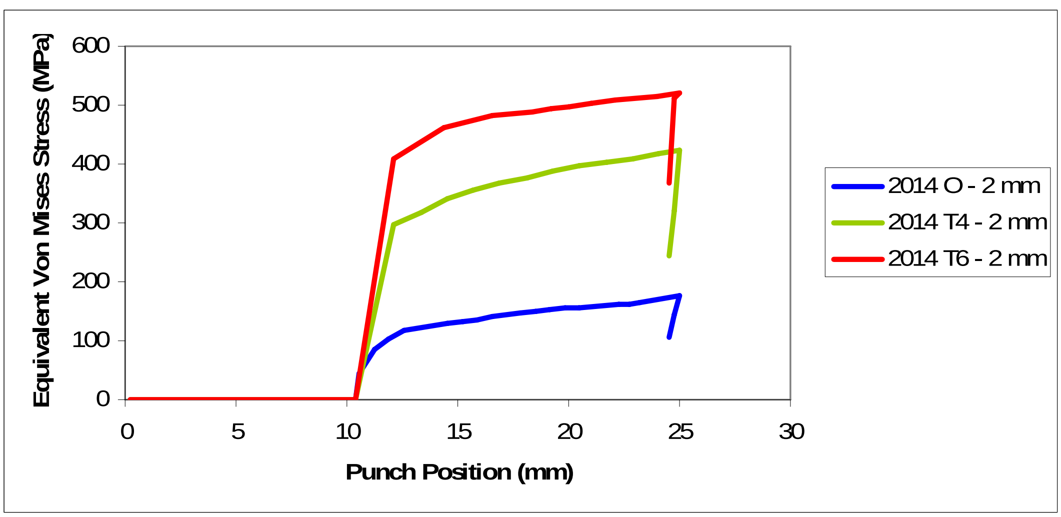

Figure 6.2 Maximum Equivalent Von Mises stress vs. punch position of 2mm thick AA 2014 under different heat treatment conditions for 60˚ V-bending.

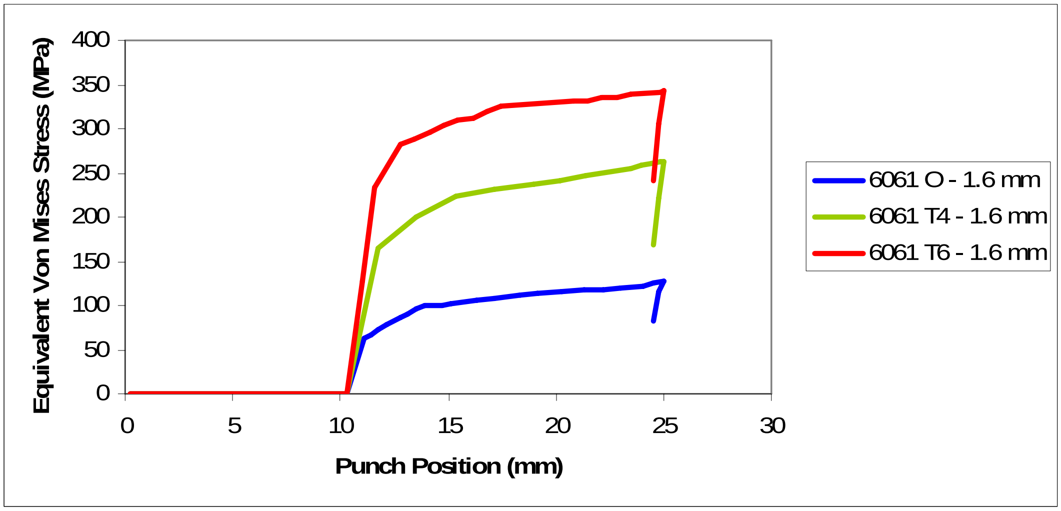

Figure 6.3 Maximum Equivalent Von Mises stress vs. punch position of 1.6 mm thick AA 6061 under different heat treatment conditions for 60˚ V-bending.

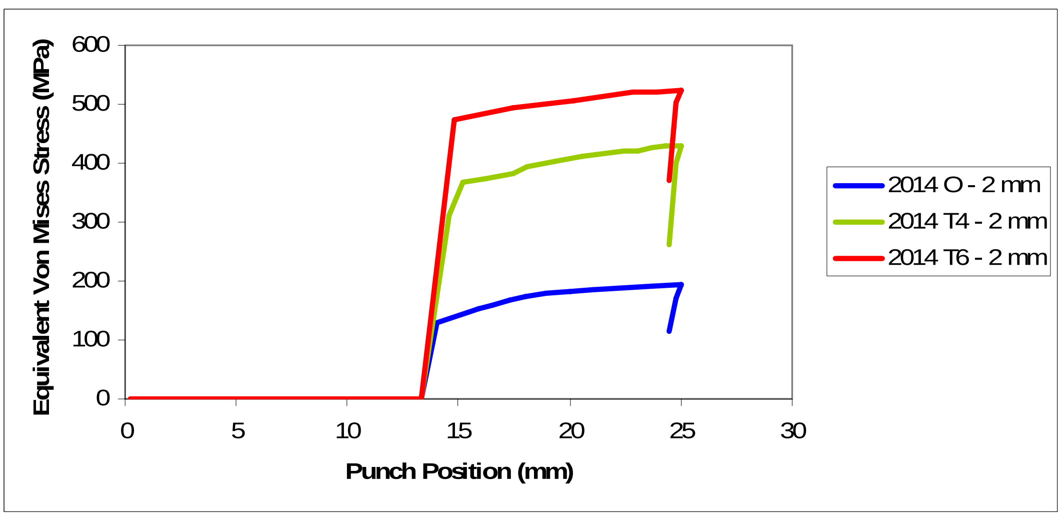

Figure 6.4 Maximum Equivalent Von Mises stress vs. punch position of 2mm thick AA 2014 under different heat treatment conditions for 90˚ V-bending.

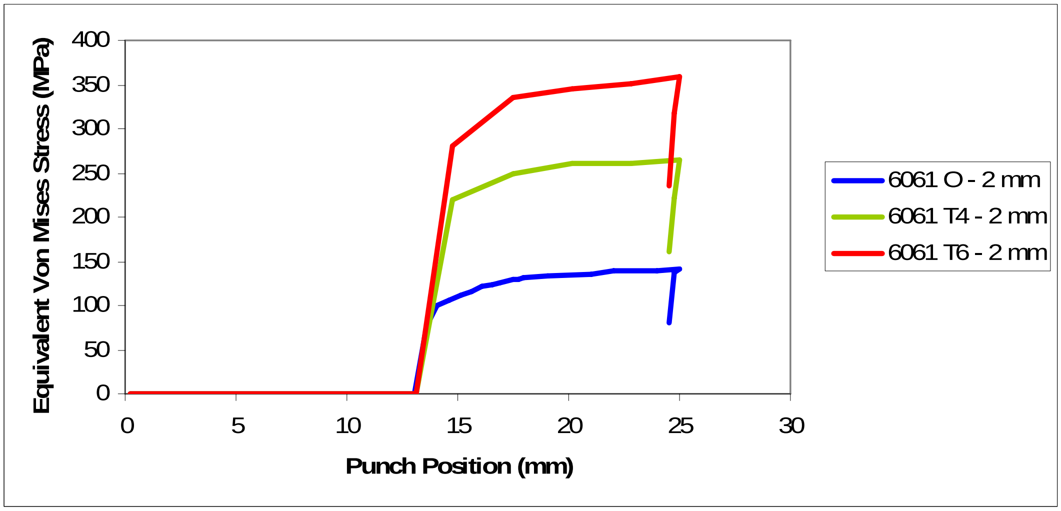

Figure 6.5 Maximum Equivalent Von Mises stress vs. punch position of 1.6 mm thick AA 6061 under different heat treatment conditions for 90˚ V-bending

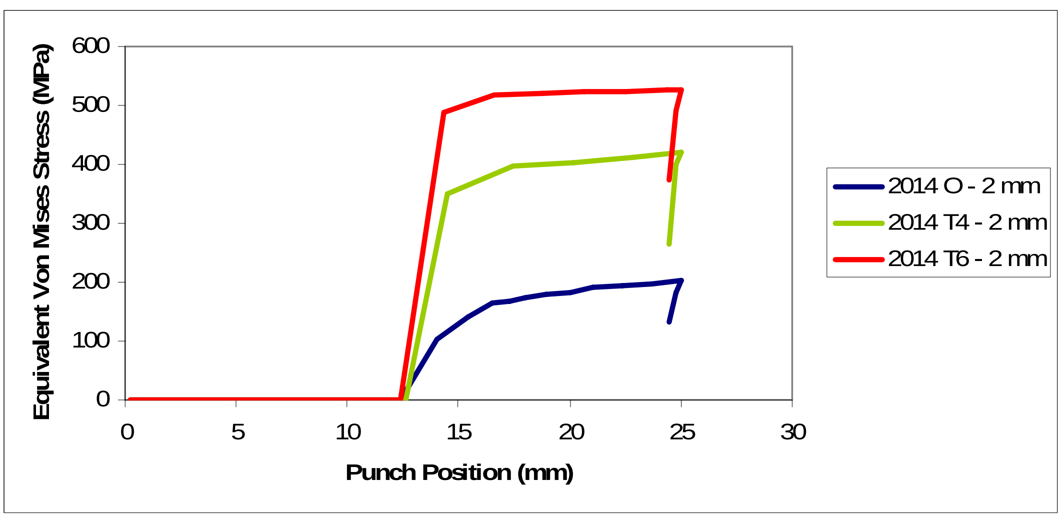

Figure 6.6. Maximum Equivalent Von Mises stress vs. punch position of 2 mm thick AA 2014 under different heat treatment conditions for 120˚ V-bending

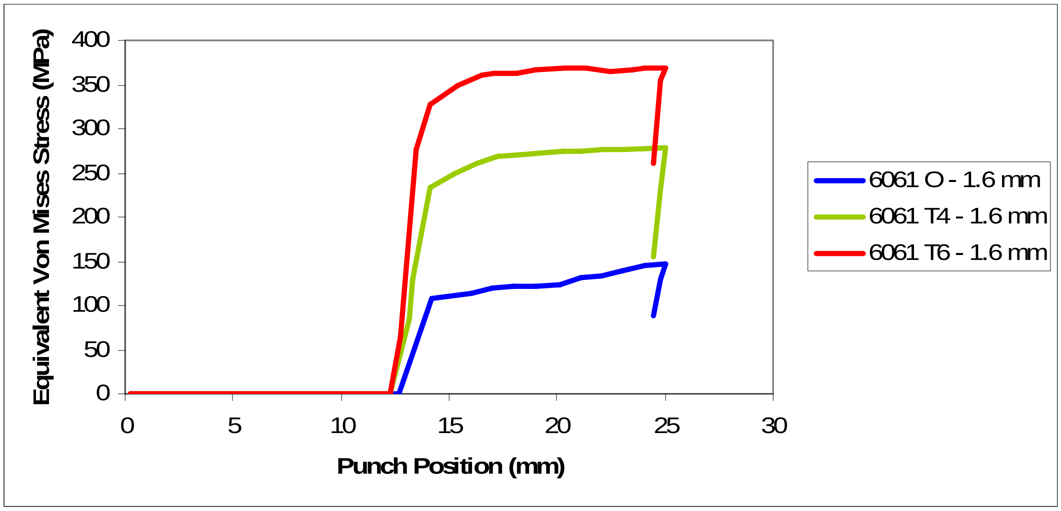

Figure 6.7 Maximum Equivalent Von Mises stress vs. punch position of 1.6 mm thick AA 6061 under different heat treatment conditions for 120˚ V-bending

FEM results showed that, for both material AA 2014 and AA 6061, maximum von Mises stresses are observed the highest in T6 condition whereas the lowest in O condition. Von Mises stress values increase as the punch moves down and at fully loaded stage, 25 mm movement of the punch tip, maximum von Mises stress values are obtained in sheet material. However, upon removal of the load, equivalent von Mises stress values began to drop suddenly beacause of elastic recorvery.

6.3. Total Equivalent Plastic Strain Values

Total equivalent plastic strain values of each heat treated material for 60˚, 90˚, 120˚ V-bending are graphically demonstrated in Figure 6.8, Figure 6.9, Figure 6.10, Figure 6.11, Figure 6.12 and Figure 6.13.

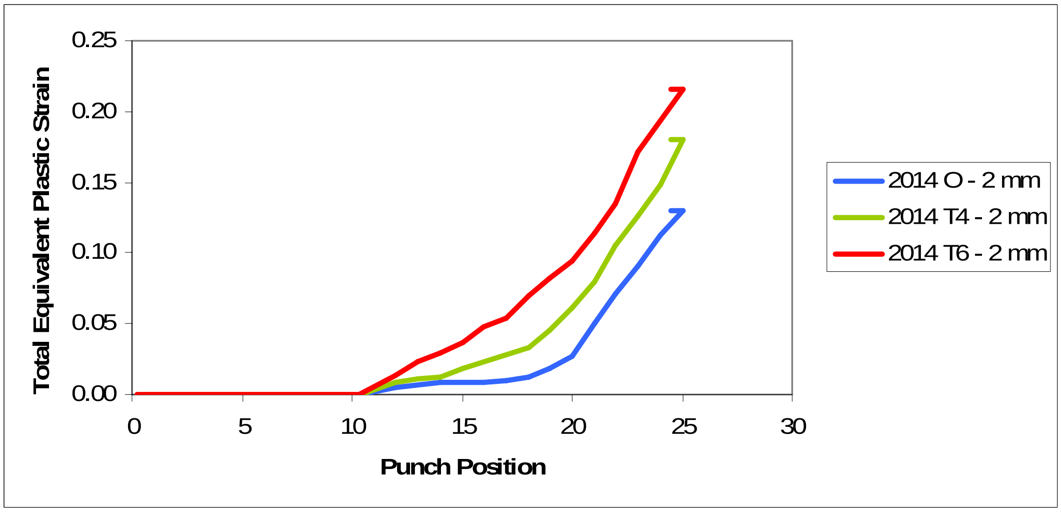

Figure 6.8 Total Equivalent Plastic Strain vs. punch position of 2 mm thick AA 2014 under different heat treatment conditions for 60˚ V-bending

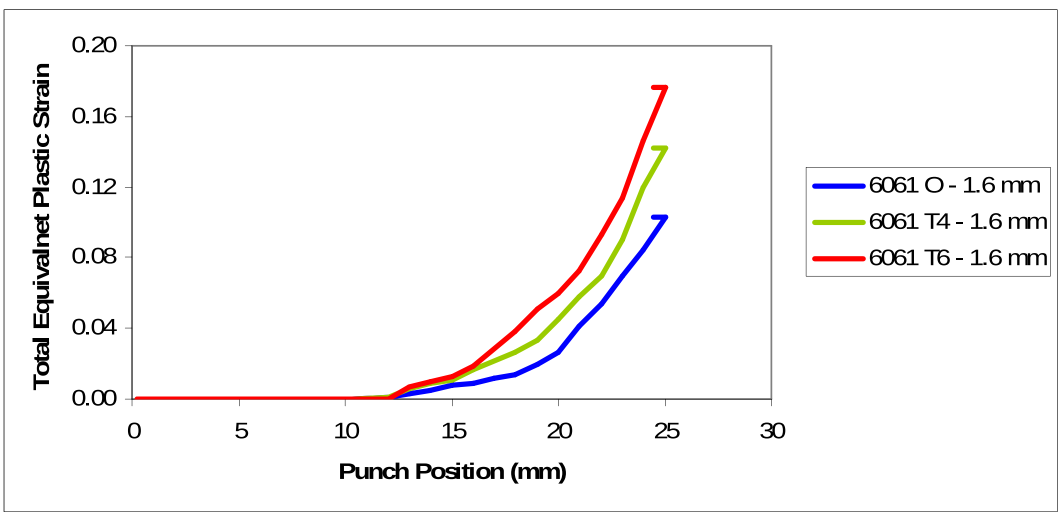

Figure 6.9 Total Equivalent Plastic Strain vs. punch position of 1.6 mm thick AA 6061 under different heat treatment conditions for 60˚ V-bending

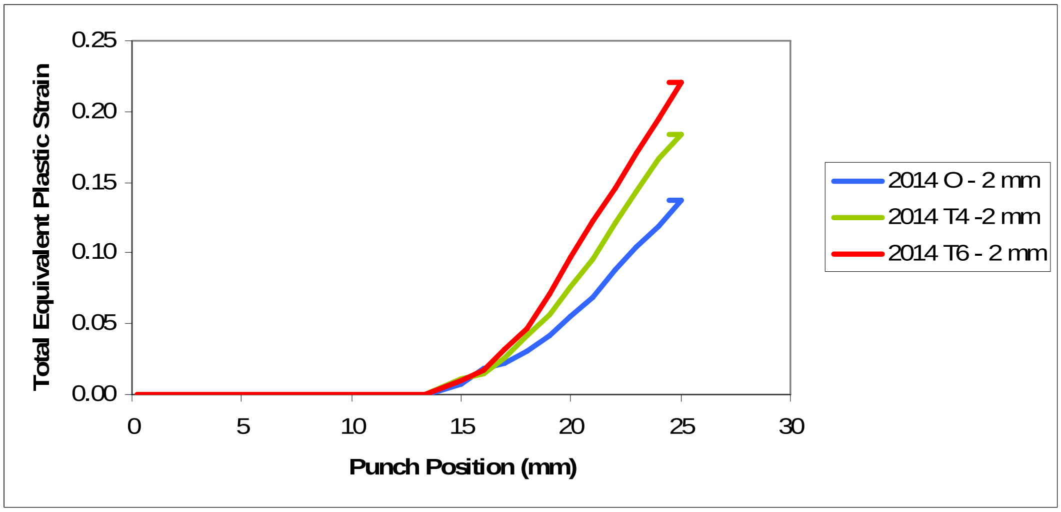

Figure 6.10 Total Equivalent Plastic Strain vs. punch position of 2 mm thick AA 2014 under different heat treatment conditions for 90˚ V-bending

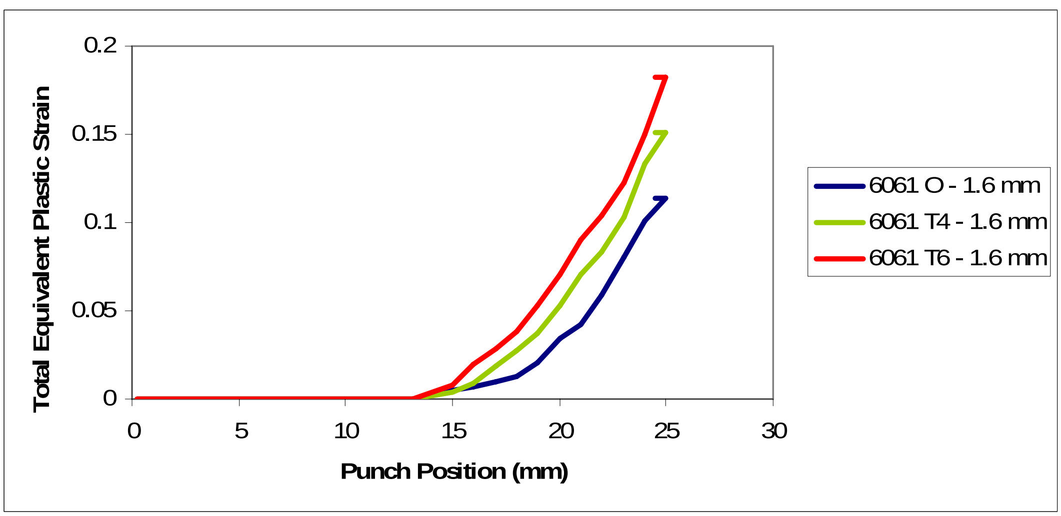

Figure 6.11 Total Equivalent Plastic Strain vs. punch position of 1.6 mm thick AA 6061 under different heat treatment conditions for 90˚ V-bending.

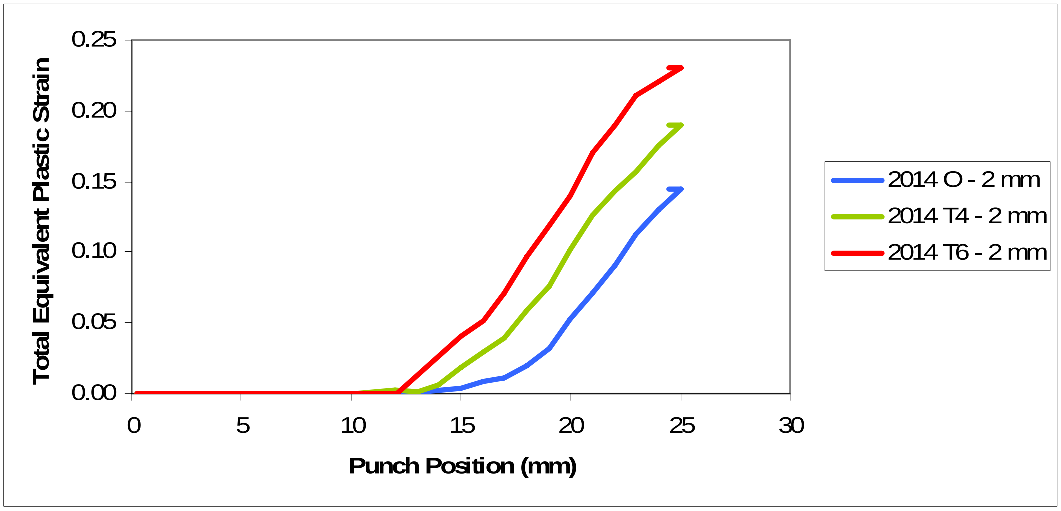

Figure 6.12 Total Equivalent Plastic Strain vs. punch position of 2 mm thick AA 2014 under different heat treatment conditions for 120˚ V-bending.

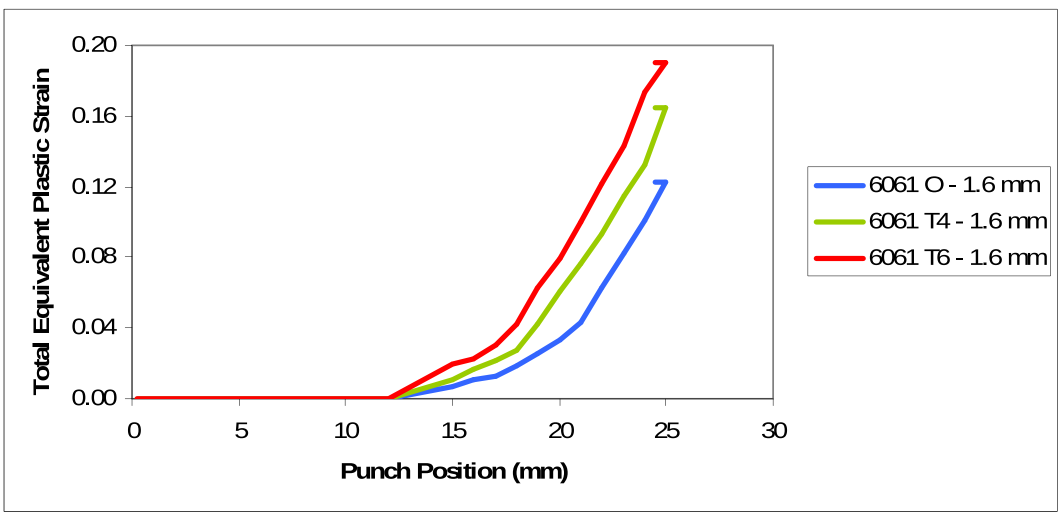

Figure 6.13 Total Equivalent Plastic Strain vs. punch position of 1.6 mm thick AA 6061 under different heat treatment conditions for 120˚ V-bending.

Maximum total equivalent plastic strain distributions given in the case studies indicate that the material in O condition is subjected to smaller equivalent plastic strain values than the material in temper conditions T4 and T6. Maximum plastic strain values are observed at the fully loaded stage. Thereafter, removal of the punch, the total equivalent plastic strains remains constant.

6.4. Punch Loads

Punch load values of each heat treated material for 60˚, 90˚, 120˚ V-bending are graphically demonstrated in Figure 6.14, Figure 6.15, Figure 6.16, Figure 6.17, Figure 6.18 and Figure 6.19.

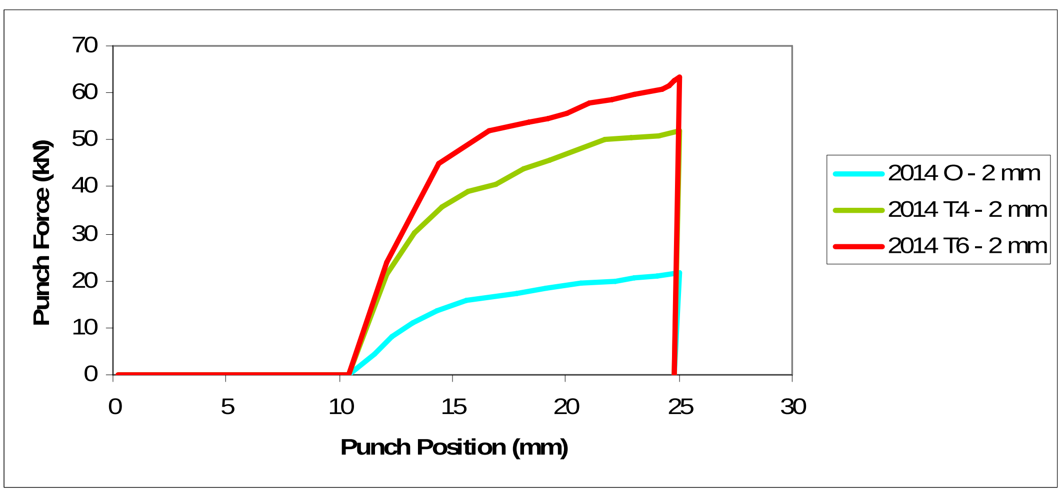

Figure 6.14 Punch Force vs. Punch Position of 2 mm thick AA 2014 under different heat treatment conditions for 60˚ V-bending.

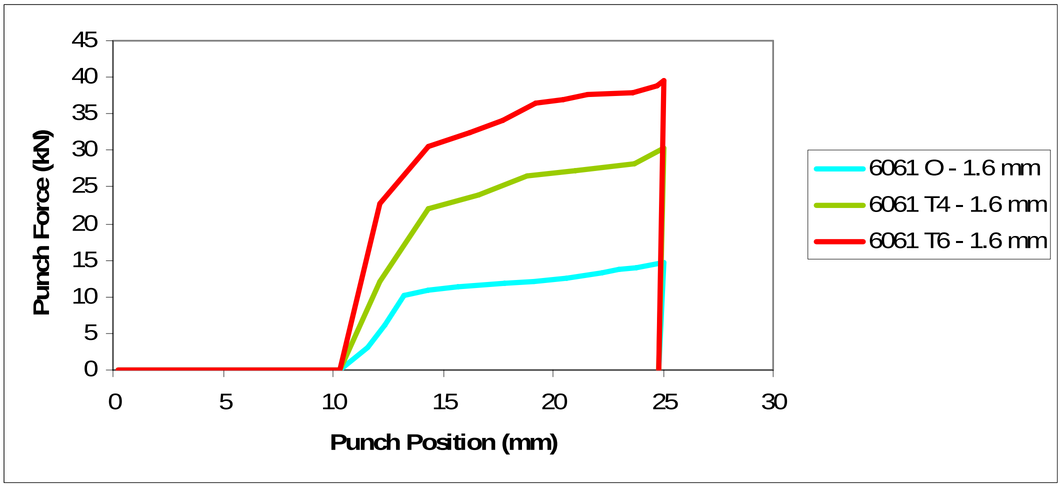

Figure 6.15 Punch Force vs. Punch Position of 1.6 mm thick AA 6061 under different heat treatment conditions for 60˚ V-bending.

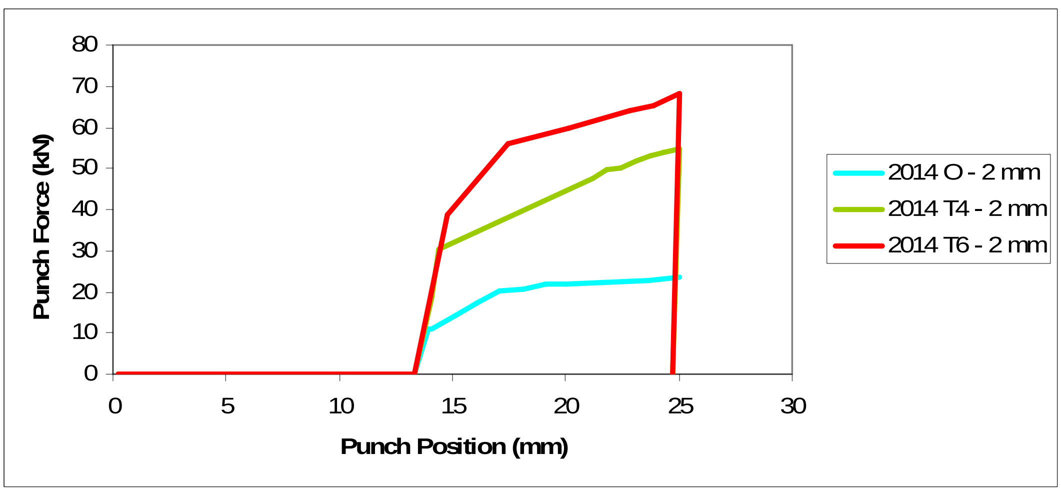

Figure 6.16 Punch Force vs. Punch Position of 2 mm thick AA 2014 under different heat treatment conditions for 90˚ V-bending.

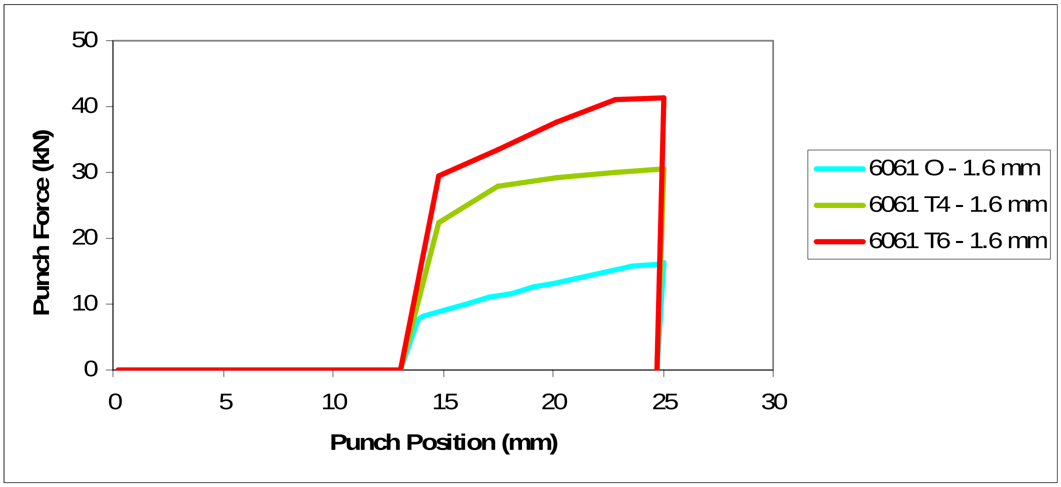

Figure 6.17 Punch Force vs. Punch Position of 1.6 mm thick AA 6061 under different heat treatment conditions for 90˚ V-bending.

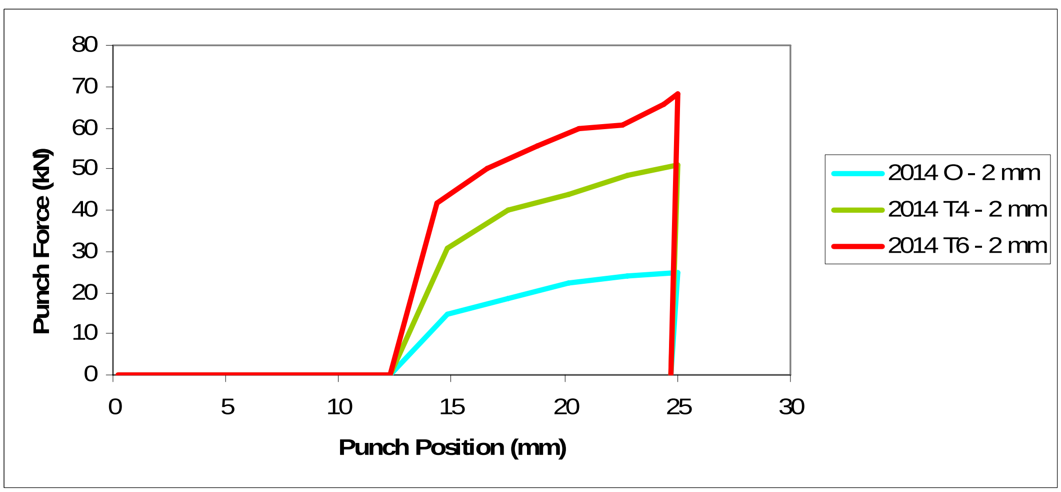

Figure 6.18 Punch Force vs. Punch Position of 2 mm thick AA 2014 under different heat treatment conditions for 120˚ V-bending.

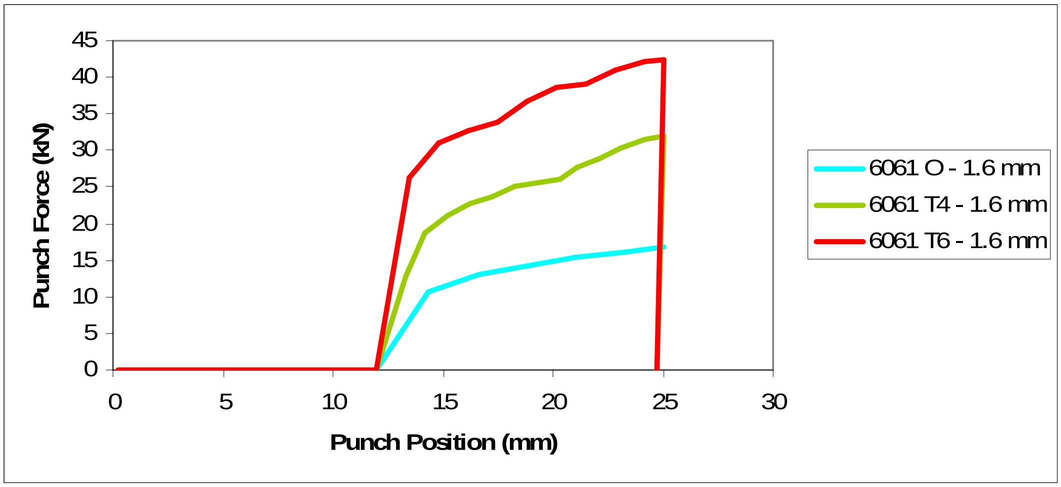

Figure 6.19 Punch Force vs. Punch Position of 1.6 mm thick AA 6061under different heat treatment conditions for 120˚ V-bending.

Regarding of FEM results, force required to bend sheet metal for T6 heat treatment is higher than the T4 heat treatment condition. Whereas required punch force for V-bending is the minimum in O heat treated material as expected.

CHAPTER 7

CONCLUSIONS

7. 1. General Conclusions

In this thesis, several bending operations have been analyzed in order to determine the effect of heat treatment to the springback. For this purpose, three different types of heat treatment are applied to the alloys AA 2014 and AA 6061, and the amount of springback have been determined under both circumstances. Moreover, the effect of bend angle and thickness to the springback is also studied individually in the scope of this work. Hence, the general conclusions attained in this study can be stated as follows:

i. The materials used have the highest yield strength in T6 condition compared to temper T4 and O and it is observed that higher springback values are obtained in temper T6 in comparison with temper T4 and O.

ii. It is seen that as the yield strength of the material is increased by heat treatment higher maximum von Mises stress values are observed. For same bending conditions, maximum von Mises stress values occured in T6 condition whereas it happens to be minimum in O condition.

iii. Maximum total equivalent plastic strain distributions indicated that the material in O condition is subjected to smaller equivalent plastic strain values than the material in temper conditions T4 and T6.

iv. For a particular temper type of the materials used, when the thickness of the material increases, springback amounts decrease.

v. For a particular material used, when thickness of the sheet increases, total equivalent plastic strain amounts grow for identical conditions.

vi. When the thickness of the sheet increases for the particular materials used, von Mises stress amounts increase.

vii. It is shown that the increment in bend angle causes increase in springback.

viii. In V-bending process, there exist two different bent-up regions, which cause springback in opposite directions. Thus, it is possible to obtain negative springback for some configurations of V-bending.

ix. FEM results also showed that, in T6 condition, required punch force to bend the sheet metal is higher than the material in T4 condition where the lowest in O condition.

x. It is observed that numerical and experimental results are in good agreement.

7. 2. Future Recommendations

One of the future studies related to this study may be the simulation and analysis of different bending operations such as U-die bending and bending with flexible tooling. In such a case, the tooling configurations may be varied and the changes in the processes may be investigated.

Another further study may be to analyze more complex bending operations by utilizing hot forming processes. Effect of material model to the bending and springback simulation may also be studied.

Finally, FEM may be used in conjuction with optimization software, by which new algorithms may be created and tooling design of complicated bending processes may be accomplished.

REFERENCES

[1] Tschaetsch, H**, Metal Forming Practise,** 7th Ed., Springer, 2006.

[2] Boljanovic, V., **Sheet Metal Forming Processes and Die Design,** 1st Ed, Industrial Press Inc., 2004.

[3] A. Schey J., **Introduction to Manufacturing Processes,** 2nd Ed., McGraw-Hill Book Company, Inc., 1987.

[4] Suchy, I., **Handbook of Die Design**, 2nd Ed., McGraw-Hill Book Company, Inc., 2006

[5] Marciniak Z., Duncan J. L**. Mechanics of Sheet Metal Forming** , 2nd Ed., Elsevier Science, 2002.

[6] Johnson, W., and Mellor, P. B., **Engineering Plasticity,** Van Nostrand Reinhold Company, London, 1978.

[7] SME (Society of Manufacturing Engineers), **Die Design Handbook,** 3rd Ed., McGraw-Hill Book Company, Inc., 1990

[8] Amstead, B. H., Ostwald, P. F., and Begeman, M. L., **Manufacturing Processes**, John Wiley & Sons, 1986.

[9] ASM Handbook, Volume 4, Heat Treating

[10] Alcoa, Alloy 6061 Tech Sheet,

[11] Varlı, A. E., Ms Thesis **"Fatigue Crack Growth Behavior of AA 6063 Aluminum Alloy at Different Aging Conditions",** 2006

[12] Lei Li-Ping-, Hwang S., Kang B. S., "**Finite Element Analysis and Design in Stainless Steel Sheet Forming and its Experimental Comparison** ", Journal of Materials Processing Technology, Vol 110, 2001, ppp. 70-77.

[13] Nishino S., Ohya K., **"Proposal for Reducing Press Working Load and High Accurate Evaluation of Springback Error in Bending Automobile Sheet Metal"** JSAE Review, Vol 24, 2003, pp. 283-288.

[14] Chou, I., Hung C., "**Finite Element Analysis and Optimization on Springback Reduction**", International Journal of Machine Tools & Manufacture, Vol. 39, 1999, pp. 517-536.

[15] Karafillis, A. P., and Boyce, M. C., "**Tooling Design in Sheet Metal Forming Using Springback Calculations**", International Journal of Mechanical Sciences, Vol. 34, No. 2, 1992, pp. 113-131.

[16] Palaniswamy, H., Ngaile, G., **"Optimization of Blank Dimensions to Reduce Springback in the Flexforming Process"** Journal of Materials Processing Technology, Vol 146, 2004, pp.28-34.

[17] **Lee, Sang-Work., "A study on the Bi-Directional Springback of Sheet Metal Stamping".,** Journal of Materials Processing Technology, Vol 167, 2005, pp.33-40.

[18] Zhao, K. M., Lee, J. K., "**Finite Element Analysis of three-point Bending of Sheet Metals**", Journal of Materials Processing Technology, Vol 122, 2002, pp. 6-11.

[19] Gan W., Wagoner R.H., "Die Design Method for Springback", International Journal of Mechanical Sciences, Vol. 46, 2004, pp. 1097-1113.

[20] Wu Longwu., "**Tooling Mesh Generation Technique for Iterative FEM Die Surface Design Algorithm to Compensate for Springback in Sheet Metal Stamping**", Engineering Computation, Vol. 14, 1997, pp. 630-648.

[21] Cheng S. H., Cao J., "**An Accelerated Springback Compensation Method**", International Journal of Mechanical Sciences, Vol. 49, 2007, pp. 267-279.

[22] Wagoner R. H., Li M., "S**imulation of Springback : Through-Thickness Integration**"., International Journal of Plasticity, Vol. 23, 2007, pp. 345-360.

[23] Oliveira M. C., Alves J. L**.,** "**Study on the Influence of Work-Hardening Modeling in Springback Prediction**", International Journal of Plasticity ,Vol 23 , 2007 , pp.516-543.

[24] Fu B. L., Chen Y. J., "**Springback Variational Principles of Bending of Straight Beams with Large Deflection**", Journal of Materials Processing Technology , Vol. 188, 2007, pp.40-44

[25] Hilditch T. B. , Speer J.G., **"Influence of Low-Strain Deformation characteristics of high strength sheet steel on curl and springback in bend-under-tension tests.** Journal of Materials Processing Technology, Vol. 182, 2007, pp.84-94

[26] Firat M. **" U-Channel Forming Analysis with An Emphasis on Springback Deformation"** Materials and Design, Vol. 28, 2007, pp. 147-154.

[27] Panthi S. K., Ramakrishnan N., "**An Analysis of Springback in Sheet Metal Bending Using Finite Element Method (FEM)"** Journal of Materials Processing Technology, Vol. 180, 2007, pp.80-85

[28] Narasimham N., Lovell M. **"Predicting Springback in Sheet Metal Forming: An Explicit to Implicit Sequential Solution Procedure"**, Finite Elements in Analysis and Design, Vol.33, 1999, pp.29-42.

[29] Esat V., Darendeliler H., **"Finite Element Analysis of Springback in Bending of Aluminum Sheets"**, Materials and Design, Vol.23, 2002, pp. 223-229.

[30] **Papeleux L., Ponhot P., "Finite Element Simulation of Springback in Sheet Metal Forming",** Journal of Materials Processing Technology, Vol. 125-126, 2002, pp.785-791.

[31] Park D. W., Oh S. I, "A Four-Node Shell Element with Enhanced Bending Performance for Springback Analysis" , Comput. Methods Appl. Mech. Engrg., Vol. 193, 2004, pp.2105-2138.

[32] Sriram S., Wagoner R. H., **"Adding Bending Stiffness to 3-D Membrane FEM Programs."** International Journal of Mechanical Sciences ,Vol 42 , 2000 , pp.1753-1782.

[33] Livatyali H., Wu H.C., **"Prediction and Elimination of Springback in Straight Flanging using Computer-Aided Design Method Part 1: Experimental Investigations",** Journal of Materials Processing Technology, Vol. 117, 2001, pp. 262-268.

[34] Livatyali H., Wu H.C., **"Prediction and Elimination of Springback in Straight Flanging using Computer-Aided Design Method Part 2: FEM Predictions and Tool Design",** Journal of Materials Processing Technology, Vol. 120, 2002, pp. 348-354.

[35] Kutt L. M., Nardiello J. A., **"Non-Linear Finite Element Analysis of Springback"**, Communications in Numerical Methods in Engineering., Vol. 15, 1999, pp. 33-42.

[36] Fei D., Hotgson P., **"Experimental and Numerical Studies of Springback in Air V-Bending Process For Cold Rolled Trip Steels."** Nuclear Engineering and Design, Vol. 236, 2006, pp. 1847-1851

[37] Garcia-Romeu M. L., Ciurana J**. "Springback Determination of Sheet Metals in an Air Bending Process Based on an Experimental Work",** Journal of Materials Processing Technology, Vol. 191, 2007, pp. 174-177.

[38] Zhan M., Yang H., **"Springback Analysis of Numerical Control Bending of Thin-Walled Tube using Numerical-Analytical Method"** Journal of Materials Processing Technology, Vol. 177, 2006, pp. 197-201.

[39] Tekaslan O., Seker U., **"Determining Springback Amount of Steel Sheet Metal Has 0.5 mm. Thickness in Bending Dies"** Johnson, W., and Yu, T.", Materials and Design, Vol. 27, 2006, pp. 251-258.

[40] Tekiner, Z., **"An Experimental Study on the Examination of Springback of Sheet Metals with Several Thicknesses and Properties in Bending Dies"** Journal of Materials Processing technology, Vol. 145, 2004, pp. 109-117.

[41] Hsu, T. C., Shien, I. R., **"Finite Element Modeling of Sheet Forming Process with Bending Effects",** Journal of Materials Processing Technology, Vol. 63, 1997, pp. 733-737.

[42] Muderrisoglu, A., Livatyali, H., Ahmetoglu, M., and Altan, T., "**Computer Aided Design for Bending, Flanging and Hemming of Steels and Aluminum Alloys**", PMA-Metal-Form Conf., Chicago, 1997.

[43] Forcellese, A., Fratini, L., Gabrielli, F., and Micari, F., "**Computer Aided Engineering of the Sheet Bending Process**", Journal of Materials Processing Technology, Vol. 60, 1996, pp. 225-232.

[44] Gau, J.-T., and Kinzel, G. L., "**An Experimental Investigation of the Influence of the Bauschinger Effect on Springback Predictions**", Journal of Materials Processing Technology, Vol. 108, 2001, pp. 369-375.

[45] Li, X., Yang, Y., Wang, Y., **" Effect of the Material-Hardening Mode on the Springback Simulation Accuracy of V-Free Bending"**, Journal of Materials and Technology, Vol. 123, 2002, pp. 209-211.

[46] Antonelli, L., Salvini, P. **"Identification of Elasto-Plastic Characteristics by means of Air-Bending Test",** Journal of Materials and Technology, Vol. 183, 2007, pp. 127-139.

[47] Bruni, C., Forcellese, A., **"Air Bending of AZ31 Magnesium Alloy in Warm and Hot Forming Condition"**, Journal of Materials and Technology, Vol. 177, 2006, pp. 373-376.

[48] Chan, K. C., and Wang, S. H., **"The Grain Shape Dependence of Springback of Integrated Circuit Leadframes"** Materials Science and Design, Vol. 270, 1999, pp.323-329.

[49] Carden, W.D., Geng, L.M., **"Measurement of Springback"**, International Journal of Mechanical Sciences, Vol. 44, 2002, pp. 79-101.

[50] Jiang, C., Han, X., **"The Optimization of the Variable Binder Force in U-Shaped Forming with Uncertain Friction Coefficient"** Journal of Materials and Technology, Vol. 182, 2007, pp. 262-267.

[51] Zhong, H., **"Elasto-Plastic Solutions for Springback Angle of Pipe-Bending using Local Induction Heating"**, Journal of Materials and Technology, Vol. 102, 2000, pp. 103-108.

[52] Lee, S. W., and Yang, D. Y., "**An Assessment of Numerical Parameters Influencing Springback in Explicit Analysis of Sheet Metal Forming Process**", Journal of Materials Processing Technology, Vol. 80-81, 1998, pp. 60-67.

[53] Moon, Y.H., Kang, S.S., **"Effect of Tool Temperature on the Reduction of the Springback of Aluminum Sheets"**, Journal of Materials Processing Technology, Vol. 132, 2003, pp. 365-368.

[54] Kim. H.S, Koc, M., **"Numerical Investigations on Springback Characteristics of Aluminum Sheet Metal Alloys in Warm Forming Conditions"** Journal of Materials Processing Technology, Vol. 183, 2007, pp. 40-64.

[55] Inamdar, M.V, Date, P. P., **" On the Effects of Geometric Parameters on Springback in Sheets of five Materials Subjected to Air Vee Bending"**, Journal of Materials Processing Technology, Vol. 123, 2002, pp. 459-463.

[56] Geng, L., Wagoner R.H., " Role of Plastic Anisotropy and its Evolution on Springback", International Journal of Mechanical Sciences, Vol. 44, 2002, pp. 123-148.

[57] Asgari, S.A., Pereira, **"Statistical Analysis of Finite Element Modeling in Sheet Metal Forming and Springback Analysis"**, Journal of Materials Processing Technology, Vol. 183, 2007, pp. 80-88.

[58] Cantelli, J.A., Cantero, J.L., **"Theoretical analysis of Air Bending at High Temperature",** Journal of Materials Processing Technology, Vol. 190, 2008, pp. 101-110.

[59] Meinders, T., Burchitz, I.A., **"Numerical Product Design: Springback Prediction, Compensation and Optimization"**, International Journal of Machine Tools & Manufacture, Vol. 48, 2008, pp. 499-514.

[60] Kawka, M., Kakita, T., and Makinouchi, A., "**Simulation of Multi-step Sheet Metal Forming Processes by a Static Explicit FEM Code**", Journal of Materials Processing Technology, Vol. 80-81, 1998, pp. 54-59.

[61] Esat V., Ms Thesis **"Finite Element Analysis of Bending",** 2002

[62] **Marc – Volume A – Theory and User Information**, MARC Analysis Research Corporation, 1996.

[63] **Marc – Volume B – Element Library**, MARC Analysis Research Corporation, 1996.

[64] **Wagoner H.R, Cheot J.L, Fundamentals of Metal Forming,** 1st Ed., John Wiley & Sons, Inc., 1997.